Pathophysiology of Anoctaminopathy (LGMD2L)

Calum Norman Robert Kirk

A thesis submitted for the degree of Doctor of Philosophy

Institute of Genetic Medicine

Newcastle University

May 2017

Abstract

Anoctamin 5 (ANO5) is the causative gene underlying limb girdle muscular dystrophy type 2 (LGMD2L), a highly heterogeneous musculoskeletal disease characterised by weakness of the shoulder and hip musculature, generally increasing in severity with age. A re-examination of ANO5 prevalence in previously undiagnosed patients has found that LGMD2L is the third most prevalent LGMD in the North East of England. However, very little is known about ANO5 or of possible treatment strategies for LGMD2L patients.

Anoctamin 5 is one of a ten-member family of proteins, some of which have confirmed biochemical or physiological functions. Anoctamin 6, the most closely related family member, has been suggested to be a phospholipid scramblase. Deficiency of anoctamin 6 causes Scott syndrome, a blood clotting disorder caused by failure to expose phosphatidylserine (PS) on the external plasma membrane of red blood cells. More widely, PS exposure is also required to identify and remove apoptotic cells in many cell types. One hypothesis for anoctamin 5 function is that of a phospholipid scramblase in muscle tissue; a dystrophic phenotype resulting from impaired PS exposure leading to an increased inflammatory response and a failed muscle repair process overall.

To clarify our understanding of anoctamin 5, this hypothesis was investigated along with general examination into potential interacting proteins and the subcellular localisation of anoctamin 5.

Lacking a suitable antibody against anoctamin 5, subcellular localisation was investigated using co-expression of fluorescently tagged ANO5 constructs with both organelle specific markers and GFP-tagged dysferlin constructs. Dysferlin (DYSF) is of interest as mutations are causative for LGMD2B which has an overlapping phenotype with LGMD2L. ANO5 localises to the sarcoplasmic reticulum and t-tubules in the C2C12 myoblast cell line, overlapping with the dysferlin expression pattern.

Anoctamin 5 function was investigated using ANO5 knock down C2C12 cell lines developed during this project. These cell lines were characterised using 2-dimensional electrophoresis followed by MALDI-MS/MS of selected protein spots. Expression of annexin A2 (ANXA2) in C2C12 is affected when anoctamin 5 is knocked down.

Anoctamin 5 function as phospholipid scramblase was investigated in ANO5 knock down C2C12 using an annexin V apoptosis detection kit, modified to include a stain for active caspase 3, another marker of apoptosis. The number of annexin V-positive and caspase 3-positive cells were then assessed using fluorescent microscopy. Significantly fewer annexin V-positive cells were found in ANO5 knock down C2C12 compared to Control C2C12. However, there was no significant difference between the number of active caspase 3-positive cells, suggesting that the knock down of anoctamin 5 has a specific effect on PS exposure and not a general effect to apoptotic processes.

These data suggest a possible extension to the initial anoctamin 5 as phospholipid scramblase hypothesis, reconciling the observations that anoctamin 5 is internally localised but also has a significant effect on PS exposure at the plasma membrane. This interpretation suggests that ANO5 functions within a novel subcellular vesicle population activated by apoptotic triggers. These hypothetical vesicle populations, containing ANO5, ANXA2 and PS, transit to the external plasma membrane when required where ANXA2 binds to the plasma membrane. Activation of ANO5 leads to normalisation of PS between the inner and outer leaflets of the vesicle, which is inserted into the membrane in a process requiring ANXA2 and /or dysferlin, identifying the cell as dead marking it for phagocytosis.

This project investigates novel avenues of anoctamin 5 research and suggests potential future research directions.

Declaration

The work contained in this thesis has not been submitted as part of any other degree or qualification. All work has also been carried out by the author and all sources of information fully referenced and all collaborators fully acknowledged.

Dedication

This thesis is dedicated to all LGMD and anoctaminopathy patients.

Acknowledgements

I would like to first thank Professor Hanns Lochmüller, Professor Katie Bushby, Dr Steve Laval and Dr Debbie Hicks who have supervised and advised me variously throughout my PhD. Their help, advice and support have been invaluable throughout this project.

This work would not have been possible without the help and contributions of the members of the John Walton Muscular Dystrophy Research Centre and the Institute of Genetic Medicine, past and present. Thank you to my PhD progress assessors Professor Sir John Burn and Professor Rita Horvath for their suggestions and input, Dr Andreas Roos for his essential input in the write up and submission of this thesis and to Dr Rita Barresi for her expert advice throughout the project. Thanks to Dr Mojgan Reza for carrying out and advising me on the electroporation experimentation. Thanks to Dr Morten Ritso for teaching me the optimal way to work in a tissue culture suite. To Liz Greally and the staff of the Functional Genetics Unit for all the help with the animal work and to Professor Volker Straub for letting me conduct my mouse work under his licence. Thanks to Dr Andrew Filby and the Flow Cytometry team based at the Centre for Life for their expert advice and suggestions, particularly Dr Gillian Hulme and Dr Lothar Marischen. Thanks to Dr Emily McIlwaine for assistance with the miniBradford assay. To Lisa Hodgson for training and assistance in microscopy techniques.

I also thank the Muscle Tissue Culture Collection (MTCC) for providing patient primary cell samples. The Muscle Tissue Culture Collection is part of the German network on muscular dystrophies (MD-NET) and the German network for mitochondrial disorders (mito-NET, project D2, 01GM1113A) funded by the German ministry of education and research (BMBF, Bonn, Germany). The Muscle Tissue Culture Collection is a partner of EuroBioBank (www.eurobiobank.org) and TREAT-NMD (www.treat-nmd.eu).Thanks also to Alphalyse for carrying out the mass spectrometry analysis on my selected protein spots

To Mum, Dad and my friends and family outside of the IGM for letting me unwind by talk their collective ears off about the latest or strangest scientific discoveries. Finally, Patsy. Thank you for your boundless support and patience over the years. You were always there when I needed you and I could not have finished this without you.

This work was funded by Muscular Dystrophy UK and the Medical Research Council UK.

Table of Contents

List of Figures

List of Tables

List of Abbreviations

2DE	2 dimensional electrophoresis
4% PFA/PBS	4% paraformaldehyde in phosphate buffered saline
aC3	active Caspase 3
ANO#	Anoctamin (#= 1, 2, 3, 4, 5, 6, 7, 8, 9, 10)
BIN-1	Bridging Integrator 1
BL10	C57BL/10 mouse model
BMD	Becker Muscular Dystrophy
bp	Base pairs
BSA	Bovine Serum Albumin
CaCC	Calcium activated chloride channel
CAPN3	Calpain 3
cDNA	Complementary DNA
CK	Creatine kinase
DAPI	4',6-diamidino-2-phenylindole
DFL	Specific dysferlin construct designed by Dr Steve Laval
dH2O	Distilled water
DMD	Duchenne Muscular Dystrophy
DMEM	Dulbecco's Modified Eagle's Medium
DMSO	Dimethyl sulfoxide
DNA	Deoxyribonucleic acid
DYSF	Dysferlin
EDTA	Ethylenediaminetetraacetic acid
EGTA	Ethylene glycol tetraacetic acid
ER	Endoplasmic Reticulum
eYFP	Enhanced Yellow Fluorescent Protein
FACS	Fluorescence Assisted Cell Sorting
FBS	Foetal Bovine Serum
FITC-AV	FITC conjugated Annexin V
FSC-A	Forward Scatter Area
FSC-H	Forward Scatter Height
FSHD	Facioscapulohumeral muscular dystrophy

GAPDH	Glyceraldehyde 3-phosphate dehydrogenase
GFP	Green Fluorescent Protein
IEF	Isoelectric focussing
IF	Immunofluorescence
IPG	Immobilised pH gradient
kbp	Kilo base pair
kDa	Kilo daltons
LDS	Litium dodecyl sulphate
LGMD	Limb Girdle Muscular Dystrophy
MALDI MS/MS	Matrix assisted laser desorption/ionisation tandem mass spectrometry
mdx	C57BL/10ScSn-Dmdmdx mouse model
MMD	Miyoshi Muscular Dystrophy
MS	Mass spectrometry
NCBI	National Centre for Biotechnology Information
NET	Fractionation buffer
NL	Non linear
NS	Non-significant
OCT	Optimum Cutting Temperature
PBS	Phosphate Buffer Saline
PCR	Polymerase chain reaction
PFA	Paraformaldehyde
PI	Propidium Iodide
PK	Protein Kinase
PS	Phosphatidylserine
RNA	Ribo Nucleic Acid
rt-PCR	Reverse transcription polymerase chain reaction
SCRD	Scrambling domain
SDS	Sodium dodecyl sulphate
SDS-PAGE	Sodium dodecyl sulphate polyacrylamide gel electrophoresis
SEAL	Surface Epitope Antibody Library
shRNA	short hairpin RNA
SSC-A	Side Scatter Area

Stauro or Stspn	Staurosporine
STM	Fractionation buffer consisting of Sucrose, Tris and Magnesium chloride
TA	Tibialis Anterior
TAE	Tris acetic acid EDTA buffer
TBS	Tris buffered saline
TBS-T	Tris buffered saline with Tween20
TOF	Time of Flight

Chapter 1 Introduction

1.1 Muscular Dystrophies

Muscular dystrophies are a group of rare, highly heterogeneous diseases (Emery, 2002). While they share progressive weakness of voluntary muscles and are genetically inherited, muscular dystrophies vary in inheritance pattern, pattern of muscle involvement, age of onset, rate of progression and associated phenotypes such as heart or lung disease (Emery, 2002; Mercuri and Muntoni, 2013).

Duchenne muscular dystrophy (DMD) is the most common muscular dystrophy (prevalence - 1 in 3,600 to 1 in 6,000 male births (Bushby *et al.*, 2010)) and was the first to be characterised. DMD is named after Guillaume Duchenne who conducted detailed characterisation of the disease in the 1860s, though it has since been recognised that reports of DMD patients had been described earlier, notably by Conte and Gioja in 1836 and Meryon in 1852 (Meryon, 1852; Emery and Emery, 1993). As an X-linked disease, the majority of patients are male and experience muscle weakness from a young age, typically losing ambulation before their early teens (Laing *et al.*, 2011). In the 164 years since the description and characterisation of DMD, several other groups of muscular dystrophy, themselves often comprised of multiple subtypes, have been identified (Table 1.1).

Of these groups, Oculopharyngeal (OPMD) and the Myotonic dystrophies (DM1 and DM2) both have an autosomal dominant pattern of inheritance while the Congenital muscular dystrophies (CMD) have a recessive pattern. The CMDs are a heterogeneous group of muscular dystrophies connected by severe hypotonia from birth and the onset of muscle weakness within a year (Bonnemann *et al.*, 2014). The increased understanding in the subtleties between different muscular dystrophies is in large part thanks to the implementation of molecular genetics techniques such as next-generation sequencing (Thompson and Straub, 2016).

In the case of Facioscapulohumeral dystrophy (FSHD), while it is also autosomal dominantly inherited, it has only been after several decades of genetic and clinical investigation that a consensus on its pathophysiology has recently been reached (Tawil *et al.*, 2014). FSHD was formally characterised in the 1950s (Tyler and Stephens, 1950) but until recently, the two genetically distinct FSHD subtypes (FSHD1 and FSHD2) were clinical indistinguishable. It is now thought that changes in the expression of

DUX4, caused by disruption to the repression of D4Z4 macrosatellite repeats, leads to FSHD in skeletal muscle (Tawil *et al.,* 2014). Similarly, the increased utility of molecular genetic techniques has greatly increased the identification and understanding of the many different subtypes of limb girdle muscular dystrophies. The limb-girdle muscular dystrophies are of particular interest to this project and are discussed in further detail in the following section.

There are currently no cures for any muscular dystrophy, though therapies and management options are available for several which have increased patient life expectance and greatly improved quality of life for sufferers (Eagle *et al.,* 2002; Bach and Martinez, 2011). For DMD, the treatments developed since its first discovery include steroid therapy (Daftary *et al.,* 2007; Markham *et al.,* 2008) and ventilators (Eagle *et al.*, 2002). Current DMD research is exploring effective prediction of muscle loss using MRI (Kinali *et al.*, 2011; Wokke *et al.*, 2014) and treatment options for muscle loss including exon skipping, a form of gene therapy to effectively turn DMD into its less severe form, Becker muscular dystrophy (BMD) (Niks and Aartsma-Rus, 2017). Due to the relatively rare prevalence of many of the muscular dystrophies research into muscular dystrophies, and the LGMDs in particular, are greatly supported by the establishment and expansion of clinical registries and networks (Thompson and Straub, 2016).

Dystrophy	**Prevelance (per 100,000)**	**Location**	**Identified Protein (Gene Name)**
Congenital (CMD)			
MDC1A	0.60	6q22.33	Laminin alpha-2 (LAMA2)
Walker-Warburg syndrome	0.03	9q34.13	Protein O-Mannosyltransferase 1 (POMT1)
Ullrich (UCMD)	0.13	2q37.3	Collagen, type VI, alpha-3 (COL6A3)
		21q22.3	Collagen, type VI, alpha-1 (COL6A1) and Collagen, type VI, alpha-2 (COL6A2)
Rigid spine (RSMD1)	0.13	1p36.11	Selenoprotein N, 1 (SEPN1)
Dystrophinopathies			
Duchenne (DMD)	8.29	Xp21.2-p21.1	Dystrophin (DMD)
Becker (BMD)	7.29		
Facioscapulohumeral (FSHD)	3.95		
1		4q35	Currently Unclear, hypothesised to involve DUX4
2		18p11.32	
Limb Girdle Muscular Dystrophies	2.27	Detailed in full in Table 1.3	
Oculopharyngeal (OPMD)	0.13	14q11.2	Polyadenylate-binding protein, Nuclear 1 (PABPN1)
Myotonic			
DM1	10.4	19q13.32	Dystrophia myotonica protein kinase gene (DMPK)
DM2	0.17	3q21.3	Zinc Finger Protein 9 (ZNF9)

Table 1.1 List of the six most common muscular dystrophy groups in the North East of England Table compiled from data in Norwood et al. (2009), with additional facioscapulohumeral information from Richards et al. (2012) and "Location" information (chromosome position) from OMIM (http://omim.org/). Information for LGMD is omitted from this table as it is detailed more fully separately in Table 1.3. Groups are arranged alphabetically and not in order of frequency. The prevalence (per 100,000 people in the population), gene position and causative protein (if known) are listed.

1.2 Limb Girdle Muscular Dystrophies

The limb girdle muscular dystrophy (LGMD) group is characterised by wasting of the limb-girdle musculature, typically sparing the facial muscles (Walton and Nattrass, 1954). Diagnosis of specific LGMD subtypes has always been challenging due to the high phenotype heterogeneity seen within the group and potentially within each subtype (e.g. location of muscle weakness, age of onset, severity of disease and rate of progression; (Bushby, 1999; Thompson and Straub, 2016)). Additionally, other muscular dystrophies, for example FSHD and the dystrophinopathies (DMD and BMD), present with similar weakness and are more common in clinical populations than the LGMDs (Bushby, 2009). Exclusion of these alternative muscular dystrophies must therefore be achieved before a LGMD diagnosis can be reached. The majority of LGMD diagnostic issues are now resolved by investigation and identification of causative genes, often through use of next generation sequencing techniques (Narayanaswami *et al.*, 2014; Ghaoui *et al.*, 2015; Kuhn *et al.*, 2016).

However, access to advanced molecular diagnostic tools such as immunohistochemistry, immunoblotting and next generation whole exome sequencing, varies between and within countries. As a result it is very difficult to fully assess the global prevalence of LGMDs. Furthermore robust methods of reporting suspected cases have not been established in all countries making establishment of cohorts and corroboration of candidate genes very difficult (Bastian *et al.*, 2015). The lack of robust universal diagnosis also extends to understanding the progression of identified subtypes in successfully diagnosed patients.

Despite these difficulties, current advancements in molecular research techniques have so far allowed for identification of thirty two distinct LGMD subtypes, many with an identified causative gene (Table 1.3). These subtypes are grouped into autosomal dominant (LGMD1 [MIM# 159000]) and recessive (LGMD2 [MIM# 253600]) subtypes, with recessive subtypes being more prevalent than dominant forms making up approximately 90% of the diagnosed patient population (Cotta *et al.*, 2014; Nigro and Savarese, 2014).

LGMDs as a group however are still rare. For example in a 2009 snap shot of the clinical population of the North East of England attending specialist muscle clinics, the LGMDs as a whole made up 6.2% of the clinical population (or 2.27/100.000 prevalence of the general population) while the commonest form of muscular dystrophy,

Duchenne muscular dystrophy, typically appeared with a frequency of 8.29/100,000 in the general population, or 11.2% of the muscle patients (Norwood *et al.*, 2009).

In all LGMDs, the identification of causative genes and correct differential diagnosis allows for a better understanding of disease progression, associated complications and most importantly, therapeutic possibilities and improved patient care (Bushby, 1999; Cotta *et al.*, 2014). However the function of many of these causative genes is still unknown and it is estimated that 30% of patients lack a definitive diagnosis of their particular LGMD even following genetic testing (Bushby, 2009).

1.2.1 Autosomal dominant LGMDs

There are currently eight identified dominant limb girdle muscular dystrophy subtypes, 1A-1H. Two of these eight subtypes have been identified only in single families in Spain (LGMD1F (Gamez *et al.*, 2001; Peterle *et al.*, 2013) and Italy (LGMD1H (Bisceglia *et al.*, 2010)). LGMD1G had also initially only been identified within a single Brazilian family but has since been identified in a family in Uruguay (Starling *et al.*, 2004; Vieira *et al.*, 2014). Conversely LGMD1A has been described in a number of families worldwide including North America (Gilchrist *et al.*, 1988; Hauser *et al.*, 2000), Argentina (Hauser *et al.*, 2002) and Japan (Shalaby *et al.*, 2009).

Generally, dominant LGMDs have a later age of onset and slower disease progression than the recessive LGMDs, though the age of onset varies greatly both between and within sub-types (Bastian *et al.*, 2015). A variety of symptoms such as toe and finger flexion limitation (LGMD1G (Starling *et al.*, 2004; Vieira *et al.*, 2014)), contractures (LGMD1B (van der Kooi *et al.*, 1996)), tight Achilles tendons (LGMD1A (Gilchrist *et al.*, 1988)) and calf hypertrophy (LGMD1C and LGMD1H (Minetti *et al.*, 1998; Bisceglia *et al.*, 2010)) have been recorded in some sub-types along with the expected proximal weakness. LGMD1B is notable for the addition of cardiac involvement, including arrhythmias, conduction disturbances and dilated cardiomyopathy which in LGMD1B can lead to sudden death (van der Kooi *et al.*, 1996).

Autosomal Dominant		
Subtypes	**Location**	**Identified Protein (Gene Name)**
LGMD1A	5q31.2	Myotilin (TTID)
LGMD1B	1q22	Lamin A/C (LMNA)
LGMD1C	3p25.3	Caveolin 3 (CAV3)
LGMD1D	7q36	DnaJ heat shock protein family member B6 (DNAJB6)
LGMD1E	2q35	Desmin (DES)
LGMD1F	7q32.1	Transportin 3 (TNPO3)
LGMD1G	4p21.22	Heterogeneous nuclear ribonucleoprotein D-like protein (HNRNPDL)
LGMD1H	3p25.1-p23	Unknown

Table 1.2 List of the eight autosomal dominant LGMD subtypes currently identified. Table compiled from data in Nigro and Savarese (2014) and additional "Location" information (chromosome position) from OMIM (http://omim.org/), though the classification of the LGMD1E nomenclature appears to be just in Nigro and Savarese (2014). The currently identified LGMD subtypes are listed along with their mode of inheritance, chromosome position and causative protein (and gene).

1.2.2 Autosomal recessive LGMDs

There are currently twenty four autosomal recessive subtypes of LGMD which, as with the autosomal dominant subtypes, have a wide variation in population frequency and range of pathologies. LGMD2A is estimated to be the most common form of recessive LGMD, accounting for approximately 30% of all recessive LGMD cases (Richard *et al.*, 2016). LGMD2A has also been reported as the most common LGMD in in Spain, Italy, Czech Republic and Romania (Fanin *et al.*, 2005; Cotta *et al.*, 2014; Stehlikova *et al.*, 2014; Bastian *et al.*, 2015). LGMD2I is reported to be the most common in Denmark (Sveen *et al.*, 2006), LGMD2B the most common in the United States (Moore *et al.*, 2006) and LGMD2C, 2D, 2E and 2F (the sarcoglycanopathies) are common in Turkey, North Africa (Bushby, 1995; Zatz *et al.*, 2003) and Brazil (Cotta *et al.*, 2014).

LGMD2I was initially reported as the most common LGMD in the UK (Poppe *et al.*, 2003), but specific investigation of the patient population in the North of England now suggests that LGMD2A is the most common in this particular sub-population (Norwood *et al.*, 2009). Follow up in this geographic region has also identified increased prevalence of other recessive LGMDs such as LGMD2L which is now suggested to have a prevalence of 0.27/10,000 potentially making it the third most common form of

LGMD in the UK (Hicks *et al.*, 2011). The LGMD2L subtype was first identified in a cohort of eight families of French-Canadian descent based on linkage analysis to chromosome 11 (Jarry *et al.*, 2007). Since then, populations of LGMD2L patients have been identified in several European populations including Holland (van der Kooi *et al.*, 2013), Finland (Penttila *et al.*, 2012), France (Behin *et al.*, 2011), Italy (Magri *et al.*, 2011) as well as the aforementioned prevalence in the UK (Hicks *et al.*, 2011).

Increased identification of the number of affected individuals has increased our understanding of the range and historical progression of the geographic distribution of some LGMDs. For example LGMD2H was initially thought to appear only in the Hutterite ethnic group in Manitoba, Canada (Shokeir and Kobrinsky, 1976) but has now been recorded in other European non-Hutterite patients such as Croatia (Saccone *et al.*, 2008). Additionally, all patients in the Manitoba population were found to have the same causative c.1459G>A mutation in the gene TRIM32 (Weiler *et al.*, 1998; Frosk *et al.*, 2002). This is of particular interest as LGMD2I is also present in both Hutterite and European populations. Indeed, the c.826C>A (L276I) mutation causative for LGMD2I in Hutterite populations is the same as that identified in European patient populations, suggesting a European founder event (Frosk *et al.*, 2005). A similar founder event may have occurred for LGMD2H, but has gone unreported as the representatives in the European populations remain undiagnosed. Similarly a common c.191dupA mutation has been identified in many LGMD2L patients. The distribution of this common mutation as well as other identified causative LGMD2L mutations suggests a founder effect in Northern European populations (Hicks *et al.*, 2011).

Autosomal Recessive		
Subtypes	**Location**	**Identified Protein (Gene Name)**
LGMD2A	15q15.1	Calpain 3(CAPN3)
LGMD2B	2p13.2	Dysferlin (DYSF)
LGMD2C	13q12.12	Sarcoglycan, Gamma (SGCG)
LGMD2D	17q21.33	Sarcoglycan, Alpha (SGCA)
LGMD2E	4q12	Sarcoglycan, Beta (SGCB)
LGMD2F	5q33.2-q33.3	Sarcoglycan, Delta (SGCD)
LGMD2G	17q12	Titin-Cap (TCAP)
LGMD2H	9q33.1	Tripartite Motif-Containing Protein 32 (TRIM32)
LGMD2I	19q13.32	Fukutin-Related Protein (FKRP)
LGMD2J	2q31.2	Titin (TTN)
LGMD2K	9q34.13	Protein O-Mannosyltransferase 1 (POMT1)
LGMD2L	11p14.3	Anoctamin 5 (ANO5)
LGMD2M	9q31.2	Fukutin (FKTN)
LGMD2N	14q24.3	Protein O-Mannosyltransferase 2 (POMT2)
LGMD2O	1p34.1	Protein O-Mannose Beta-1, 2-N-Acetylglucosaminyltransferase (POMGNT1)
LGMD2Q	8q24.3	Plectin 1(PLEC1)
LGMD2R	2q35	Desmin (DES)
LGMD2S	4q35.1	Trafficking Protein Particle Complex, subunit 11 (TRAPPC11)
LGMD2T	3p21.31	GDP-Mannose Pyrophosphorylase B (GMPPB)
LGMD2U	7p21.2	Isoprenoid Synthase Domain-Containing Protein (ISPD)
LGMD2V	17q25.3	Acid Alpha-Glucosidae (GAA)
LGMD2W	2q14.3	LIM and senescent cell antigen-like-containing domain protein 2 (*LIMS2/ PINCH2)*
LGMD2X	6q21	Popeye domain–containing 1 (POPDC1)
LGMD2Y	1q25.2	Torsin A-Interacting Protein 1 (TOR1AIP1)
LGMD2Z	3q.13.33	Protein O-Glucosyltransferase 1 (POGLUT1)

Table 1.3 List of the twenty five autosomal recessive LGMD subtypes currently identified. Table compiled from data in Nigro and Savarese (2014), Schindler et al. (2016), Ghaoui et al. (2016), (Servian-Morilla et al., 2016) and additional "Location" information (chromosome position) from OMIM (http://omim.org/). The currently identified LGMD subtypes are listed along with their mode of inheritance, chromosome position and causative protein (and gene).

1.2.3 LGMDs have overlapping phenotypes and pathways with other muscular dystrophies

Due to the interplay between proteins and pathways involved in correct muscle function a few dominant and recessive LGMDs share overlapping phenotypes to both other LGMDs and other muscular dystrophies. For example, the dystrophin glycoprotein complex (DGC) is a sophisticated organisation of protein subunits which connects the extracellular matrix of muscle to the cytoskeleton (Ervasti and Campbell, 1993; Rybakova *et al.*, 2000) and together correctly regulates the constant contraction and elongation required of skeletal and cardiac muscle (Gumerson and Michele, 2011). Muscular dystrophy often results from mutations in genes which code for proteins required for correct function of the DGC.

For example, four transmembrane sarcoglycans, alpha, beta, delta and gamma, form a subunit within the DGC, the sarcoglycan complex (Yoshida *et al.*, 1994). The sarcoglycan complex is thought to assist in the stability of the plasma membrane though the precise function is not clear (Durbeej and Campbell, 2002). Mutations in the gamma, alpha, beta and delta sarcoglycans disrupt the plasma membrane of skeletal and cardiac muscle leading to the LGMDs 2C (Noguchi *et al.*, 1995), 2D (Roberds et al., 1994), 2E (Bonnemann *et al.*, 1995) and 2F (Nigro *et al.*, 1996) respectively. Differential diagnosis between the sarcoglycanopathies and DMD, now routinely achieved through genetic screening (Grimm, 1984), is often required as mutations to dystrophin, another key DGC protein, lead to DMD and BMD

Caveolin 3 is another protein required for the correct functioning of the DGC (Song *et al.*, 1996), indeed upregulation of the protein has been associated with DMD (Repetto *et al.*, 1999). Caveolin 3 is the muscle-specific member of the caveolin family and the principle component of caveolae; invaginations of the plasma membrane involved in cellular trafficking and correct muscle development (Simionescu *et al.*, 1975; Parton and Simons, 2007). Caveolin 3 is coded for by CAV3, mutations to which are causative for LGMD1C (Minetti *et al.*, 1998) but mutations to which have also been identified in familial isolated hyperCKemia (Carbone *et al.*, 2000), rippling muscle disease (Betz *et al.*, 2001; Vorgerd *et al.*, 2001) and a form of distal myopathy (Tateyama *et al.*, 2002; Gonzalez-Perez *et al.*, 2009). Evidence for an interaction between CAV3 and DYSF, mutations to which are causative for LGMD2B (Bashir *et al.*, 1998), comes from the discovery that CAV3 co-immunoprecipitates with dysferlin in human skeletal muscle,

dysferlin localisation is altered in LGMD1C muscle and several amino acid sequences in dysferlin correspond to binding motifs in CAV3 (Matsuda *et al.*, 2001).

Other LGMD not directly involved with the DGC also have overlapping pathologies with other forms of muscle weakness and muscular dystrophies. For example, mutations to the gene for myotilin are causative for LGMD1A but have also been identified as causative for a subgroup of myofibril myopathy (MFM/MYOT) which present with a distal pattern of muscle weakness (Selcen and Engel, 2004; Olive *et al.*, 2005). Another example is LGMD2I which is caused by mutations in the Fukatin Related Protein (FKRP) and is allelic with the congenital muscular dystrophy, MDC1C (Brockington *et al.*, 2001a). Generally the pathology of LGMD2I is much less severe than MDC1C, with later age of onset (late child or adulthood compared to first few months of life) and reduced risk of ambulation loss, which is likely due to the secondary deficiency of α-dystroclycan (Brockington *et al.*, 2001b). Additionally a genotype/phenotype correlation is present within LGMD2I patients as the causative 826C>A FKRP mutation leads to a more severe phenotype when compound heterozygous (Brockington *et al.*, 2001b; Walter *et al.*, 2004).

In all, several of the genes responsible for LGMDs are causative for other musculoskeletal diseases. Indeed, several of these diseases are now considered to be parts or ends of spectrums of disorders, rather than distinct diseases (Linssen *et al.*, 1997; Gazzerro *et al.*, 2010; van der Kooi *et al.*, 2013). Of particular interest to this research project is gene coding anoctamin 5 (ANO5), mutations for which are causative for limb girdle muscular dystrophy type 2L (LGMD2L) and Myoshi Myopathy Type 3 (MMD3) (Bolduc *et al.*, 2010).

1.2.4 LGMD2L similarity to LGMD2B

LGMD2B is also allelic with a distal myopathy (Emery, 2002). Missense and frameshift mutations in the dysferlin gene (DYSF, MIM# 603009) cause LGMD2B as well as Miyoshi myopathy 1 (MMD1). Furthermore, both LGMD2L and 2B present with very similar phenotypes. Both have a variable, late onset, infrequent cardiac and respiratory involvement and muscle wasting initially of the lower limbs which may present asymmetrically, with potential progression to the shoulder musculature (Jarry *et al.*, 2007; Urtizberea *et al.*, 2008). Like anoctamin 5, the function of dysferlin is not fully understood but is strongly suspected to be involved in muscle cell repair (Bansal *et al.*,

2003). Similarities between LGMD2L/MMD3 and LGMD2B/MMD1 phenotypes, as well as relevant data on cell repair in dysferlin deficient and non-dysferlin deficient cells has suggested that anoctamin 5 may act in the cell repair pathway with dysferlin (Mahjneh *et al.*, 2010).

1.3 The anoctaminopathies - LGMD2L and MMD3

1.3.1 Recessive anoctamin 5 mutations are causative in LGMD2L and MMD3

Several recessive mutations in the anoctamin 5 gene (ANO5 (MIM# 608662)) have been found to be causative for LGMD2L (Bolduc *et al.*, 2010; Hicks *et al.*, 2011; Magri *et al.*, 2011; Milone *et al.*, 2012; Penttila *et al.*, 2012; Little *et al.*, 2013) and MMD3 in Dutch and Finnish families (Linssen *et al.*, 1998; Jaiswal *et al.*, 2007; Bolduc *et al.*, 2010; Penttila *et al.*, 2012) as well as isolated hyperCKaemia (Milone *et al.*, 2012) and collectively these disease are termed the anoctaminopathies (Marlow *et al.*).

ANO5 maps to chromosome 11p14.3 (Katoh and Katoh, 2004). There are currently 71 reported unique sequence variants (www.lovd.nl/ANO5) distributed across the length of the gene, 41 of which are considered pathogenic. A common point mutation (c.191dupA) has been identified and appears at a relatively high frequency in several populations and in homozygous, heterozygous and compound heterozygous states (Hicks *et al.*, 2011; Sarkozy *et al.*, 2013). The c.191dupA mutation on exon 5 of ANO5, results in a frameshift and premature termination of the protein leading to a loss of function of ANO5 (Bolduc *et al.*, 2010). However, in Finnish populations the c.2272C>T mutation is more common though this does not appear to be due a founder event in Finland (Penttila *et al.*, 2012). The c.2272C>T mutation is a missense mutation located on exon 20 and also appears in homozygous, heterozygous and compound heterozygous states (Penttila *et al.*, 2012; Sarkozy *et al.*, 2013). Other identified variants in ANO5 appear as splice site, nonsense stop, synonomous and intronic mutations (Sarkozy *et al.*, 2013).

However, there has yet to be any identified genotype/phenotype correlation in anoctaminopathy patients. For example, Penttila *et al.* (2012) found in an analysis of Finnish patients both c.191dupA and c.2272C>T mutations are causative for severe to mild distal, proximal and proximodistal phenotypes. While the mutation frequency for ANO5 has been suggested to be high (Hicks *et al.*, 2011; Penttila *et al.*, 2012) it is still difficult to accurately assess due to high heterogeneity of phenotypes and the subclinical presentation of many patients, despite homozygosity or compound heterozygosity for known pathogenic mutations (Liewluck *et al.*, 2013; Savarese *et al.*, 2015).

1.3.2 Increased understanding of anoctaminopathy phenotype

As the number of diagnosed patients has increased, the symptoms of LGMD2L have become better defined. It presents predominately in adults with a mean age of onset of

32.7 years (Jarry *et al.*, 2007), though the range has been recorded as between 11 and 70 years (Jarry *et al.*, 2007; Sarkozy *et al.*, 2013). Male predominance is significant with most female patients positive for ANO5 mutations being either asymptomatic or presenting with only mild symptoms (Sarkozy *et al.*, 2013). MRI investigation has confirmed that muscle pathology is asymmetrical, though it predominantly affects the quadriceps femoris (Sarkozy *et al.*, 2012). Myalgia following exercise is common and a high creatine kinase (CK) level of above 1000 U/L has been recorded in the majority of patients (Milone *et al.*, 2012). Interestingly, asymptomatic patients positive for the causative mutations have been recorded with similarly high CK levels (Milone *et al.*, 2012; Sarkozy *et al.*, 2013). Additionally, a cohort of Dutch patients newly diagnosed with LGMD2L were found to have engaged in extensive physical activity before the onset of symptoms (van der Kooi *et al.*, 2013). The contractures, facial weakness and cardiomyopathy seen in other muscular dystrophies, are very rare.

MMD3 (MIM# 613319) patients share similar phenotypes with LGMD2L patients namely initial, often asymmetric, weakness of the leg muscles with potential progression to upper arm musculature, elevated CK levels (above 2000 U/l), male predominance and an adult age of onset (mean age of onset = 34, range of 13-52) (Linssen *et al.*, 1997; Linssen *et al.*, 1998). Some diagnosed LGMD2L patients have been shown to present with distal as well as proximal muscle weakness (van der Kooi *et al.*, 2013) and some Dutch MMD3 patients also develop proximal weakness of the hips and shoulders (Linssen *et al.*, 1997). Therefore, MMD3 and LGMD2L are more accurately described as opposing ends of a pathological spectrum rather than distinct disorders.

1.3.3 Gnathodiaphyseal Dysplasia

Dominant missense ANO5 mutations have found to be causative for the rare bone syndrome Gnathodiaphyseal dysplasia (GDD, MIM# 166260) (Riminucci *et al.*, 2001; Tsutsumi *et al.*, 2004). Causative heterozygous missense mutations have been identified in a number of geographically diverse families though two different mutations have been identified in the same cysteine residue of amino acid 356. In a large Japanese family (21 affected members) c.1066T>G has been identified while in two members of an African-American family the mutation is c.1066T>C (Akasaka *et al.*, 1969; Tsutsumi *et al.*, 2004). More recently a c.1538C>T mutation in exon 15 has been identified in a large Italian family (Marconi *et al.*, 2013). Unlike recessive ANO5 mutations, these

dominant mutations lead to disease phenotypes in both male and female patients (Ahluwalia *et al.*, 2007).

Furthermore, the cysteine residue at amino 356 where the GDD mutations are found, is conserved throughout vertebrate (human, mouse and zebrafish) and invertebrate (fruit fly and mosquito) species, and located to the proposed extracellular loop between transmembrane domains one and two (Tsutsumi *et al.*, 2004). This extracellular loop location has been noted as similar to mutations for MMD3 which are found on the loop between transmembrane domains seven and eight (Bolduc *et al.*, 2010).

GDD patients present with deformities of both jaw and long bones and skeletal fragility (Akasaka *et al.*, 1969; Riminucci *et al.*, 2001). Many patients suffer from frequent fractures of femur, radius/ulna and vertebrae bones from trivial trauma at a young age though with apparently normal healing. Cortical thickening and bowing of the tubular bones can also occur, with bowing being caused by asymmetrical healing of the bones. The spine and growth plates however appear to develop normally and growth of the patients appears to be unaffected. As patients age cemento osseous lesions of the jawbone occur, often from poor healing following tooth extraction, causing deformity of the jawbone. Examination of the lesions has shown them to be formed from a combination of fibroblasts and mineralisation of blood vessels (Akasaka *et al.*, 1969; Riminucci *et al.*, 2001; Marconi *et al.*, 2013). Initially named "hereditary gnatho-diaphyseal sclerosis" (Akasaka *et al.*, 1969), GDD was renamed to a dysplasia when it was noted that sclerosis (increases in bone density or hardening) was not associated with the jaw deformations (Riminucci *et al.*, 2001).

1.4 The Anoctamin family

Anoctamin 5 was previously named TMEM16E (Trans MEMbrane domain containing family 16, member E) due to its close homology to the TMEM16 family of proteins (Katoh, 2004; Katoh and Katoh, 2004). At the time, this family included the previously described genes TMEM16A (FLJ10261 or ORAOV2), TMEM16B (C12orf3), TMEM16C (C11orf25) and TMEM16D (FLJ34272), characterised by the eight transmembrane domains that they code for, with both the NH2 and COOH termini located within the plasma membrane (Tsutsumi *et al.*, 2004) (Figure 1.1). The TMEM16 family currently contains 10 members (1-10) and is now collectively known as the anoctamin family, with 'ANO' replacing the 'TMEM16' nomenclature. Several assumptions about anoctamin 5 function have been made but currently, a comprehensive understanding of the range of ANO5 functions remains elusive. However, a number of other anoctamins have been extensively investigated.

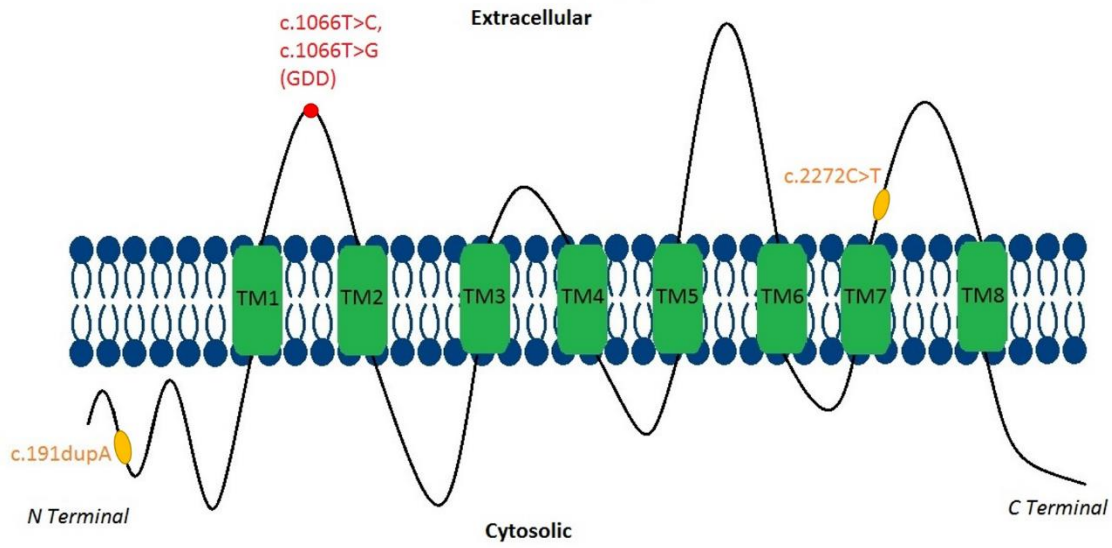

Figure 1.1 Predicted topology of anoctamin 5. Figure created using information from Penttila et al. (2012) and Savarese et al. (2015). The approximate positions of c.191dupA (the most common causative mutation for LGMD2L in most European populations) and c.2272C>T (the most common mutation for LGMD2L in Finnish populations) are labelled in orange. The approximate positions of known GDD mutations c.1066T>C and c.1066T>G are labelled in red.

Phylogenetically, the anoctamin family is highly conserved, retaining considerable protein homology between vertebrate species (Duran and Hartzell, 2011) (Figure 1.2). Early research on anoctamin 1 (MIM# 610108), found to be upregulated in cancer tumours (West *et al.*, 2004; Carles *et al.*, 2006), led to the suggestion that this protein

forms a calcium activated chloride channel (CaCC) at the cell membrane, which led to the assumption that all anoctamins fulfilled the same function (Caputo *et al.*, 2008; Yang *et al.*, 2008). However, another anoctamin associated with disease, ANO6, was soon identified as a phospholipid scramblase (Suzuki *et al.*, 2010; Castoldi *et al.*, 2011) and an unconfirmed ion channel (Scudieri *et al.*, 2015). Current research into nhTMEM16 and afTMEM16, fungal homologs of the ANOs, have broadened our understanding of the family even further and now suggests an evolutionary path from one function to the other (Brunner *et al.*, 2014; Whitlock and Hartzell, 2016a).

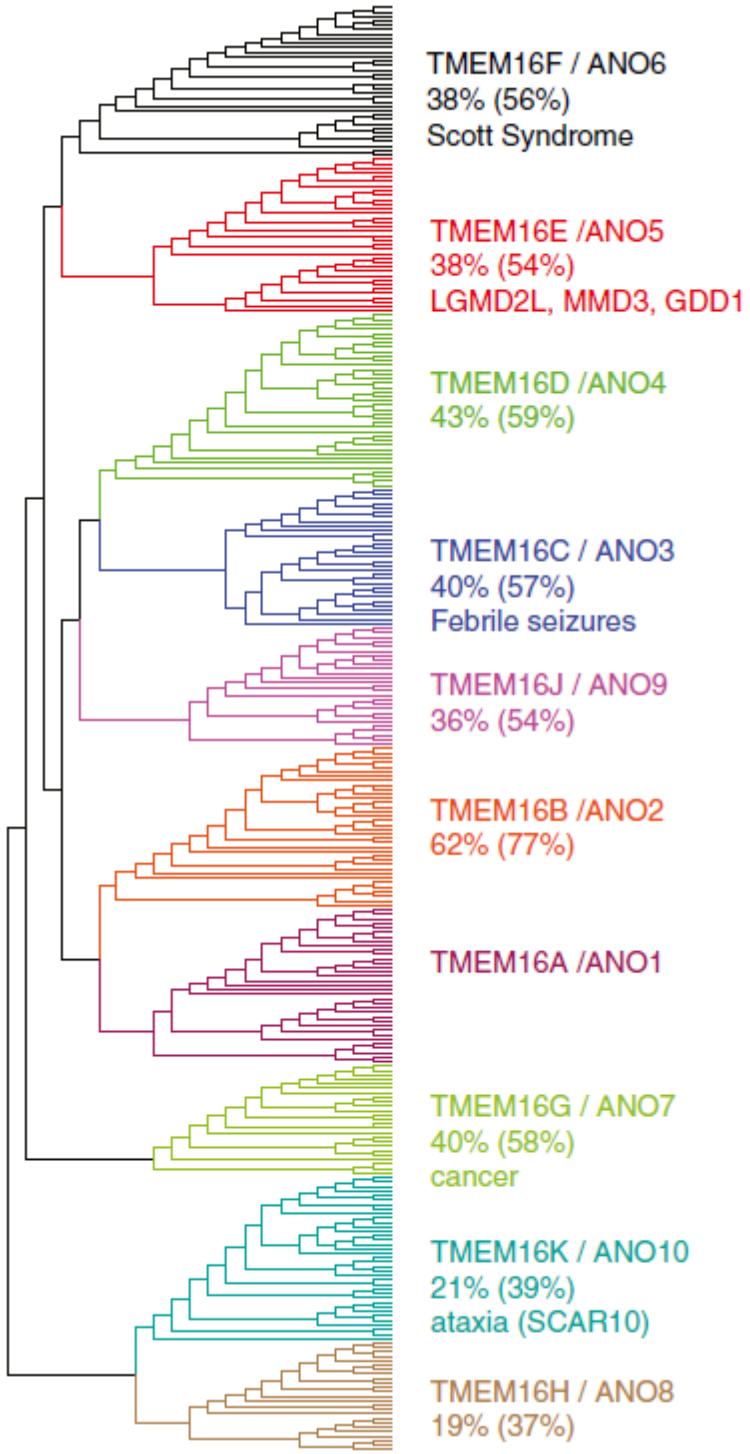

Figure 1.2 Rooted phylogenetic tree of the anoctamin family. Figure taken from Whitlock and Hartzell (2016b). Below each anoctamin name is the percent identity and (similarity) to ANO1 as well as any associated diseases. For each, both the anoctamin and TMEM16 nomenclature are given. The original authors used a subset of 1650 anoctamin sequences acquired from Uniprot to build the tree. A subset was used to remove duplicates and splice variants.

1.5 Development of ANO5 knockout mouse models and improved understanding of anoctamins as scramblases

There were no mouse models, cell lines or reliable antibodies available for anoctamin 5 prior to the start of this project. As such, investigation of ANO5 specific antibodies and development of model knockdown cell lines formed an integral part of this project. However, in the last two years of this project, three ANO5 knockout mice have been published by different labs (Gyobu *et al.*, 2015; Xu *et al.*, 2015; Griffin *et al.*, 2016). As these mice were not available to this project they were not investigated, but the implications from the characterisation of these mice is discussed in greater detail in chapter 6 of this thesis.

Additionally, in the last year a great deal has been learned about the scramblase ability of the anoctamin family members and their fungal homologs. This recent information has been included within this introduction to provide an up to date view of the current understanding of the anoctamins, though these details were unpublished or speculative at the start of this project.

1.6 Anoctamins as calcium activated chloride channels

CaCCs are known to be important in several physiological functions including amplification of olfactory transduction (Matthews and Reisert, 2003), stabilization of membrane potential in photoreceptors (Lalonde *et al.*, 2008), fluid secretion in glands and airway epithelia (Kunzelmann *et al.*, 2009), neuron action potential waveform and both firing and regulation of smooth muscle contraction (Hartzell *et al.*, 2009). However, until the discovery of anoctamin 1 and its closest related family member anoctamin 2 (MIM# 610109), the identity of the genes coding for CaCCs remained unknown. Homologues of anoctamin 1 prepared from both Xenopus oocytes and mice have been show to produce the same CaCC currents as native Axolotl oocyte CaCC when injected with Xenopus oocytes and mouse mRNA (Schroeder *et al.*, 2008).

Since their discovery, anoctamins 1 and 2 have been confirmed to function in the same processes and tissues as other recorded CaCCs. They have been identified as regulators of airway smooth muscle contraction (Huang *et al.*, 2012), in the rod photoreceptor terminals of mice retina (Stohr *et al.*, 2009; Dauner *et al.*, 2013) and in murine taste (Cherkashin *et al.*, 2015) and olfactory tissues (Dauner *et al.*, 2012). However, several studies have also expanded on their tissue specific functions, identifying them as CaCCs responsible for insulin secretion in mouse β-cells (Crutzen *et al.*, 2015) and microvilli length and surface area in frog oocytes (Courjaret *et al.*, 2016). Anoctamin 1 specifically has been found to play an important role in cancer development. It has been identified as a potential biomarker in esophageal cancer (Shang *et al.*, 2016) and that tumour cell proliferation an migration are promoted by its overexpression (Guan *et al.*, 2016).

Due to the high sequence homology within the anoctamin family, the other anoctamins were also thought to act as CaCCs, although confirmation of this was difficult to establish (Duran and Hartzell, 2011). Several studies claimed to have identified chloride conductance induced by expression of other anoctamins. For example, anoctamins 6, 7 and 10 have been recorded producing chloride channels of various intensities. However the intensity of the ion flux recorded for these three anoctamins was less than 10% that of the flux recorded for anoctamin 1. Additionally, while a short form of anoctamin 7 has also been identified without any transmembrane domains making it an unlikely ion channel, it still produces an ion flux of the same intensity as the full form of anoctamin 7 (Schreiber *et al.*, 2010). The suggestion was made that due the presence of at least one

anoctamin in any one cell line, expression experiments of anoctamin conductance have the potential to be contaminated by endogenous anoctamins (Kunzelmann *et al.*, 2009; Schreiber *et al.*, 2010).

1.7 Asymmetry, pathways and essential components of the plasma membrane

All cell membranes are built from a complex amalgam of lipids and proteins, relying on the amphipathic nature of lipids to arrange into two symmetrical monolayers (van Meer *et al.*, 2008). The hydrophilic head groups of the lipids face the aqueous outer environment, while their attached hydrophobic hydrocarbon chains point towards one another at the centre of the bilayer (van Meer *et al.*, 2008; Whitlock and Hartzell, 2016a).

Ordinarily phosphatidylcholine, sphingomyelin and glycolipids are maintained on the exoplasmic leaflet of the membrane while phosphatidylserine, phosphatidylethanolamine and phosphatidylinosital are retained on the cytoplasmic leaflet (Zachowski, 1993; Daleke, 2007). Maintaining plasma membrane asymmetry is an essential part of proper cell function as movement of lipids from one membrane leaflet to another are required for membrane stability, cell signalling, blood coagulation, apoptosis and membrane protein regulation (Andersen *et al.*, 2016). The redistribution of phospholipids between bilayers, for example the movement of phosphatidylethanolamine into phosphatidylcholine rich areas of the membrane (van Meer *et al.*, 2008), is also required for initiating curvature of the plasma membrane which is further required for vesicle budding and fusion (Pomorski and Menon, 2006).

The structure of the membrane bilayer is such that transition from one monolayer to another is highly energy demanding (Pomorski and Menon, 2006; Andersen *et al.*, 2016), with spontaneous diffusion of a single lipid taking 24 hours on average (Nakano *et al.*, 2009). Three groups of transmembrane lipid transporter protein are involved in maintaining and redistributing the plasma membrane, depending on the stimulus or required function. The heterogeneous distribution of lipids is maintained by ATP dependant flippases and floppases working in counter balance to one another (Daleke, 2003). Flippases preferentially transport lipids, most notably phosphatidylserine (PS), from the exoplasmic to the cytoplasmic leaflet (Pomorski and Menon, 2006) while floppases work in the reverse (Borst *et al.*, 2000). There are several types of both transporter types as each have different specificities and cell types. For example ATP-binding cassette (ABC) transporters as floppases (van Helvoort *et al.*, 1996) and the P4 subtype of P-type ATPases and aminophospholipids as flippases (Daleke and Lyles, 2000; Lopez-Marques *et al.*, 2014).

1.7.1 Phospholipid Scramblases and Phosphatidylserine exposure

Scramblases are the third group of transmembrane lipid transporter proteins. They act during specific cellular processes to rapidly disrupt lipid asymmetry and non-selectively expose lipids to the outer surface of the plasma membrane (Bevers *et al.*, 1983; Williamson *et al.*, 1992; Williamson *et al.*, 1995). Phospholipid scramblases are activated by increases to cytosolic calcium concentration (Zwaal and Schroit, 1997; Williamson *et al.*, 2001), which simultaneously inhibits flippase activity (Bitbol *et al.*, 1987) and lower the energy requirement for transition across the bilayer (Whitlock and Hartzell, 2016a). Current research carried out using computer models of nhTMEM16, suggests that scramblases reduce the energy demand by bending the plasma membrane and reducing the distance between the two leaflets of the membrane. Distortion of the membrane is greatest around the hydrophilic groove where the distance between membranes reduces from 28.5 Å to 18.3 Å. Furthermore, the presence of water within the hydrophilic groove of the scramblase and collections of lipid head groups at either end of this groove appear to facilitate the moment of lipids from one membrane to the other. Dipole stacks grow halfway into the groove from a high density lipid head group on the cytoplasmic leaflet of the membrane (termed the S_C region). The dipole stacks provide a scaffold for lipids to move along by forming dipole-dipole interactions as they pass through (Bethel and Grabe, 2016). Binding sites lining a channel pore, acting as a stepping stone mechanism, have also been observed in ion channels (Doyle *et al.*, 1998).

PS is a key lipid often exposed to the extracellular leaflet during scrambling events, where it acts as a marker to other cells. PS is exposed by scramblases during blood coagulation (Lhermusier *et al.*, 2011), apoptosis (Fadok *et al.*, 1992; Schlegel and Williamson, 2001), differentiation and microvesicle formation (Sessions and Horwitz, 1983; Schlegel and Williamson, 2001; van den Eijnde *et al.*, 2001). It is also becoming increasingly clear that PS plays a key role in sarcolemma wound healing (Middel *et al.*, 2016), a pathway also associated with dysferlin function.

1.7.2 Dysferlin, membrane repair and phosphatidylserine

Dysferlin is homologous with the FER-1 gene in *Caenorhabditis elegans* (Bashir *et al.*, 1998; Liu *et al.*, 1998; Bansal *et al.*, 2003), which is responsible for the fusion of large vesicles called membranous organelles to the plasma membrane (Achanzar and Ward, 1997). Studies of dysferlin have indicated that in wild type mouse muscle, dysferlin

enriched vesicles seal sites of muscle cell damage by fusing to the sarcolemma (muscle cell membrane). However, dysferlin-deficient mouse muscle shows vesicle accumulation at the site of damage, but a lack of vesicle fusion to the sarcolemma (Bansal *et al.*, 2003). In all muscle, sarcolemmal damage is caused by mechanical stress from regular muscle function (McNeil and Khakee, 1992; Cohn and Campbell, 2000). In dystrophic muscle mechanical stress has also been shown to lead to necrosis with membrane damage occurring in the initial stages (Straub *et al.*, 1997). Ineffective cell repair following damage has therefore been suggested as causative for LGMD2B and MMD1 (Liu *et al.*, 1998; Bansal *et al.*, 2003).

Very recently, the role of dysferlin in membrane repair has been more fully investigated furthering the understanding of the extent of the complexity of membrane repair. Demonbreun *et al.* (2016b) identified two structures which rapidly form following plasma membrane wounding. They term these structures the "repair cap" and the "shoulder" proteins. The authors define the "shoulder" as the region adjacent to the "repair cap" which its self lies above the area of damage. They identify dysferlin as a key "shoulder" protein as it is rapidly recruited immediately following laser injury and because they identified significant delay in membrane resealing in dysferlin-deficient myofibers. They also suggest that there is a level of safe-guarding in these shoulder proteins as they also investigated the related protein myoferlin. Myoferlin and dysferlin-deficient myofibers showed similar delay in membrane resealing while myofibers deficient for both proteins showed the greatest delay in repair. Demonbreun *et al.* (2016b) suggest that lateral membrane recruitment, that is recruitment of proteins from the surrounding plasma membrane rather than from cytoplasmic stores, leads to the accumulation of these proteins within the shoulder region.

The "repair cap" is comprised of aggregated annexin A6 (ANXA6) and also forms rapidly following membrane wounding. The aggregation of other annexins including annexin A1 and A2 follow soon after. Dysferlin is known to bind annexin A1 and A2 proteins (Lennon *et al.*, 2003; Cagliani *et al.*, 2005) and they have also been suggested as important in membrane repair (Boye and Nylandsted, 2016). Demonbreun *et al.* (2016b) also locate PS within the shoulder region during repair though after the recruitment of both the shoulder proteins and the repair cap. This highly ordered recruitment of dysferlin, annexin A6 then annexin A1 and A2 following membrane damage has also been recorded in zebrafish (Roostalu and Strahle, 2012)

1.7.3 The Annexins

Annexins are a group of calcium-dependant membrane-binding proteins, which form a superfamily of over 100 different proteins found throughout the animal kingdom (Moss and Morgan, 2004). As such they are divided into separate groups (labelled A-E); human annexins and orthologs (ANXA), invertebrates (ANXB), plants (ANXC), fungi (ANXD) and protists (ANXD) (Gerke and Moss, 2002; Moss and Morgan, 2004). Twelve annexins have been identified in humans, ANX1-11 and ANX13 (there is no protein currently assigned to ANXA12) (Gerke and Moss, 2002; Mirsaeidi *et al.*, 2016).

Annexins are intracellular proteins which bind with phospholipids found preferentially in the cytoplasmic leaflet of the plasma membrane and so localise either to the cytosol or plasma membrane, depending on the presence of calcium (Gerke and Moss, 1997). They are found in a diverse range of cells and tissues (Moss and Morgan, 2004). Annexins play a part in multiple cellular pathways such as regulation of membrane trafficking (Gerke *et al.*, 2005), ion channel regulation (Gerke and Moss, 2002), calcium homeostasis and adaptation during cellular stress (Monastyrskaya *et al.*, 2009), anticoagulation, phospholipase A2 inhibition (Raynal and Pollard, 1994), vesicle aggregation (Bitto and Cho, 1998; Spenneberg *et al.*, 1998), endocytosis (Creutz and Snyder, 2005), interactions with the cytoskeleton (Oliferenko *et al.*, 1999) and the aforementioned plasma membrane repair pathway (Roostalu and Strahle, 2012; Demonbreun *et al.*, 2016a; Demonbreun *et al.*, 2016b).

Each annexin is formed of a NH_2-terminal "head" domain and a conserved COOH-terminal protein core domain itself formed of four homologous repeats (Geisow *et al.*, 1986; Moss and Morgan, 2004), though annexin A6 has eight repeats (Avila-Sakar *et al.*, 2000). Each repeat contains five α-helices (Huber *et al.*, 1990), a calcium binding site (Geisow *et al.*, 1986) and are all highly conserved both between annexin family members and between the repeats themselves (Moss and Morgan, 2004).

1.7.4 Apoptosis and phosphatidylserine exposure

Exposure of PS to the cell surface is also required during apoptosis, the programmed and controlled death of a cell (Li *et al.*, 2003). Apoptosis is a critical and evolutionary conserved process, involved in killing infected or malignant cells (Hochreiter-Hufford and Ravichandran, 2013) but also as a counter processes to cell proliferation, removing excess cells during development and growth (Kerr *et al.*, 1972). For example,

incomplete or disturbed apoptosis can lead to several developmental disorders including malformation of limbs (Guha *et al.*, 2002), congenital brain malformation and respiratory distress syndromes (Li *et al.*, 2003).

It is the programmed and ordered nature of apoptosis which distinguishes it from necrosis and other types of cell death (Kerr *et al.*, 1972). Apoptosis of mammalian cells can be initiated either through extracellular proteins binding to death-receptors on the cell surface (extrinsic pathway), or through the release of intracellular proteins following stress to the cell (intrinsic pathway) (Putcha *et al.*, 2002). Both pathways ultimately lead to the release of mitochondrial proteins such as cytochrome c, activation of caspases and ultimately cell death involving cell shrinkage, DNA fragmentation, condensation of chromatin, membrane blebbing and formation of apoptotic bodies (Thornberry and Lazebnik, 1998; Towomey and McCarthy, 2005).

The caspases are a family of highly specific proteases which are key proteins in apoptosis. There are thirteen caspase family members in mammals, though caspases 11 and 12 are murine homologs and do not exist in humans (Thornberry and Lazebnik, 1998). The three key roles of caspases in apoptosis are inhibition of apoptosis inhibitors like I^{CAD} and Bcl-2 (Cheng *et al.*, 1997; Enari *et al.*, 1998), destruction of cell structure (leading to cell shrinkage) and interruption of protein activity (Thornberry and Lazebnik, 1998). Caspase independent apoptosis has also been recorded in several cells however. This process also involves the release of mitochondrial proteins (AIF, EndoG and Omi), though these proteins activate apoptotic characteristics such as chromatin condensation and endonuclease activity without involvement from caspases (Towomey and McCarthy, 2005).

The final stages of apoptosis are the removal and final destruction of the dying cell by phagocytes, which is necessary to stop the leakage of cellular components into the extracellular space and initiation of the inflammatory response (Kerr *et al.*, 1972). PS exposure is one of the most ubiquitous “eat me” signals used to signal to phagocytes (Fadok *et al.*, 2001) and an early indicator of an apoptotic cell (Kurosaka *et al.*, 2003) though other proteins have been identified as exposed on the cell surface during apoptosis (Dini *et al.*, 1996; Taylor *et al.*, 2000). For example annexin A1 has been shown to co-localise with PS on the plasma membrane where its presence has been suggested to enhance uptake by phagocytes (Arur et al. 2003; Gardai et al. 2005).

Increases in intracellular calcium are required for exposure of PS in apoptotic cells. Research has shown that apoptotic cells lacking intracellular calcium experience normal cell shrinkage, membrane blebbing and protein cleavage but reduced PS exposure. Re-addition of calcium to these deprived cells rescued PS exposure (Hampton *et al.*, 1996). Similarly, phagocytes derived from PS receptor deficient mice display a 50% reduction in phagocytotic ability (Li *et al.*, 2003). Finally PS expressing liposomes have also been observed as reducing mouse forepaw oedema in a dose dependant manor (Ramos *et al.*, 2007).

Timely exposure of PS identifies the cell for phagocytosis which in turn release anti-inflammatory signals thereby avoiding activation of the inflammatory pathway (Kurosaka *et al.*, 2002). While inflammation is a vital process in keeping the site of injury or infection clear of further damage (Rock and Kono, 2008), failure to remove accumulated lysed or infected cells will lead to an inflammatory response in turn leading to delayed repair or recovery and other complications including muscular dystrophy as is the case with the dysferlinopathies (Tidball, 2005; Rawat *et al.*, 2010).

1.8 Anoctamins as phospholipid scramblases

1.8.1 Development of an ion transporter from a phospholipid scramblase

Despite the initial assumption that all anoctamins are CaCCs, very recent investigation of the anoctamin family and related fungal homologs, nhTMEM16 and afTMEM16, now suggests that the anoctamins originated as scramblases with ANO1 and ANO2 developing into CaCC, rather than the other way round (Whitlock and Hartzell, 2016a). It was the observation of phospholipid scrambling following purification and reconstitution into liposomes of fungal ANO homologs that finally indicated that anoctamins were historically scramblases (Brunner *et al.*, 2014). However the structural differences between common ion transporters and the anoctamin scramblases seem to be incompatible.

The conventional ion channel is a funnel, with the protein surrounding the entire channel and providing a selective path for specific ions (MacKinnon, 2004). The anoctamins however appear to better fit the predicted model for scramblases with a hydrophilic "furrow" on one side of their surface, specifically formed of membrane helices 4 and 6 (Pomorski and Menon, 2006; Brunner *et al.*, 2014; Whitlock and Hartzell, 2016b). In ANO6, the furrow also contains the scramblase domain that has been recently identified (Yu *et al.*, 2015). The hydrophilic environment within this furrow is essential as it allows the hydrophilic lipid head groups to transition from one bilayer to the other while the hydrophobic acyl tails remains within the internal phase of the lipid bilayer.

This structural arrangement would be incompatible for ion transport as the ion would be permanently exposed to the bilayer on one side. Transition from scramblase to ion transporter however is supported by mutagenesis studies which show that the ion selection and conduction residues are homologous to the scramblase regions of the rest of the family (Whitlock and Hartzell, 2016b). Two hypotheses have been proposed to rectify this conflict. First, Whitlock and Hartzell (2016b) suggest that the pore of ANO1 and ANO2 is adjacent to a non-bilayer with the lipid head groups of this bilayer orientated towards the furrow of the anoctamin. Chloride ions would then transition along the furrow between the lipid head groups. Alternatively Brunner *et al.* (2014) suggest that the anoctamins form dimers, with the dimer structure of ANO1 and ANO2 differing from that of the scramblase anoctamins. In this model the furrows of ANO1 and ANO2 dimers are orientated towards each other, forming a funnel structure similar

to the conventional ion channel. The scramblase anoctamins meanwhile, form dimers with furrows orientated away from each other, in effect creating dimers that each have two furrows with which to facilitate scramblase function.

1.8.2 Anoctamin 6 is a phospholipid scramblase

Anoctamin 6 is the closest related family member to anoctamin 5 (Hartzell *et al.*, 2009) and has been found to play a role in the extremely rare bleeding disorder Scott Syndrome (Suzuki *et al.*, 2010; Castoldi *et al.*, 2011). Patients with Scott Syndrome present with moderately mild bleeding episodes due to ineffective phospholipid scramblase action in thrombocytes and related blood cells (Lhermusier *et al.*, 2011). Very few Scott syndrome patients have so far been identified (Weiss *et al.*, 1979; Toti *et al.*, 1996; Munnix *et al.*, 2003; Suzuki *et al.*, 2010; Castoldi *et al.*, 2011) which has led to the suggestion that Scott Syndrome is underdiagnosed due to the mildness of the bleeding episodes and because phospholipid scrambling assays are not routine investigative tools (Solari *et al.*, 2016). Platelets from ANO6-deficient mice have also been found to be defective for phospholipid scramblase activity (Fujii *et al.*, 2015; Mattheij *et al.*, 2015). Specifically, the exposure of PS on platelet surfaces following calcium treatment as well as microparticle shedding and thrombin production are impaired in platelets from ANO6-deficient mice (Fujii *et al.*, 2015). These mouse models also show unaffected clot retraction and normal bleeding times which closely replicates the patient phenotype (Fujii *et al.*, 2015).

During normal blood coagulation, scramblases redistribute the phospholipid bilayer of thrombocytes and expose PS which in turn triggers the blood clotting cascade (Spronk *et al.*, 2014). The identification of mutations in ANO6 in Scott Syndrome patients led to the suggestion that anoctamin 6 either interacts with vital molecules in the pathway, such as scramblases or calcium detecting molecules, or is itself the scramblase, actively binding to calcium and activating the cascade (Suzuki *et al.*, 2010).

While similarity of structure does not always equal similarity of function, the very high sequence homology between anoctamin 5 and 6 suggests that both are involved with phospholipid scrambling and exposure of PS. Inhibition or distortion of anoctamin 5, which is most highly expressed in muscle cells, may lead to ineffective cellular function and eventual muscle weakness.

1.9 Hypotheses of anoctamin 5 function

Improvements in the genetic diagnosis of LGMD2L and the identification of more anoctaminopathy patients reinforces the need to identify the function of anoctamin 5. A number of hypotheses on anoctamin 5 function have been formed based on the similar LGMD2L and 2B pathologies and the confirmed functions of some of the other anoctamin family members.

Initially, the most common assumption was that the whole anoctamin family were CaCCs as anoctamin 1 and 2 had been shown to be robust CaCCs, in different tissues (Hartzell *et al.*, 2009). Despite extensive testing though, no robust CaCC activity has yet been demonstrated for anoctamin 5 (Schreiber *et al.*, 2010; Duran and Hartzell, 2011). At the outset of this project, the anoctamins were still strongly suspected of being a family of CaCCs, though current research now suggests that this function has evolved from their initial function as scramblases. However calcium is the trigger mechanism in several important cellular functions such as membrane repair (Bansal *et al.*, 2003) and phospholipid scrambling (Mirnikjoo *et al.*, 2009a). Therefore if anoctamin5 is a CaCC, mutations in ANO5 leading to a non-functioning protein could lead to disturbed calcium signalling and downstream alterations to these other cellular processes.

Membrane repair is also often hypothesised as one of the potential cellular roles for both anoctamin 5 and dysferlin. Faulty cell repair has been observed in non-dysferlin deficient fibroblasts from MMD3 patients despite the presence of lysosomes and enlargeosomes, compartments thought to aid in repair, at the wound site (Jaiswal *et al.*, 2007). Coupled with the observations of similarities in phenotype between LGMD2L/MMD3 and LGMD2B/MMD1, the hypothesis suggested was that anoctamin 5 may act upstream of dysferlin in the cell repair pathway. The role of anoctamin 5 in this pathway has yet to be fully characterised and so far, no other anoctamin has been recorded as being involved in a similar pathway.

An alternative hypothesis formulated from the functions of the other non-CaCC anoctamins, is that anoctamin 5 acts as a phospholipid scramblase, specifically in the exposure of PS on the outer plasma membrane. As an apoptotic marker normally located on the internal leaflet of the plasma membrane, exposure of PS on the outer leaflet marks the cell for destruction by phagocytes (Verhoven *et al.*, 1995). Removal of damaged or dead cells is an essential part of the inflammatory process after tissue

damage and maintains healthy tissue function (Hochreiter-Hufford and Ravichandran, 2013).

If ANO5 has a similar function to ANO6 and is either interacting with or is itself a phospholipid scramblase, mutations would lead to a loss of this function. Effective phospholipid scrambling would therefore not take place, PS would not be exposed at the cell surface and apoptotic signalling would not occur. Loss of apoptotic signalling may then delay or inhibit recruitment of phagocytes and the removal of damaged cells.

PS is also required for fusion of cell membranes and is exposed at the cell-to-cell contact points during differentiation of C2C12 (van den Eijnde *et al.*, 2001). An alternative hypothesis is therefore that impaired PS exposure in ANO5 deficient cells leads to impaired myoblast differentiation or fusion of satellite cells to areas of muscle damage. Ultimately, impaired PS exposure may lead to impaired muscle regeneration and potential onset of the anoctaminopathy phenotype.

1.10 PhD Aims

This PhD aims to discover the subcellular location and function of ANO5. A better understanding of these aspects of anoctamin 5 would be invaluable in understanding how anoctamin 5 mutations cause three different musculoskeletal diseases. This information could then potentially lead to a better understanding of the other muscular dystrophies with similarly dichotic presentations, e.g. mutations in DYSF leading to MMD1 and LGMD2B. Additionally, identifying the subcellular location and function of anoctamin 5 will improve the current understanding of anoctamin biology.

Identification of anoctamin 5 localisation will be accomplished through transfection of various tagged ANO5 constructs into several cell lines. Immunofluorescence and co-localisation with cell compartment markers will then allow for identification of localisation in these transfected cell lines. These constructs will then be used to investigate *in vivo* localisation of overexpressed ANO5.

Identifying the function of anoctamin 5 will be accomplished in two ways, both using ANO5 knock down C2C12 cell lines (a mouse myoblast line) developed during this project. The first route of investigation will be unbiased characterisation of the knock down cells, achieved using 2-dimenstional gel investigation. Proteins with altered expression levels in ANO5 knock down C2C12 compared to Control knock down and wild type C2C12 will be identified by spot differences in 2-dimensional gels and MALDI-MS/MS analysis. Inferences about these proteins relationship to ANO5 will then be made.

The second route of investigation will be a biased, specific examination of phospholipid scramblase activity in the knock down C2C12, investigated using functional assays for scramblase activity. FITC conjugated annexin V, which preferentially binds to PS, will be used to visualise the exposure of PS during differentiation and induced apoptosis. Quantitative differences between ANO5 knock down and Control knock down C2C12 will then be made. Finally, this assay will then be used to investigate the scramblase activity of ANO5 patient primary myoblasts.

Chapter 2 Materials and Methods

2.1 Tissue Culture

Cell lines were cultured in a Hera Cell 240 incubator set to 37°C in 5% CO_2 and all work was carried out in a Hera Safe Cabinet. HeLa, HEK, MIN6, NIH 3T3 and wild type C2C12 cell lines were cultured in growth media while ANO5 knock down and Control knock down C2C12 were cultured in selection media. Primary patient cells were cultured in Skeletal Muscle Cell Growth Media and were kindly donated by the Muscle Tissue Culture Collection in Munich (LGMD2L and LGMD2B patient cells) and from the John Walton Muscular Dystrophy Research Centre Biobank (control patient cells).

Cultures were maintained by cycles of 0.05% trypsin dissociation from the culture vessel, centrifugation in an Eppendorf 5804 R centrifuge to remove the trypsin and reseeded at lower densities onto clean plasticware. Details of the specific plasticware used are indicated in the corresponding techniques below. Stocks of each cell line were made using the same trypsin dissociation steps described above but with the cell pellet resuspended in either commercially sourced Recovery Cell Culture Freezing Media or freezing media made in house. 1ml aliquots of resuspended cells were placed in cryogenic vials and were frozen overnight in a Mr Frosty Cryo 1°C Freezing Container in a -80°C freezer. Aliquots were then moved to plastic box racks in the same -80°C freezer or to liquid nitrogen storage for long term storage.

2.1.1 C2C12 Differentiation

C2C12 myoblasts were differentiated into myotubes by replacing growth media with differentiation media. Upon reaching ~50-60% confluence, cells were washed once with 2ml differentiation media and then treated with 4ml differentiation media. This was the D0 time point. Differentiation media was then replaced and refreshed one day (D1 timepoint), three days (D3) and five days (D5) following this. If D5 was the experimental end time point then cells were fixed in 4% PFA in PBS rather than having differentiation media refreshed.

2.2 ANO5 knock down C2C12 production

2.2.1 ANO5 and Control shRNA

Control and ANO5 specific Short Hairpin RNAs (shRNA) were purchased from Santa Cruz Biotechnology. The ANO5 shRNA consisted of a pool of three different shRNA plasmids, each with a different sense and antisense sequence. The Control shRNA consisted of a scrambled sequence which would therefore not target any gene for knock down, but still produce antibiotic resistant cells. Both shRNA's conferred puromycin resistance to successfully transfected cells.

2.2.2 shRNA Transfection

C2C12 cells were seeded into twelve 100mm tissue culture petri dishes and cultured in growth media until 50-70% confluent. Individual solutions for shRNA constructs, GFP construct and plasmid transfection reagent were made (Table 2.1). 3000µl of shRNA Plasmid Transfection Reagent solution was added to each of the other solutions. Mixed solutions were gently mixed by pipetting and incubated for 45 minutes at room temperature.

	Control shRNA	**ANO5 shRNA**	**GFP plasmid**	**shRNA PTR**
Reagent Volume	60µl	60µl	12µl	432µl
DMEM	2940µl	2940µl	1188µl	6768µl

Table 2.1 Solution components for shRNA transfections. Total volumes of each component are given. Plasmid and shRNA solutions were prepared at a concentration 6µg per 100mm dish, diluted 0.5µg/µl (Control and ANO5 shRNA) and 1µg/µl (GFP). shRNA Plasmid Transfection Reagent (shRNA PTR) was prepared at a concentration of 36µl per 100mm dish.

Each culture dish was washed twice with 4000µl of DMEM before 8800µl DMEM was added to each dish. 1200µl of combined solutions were added drop wise to individual 100mm culture dishes (Control to five dishes, ANO5 to five dishes, GFP to two dishes) and were mixed by gentle pipetting. Dishes were incubated overnight in standard tissue culture conditions before 5000µl of DMEM plus 20% FBS was added to each dish. Cells were then incubated for an additional day under standard tissue culture conditions before the medium was aspirated from each dish and replaced with 10ml fresh selection media. Dishes were checked daily for clone formation and the replacement of selection media.

2.2.3 Clone selection, proliferation and differentiation

Once stable clones were of a sufficient size, cloning cylinders and trypsin cell dissociation media were used to pick clones and transfer them to an individual well of a 24 well plate. Cells continued to be cultured in selection media, using PBS washes, trypsin dissociation, centrifugation and reseeding cycles to transfer cells to larger tissue culture plates until a clone occupied all wells of a 6 well plates. At this stage all wells were washed with PBS, trypsinised, divided into two separate 15ml falcon tubes and centrifuged. The cell pellet from one falcon was resuspended in 2ml of Cell Recovery Freezing Medium and aliquoted into two cryotubes for storage at -80 and later use. The other cell pellet was seeded into another 6 well plate for differentiation.

Upon reaching ~70-80% confluency all wells were imaged using an Eclipse TS100 using NIS Elements (D 3.2) image acquisition software. Three wells were then washed with PBS, trypsinised, centrifuged at 4000rpm for 5 minutes and stored at -80 for later extraction of Day 0 RNA. The remaining 3 wells were differentiated using the protocol given in section 2.1.1. Images were taken at D0, D3, D5 and D7 time points to track differentiation progression. At the D7 time point cells were stored at -80 for RNA extraction.

2.2.4 RNA Extraction

D0 and D7 time point cell pellets were resuspended in 1ml of Trizol and transferred to an RNase free eppendorf tube. To each sample, 200µl of RNase free chloroform was added and inverted to produce an emulsion. Eppendorf's were spun at 14000rpm for 10 minutes in an Eppendorf 5810 R centrifuge and the clear fraction of the resulting solution pipetted into new eppendorf tubes. 2µl of Pellet Paint and 0.5ml of isopropanol were added to the solution and the eppendorf inverted before being spun again at 14000rpm for 10 minutes. The isopropanol was removed and 200µl of 75% ethanol in nuclease free water was added without disturbing the pellet, followed by brief spinning. The ethanol was removed with residual ethanol removed by brief centrifugation and careful pipetting and gentle warming in a heat block. The pellet was then resuspended in 30µl nuclease free water before quantification using a Nanodrop 8000 UV-Vis Spectrophotometer.

2.2.5 cDNA Preparation

RNA was then converted to cDNA using Superscript III RT. 1µl of random primers, 6µl of sample RNA (100ng/µl) and 1µl of 10mM dNTP mix (10mM each dATP, dGTP, dCTP and dTTP at neutral pH) were added to one well of a 96 well PCR plate, covered by 8 well domed strip caps. The plate was then heated to 65˚C for 5 minutes in a Labcycler PCR machine and incubated on ice for 1 minute immediately afterwards. 4µl of 5X First-Strand Buffer, 1µl 0.1M DTT, 1µl RNaseOUT Recombinant RNase Inhibitor (40units/µl) and 1µl Superscript III RT (200units/µl) were then added to each well. Each mixture was mixed by gentle pipetting and the plate placed back in PCR machine. The plate was incubated at 50˚C for 1 hour, then 70˚C for 15 minutes and stored at +4˚C (short term) or -20˚C (long term).

2.2.6 Reverse transcription PCR

The resulting cDNA was then used in a standard PCR reaction to confirm the presence or absence of ANO5 in C2C12. Two 96 well plates were run to test ANO5 knock down cDNA with ANO5 and GAPDH primers (Table 2.2). Two master mixes were also prepared, each with a different primer pair. Both master mixes contained 70µl 10nM dNTPS, 175µl 10xPCR Buffer, 140µl PCR Enhancer, 70µl Moltaq, 70µl of each of the corresponding forward and reverse primers and dH_2O up to a final volume of seventy 25µl reactions. For the ANO5 primer plate 3µl of each ANO5 knock down cDNA sample was put into 66 wells, while only 1µl of ANO5 knock down cDNA were put into the corresponding 66 wells of the GAPDH primer plate. Both plates were then run simultaneously on Labcycler PCR machines (SensoQuest) using the same PCR programme (Table 2.3). 5µl of each PCR product was mixed with 2µl of loading dye and loaded, with a 1kbp reference ladder, on a 1% (w/V) agarose gel in TAE buffer prepared with 5µl of SafeView stain. Samples were separated by molecular weight with application of an electrical current at a constant 100v for 1 hour.

Gene Target	Forward Primer Sequence	Reverse Primer Sequence
ANO5	CAAGAACTGGGCTCGATTTT	AGGTCACTGTGGTCCCTGAC
GAPDH	GGGTGTGAACCACGAGAAAT	GCCATGTAGGCCATGAGGT

Table 2.2 Forward and reverse ANO5 and GAPDH primer sequences. Both primers were designed to amplify a 500bp region of the gene targets.

Step	Temp (°C)	Time (s)	Passes	Notes
1	94	120	1	
2	94	10	19	
3	55	30	19	
4	72	150	19	
5	94	10	19	plus 20s on each pass
6	55	30	19	plus 20s on each pass
7	72	120	19	plus 20s on each pass
8	4	-	-	

Table 2.3 PCR programme for amplification of shRNA transfected C2C12 cDNA. Steps 2-4 and 5-7 were repeated for the number of passes indicated before proceeding to the subsequent step. Samples were held at step 8 at 4°C until removed from the Labcycler.

2.3 Cell Transfection

2.3.1 Lipofectamin 2000

Lipofectamin 2000 was used to transiently transfect MIN6, NIH3T3 and HeLa cell lines. All cell lines were cultured to ~90% confluence on glass 8 well chamber slides under normal tissue culture conditions. For each experiment separate solutions were made for Lipofectamine 2000 and each construct transfection condition. 1µl of Lipofectamine 2000 was used for each transfected well, diluted 1:10 in DMEM. Constructs were prepared at a total concentration of 1µg per well, diluted 1:50 in DMEM. Co-transfections therefore used 0.5µg of each construct. Complexes were left to incubate for 5 minutes at room temperature before 10µl of construct solution and 10µl of Lipofectamine 2000 solution were gently mixed together in new eppendorf tubes. Combined solutions were left to incubate for a further 20-40 minutes at room temp. 20µl of the combined solutions were then added to the corresponding wells of the 8 well chamber slide, mixed by gently pipetting. Slides were incubated overnight under standard tissue culture conditions before fixation in 4% PFA in PBS.

2.3.2 FuGene

FuGene was used to transfect wild type undifferentiated C2C12 cells prior to differentiation into myotubes. C2C12 were cultured to ~50-60% confluence on slideflasks under standard tissue culture conditions. For each slideflask, 4ml of fresh growth media was replaced prior to addition of 100µl of transfection solution consisting of 5µl FuGene transfection reagent, 10µl total plasmid construct (5µl of each plasmid in co-transfections) and 85µl DMEM. Slides were incubated overnight in standard tissue culture conditions, before fixation in 4% PFA in PBS.

2.3.3 Amaxa

Amaxa was used to transfect wild type undifferentiated C2C12 cells prior to differentiation into myotubes. Cells were removed from culture vessels using standard trypsin methods and the cell density calculated using a haemocytometer. 1×10^6 cells were resuspended in 100µl Cell Line Nucleofector Solution V and combined with 2µg of plasmid. The entire suspension was then transferred into a cuvette, with the sample covering the bottom with no air bubbles, and sealed with a cap. Each cuvette was then inserted into the holder of a Nucleofector® I Device and the programme B-32 used to

treat the cells. Immediately after the programme had completed (<60 seconds), the cuvette was taken out of the holder and 500µl of culture medium was added to the cuvette. 500µl of the solution was then transferred to a single well of a 6-well plate pre-treated with 1ml of growth media (final volume 1.5ml media per well). Cells were then incubated overnight in standard tissue culture conditions, before fixation in 4% PFA in PBS.

2.3.4 GeneJuice

GeneJuice was used to transfect wild type undifferentiated C2C12 with tagged ANO5 constructs, prior to apoptosis treatment. 36µl of GeneJuice was mixed with 600µl DMEM minus serum, vortexed briefly and left to stand for five mins. 350µl of this solution was mixed with 14µl ANO5-Myc, 250µl was mixed with 5µl GFP and incubated at room temperature for 15 mins. 50µl of the appropriate mixture was then added to the corresponding wells and incubated overnight under normal tissue culture conditions, before fixation in 4% PFA in PBS.

2.4 Electroporation and Cryosectioning of Mouse Muscle

All animal work was conducted following Home Office guidelines under Professor Volker Straub's project licence 60/4137. As such I merely observed the actually electroporation conducted by Dr Mojgan Reza, but assisted with weighing the mice and conducted the dissections of the tibialis anterior (TA) muscle myself. C57BL/10 (BL10) and C57BL/10ScSn-Dmd^{mdx} (*mdx*) mice stocks were maintained by Elizabeth Greally (personal licence number 60/10222).

For each electroporation, age and gender matched mice were weighed and administered with isoflurane. The corresponding volume of pain relief was then administered subcutaneously (carprofen at 50mg/kg). After shaving the animals legs, 25µl of hyaluronidase (0.4U/µl), an enzyme which helps to increase tissue permeability, was then administered directly to the TA muscle of each leg. The final injection of 50µl of construct (~1µg/µl) was then administered to the central portion of the TA muscle. In the fourth round of electroporation GFP and ANO5 constructs were mixed with the mini-dysferlin construct before injection and a total volume of 50µl was administered. Immediately following injection each leg was electroporated with 8x20ms pulses of 200V/cm at intervals of 250ms. After suitable recovery time mice were sacrificed by cervical dislocation and their TA muscles dissected and mounted in OCT on cork disks and snap frozen in isopentane for storage at -80.

A Microm HM 560 cryostat was used to cut 8 nm thick serial sections from embedded TA muscle, which were then serially mounted on sets of 10 permafrost slides (6-7 sections per slide). Sections were stored wrapped in cling film at -80°C until the day of staining.

2.5 Immunocytochemistry, Immunohistochemistry and Haematoxylin and Eosin Staining

2.5.1 Immunofluorescence (IF) staining

HeLa, MIN6 and NIH 3T3 cell lines were cultured on glass eight well chamber slides. Undifferentiated and differentiated C2C12 were cultured on permanox 4 well chamber slides and slide flasks. Relative reagent volumes for each culture vessel are given in Table 2.4. All cell lines were fixed in 4% paraformaldehyde in PBS (4% PFA/PBS) for 10 minutes at room temperature in the dark. Slides were then washed once with 1xPBS before addition of blocking solution to each well of multi-well chamber slides or the entire surface of chamber slides. Slides were incubated for 1 hour at room temperature in the dark. Blocking solution was replaced in the corresponding wells/slideflask with primary antibody diluted in blocking solution and incubated for another hour in the dark. Primary antibody negative conditions were treated with the same volume of 1xPBS.Slides were washed three times in 1xPBS for 20 minutes in the dark, before replacement with secondary antibody diluted in blocking solution for an hour in the dark. Slides were washed again three times in 1xPBS for 20 minutes in the dark before chamber gaskets were removed.

For eight well chamber slides this was achieved by applying 100µl of ice cold methanol to each well, incubating for 7 minutes at room temperature and levering the chamber gasket from the slide. For 4 well chamber slides and slideflasks, gasket chambers were levered from the slide. Slides were briefly washed in PBS, air dried in the dark, mounted using a few drops of Vectashield plus DAPI and covered with a cover slip. Slides were stored at +4°C in the dark until imaging.

Solution	**8 wells**	**4 wells**	**Slideflask**
4% PFA/PBS	100µl	300µl	500µl
Blocking solution	100µl	300µl	500µl
Antibodies	100µl	300µl	500µl
Washes	500µl	500µl	1000µl

Table 2.4 Adjusted immunofluorescence staining reagent volumes for each culture vessel used. Volumes given are per well of the culture vessel except for chamber slides where volumes refer to the entire surface area of the slide.

2.5.2 Haematoxylin & Eosin staining

Selected slides were defrosted and air dried on the bench for 30 minutes and then submerged in Haematoxylin stain for seven minutes, before being washed in water for two minutes. Slides were then dipped in 1% hydrochloric acid in 70% ethanol, washed in water for 30 seconds submerged in eosin for 30 seconds and then washed in water again for 30 seconds. All wash steps were under a constantly flowing tap. The slides were then immediately submerged in increasing concentrations of ethanol solution; 5 seconds in 70% ethanol, 5 seconds in 90% ethanol and then 1 minutes in 100% ethanol. Slides were then immediately submerged in histoclear (National Diagnostics) for 3 minutes and then in another container of fresh histoclear for an additional 3 minutes. Finally, slides were then mounted with coverslips using hard setting DPX. Slides were kept in histoclear solution until mounting to ensure that the stained muscle sections did not dry out before mounting.

2.5.3 Immunohistochemistry staining

Slides were removed from -80°C freezer storage and thawed for 30 minutes at room temperature wrapped in cling film. Slides were unwrapped and laid out on a square plastic tray (humidified with damp towels) for a further 30 minutes. During this warm up period, an ImmEdge Pen was used to encircle each muscle section with a waterproof wax boundary. After the warm up period and wax boundaries had dried, the slides were placed in a Hellendahl jar and immersed in 0.1% Triton X-100 in PBS for 15 minutes. Slides were then washed in PBS for 5 minutes before being removed from the jars, excess buffer blotted from the slides and arranged on the same humidified square plastic tray. Slides to be treated with non-mouse derived primary antibodies were then blocked in 2 drops of Odyssey protein block. However slides to be treated with mouse derived antibodies were blocked in M.O.M mouse Ig Blocking Reagent (2 drops of stock solution in 2.5ml PBS). Slides were then covered and blocked for 30 minutes at room temperature. Protein block was then flicked off and the slides washed in PBS for 15 minutes in Hellendahl jars.

Anti-GFP and Anti-Dystrophin primary antibodies were diluted in Odyssey protein block while Anti-Myc was diluted in M.O.M diluent. Slides treated with M.O.M mouse Ig Blocking Reagent were incubated in M.O.M diluent for 5 minutes at room temperature, while 50µl of appropriate primary antibody was added to each section of

the non-M.O.M treated sections. 50µl of Anti-Myc was then applied to M.O.M treated sections, the tray covered with the tray lid and all sections were left at +4˚C overnight.

The following morning, slides were left to warm for 1 hour on the bench. Slides were the rinsed in 1x PBS solution applied from a plastic squeeze bottle before slides were washed for 30 minutes in 1xPBS in Hellendahl jars. 1xPBS was refreshed after the first 7 minutes. Secondary antibody Donkey anti-Rabbit 594 (Abmart) diluted in Odyssey protein block was prepared for anti-GFP and anti-Dystrophin slides, while secondary antibody Goat anti-Mouse 488 (Abmart) diluted in M.O.M diluent was prepared for anti-Myc slides. 50µl of secondary antibody was then applied to the corresponding muscle sections and incubated at room temperature for 90 minutes, covered by the tray lid. Slides were washed in 1xPBS for 30 minutes, with the 1xPBS again replaced after 7 minutes. Slides were then dried a few at a time (to avoid sections from drying out), before a few drops of vectashield+DAPI were added and the sections covered by a glass coverslip. Slides were then stored at +4˚C until imaging.

2.5.4 Lysosome staining

To optimise LysoTracker staining of lysosomes, ~90% confluent wild type C2C12 on two 8 well chamber slides were stained with 50nM, 60nM and 70nM concentrations of LysoTracker for 1 hour and 30 minutes. 70nM solution was made from 0.7µl lysotracker in 10ml Growth media and subsequently diluted to 60nM (1371.4µl in 228.6µl Growth media) and 50nM solutions (1142.9µl in 457.1µl Growth media). Slides were then fixed, washed in PBS and mounted using Vectorshield + DAPI and coverslips.

Tandem LysoTracker and IF staining was achieved using the above LysoTracker method followed by standard fixation and IF staining protocols (1:100 9E10 primary antibody, 1:3000 goat anti-mouse 488 secondary antibody) described in Section 2.5.1. Cells were transiently transfected using the GeneJuice method (Section 2.3.4) the day before staining.

2.6 Phosphatidylserine exposure detected using FITC conjugated Annexin V staining

2.6.1 Phosphatidylserine exposure during differentiation

Wild type C2C12 cells were cultured on slideflasks and differentiated to day 1 (D1), day 3 (D3) and day 5 (D5) time points, using established tissue culture techniques (Section 2.1). Upon reaching the required time point slide flasks were washed with 1ml ice cold 1xPBS and immediately incubated in 900µl FITC-AV solution in the dark for 15 minutes as per manufacturer instructions. Slides were then washed twice in 1ml of 1x binding buffer (1ml 10x binding buffer + 9ml dH_2O) and fixed in 500µl of 4% PFA/PBS for 10 mins. Slides were stored in PBS at +4° overnight or blocked for 1 hour at room temperature in 1ml blocking solution.

To track differentiation of the cells, immediately following blocking, slides were incubated in 900µl phalloidin 594 (diluted 1:300 in IF blocking solution) at room temperature for 1 hour. Finally, slides were washed in 1ml of 1xPBS three times, for 20 minutes before the chamber was removed, the slide air dried and mounted with Vectashield + DAPI and a coverslip. Slides were stored at +4° before imaging.

2.6.2 Phosphatidylserine exposure during apoptosis

Cells were cultured on permanox 8 well chamber slides until ~90% confluent. Apoptosis was induced in six wells using combinations of 50µM staurosporine (a PK inhibitor) and 3mM EGTA (a calcium chelator) in growth media (Table 2.5). Two wells were left untreated (growth media only) as negative controls. Slides were incubated for four hours at 37° and 5% CO_2. Media was removed following incubation and all wells washed in 400µl of 1xPBS. Each well was then incubated in 100µl of FITC-AV solution for 15 minutes at room temperature in the dark. Wells were then washed twice in 200µl of 1x binding buffer before fixation in 100µl of 4% PFA/PBS per well for 10 minutes and mounting with Vectashield + DAPI and a coverslip.

Solution ID	Solution Components	Expected Observation
A.	50µM staurosporine + 3mM EGTA in 100µl DMEM + 10% FBS	Apoptosis, but with less annexin V positivity compared to solution B
B.	50µM staurosporine in 100µl DMEM + 10% FBS	Apoptosis with high annexin V positivity
C.	3mM EGTA in 100µl DMEM + 10% FBS	No induced apoptosis and therefore very little annexin V positivity

Table 2.5 Composition of experimental and control solutions used to induce apoptosis. Solutions A and C were control solutions as the EGTA would chelate intracellular calcium and reduce the apoptotic effect caused by the staurosporine. Solution B was the experimental solution as the staurosporine would inhibit protein kinase, triggering apoptosis.

2.6.3 Phosphatidylserine exposure potential of knock down C2C12 investigated using FITC-AV staining and anti-activated caspase 3 staining

The initial FITC-AV staining was modified to include an additional anti-active caspase 3 stain. Apoptosis induction remained the same but following this only half of the wells were treated with Annexin V assay solution (Figure 2.1 Layout of FITC-Annexin V + active Caspase 3 assay eight well chamber slides.Figure 2.1). The other wells were kept in 1xPBS until fixation in 4% PFA/PBS. Following fixation, 100µl of blocking solution was added to each well and the slide incubated at room temperature for 1 hour in the dark. After incubation, 100µl of anti-active caspase-3 antibody (Abcam, ab2302), diluted 1:100 in blocking solution was added to all wells and incubated in the dark at +4° overnight.

The following morning, slides were washed three times for 20 minutes in 400µl 1x PBS in the dark. 100µl of anti-Rabbit alexa fluor 594 secondary antibody diluted 1:3000 in blocking solution was applied to each well and left to incubate in the dark for 1 hour at room temperature. All wells were again washed three times for 20 minutes in 400µl 1x PBS in the dark. The chamber gasket was removed from the slide, excess PBS gently removed, slides air dried in the dark and mounted with Vecta Shield + DAPI and a glass coverslip. All slides were stored at +4° until imaging, blinding and cell counting.

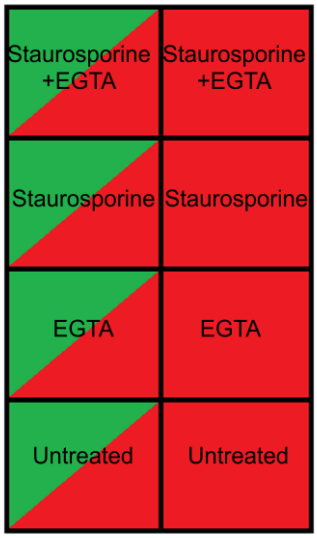

Figure 2.1 Layout of FITC-Annexin V + active Caspase 3 assay eight well chamber slides. Squares filled half red and green indicate wells treated with both FITC-AV and aC3 primary antibody + alexa fluor 594 secondary. Red filled squares indicate wells only stained with aC3 and alexa fluor 594 secondary. Reagents used to induce apoptosis are given in each well.

2.7 Lysate Preparation

2.7.1 Western Blot Lysate Preparation

Lysates were made from GFP-ANO5-MycHis transfected HeLa cells (transfected using the Lipofectamin 2000 protocol in section 2.3.1) and untransfected HEK cells, cultured in 6 well plates. Media was removed, plates placed on ice and each well washed with 1ml of ice cold PBS. PBS was removed, 150µl of ice cold lysis buffer applied to each well, cells scraped from each well using a plastic scraper and the suspension transferred to a 1.5ml Eppendorf tube on ice. Suspensions were constantly agitated for 30 minutes at 4°C then centrifuged at 12000rpm for 20 minutes at 4°C. The supernatant from each tube was then transferred to a fresh Eppendorf on ice, quantified using a Qubit fluorometer as per the manufacturer's instructions and stored at -20°C.

2.7.2 Subcellular fractionation by differential centrifugation and 2D gel lysate preparation

The subcellular fractionation protocol used was taken from Dimauro *et al.* (2012) (Figure 2.2). C2C12 cells were grown to 90% confluence in either four T75's or two T150's. Flasks were washed once with ice cold PBS (each T75 with 3ml; each T150 with 6ml) and then immediately treated with STM buffer (each T75 with 0.5ml; each T150 with 1.5ml). Cells were then manually removed using a plastic cell scrapper and collected into one 15ml falcon tube per cell line. Cells were pelleted by centrifugation in an Eppendorf 5804 R centrifuge for the first step and then in an Eppendorf 5810 R centrifuge for all subsequent steps. Where stated, cell pellets were resuspended in 500µl of STM buffer, 100µl of NET buffer and 300µl of solubilisation solution. Where stated, cell suspensions were mixed with 2.5ml of 100% acetone (five volumes of cell suspension) and 800µl of solubilising solution (eight volumes of cell suspension). P5 was further lysed by being passed sequentially through a 19G and 21G Microlance 3 needle on Micro-Fine 0.5ml syringes. All steps were carried out over ice.

For use in 2D gels, wild type and knockdown C2C12 subcellular fractionations were either mixed with 800µl or resuspended in 300µl of solubilisation solution.

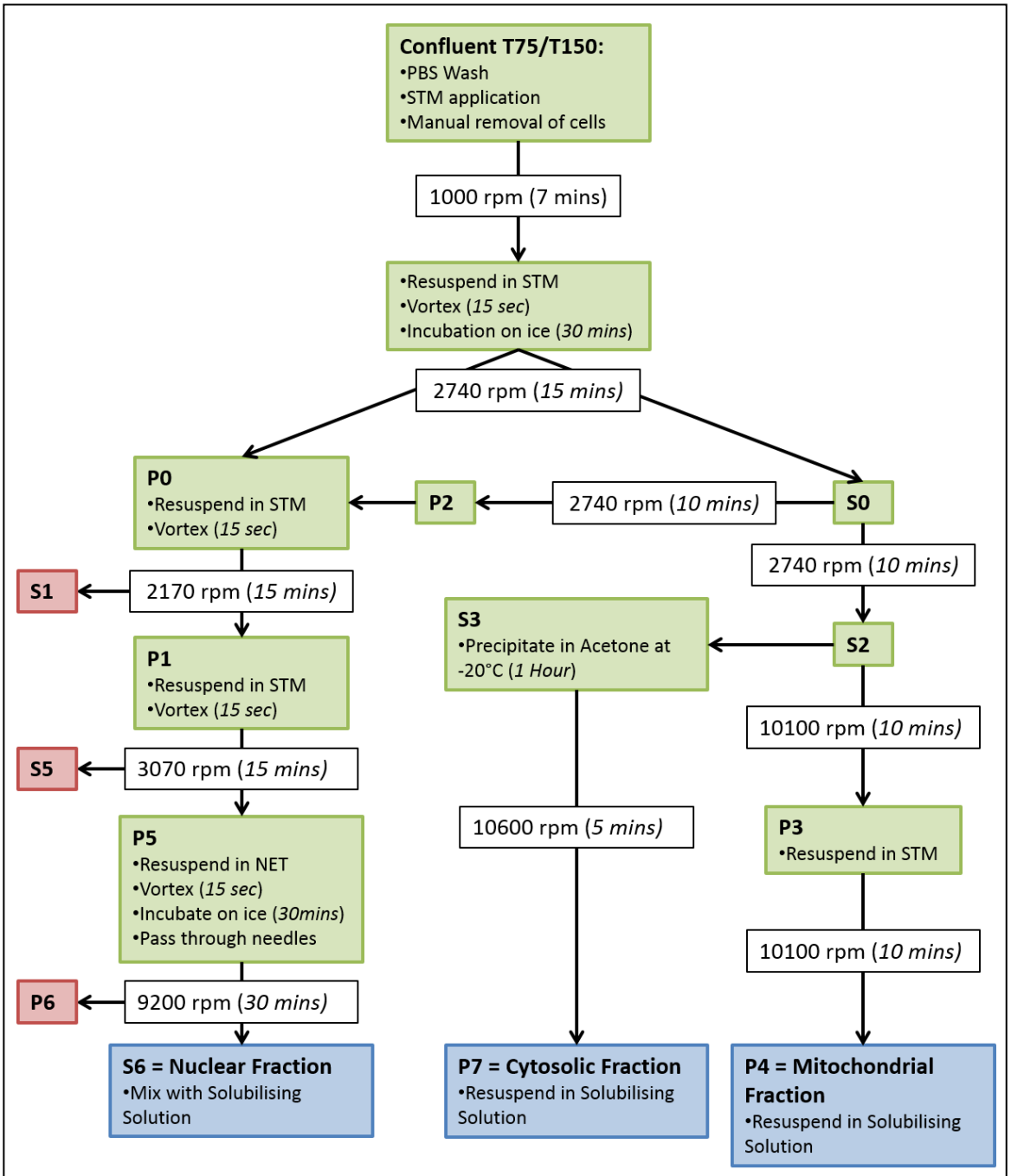

Figure 2.2 Subcellular fractionation work flow adapted from Dimauro et al (2014). "S" denotes supernatant fraction, "P" denotes pellet fraction. Green boxes indicate treatment (if any) of pellets or supernatants that were further fractionated. Blue boxes represent final experimental pellet and supernatants. Red boxes indicate discarded pellets or supernatants. White boxes indicate centrifuge speeds and times for each step.

2.8 Protein Quantification

2.8.1 Quantification by Qubit Protein Assay

The protein concentration of all transfected HeLa and untransfected HEK lysates were measured using the Qubit Protein Assay on a Qubit 2.0 fluorometer. The Qubit fluorometer was calibrated for each protein quantification run, so an additional three 0.5mL PCR tubes were prepared each time for the required standards (identified as 1, 2 and 3). Tubes were labelled and enough Qubit working solution prepared for each sample and standard to be run (1µl Qubit Protein Reagent in 200µl Qubit Protein Buffer for each sample). 190µl and 199µl of Qubit working solution was added to 10µl of standards and 1µl of samples respectively. Tubes were vortexed for 2 to 3 seconds before being incubated at room temperature for 15 minutes in the dark. The three standards were then read on the Qubit in sequential order to calibrate the machine before samples were run and the protein concentration recorded for each.

2.8.2 Quantification by MiniBrandfrod Assay

All fractionated lysates were treated the same no matter which buffer was used for preparation. A standard curve was first prepared using six samples of Bovine Serum Alubumin (BSA, 1mg/ml) in increasing concentrations plus Protein Assay Dye Reagent Concentrate and dH_2O (Table 2.6). Initial volumes of 1µl were used for each lysate sample. All samples were mixed together in disposable semi-micro polystyrene cuvettes (340-900nm range), run on a BioPhotometer and the A595 fluorescence values recorded. If lysate sample fluorescence was lower than the value recorded for the 1µl standard curve sample, the lysate sample was re-run with 10µl of lysate to ensure the fluorescence value fell within the curve.

The A595 fluorescence values were inputted into Microsoft Excel (fluorescence values on the y axis and BSA concentrations on the x axis) to plot the standard curve. y equation values from the resulting curve generated by Excel were inputted into Equation 2.1 to calculate the concentration (mg/ml) of lysates. Concentration values were divided by ten for lysates which used 10µl of sample rather than 1µl.

BSA	Protein Assay Dye	dH_2O
1	799	200
3	797	200
5	795	200
10	790	200
15	785	200
20	780	200

Table 2.6 Sample components for creation of BSA standard curve. All values are given in µl.

$$Concentration = (absorbance - yb)/ya$$

Equation 2.1. Calculation of lysate concentrations. 'Absorbance' is the A595 value obtained from the BioPhotometer readout. 'ya' is the first value given in the y equation and 'yb' is the second value, i.e. y= ya + yb

2.9 2D gel electrophoresis

Mitochondrial, nuclear and cytoplasmic subcellular fractionations were run out using 2 dimensional (2D) electrophoresis using the ZOOM runner IPG system. For each 3-10NL ZOOM IPG strip to be run (to a maximum of eight per cassette), 140µl of subcellular fraction lysate was loaded into the individual sample loading well of a ZOOM IPGRunner Cassette. Each strip was loaded into the cassette with the positive end orientated at the bottom of the cassette. Strips were sealed into the cassette using sealing tape and rehydrated for an hour at room temperature. The Sealing Tape and Sample Loading Devices were removed from the cassette, and an electrode wick attached to the now exposed adhesive at each end of the cassette. 600µl of deionised water was applied to each wick. The cassette was sandwiched against one side of a ZOOM IPGRunner Core with the electrode wicks touching the electrodes of the core. A second cassette or a buffer dam was placed on the other side of the runner core and the assembled sandwich placed into a Mini-Cell Chamber, secured in place with a Gel Tension Wedge. The outer chamber was filled with 600ml of deionised water, with extra care taken to ensure none got into the inner chamber. The lid of the chamber was secured with the correct electrodes connected to the corresponding power pack ports. Isoelectric focusing (IEF) was performed on the IPG strips using a three step set programme on a Bio-Rad PowerPac HC; 175 volts for 1 hour, slow ramping up to 2000 volts for 45 minutes and held at 2000 volts for a further 45 minutes.

Following IEF, the rig was carefully disassembled, taking extra care not to get water on the cassette surface. IPG strips were then either wrapped in cling film and stored at -80°C for future running of the second dimension or immediately run through the equilibration step. For equilibration, each IPG strip was submerged in 5mL of sample reducing buffer for 15 minutes and 5mL of 125mM Alkylating solution for an additional 15 minutes. Frozen IPG strips were defrosted for ~15 minutes before the equilibration step and resumption of the protocol.

SDS page was performed on equilibrated IPG strips using 4-12% Bis-Tris ZOOM protein gels. The IPG strip was inserted into the well of the gel with the negative end of the strip closest to the ladder lane. A scalpel was used to push the IPG strip so it touched the gel and removed any trapped air bubbles which would distort the SDS page run. The gel was inserted into the XCell SureLock® Mini-Cell with either another gel or a buffer dam on the opposite side of the core. Approximately 350µl of 0.5% agarose, dissolved

in MES running buffer, was used to seal in the IPG strip. The inner and outer chambers were filled with MES running buffer and 0.5ml of NuPAGE® antioxidant was added to the inner chamber. 10µl of Chameleon Duo Pre-stained Protein Ladder was loaded into the ladder well and the lid attached to the Mini-Cell. Gels were then run for 45 minutes at 200v on a Bio-Rad PowerPac HC.

2.9.1 Coomassie Staining

Proteins present in 2D gels were visualised by Coomassie staining using SimplyBlue SafeStain. Gels were removed from the Mini-Cell chambers, carefully removed from their plastic cassette containers and transferred to large weight boats. Gels were washed with 100mL dH_2O three times for 5 minutes with continuous shaking. Gels were stained with approximately 15ml SimplyBlue SafeStain for 1 hour at room temperature with gentle shaking. SimpleBlue SafeStain was discarded and gels were washed in 100ml dH_2O over night before being imaged on an Odyssey CLx.

2.10 Western Blotting

2.10.1 Stacking and Resolving gel preparation

Hand cast gels (15%) were made to western blot for S100-A4 protein. 0.75mm glass moulds were assembled on an Mini-PROTEAN Tetra Cell Casting Module. 5ml of resolving gel solution was assembled and poured into the glass moulds (Ammonium persulphate and TEMED were added immediately before pouring as these cause the solution to solidify). Solutions were topped with 100% isopropanol to level the resolving gel. Isopropanol was poured off after the resolving gel had set, the gel was washed with dH_2O and briefly dried. 3ml of the stacking gel solution was then assembled (Ammonium persulphate and TEMED again added immediately before pouring) and poured on top of the resolving gel. A 10 well comb was then inserted into the mould. Gel was then left to dry before either immediately used for SDS page or wrapped in cling film in an excess of dH_2O and stored at 4°C for later use. Commercially sourced NuPage Bis-Tris gels were used for all other proteins.

2.10.2 SDS PAGE

Western blots were run fresh for each experiment. 25µg of protein were prepared in a final volume of 20µl of running buffer in an eppendorf tube. 7.5µl NuPage LDS sample buffer x4 and 3µl NuPage reducing agent 10 x were added to prepared lysates and denatured at 90-100 °C for 5 mins. Commercially sourced gels were assembled gel with the front of the gel facing the inner chamber of a Mini-Cell chamber. Hand poured gels were assembled into Mini-PROTEAN Tetra Electrode Assembly. If only running one gel a buffer dam was placed on the opposite side before the entire sandwich is clamped in place inside the chamber. The inner chamber was filled with running buffer and checked for leaks before the outer chamber is filled with the remaining running buffer. The wells were then flushes with a syringe before loading with 20µl (HeLa and HEK lysates) or 30µl (C2C12) of samples and 10µl of SeeBlue Plus2 ladder (ECL detection) or chameleon duo ladder (Li-Cor detection). Gels were then run at 200V for approximately 50 minutes or until the yellow loading buffer tide line reached the bottom of the gel

2.10.3 Protein Transfer

Gels were removed from the Mini-Cell chambers, carefully removed from their plastic cassette containers or glass moulds and placed on top of Immobilon-FL PVDF membrane, cut to size. The membrane had been pre-wet in 100% methanol and rinsed in chilled transfer buffer. Together they were placed between four squares of cut to size blotting paper and two sponges, all soaked in chilled transfer buffer. This "sandwich" was placed in a transfer cassette and placed in a transfer tank, with the membrane orientated closest to the positive electrodes. Two gels were run in the same tank, if required, which was filled with chilled transfer buffer. Proteins were transferred for 90 minutes at 350mA using a Bio-Rad PowerPac HC. Protein transfer to the membrane was confirmed using Ponceau staining (Sigma) of the membrane for 5 minutes.

2.10.4 Antibody probing and washing

Two different protocols were used depending on the method of eventual visualisation to be used.

For ECL detection, following ponceau staining, the membrane was destained in dH_2O, blocked for 1 hour at room temperature in 5% milk in TBST on a shaker, cut into strips so that it could be probed by different primary antibodies and then incubated overnight at +4° in primary antibody prepared in 5% milk in TBST. The following morning primary antibody was removed, the membrane washed in TBST three times for 10 minutes, incubated for 90minutes in horseradish peroxidase (HRP) conjugated secondary antibody prepared in 5% milk in TBST and washed again three times for 10 minutes in TBST before ECL detection.

For Li-Cor Odyssey detection, following ponceau staining, the membrane was pre-wet for 1 minute in 100% methanol, rinsed with ultrapure water, wet in 1x TBS for 2 minutes and incubated for one hour in TBS Odyssey Blocking Buffer with gentle shaking. During this time primary antibodies were prepared to a final dilution of 5ml in TBS-Ta Blocking solution. Membranes were blotted in primary antibody overnight at 4°C with gentle shaking.

The following morning membranes were washed three times in ~10ml TBS-T Wash buffer with vigorous shaking for 5 minutes. During the washes the IRDye secondary antibodies were diluted in TBS-Tb to a final volume of 5ml. Blots were incubated in

secondary antibody for one hour at room temperature, protected from light with gentle shaking. Following incubation, blots were again washed three times for 5 minutes with vigorous shaking in ~10ml TBS-T Wash buffer, whilst also being protected from light. Membranes were rinsed a final time in 1x TBS to remove residual Tween 20 and stored in 1x TBS in the dark at 4 °C or imaged immediately with the Odyssey CLx.

2.11 Visualisation of Western blot and Coomassie stains

2.11.1 ECL Detection and development

Standard Western blot membranes of HeLa and HEK cell lysates were visualised in a dark room on using SuperSignal West Dura Chemiluminescent Substrate kit. Each section of membrane was incubated for 5 minutes at room temperature in 1ml of ECL substrate, prepared from equal parts solutions A and B provided in the kit. Photographic film was then exposed to the membrane for a determined amount of time in a sealed film cassette, separated by transparent plastic film, before development of the film and final visualisation of the blot.

2.11.2 Odyssey CLx Gel Scanning

All knockdown C2C12 lysate Coomassie stained gels and standard and 2D Western blot membranes were imaged using an Odyssey CLx and Image Studio Ver 4.0 software. Gels were placed on the scanning surface of the Odyssey CLx in an excess of dH_2O or 1x TBS, to ensure the gels and membrane didn't dry out during scanning. Test images were taken to ensure the gel or membrane was fully within the scanning area of the Odyssey and then scanned only in the 700 nm spectrum (Coomassie gels) or simultaneously in the 700 nm and 800nm spectrums (western blots) at 21µm/pixel resolution and medium quality.

2.12 Microscopy and Image Analysis

All immunofluorescent, immunohistochemical and Annexin V assay images were taken on the AxioImager (Zeiss) microscope using AxioVisions40 (V 4.8.2.0) image acquisition software. Heamotoxinalin and Eosin staining images were taken on the Axioplan (Zeiss) microscope using AxioVision (V 4.8.1.0) image acquisition software. Brightfield images of knock down C2C12 clone selection and differentiation were taken on an Eclipse TS100 (Nikon) using NIS Elements (D 3.2) image acquisition software.

In experiments involving detection of fluorescent tags, initial values of laser exposure required to optimally detect each fluorophore at each magnification were maintained across all subsequent wells or slides containing the same experimental condition and their controls.

2.12.1 Annexin V assay imaging and cell counting

For each image, individual image files were created for each fluorescence channel and exported in a .tiff format. Each image folder containing these multiple files was blinded prior to cells counting using the Cell Counter plugin of Image J. Each fluorescence channel file was opened individually (DAPI only, FITC-AV+DAPI, Caspase 3+DAPI, all channels) and the number of positive cells recorded to an excel spreadsheet before un-blinding the images and statistical analysis.

2.13 Flow cytometry analysis using FACSCanto

2.13.1 Cell sample preparation

Three different experimental flow cytometry set ups were used, referred to as 1µM Time Series, 50µM Time Series and 50µM Apoptosis. In each, C2C12 and patient myoblasts were cultured in 6 well plates using standard tissue culture methods, as described in section 2.1.

For 1µM and 50µM Time Series experiments, a master mix of 1µM or 50µM staurosporine in 2000µl growth media was prepared. Apoptosis was induced in ~95% confluent cells by replacing culture media in a single well with 500µl of the master mix and returning to normal tissue culture conditions for one hour. This process was repeated three times producing 4hour, 3hour, 2hour, 1hour and two 0hour time points.

For 50µM Apoptosis, normal culture media was removed from two wells of ~95% confluent cells and replaced with 50µM staurosporine in 500ul growth media in one well and 50µM staurosporine and 3mM EGTA in 500ul growth media in the second well. Plates were incubated for 4 hours under normal tissue culture conditions.

Collection of cell populations was consistent across experimental set ups. Following incubation, media from each well was transferred to individual 15ml falcon tubes and the wells were washed with 500µl of ice cold PBS, which was also added to the same 15ml falcon tubes. Remaining adherent cells were removed by applying 300µl of TrypLE trypsin to each well and incubating for 5 minutes in normal tissue culture conditions. 500ml of ice cold PBS was added to each well to dilute the TrypLE and the total 800µl solution removed from each well and added to the corresponding 15ml falcon. Finally, the wells were washed again with 500µl of ice cold PBS, with washes again added to the corresponding falcon tube. Collected cells were pelleted by centrifuging at 1000rcf for 5 minutes in a Eppendorf 5804 R centrifuge. Cells were washed by resuspension in 500µl of ice cold PBS followed by centrifugation at 1000rcf for 5 minutes, discarding the PBS afterwards.

Cell pellets were resuspended in different Annexin V assay solutions. For 1µM and 50 µM Apoptosis set ups, three different solutions were prepared. Both populations of treated cells and one population of untreated cells were resuspended in 100µl of Solution 1, one population of untreated cells was resuspended in 100µl of Solution 2 and another untreated population in Solution 3 (Table 2.7). For Time Series set up, all

populations of treated cells and one untreated population were resuspended in 100µl of Solution 1. The last population in each set up remained unstained as a negative control and was resuspended in 500µl of 1x Binding Buffer (1ml 10x Binding Buffer + 9ml dH_2O).

Resuspended cells were then transferred to clean FACS tubes (Corning) and left to incubate for 15 minutes at room temperature in the dark. Following incubation, 400µl of 1x Binding Buffer was added to each FACS tube containing stained cell populations and all populations immediately analysed by Flow cytometry.

Solution 1	**Solution 2**	**Solution 3**
3µl FITC Annexin V conjugate	1µl FITC Annexin V conjugate	-
30µl Propidium Iodide	-	10µl Propidium Iodide
30µl 10x Binding Buffer	10µl 10x Binding Buffer	10µl 10x Binding Buffer
237µl dH_2O	89µl dH_2O	80µl dH_2O

Table 2.7 Composition of annexin V staining solutions for flow cytometry. Total volumes required to stain the number of samples for each condition.

2.13.2 Flow Cytometry

Fluorescence data of stained and unstained C2C12 and patient myoblast cell populations was collected using a FACSCantoII (BD) equipped with 2-488/530/30-A and 2-488/585/42-A lasers to capture FITC-Annexin V (FITC-AV) and propidium iodide (PI) fluorescence signal respectively. Samples were interrogated and manually gated using FACSDiva (BD) software. While automated procedures are available and recommended for large datasets (Verschoor *et al.*, 2015), manual gating analysis is still a valid and relatively fast method of analysis when dealing with smaller sample sizes (e.g. fewer than 40 samples). A total of 10,000 events (i.e. cells passing through the path of the lasers) were captured per sample.

2.14 Statistical Analysis

All statistical analyses were carried out in Microsoft Excel. Chi^2 calculations (Equation 2.2) were used to test the difference in the number of positive cells between ANO5 and Control knock down C2C12 and between LGMD2L or LGMD2B and wildtype patient myoblasts in each treatment condition. Chi^2 was used as the data was non-parametric and categorical (i.e. yes or no for positive staining). The null hypothesis tested was "ANO5 knock down does not affect PS exposure in C2C12 cells".

The Chi^2 statistic is calculated using Equation 2.2. For the analysis of knock down C2C12 images, observed values in each treatment condition were the summed counts of the number of positive cells across the five images taken of each well. For analysis of patient myoblast flow cytometry data, the number of events recorded in each quadrant in each treatment condition for each cell line were used as the observed values. The 2x2 table method was used to generate the expected values (Figure 2.3). These values were then used in Equation 2.2 to generate a Chi^2 statistic with 1 degree of freedom.

$$\chi^2 = \frac{\sum(Observed - Expected)^2}{Expected}$$

Equation 2.2 Chi^2 equation used to calculate the association between positive count values.

	Control	**ANO5**	
Number of Positive Cells	*A*	*B*	*A+B = AB*
Number of Negative Cells	*C*	*D*	*C+D = CD*
	A+C = AC	*B+D = BD*	*A+B+C+D*

Observed = B

Expected = A/AC x BD

Figure 2.3 Example of 2x2 table calculations used to generate expected values for the Chi^2 statistic. "Positive" and "Negative Cells" refer to either FITC-AV or aC3 depending on the condition being tested

2.15 Consumables and Equipment

Item	Product Code	Supplier
0.05% Trypsin	25300096	Gibco
0.45µm PES membrane	89220-712	VWR
1.5ml microfuge tube	211-2610	VWR
1000µl pipette filter tips	S1122-1830	Starlab
100mm petri dishes	734-2321	VWR
10ml serological pipettes	86.1254.001	Sarstedt
10µl pipette filter tips	S1121-3810	Starlab
15ml centrifuge tubes	430766	Corning
19G Microlance 3 needle	ND500	BD
1kb DNA ladder	G571A	Promega
2.0ml Skirted Cryovial	E3090-0013	Star Labs
200µl pipette filter tips	S1120-8810	Starlab
20µl pipette filter tips	S1120-1810	Starlab
21G Microlance 3 needle	ND434	BD
24-well plate	734-2325	VWR
25ml serological pipettes	86.1685.001	Sarstedt
2-mercaptoethanol	31350-010	Life Technologies
30% Acrylamide/Bis Solution	161-0159	Bio-Rad
50ml centrifuge tubes	430829	Corning
50ml serological pipettes	86.1689.001	Sarstedt
50ml syringes without needles	SYR6212	SLS
5ml serological pipettes	86.1689.001	Sarstedt
6-well plate	734-2323	VWR
8 well chamber slides	734-0089	VWR
8-channel spectrophotometer	ND-8000	NanoDrop

8-Strip PCR Caps, Domed	I1400-0800	Star Labs
96-well PCR plates	E1403-5200	Starlab
Acetic acid	A6283-1L	Sigma-Aldrich
Acetone	20066.330	VWR
Agarose	NBS-AG500	NBS Biologicals
Agarose gel electrophoresis tanks	1704405	Bio-Rad
Alexa Fluor 488 goat anti-mouse IgG	A11001	Invitrogen
Alexa Fluor 594 goat anti- mouse IgG	A11008	Invitrogen
Alexa Fluor 594 goat anti- rabbit IgG	A11005	Invitrogen
Alexa Fluor 594 phalloidin	A12381	Invitrogen
Ammonium Persulfate (APS) 10 g	161-0700	Bio-Rad
Ampicillin sodium salt	A9518-5G	Sigma-Aldrich
Anti-Active Caspase-3	ab2302	Abcam
Anti-Annexin A2	ab41803	Abcam
Anti-c-Myc Antibody (9E10)	sc-40	Santa Cruz Biotech
Anti-c-Myc Antibody (ab39688)	ab39688	Abcam
Anti-dystrophin antibody	ab15277	Abcam
Anti-GFP	ab290	Abcam
Anti-Hsp27	ab2790	Abcam
Anti-S100A4	ab93283	Abcam
Autoclave	RS232	Astell
Autoclave tape	817-0118	VWR
Bio-Lyte 3/10 Ampholyte 40% 10ml	163-1112	Bio-Rad
BioPhotometer	-	Eppendorf
Blue/orange 6x loading dye	G190A	Promega
Bovine Serum Albumin (BSA)	A3294-50G	Sigma
Camera BW	AxioCam HRc	Zeiss

Camera RGB	DS-Fi2	Nikon
Carprofen	33975-100MG-R	Sigma Aldrich
cDNA reverse transcription kit	4368814	App'd Biosystems
Cell Scraper, 320mm Long, pivoting blade	CC7600-0320	Starlab
Chameleon Duo Pre-stained Protein Ladder	928-60000	Li-Cor
Chloroform	C2432-1L	Sigma
Class 1 airflow cabinet	Hera guard	Heraeus
Class 2 airflow cabinet	Hera safe	Heraeus
Cloning cylinders, glass	C1059-1EA	Sigma-Aldrich
Cover glasses, 22x50mm, 0.13mm thickness	631-0137	VWR
Cryostat	Microm HM 560	Thermo Fisher Scientific (TFS)
DEPC-treated water	AM9906	Ambion
Dimethyl sulfoxide (DMSO)	D-8779	Sigma-Aldrich
Dulbecco's modified Eagle medium	41966052	Gibco
EDTA	E5134-500G	Sigma-Aldrich
EGTA	E8145	Sigma-Aldrich
EndoFree Plasmid Maxi Kit (10)	12362	QIAGEN
Ethanol	20821.33	VWR
FACS Tubes	352054	Corning
Fine scales	BD BH 110	Denver
Flask tissue culture 150cm²	430825	Corning
Flask tissue culture 75cm²	734-2313	VWR
Flow Cytometer	FACSCanto II	BD
Foetal bovine serum (FBS)	EU-000-F	SLI
Freezer -80°	U725	NB Scientific
Fridge/freezer -20°	KGV36VW32G	Bosch

FuGENE HD Transfection Reagent	E2311	Promega
GAPDH (mouse)	ab8245	Abcam
GAPDH (rabbit)	D16H11	Cell Signal Tech
GelDoc-It Imaging System	GelDoc-It310	UVP
GeneJuice	70967-6	Merck Millipore
Gentamicin	15750-037	Gibco
Glucose	G8270-100G	Sigma-Aldrich
Glycerol	G5516-100ML	Sigma-Aldrich
Glycine	G8898-1KG	Sigma-Aldrich
Haemocytometer	680030	Marienfeld
Heater magnetic stir block	101N0052	Fisher
HEPES	H3375-100G	Sigma-Aldrich
Horse serum	26050088	Gibco
Hyaluronidase	H3506	Sigma-Aldrich
Hybond PVDF membrane	RPN303F	GE Healthcare
HCl, Hydrochloric acid	84436-1L	Sigma-Aldrich
IGEPAL CA-630	I7771-50ML	Sigma-Aldrich
ImmEdge Pen	H-4000	Vector Labs
Immobilon-FL PVDF	IPFL00010	Merck Millipore
Incubator	Hera cell 240	Heraeus
Insulin syringe with needle	613-4897	VWR
Iodoacetamide	I6125-5G	Sigma Aldrich
IRDye 680RD Goat anti-Rabbit	926-68071	Li-Cor
IRDye 800CW Donkey anti-Mouse	926-32212	Li-Cor
Isopentane	M32631-2.5L	Sigma-Aldrich
Isopropanol	20842.33	VWR
Lab Armor beads	A1254301	Life Technologies

LDS sample buffer	NP0007	Invitrogen
Lens tissue	2105-841	Whatman
L-Glutamine	35050-038	Gibco
Lipofectamine® 2000	11668019	Life Technologies
Lyostracker Red DND-99	L-7528	TFS
MES SDS protein gel running buffer	NP0002	Invitrogen
Methanol	20846.326	VWR
$MgSO_4$, Magnesium sulphate	208094-500G-D	Sigma-Aldrich
Micro-Fine 2.5ml syringes	SYR2LL	Terumo
Microfuge	5415D	Eppendorf
Microscope filter DAPI	FS02	Zeiss
Microscope filter GFP	FS13	Zeiss
Microscope filter Rhodamine	FS15	Zeiss
Microscope inverted fluorescence	AxioVert200M	Zeiss
Microscope inverted light	AE20	Motic
Mini-PROTEAN Tetra Cell Casting Module	1658010	Bio-Rad
Mini-PROTEAN Tetra Electrode Assembly	1658037	Bio-Rad
Mounting medium with DAPI	H-1200	Vectorlabs
Mouse on Mouse (M.O.M.) Basic Kit	BMK-2202	Vector Labs
Mr Frosty Cryo 1°C Freezing Container	5100-0001	TSF
NaCl, Sodium chloride	S9888-5KG	Sigma-Aldrich
NaOH, Sodium hydroxide	S5881-500G	Sigma-Aldrich
Nitrile gloves	112-2755	VWR
Novex Mini-gel PAGE tanks	120801-2839	Invitrogen
Nuclease-free water (NFW)	AM9937	Ambion
Nunc Lab Tek 8 Well Permanox Slides	177445K	SLS Ltd
Nunc Lab-Tek 4 Well Permanox Slides	C6932-1PAK	Sigma-Aldrich

Nunc Lab-Tek Chamber Slides	C7182-1PAK	Sigma-Aldrich
NuPAGE antioxidant	NP0005	TFS
NuPAGE MES SDS Running Buffer (20X)	NP0002	Life Technologies
NuPAGE MOPS SDS Running Buffer (20X)	NP0001	Life Technologies
NuPAGE Novex 4-12% Bis-Tris Protein Gels	NP0321BOX	Life Technologies
Objective CFI Plan Apochromat 20x	VC 20x/0.75	Nikon
Objective CFI Plan Fluor 10x	DL-10x F/0.3	Nikon
Objective Plan Neofluar 10x	10x/0.3	Zeiss
Objective Plan Neofluar 20x	20x/0.5	Zeiss
OCT cryoembedding Matrix	12678646	TFS
Odyssey Blocking Buffer (TBS)	927-50003	Li-Cor
Odyssey Infrared Imaging System	Odyssey CLx	Li-Cor
Paraformaldehyde	P6148-1KG	Sigma-Aldrich
Pasteur pipettes 230mm	612-1702	VWR
PBS tablets	18912-014	Gibco
PCR plate adhesive sealing sheets	AB-0558	TFS
PCR thermocycler	LabCycler	Sensoquest
Pellet Paint Co-Precipitant	69049-3	Merck Millipore
Penicillin/Streptomycin	15070063	Gibco
pH meter	HI 2210	Hanna
Phenol:chloroform:isoamyl alcohol	15593031	Ambion
Phenylmethanesulfonyl fluoride	P7626-1G	Sigma-Aldrich
Phosphate buffered saline solution	20012068	Gibco
Ponceau	P7170-1L	Sigma
PowerPac	HC 1645052	Eppendorf
Protein Assay Dye Reagent Concentrate	500-0002	Bio-Rad
cOmplete protease inhibitor tablet	05892791001	Roche

QIAprep Spin Miniprep Kit	27106	Qiagen
QIAquick Gel Extraction Kit	28706	Qiagen
Qubit 2.0 flourometer	Q32866	TFS
Qubit Protein Assay Kit	Q33212	TFS
Recovery Cell Culture Freezing Medium	12648-010	Life Technologies
Refrigerated centrifuge	5804R	Eppendorf
RNase Zap	AM9780	Ambion
RNaseOUT Recombinant RNase Inhibitor	10777-019	Invitrogen
Rotor	A-4-44	Eppendorf
Rotor	F45-30-11	Eppendorf
Rotor	A-4-62	Eppendorf
SafeView nucleic acid stain	NBS-SV1	NBS Biologicals
Sample reducing agent	NP0009	Invitrogen
Scales	HL-200i	A&D
Scalpels no.22	REF0508	Swann-Morton
SDS	L3771-500G	Sigma-Aldrich
SeeBlue Plus2 protein standards	LC5925	Invitrogen
Semi-micro Polystyrene Cuvettes	634-0676	VWR
shRNA Plasmid Transfection Reagent	sc-108061	Santa Cruz Biotech
SimplyBlue SafeStain	LC6060	Invitrogen
Skeletal Muscle Cell Growth (SMCG) Media	C-23060	Promo Cell
SMCG Media Supplementary Mix	C-39365	Promo Cell
Sodium azide	S2002-5G	Sigma-Aldrich
Sodium dodecyl sulphate (SDS)	L3771-500G	Sigma-Aldrich
Sodium deoxycholate	D6750	Sigma-Aldrich
Staurosporine from Streptomyces sp.	S4400-.5MG	Sigma-Aldrich
Superfrost Plus Slides	631-0108	VWR

Superscript III Reverse Transcriptase	18080-044	Invitrogen
TACS Annexin V-FITC Apoptosis Kit	4830-01-K	R&D Systems
TEMED	161-0800	Bio-Rad
Triton X-100	T8787-50ML	Sigma-Aldrich
Trizma base	T1503-1KG	Sigma-Aldrich
TRIzol	15596026	Ambion
TrypLE Express Enzyme (1X)	12604013	Life Technologies
Tween 20	P9416-100ML	Sigma-Aldrich
Ultrapure water system	D11901	TFS
Urea	U5378-1KG	Sigma-Aldrich
Virkon	A01302780	Dupont
Water bath	JB Aqua 18 Plus	Grant
Western blot transfer tanks	1703930	Bio-Rad
ZOOM IPG Strips - pH 3-10NL	ZM0011	Life Technologies
ZOOM IPGRunner Cassettes	ZM0003	Life Technologies

2.16 Solutions

125mM Alkylating solution

Iodoacetamide	232mg
1X NuPAGE LDS Sample Buffer	10ml

15% Resolving Gel Solution

30% Acrylamide	2.5ml
1.5M Tris, pH 8.8	1.25ml
10% SDS	50µl
10% Ammonium Persulfate	50µl
TEMED	2µl
dH_2O	1.15ml

15% Stacking Gel Solution

30% Acrylamide	300µl
1.5M Tris, pH 6.8	375µl
10% SDS	30µl
10% Ammonium Persulfate	30µl
TEMED	3µl
dH_2O	2.26ml

4% (w/V) paraformaldehyde (PFA) in PBS

dH2O	500ml
PBS tablets	2
NaOH	3 pellets
PFA	40g
pH adjusted with NaOH	7.4
dH2O	to 1000ml

Annexin V solution

	Differentiation	**Apoptosis**
FITC-Annexin V conjugate	9µl	1µl
10x Binding Buffer	90 µl	10µl
dH_2O	801µl	79µl

Apoptosis Solutions

	Solution A	**Solution B**	**Solution C**
Staurosporine	50µM	50µM	-
EGTA	3mM	-	3mM
DMEM + 10% FBS	up to 100µl	Up to 100µl	up to 100µl

Differentiation Media

DMEM	48ml
Horse Serum	1.5ml
Penicillin/Streptomycin	500µl

Freezing media

DMEM	70ml
FBS	20ml
DMSO	10ml

filtered through a 0.45µm PES membrane

Growth Media

DMEM	500ml
FBS	50ml

IF Blocking Solution

Triton X-100	50µl
FBS	5ml
10x PBS	5ml
dH_2O	40ml

Lysis Buffer

Radioimmunoprecipitation (RIPA) assay buffer	150 mM sodium chloride	0.88g
	1% Triton X-100	10µl
	0.5% Sodium deoxycholate	0.5 µl
	0.1% SDS	1µl
	50 mM Tris at pH 8.0	0.61g
	dH_2O	100ml
Protease inhibitor tablet		1 tablet/10ml

MES and MOPS SDS protein running buffer

MES SDS protein running buffer (20x) or MOPS SDS protein running buffer (20x)	35ml
dH2O	700ml

M.O.M diluent

Protein Concentrate stock solution	600µl
1x PBS	7.5ml

NET Buffer

1M HEPES pH 7.9	200µl
1M $MgCl_2$	15µl
1M NaCl	5ml
100mM EDTA	20µl
Glycerol	2ml
Triton X-100	100 µl
200mM PMSF (serine protease inhibitor)	50 µl
dH_2O	up to 10ml

Phosphate buffered saline (PBS)

PBS tablets	2
dH_2O	1000ml

Tris buffered saline (TBS) 10x

Trizma base	60.5g
NaCl	87.6g
dH_2O	Up to 1L
pH adjusted with HCl	7.5

Reconstitution Buffer, for Abmart Antibodies

1% BSA	1g
0.01% Sodium Azide	0.01g
50% Glycerol	50ml
10mM HEPES at pH 7.5	0.23g
dH_2O	50ml

Selection Media

DMEM	500ml
FBS	50ml
10µg/ml Puromycin	500µl

Skeletal Growth Media (SGM)

Skeletal Muscle cell growth media	500ml
FBS	50ml
Skeletal Muscle Cell Growth Media Supplementary Mix	25.9ml
L-Glutamine	5ml
Gentamicin	300µl

STM Buffer

1M Sucrose	12.5ml
1M Tris-HCl, pH 7.4	2.5ml
1M $MgCl_2$	250µl
200mM PMSF (serine protease inhibitor)	250µl
dH_2O	up to 50ml

Solubilisation Solution

1ml Buffer A	9M urea	20ml
	2% (v/v) Nonidet P-40	400µl
	0.8% (w/v) ampholine pH 3-10	400µl
	2% (v/v) 2-mercaptoethanol	400µl
100µl Buffer B	PMSF	15.5mg
	95% ethanol	1ml

Sample Reducing Buffer

NuPAGE® Sample Reducing Agent (10X)	0.5mL
1x NuPAGE® LDS Sample Buffer	4.5mL

Tris acetic acid EDTA (TAE) buffer

Tris	400mM
EDTA	10mM
Acetic acid	11.4% (V/V)
pH (with Trizma base and acetic acid)	7.6

TBS-Ta Blocking Solution

TBS Odyssey blocking buffer	30ml
Tween 20	60µl

TBS-Tb Blocking Solution

TBS Odyssey blocking buffer	20ml
Tween 20	40µl
10% SDS	20µl

TBS-T Washing Buffer

1x TBS	200ml
Tween 20	200µl

Western blotting protein transfer buffer (PTB)

Trizma base	3.03g
Glycine	14.4g
dH2O	to 800ml
Methanol	200ml

Chapter 3 *In Vitro* and *In Vivo* localisation of ANO5

3.1 Introduction

One key indicator of the physiological function of a protein is the subcellular localisation. Early localisation studies of mouse Ano5 (a homolog for human ANO5) in murine embryogenesis found evidence for anoctamin 5 localising to the plasma membrane as well as several subcellular compartments including Golgi apparatus, trans-Golgi network, secretory vesicles, endoplasmic reticulum (ER) and endosomes (Mizuta *et al.*, 2007). Similarly, HEK (Human Embryonic Kidney), HeLa and CHO (Chinese Hamster Ovary) cell lines transfected with Green Fluorescent Protein (GFP) tagged ANO7 have been shown to display characteristic ER-like expression when colocalised with the ER marker, mCherry-17. This has led to the suggestion that all intracellular anoctamins localise to the ER (Duran *et al.*, 2012). Other early data has shown that ANO5 localises to the ER (Tsutsumi *et al.*, 2004), but has not been confirmed in all studies.

Indeed the precise localisation of anoctamin 5, other than to the cytoplasm, has yet to be determined (Duran *et al.*, 2012). Gaining a better understanding of anoctamin 5 localisation would allow inference of the functional pathways in which it is involved and other proteins with which it interacts. These pathways and interacting proteins can then be further investigated, confirming or rejecting hypotheses and adding to the overall picture of anoctamin 5 function.

For example, observing co-expression of anoctamin 5 and dysferlin may suggest that these proteins are both involved in the same pathway. As dysferlin has already been suggested to be heavily involved in membrane fusion and repair pathways in muscle, specific investigation could then be conducted into a similar role for anoctamin 5 (Bansal *et al.*, 2003; Lennon *et al.*, 2003). Investigation may then clarify the involvement of anoctamin 5 in these pathways and go a step towards reconciling the overlapping phenotypes of the anoctaminopathies and dysferlinopathies.

In general, subcellular localisation of proteins is identified using antibody staining of tissue sections (Ohlendieck *et al.*, 1991; Matos *et al.*, 2010), cell cultures (Campbell *et al.*, 1979; Mandinova *et al.*, 1998) or biochemically fractionated material (Lee *et al.*, 2010). As no verified anoctamin 5 antibody is commercially available a validated antibody would be of considerable value to the research field. Therefore as a first step

for this project, validation of a pool of customized antibodies was carried out to identify an antibody suitable for further investigation.

As an alternative approach to antibody staining, anoctamin 5 was tagged with either GFP or a small epitope (cMyc tag) to enable the exogenously expressed fusion protein to be tracked by fluorescence microscopy. In this chapter, tagged anoctamin 5 constructs were used to investigate the localisation of anoctamin 5 in cell cultures and mouse muscle.

3.2 Custom anoctamin 5 antibody validation

Nine custom mouse monoclonal antibodies were obtained from the company AbMart. This company uses a "library" approach termed SEAL (Surface Epitope Antibody Library) which targets multiple epitopes of the protein of interest and utilises multiple antigens, immunisations, fusions and clone selections to create a number of antibodies for the target protein.

Antibodies were received as ascites and resuspended in 0.5ml of reconstitution buffer suggested by Abmart. Gentle heating in a heat block with brief vortexing was also applied to improve the resuspension of antibodies, though the first batch of antibodies remained very viscous and were difficult to work with.

3.2.1 Validation by Western blotting

Validation of both sets of nine Abmart ANO5 antibodies by western blotting was achieved by investigating protein extracts derived from transiently GFP-ANO5-MycHis transfected HeLa and untransfected HEK lysates on precast gels. As ANO5 has been shown to be unexpressed in HeLa cells and endogenously expressed at low levels in HEK cells, untransfected HEK lysates were used as endogenously expressing controls to overexpressing HeLa lysates (Kunzelmann *et al.*, 2009). Following transfer, the membranes were cut vertically along the ladder so that the blot could be probed with multiple concentrations of Abmart antibodies as well a control GAPDH primary antibody. GAPDH was used as a control as a well-established loading control. Goat anti-mouse HRP and goat anti-rabbit HRP secondary antibodies were used against Abmart and GAPDH primary antibodies respectively.

The first batch of nine antibodies, with the exception of Ab9A, had a very high level of background at very high dilutions (Figure 3.1). In each case, the entire blot is mostly black and in some blots is so over exposed that some potential bands appearing as white rather than black (Figure 3.1 Ab1A, 2A, 4A, 5A and 6A). Ab9A however, produced almost no background even at a lower concentration of 1:5000, but still failed to detect a band in either cell lysate. Due to time pressure to validate these antibodies, alternative blocking methods to reduce the background were not attempted. The high level of background strongly indicated that this batch of antibodies could not be optimised for ANO5 detection and so were excluded from further experimentation and a second batch of antibodies was requested from the Abmart.

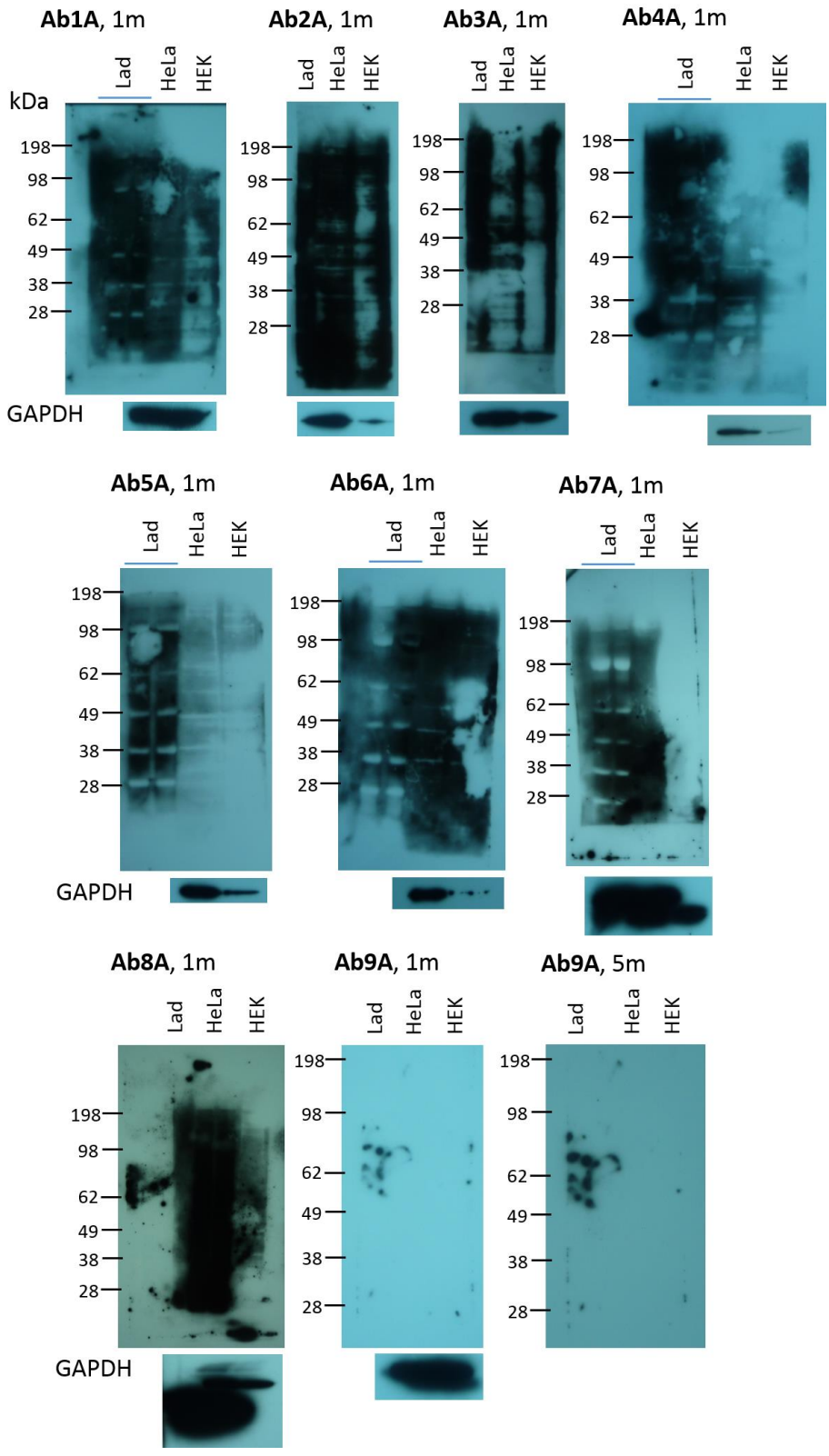

Figure 3.1 Western blots probed with nine custom ANO5 antibodies (Batch A). Ab1A to Ab8A were used at a concentration of 1:10,000. Ab9A was used at a concentration of 1:5000. Exposure times for Ab1A-8A were 1m. Exposure times of 1m and 5m were investigated for Ab9A to ensure that a faint band was not missed at the shorter exposure time. The corresponding GAPDH control blots are given under each antibody. Biological N = 9. Technical N = 1.

To rapidly optimise the second batch of antibodies, several dilutions of Ab1B were run on a blot of only transfected HeLa lysates (Figure 3.2). This blot was then analysed on a GelDoc-It imaging system following ECL treatment. These results show that there is still a high degree of background with this antibody at lower antibody concentrations (1:500). Though at higher dilutions (1:5000 and 1:10,000) there is markedly reduced background compared against the same dilutions of the batch A antibodies. More importantly, there are also two bands present on the blot at ~38 and ~36kDa and that these bands are detectable up to a dilution of 1:5000. From this initial experimentation, dilutions of 1:1000 and 1:2500 were used for Ab2B, 3B, 4B and 5B on both HeLa and HEK lysates (Figure 3.3 A., B., C. and D.). Antibodies were tested sequentially, during which it became apparent that a dilution of 1:2500 was optimal for band detection with minimal background. Therefore HeLa and HEK lystates were probed with Ab6B, 7B, 8B, and 9B at a dilution of 1:2500 only (Figure 3.3 E. and F.). These blots were all visualised using the standard X-ray developer method.

These results show that the same two bands detected by Ab1B at ~38 and ~36kDa are detected by all of the subsequent batch B antibodies but only in the transfected HeLa lysates. Antibodies Ab2B, 4B, 5B, 6B, 7B, 8B and 9B also detected a small additional band at ~62kDa in both the transfected HeLa and untransfected HEK lysates. However the expected molecular weight of ANO5 is 102kDa well above any of these bands. Despite the lack of a band at the predicted molecular weight for ANO5, this batch of antibodies were further investigated using immunofluorescence staining.

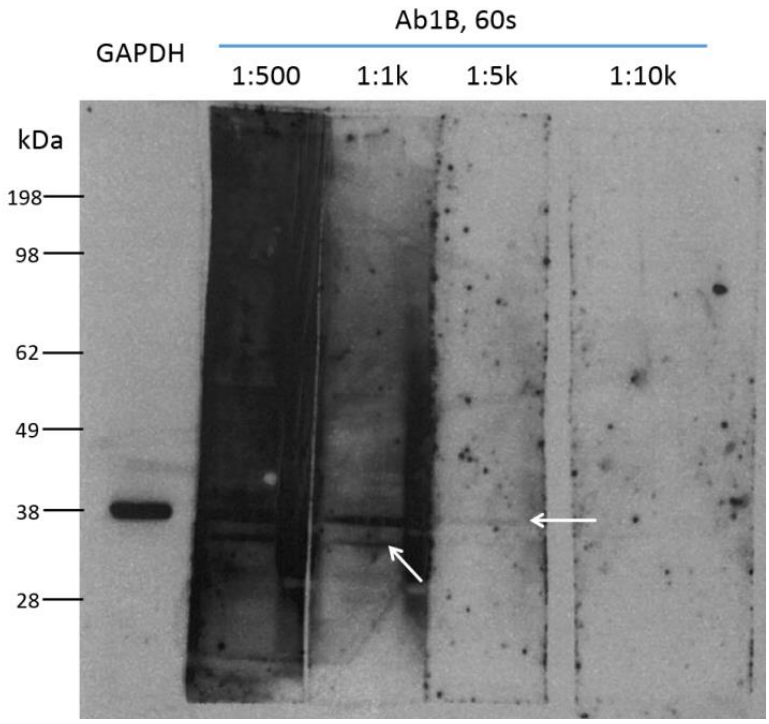

Figure 3.2 Western blot probed with increasing dilutions of Ab1B. Arrows indicate double bands detected by Ab1B at ~40 and ~37kDa. Bands are clearly detected at 1:500 and 1:1000 dilutions, faintly at 1:5000 and undetected at 1:10,000. GAPDH control, probed at a dilution of 1:10,000 is detected at 38kDa. The full blot was reassembled prior to imaging and exposed for 60 seconds. Biological N =1. Technical N = 1.

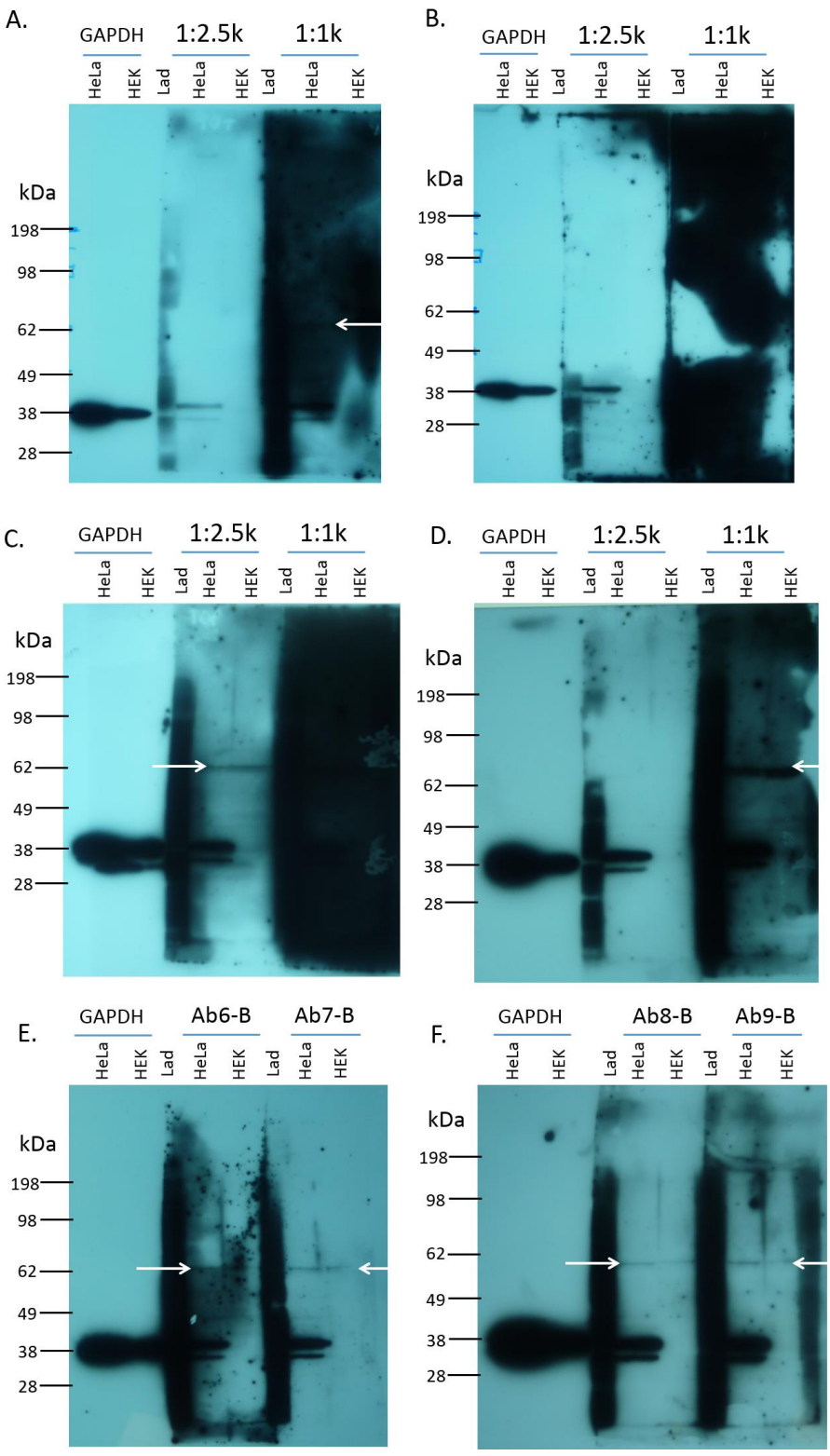

Figure 3.3 Western blots using the second received batch of custom ANO5 antibodies. A. 30 second exposure of Ab2B blot. B. 1 minute exposure of Ab3B blot. C.30 second exposure of Ab4B blot. D.30 second exposure of Ab5B blot. E. 1minute exposure of Ab6B and Ab7B blot at 1:2500. F. 1 minute exposure of Ab8B and Ab9B blot at 1:2500.The white arrows on A. C. D. E. and F. indicate the position of the 62kDa band detected by these antibodies in both lysates. GAPDH controls included on each blot are at 1:10,000. Biological N = 8. Technical N = 1.

3.2.2 Validation by immunofluorescence staining

GFP-ANO5 and ANO5-MycHis were transfected into HeLa cells cultured on 8-well chamber slides using Lipofectamin 2000 methods and analysed by immunofluorescence staining to determine the sensitivity of Abmart antibodies. Both GFP and Myc-tagged constructs were used to corroborate the data of the other and confirm antibody detection sensitivity.

Positive immunofluorescence staining showed successful transfection with an efficiency of approximately 5-7% for both constructs. However, where GFP or highly expressed Myc tag signals indicated transfection, an increase in cell staining above that seen in the surrounding cells was not detected by any Abmart antibody (Figure 3.4 and Figure 3.5). These data in concert with failure to detect of a band of the predicted molecular weight for ANO5 during western blotting indicated that no antibody could be selected as suitable for detecting ANO5.

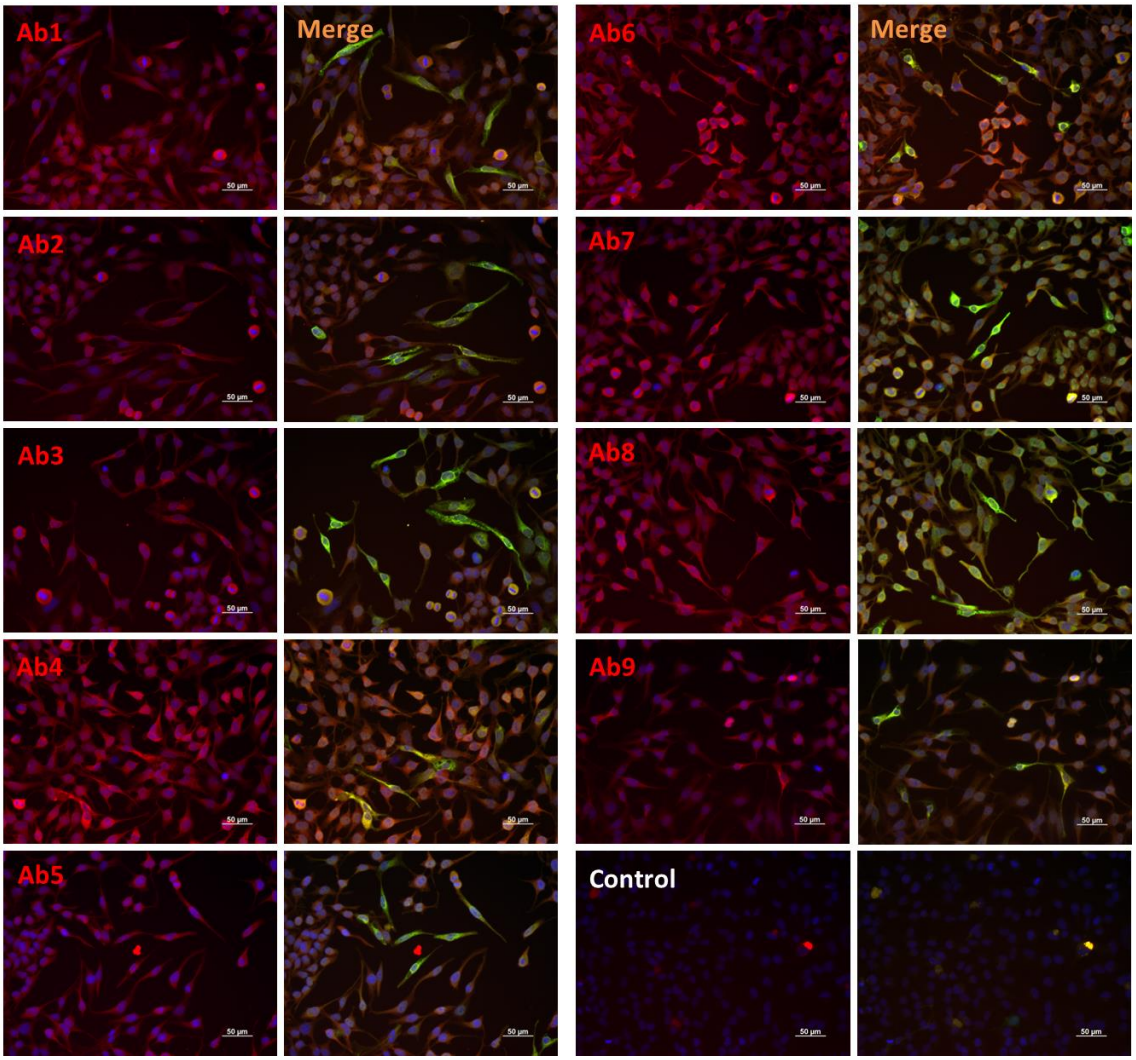

Figure 3.4 Custom ANO5 antibody immunofluorescence stain of ANO5-MycHis transfected HeLa cells. Left hand images are micrographs of red fluorescence of each Abmart antibody (labelled) + alexa fluor 594 secondary antibody. Right hand images are micrographs of the red fluorescence signal merged with green fluorescence from anti-Myc (ab39688) antibody + alexa fluor 488 secondary antibody. Bottom right image Control images show secondary antibody only condition in transfected cells. All images are at x20 magnification (scale bars = 50µm). Biological N = 10. Technical N = 2.

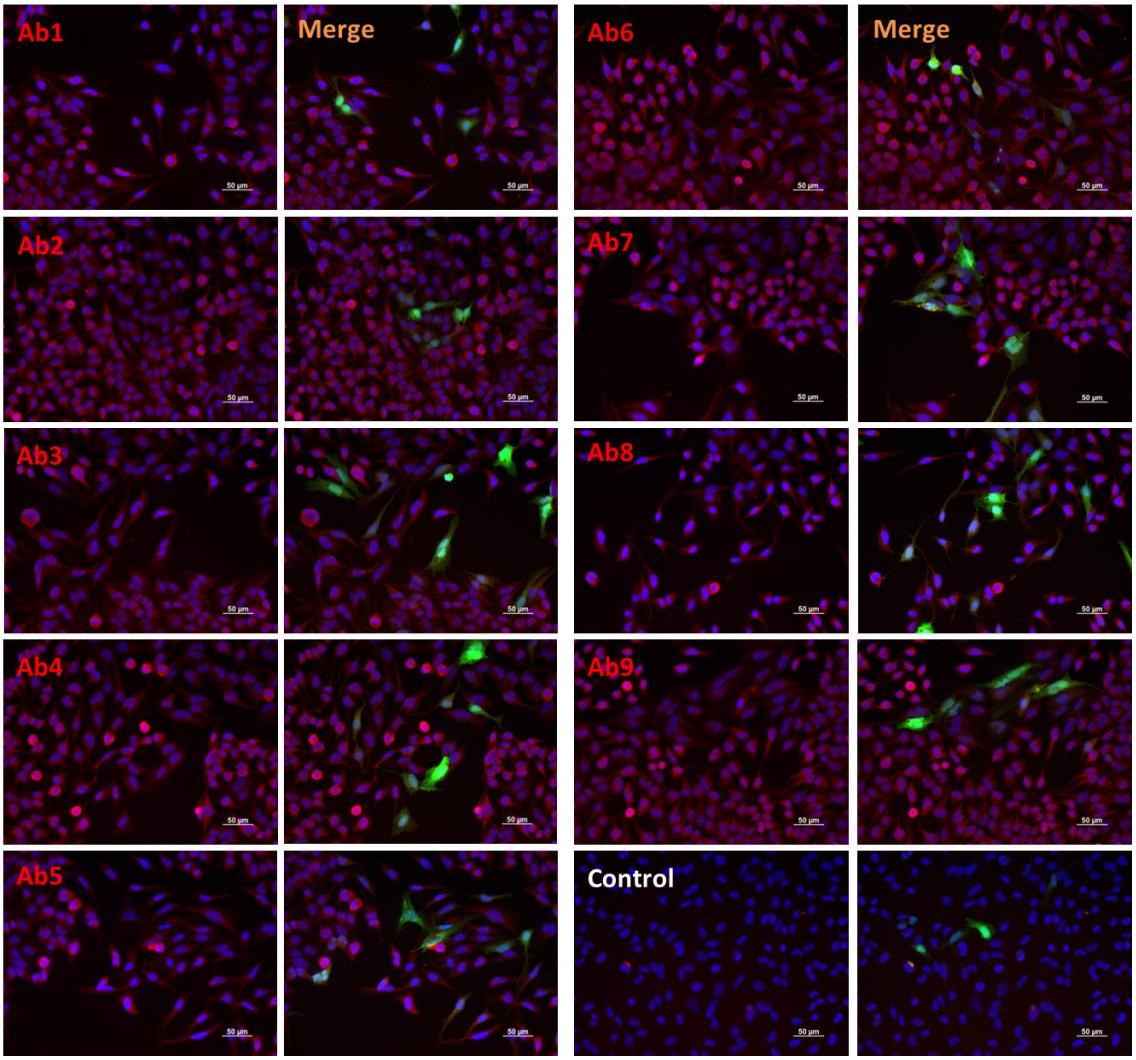

Figure 3.5 Custom ANO5 antibody immunofluorescence stain of GFP-ANO5-MycHis transfected HeLa cells. Left hand images are micrographs of red fluorescence of each Abmart antibodies (labelled) + alexa fluor 594 secondary antibody. Right hand images show the merged images with GFP fluorescence from GFP tag. Bottom right image Control images show secondary antibody only condition in transfected cells. All images are at x20 magnification (scale bars = 50µm). Biological N = 10. Technical N = 2.

3.3 Creation of GFP and MycHis tagged anoctamin 5 constructs

To better understand anoctamin 5 expression *in vitro*, GFP and YFP-tagged organelle markers were co-transfected with Myc-tagged anoctamin 5 constructs. GFP-ANO5-MycHis, GFP-ANO5, ANO5-MycHis and ANO5 only constructs were developed by Catherine Jepson prior to this project using the synthetic *Homo sapiens* cDNA clone encoding the full length of human ANO5 transcript variant A (IMAGE: 100061756) (Figure 3.6 A.-D.). GFP only, GFP-DFL (a GFP-tagged dysferlin construct) and BIN-1 constructs were developed by Dr Steve Laval (Figure 3.6 E.-G.). GFP-DFL and BIN-1 constructs included the human cDNA of the respective genes cloned into an adapted pcDNA4/TO/Myc-HIS vector (Klinge *et al.*, 2007). Fluorescent organelle constructs for Golgi, endoplasmic reticulum and endosomes (Figure 3.6 H.-J.) were commercially sourced (Takara) prior to the start of this project.

GFP has an excitation peak of 509nm (Johnson *et al.*, 1962; Morise *et al.*, 1974) and due to its stable fluorescence in other organisms, has become a common photoprotein tag (Chalfie *et al.*, 1994; Inouye and Tsuji, 1994). GFP expression has been used to confirm the transduction efficiency of plasmid and viral vectors (Smolina *et al.*, 2015) as well as to detect the subcellular expression of tagged proteins in murine models of muscular dystrophy (Li *et al.*, 2006). For example GFP tagged mini dystrophin constructs transduced into *mdx* mice have shown GFP positivity in the sarcolemma of skeletal myofibres (Li *et al.*, 2006).

Commercially sourced fluorescent organelle constructs (Golgi, ER and ENDO) contained enhanced YFP (eYFP) tags. The eYFP tag is a yellow fluorescence with an excitation maximum of 513nm. However it can also be efficiently excited at 488nm which is the standard laser emission for GFP detection. While the close spectra of these markers is an issue during simultaneous detection, for individual expression experiments they allow for detection of both GFP and eYFP using the same laser (Zimmermann, 2005; Dinant *et al.*, 2008).

Each commercial construct also contains sequences which specifically localise it to the organelle of interest. The Golgi construct contains 81 amino acids of human beta 1,4-galactosyltransferase (Human–GT). This is a membrane anchoring signal peptide which localises the construct to trans-medial region of the Golgi apparatus (Watzele and Berger, 1990). The ER construct contains the protein sequence for calrecticulin which localises to the endoplasmic reticulum (Fliegel *et al.*, 1989) and the ENDO construct

contains RhoB GTPase which localises the construct to the surface of endosomal pathway vesicles. The ENDO construct also contains a Myc tag which makes direct comparison between co-transfected ENDO and ANO5-Myc constructs impossible. This construct was still included in experiments however, as the literature suggests that ANO5 may localise to the endosome (Mizuta *et al.*, 2007). Comparison was instead made between eYFP fluorescence of the ENDO construct and the Myc fluorescence of singly transfected ANO5-Myc.

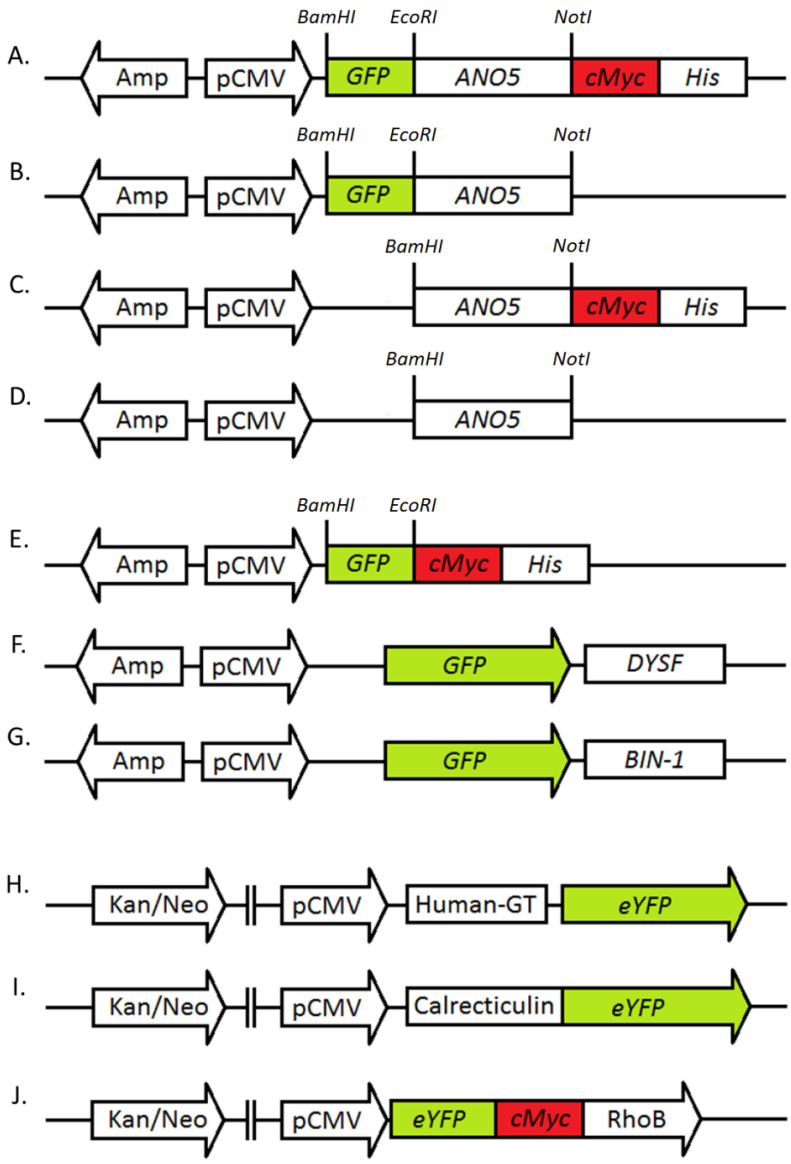

Figure 3.6 Representative diagrams of essential components of constructs used for antibody validation, organelle localisation and electroporation localisation experimentation. A.-D. Anoctamin 5 constructs developed by Catherine Jenson. Locations of BamHI, EcoRI and NotI restriction sites are indicated. E.-G. GFP construct, GFP tagged Dysferlin (GFP-DFL) and BIN-1 constructs developed by Dr Steve Laval. Locations of BamHI, EcoRI and NotI restriction sites in GFP construct are indicated. H.-J. Fluorescent Organelle constructs purchased from Takara H. Golgi construct, Human–GT marked section localises construct to the Golgi, I. ER construct, Calrecticulin marked section localises construct to the endoplasmic reticulum, J. ENDO construct, RhoB marked section localises construct to the surface of endosomal pathway vesicles. Arrows indicate the direction of DNA translation. Amp and Kan/Neo indicate the antibiotic resistances (ampicillin or kanamycin/neomycin) of the particular construct. eYFP indicates constructs with enhanced Yellow Fluorescent Protein. For simplicity diagrams are not to scale. Breaks in the diagrams indicate large distances in the sequence of the construct.

3.4 Co-expression of ANO5-Myc with fluorescently tagged organelle markers in MIN6 and NIH3T3 cell lines

The Myc tagged anoctamin 5 construct was transiently transfected into mouse pancreatic cell line MIN6 or mouse fibroblast cell line NIH 3T3 with fluorescent organelle constructs BIN-1, ENDO, ER and Golgi (Figure 3.7 and Figure 3.8).

ANO5-Myc has a punctate pattern of expression throughout the cytoplasm of both transiently transfected cell lines. These structures become denser the closer they are to the nucleus. Populations of MIN6 and NIH 3T3 cells successfully co-transfected with both ANO5-MycHis and fluorescent organelle markers indicate that all constructs localise to the cytoplasm as expected.

BIN-1, an endosomal marker in non-myoblast cell lines, shows a similar pattern of diffuse cytoplasmic distribution in NIH 3T3 cells which closely overlay with the ANO5-Myc fluorescence. BIN-1 cytoplasmic expression is denser in MIN6 cells and does not localise to the same parts of the cell so does not over lay with the ANO5-Myc pattern of expression. ENDO also has a punctate expression pattern in the cytoplasm though the spots of fluorescence are much larger than in the NIH 3T3 cells compared to the single ANO5-Myc fluorescence and so are unlikely to co-localise. Comparison of independent ENDO and ANO5-Myc fluorescence patterns in MIN6 cells is harder to distinguish as the ENDO fluorescence pattern is very similar to single ANO5-Myc fluorescence. Without co-expression images it is not possible to accurately determine co-localisation between ENDO and ANO5-Myc constructs.

In MIN6 cells ER, the endoplasmic reticulum marker, has a punctate pattern throughout the cytoplasm, overlapping with ANO5-Myc fluorescence. In NIH 3T3 cells, ER localises very densely around the nucleus and does not overlap with ANO5-Myc fluorescence.

ANO5 does not appear to localise to the Golgi apparatus in either MIN6 or NIH 3T3, though there is some overlap in localisation in Golgi signal in NIH 3T3 cells. Untransfected controls, stained with anti-Myc antibody were negative for fluorescence signal.

These data suggest that fluorescently tagged ANO5 constructs partially co-localise with ER in MIN6 cells and BIN-1 in NIH 3T3 cells (Figure 3.7 and Figure 3.8).

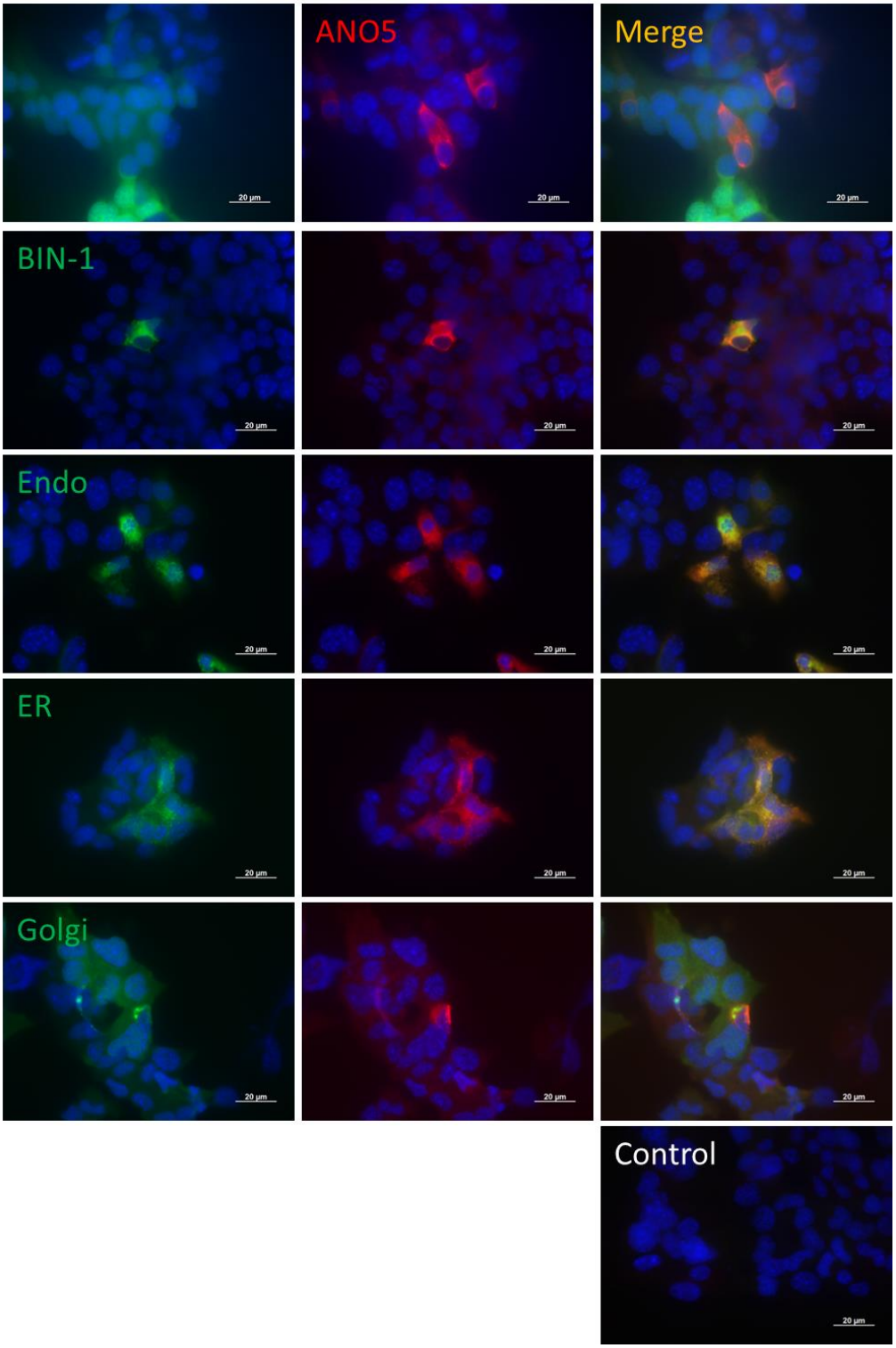

Figure 3.7 Co-expression of ANO5-MycHis and fluorescent organelle markers in MIN6 cells. Left hand images are micrographs of green fluorescence signal (BIN-1 and ENDO localise to Endosomes, ER localises to endoplasmic reticulum, Golgi localises to Goligi apparatus). The ANO5 column shows red fluorescence of anti-Myc (9E10) antibody + alexa fluor 594 secondary detecting the ANO5-MycHis construct and the right hand images show the merged images. Untransfected control cells are shown in the bottom right image. All images are at x63 magnification (scale bars = 20µm). Biological N = 6. Technical N = 2.

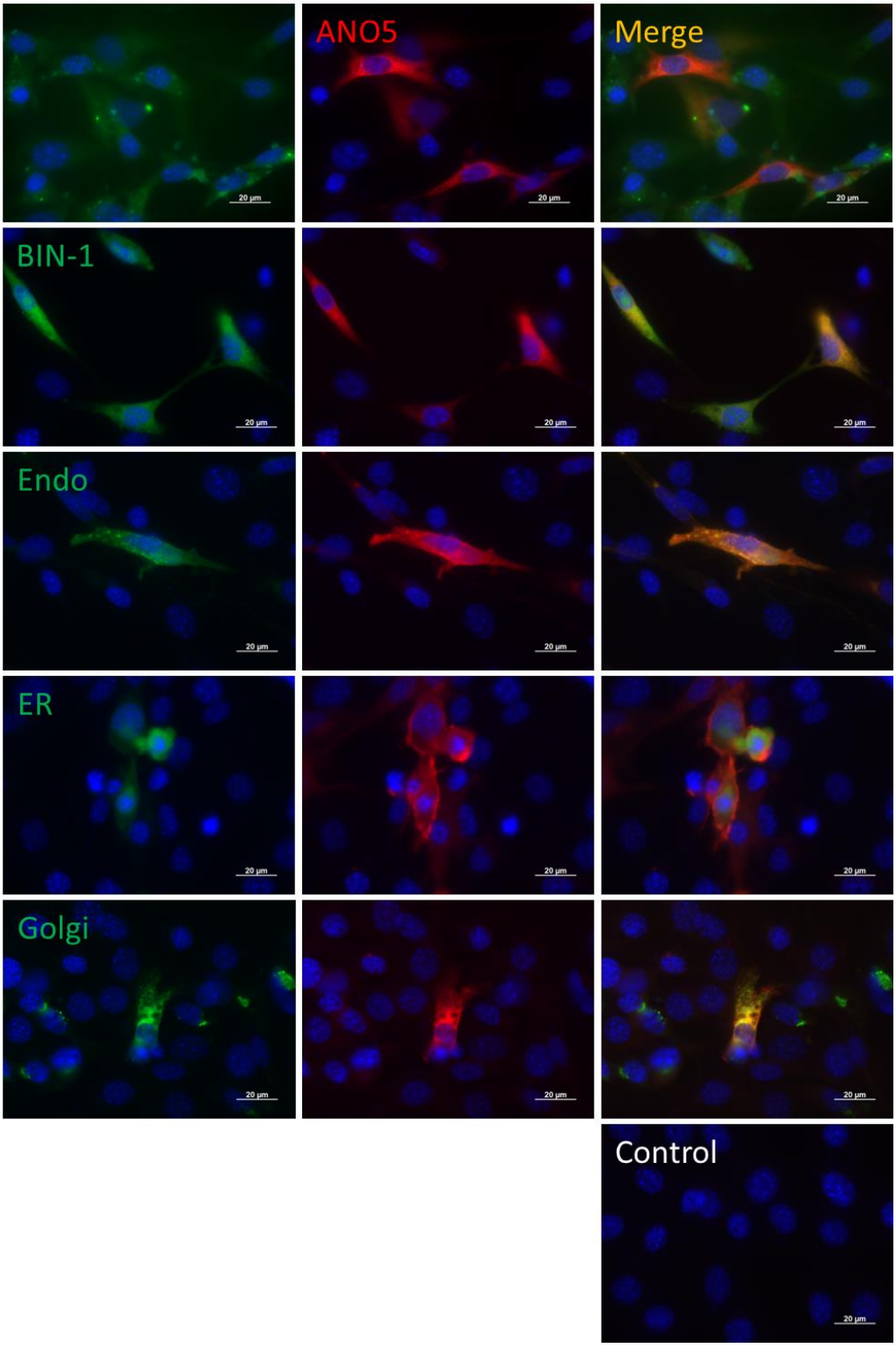

Figure 3.8 Co-expression of ANO5-MycHis and fluorescent organelle markers in NIH 3T3 cells. Left hand images are micrographs of green fluorescent organelle makers (BIN-1 and ENDO = Endosomes, ER = endoplasmic reticulum, Golgi = Goligi apparatus). The ANO5 column shows red fluorescence of anti-Myc (9E10) antibody + alexa fluor 594 secondary detecting the ANO5-MycHis construct and the right hand images show the merged images. Untransfected control cells are shown in the bottom right image. All images are at x63 magnification (scale bars = 20µm). Biological N = 6. Technical N = 2.

3.5 Co-expression of ANO5-Myc and fluorescently tagged organelle markers in undifferentiated and differentiated C2C12

T-tubules are invaginations in the sarcolemma of muscle cells and part of the cytoskeleton, responsible for transmitting electrical signals across the full width of cells and myofibrils, ultimately resulting in synchronous contraction of the full muscle (Huxley and Taylor, 1958; Bastian and Nakajima, 1974). The t-tubules have also been identified as the site of dysferlin localisation during muscle development (Klinge *et al.*, 2007) and have also been suggested as dependant on dysferlin for correct formation (Demonbreun *et al.*, 2014).

To investigate the subcellular localisation of anoctamin 5 in a more biologically relevant model and to investigate potential ANO5-Myc localisation to the t-tubules, transient transfection of the same ANO5-Myc with BIN-1 and Golgi marker constructs was carried out in undifferentiated (D0) and differentiated (D5) C2C12 mouse myoblasts (Figure 3.10). In this system the BIN-1 construct is predicted to be targeted to the t-tubules in differentiated myotubes (Lee *et al.*, 2002). Golgi marker constructs were included as a negative control as ANO5 was not expected to co-localise with these organelles.

3.5.1 Transfection optimisation

Several attempts were made to optimise transient transfection of undifferentiated C2C12 prior to myotube differentiation (Figure 3.9). Lipofectamine 2000 and Amaxa transfection methods were attempted, but these either had low initial transfection efficiencies (Lipofectamin 2000) or killed too many cells during transfection to lead to viable differentiation (Amaxa). FuGene was selected for further transfection experiments as it yielded the highest transfection efficiency in undifferentiated C2C12 and retained the GFP construct over five days of differentiation.

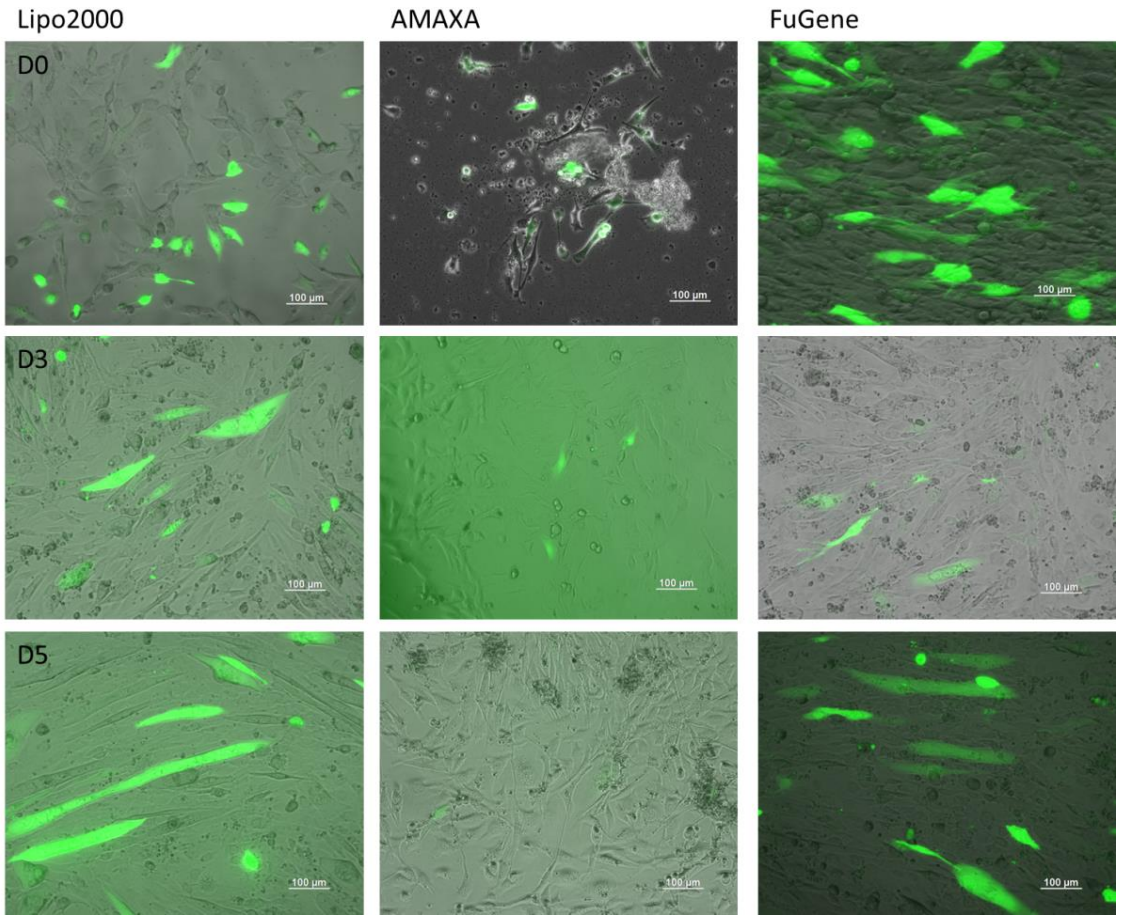

Figure 3.9 Comparison of Lipofectamin 2000, AMAXA and Fugene transfection efficiencies of GFP construct and retention during differentiation. D0 (Undifferentiated), D3 (fusing C2C12) and D5 (early myotubes) time points are shown. All images are at x10 magnification (scale bars = 100µm). Biological N = 3. Technical N = 2.

3.5.2 Co-expression of ANO5-Myc and fluorescently tagged organelle markers in undifferentiated and differentiated C2C12

D0 C2C12 successfully transfected with ANO5-Myc retain the same pattern of expression seen in MIN6 and NIH 3T3 cells. There is a punctate pattern throughout the cytoplasm with increased density in proximity to the nucleus. A similar pattern is also seen in D5 differentiated C2C12, though with the punctate pattern appearing to form slight striated patterns within the cell. This may be due to elongation of the cell and not represent actual structures within the cell.

BIN-1 is expressed throughout the cytoplasm at both D0 and D5 time points. While ANO5-Myc also localises to similar areas of the cytoplasm at both time points, the signals do not completely overlap suggesting that ANO5 only partial co-localises with BIN-1 (Figure 3.10). ANO5 does not localise to the Golgi apparatus in either D0

myoblasts or D5 myotubes. The Golgi construct localises around the nuclei and to a few concentrated clusters in the cytoplasm. C2C12 stained with only secondary antibody or transfected only with FuGene were negative for any fluorescence other than DAPI. These results suggest that ANO5 partially localises to the t-tubules in both undifferentiated and differentiated C2C12.

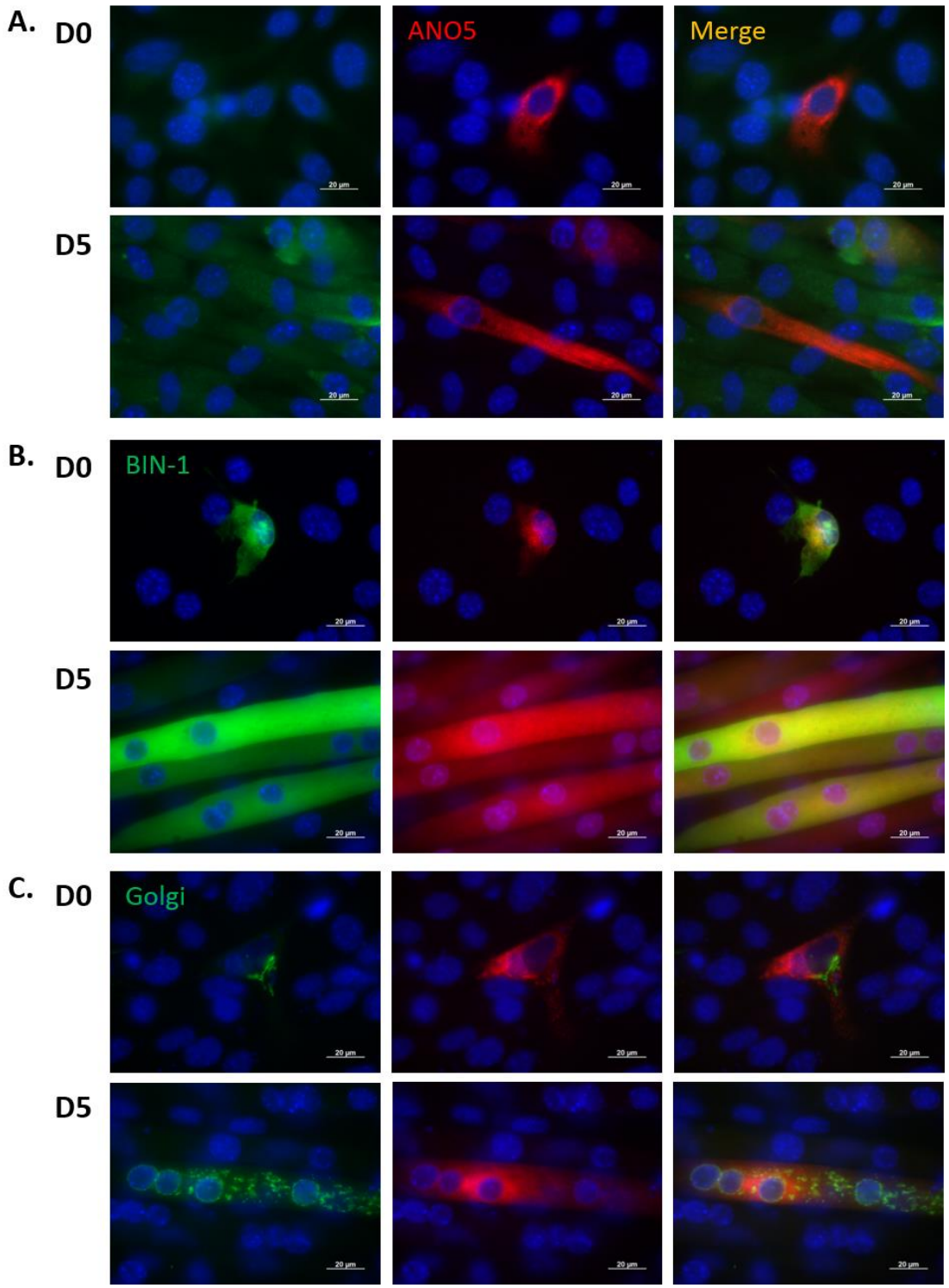

Figure 3.10 Co-Expression of ANO5-MycHis and fluorescent organelle markers in undifferentiated and differentiated C2C12. A. Control C2C12 transfected with ANO5-MycHis only. B. BIN-1 marker identifying t-tubules in green. C. Golgi marker identifying Golgi apparatus. Left hand images are micrographs of green fluorescent organelle makers, ANO5 column of images show red fluorescence of anti-Myc (9E10) antibody + alexa fluor 594 secondary antibody detecting the ANO5-MycHis construct and the right hand images show the merged images. All images taken at x63 magnification (scale bars = 20µm). Biological N = 3. Technical N =1.

3.6 Co-expression of ANO5-Myc with fluorescently tagged DYSF marker in undifferentiated and differentiated C2C12

The anoctaminopathies and dysferlinopathies share a number of clinical features including a late age of onset, infrequent cardiac or respiratory involvement and a similar rate of progression and pattern of muscle involvement (Jarry *et al.*, 2007). Anoctamin 5 co-localisation with dysferlin was investigated in undifferentiated and differentiated C2C12 cells.

Partial co-localisation of ANO5-Myc and GFP-DFL is seen in undifferentiated C2C12 cells (Figure 3.11). Anoctamin 5 is visible with the punctate pattern of expression across the cytoplasm with some clustering near the nucleus, which had been previously observed, while dysferlin has a more filamentous pattern of expression throughout the cytoplasm.

These staining patterns remain when the myoblasts fuse to become myotubes at day 5, but the dysferlin pattern is more pronounced, becoming more obviously filamentous across the length of the myotube. At both day 0 and day 5, the punctate pattern of anoctamin 5 lines up with the filamentous pattern of dysferlin, seen in the yellow signal in the merged channel. Slides stained with only secondary antibody or transfected only with FuGene were negative for fluorescence other than DAPI.

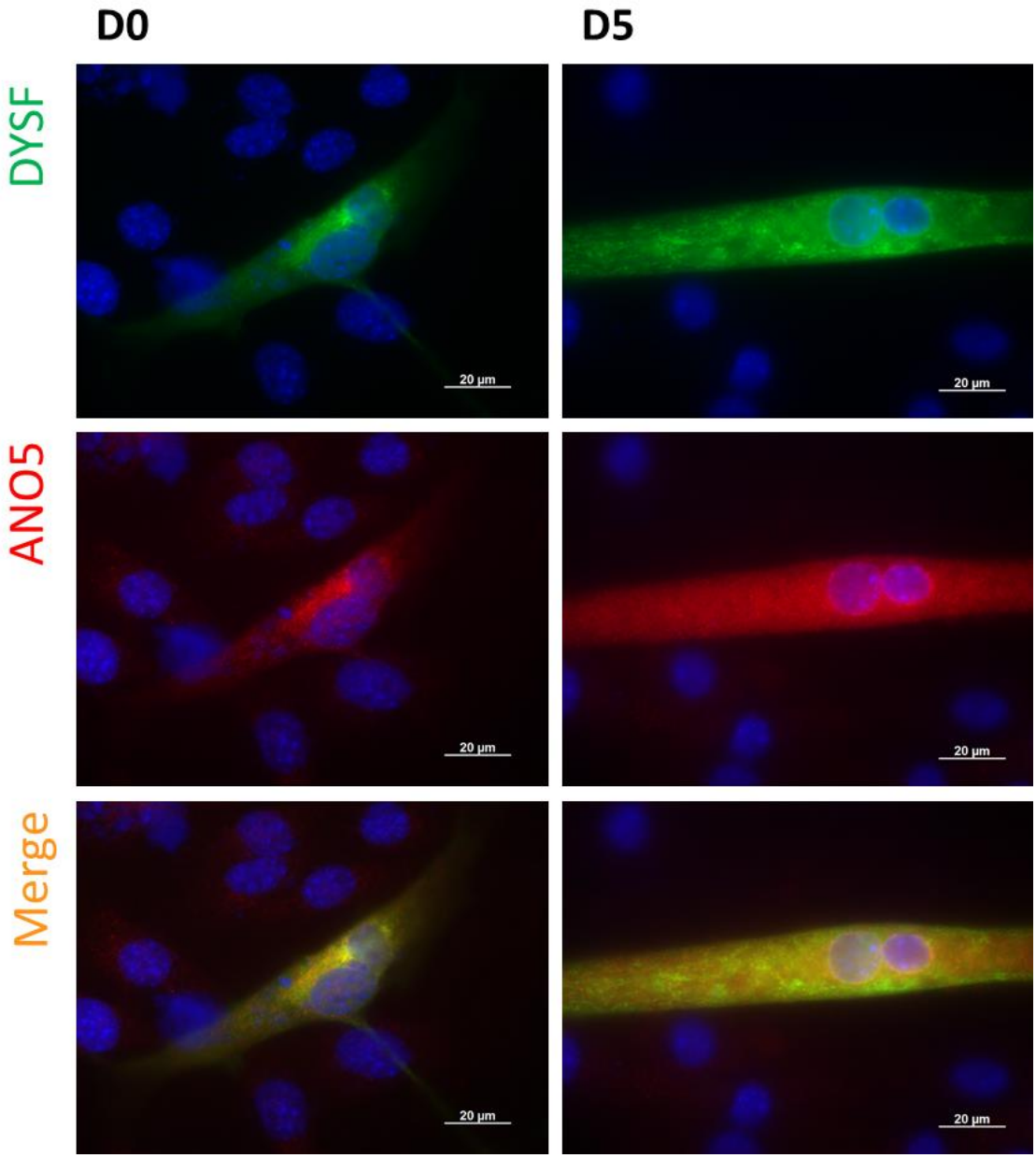

Figure 3.11 Co-Expression of ANO5-MycHis and DYSF in undifferentiated and differentiated C2C12. Top row of images are micrographs of green fluorescent GFP-tagged dysferlin (DYSF) maker, middle row of images are micrographs of red fluorescence of anti-Myc (9E10) antibody detecting the ANO5-MycHis construct and the bottom row of images are micrographs of the merged images. All images taken at x63 magnification (scale bars = 20µm). Biological N = 1. Technical N = 1.

3.7 *In vivo* localisation of anoctamin 5 using electroporation of *mdx* mouse muscle

3.7.1 Construct validation

To understand ANO5 localisation in a more biologically relevant model, electroporation was used to introduce expression constructs into the *tibialis anterior* muscle of male *mdx* mice in order to identify the *in vivo* localisation of ANO5 constructs. Electroporation experimentation were carried out using GFP, GFP-ANO5, ANO5-MycHis and mini-dystrophin constructs, either singly or in combination.

All constructs were first validated using restriction digest and expression in HeLa cells. Restriction digest products visualised on 1% (w/V) agarose gel confirmed that the constructs each contained inserts of the expected sizes (Figure 3.12). Similarly, immunofluorescent staining of GFP and Myc expression in transiently transfected HeLa cells indicate that the constructs were functionally viable and that staining methods were sufficient (Figure 3.13).

The ANO5-Myc construct shows the expected punctate pattern of expression within the cytoplasm of the cell seen in previous experiments. Both the GFP control and GFP-ANO5 constructs appear to be uniformly expressed throughout the cytoplasm, though the GFP-ANO5 construct has a comparatively lower level of fluorescence. Immunofluorescent staining with anti-GFP (ab290) appears to detect GFP only at the plasma membrane. Though as untransfected cells within the same wells did not display positive immunofluorescent staining, it was decided that this antibody was still useful as a second stain for confirming positive GFP expression.

The transfection efficiency varied between constructs with the GFP control construct having the highest (~40-50% of cells with detectable fluorescence). Of the two tagged ANO5 constructs, GFP-ANO5 had the highest transfection efficiency (~15-20%) and ANO5-MycHis the lowest (~5-10%). Mini-dystrophin construct C1 was not tested in HeLa cells as it had been used successfully by another member of the group in a previous electroporation experiment.

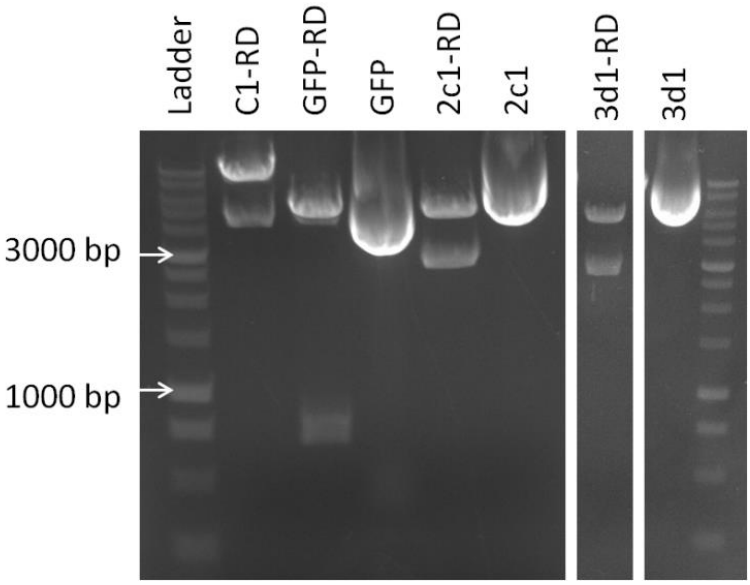

Figure 3.12 Electrophoresis gel of whole and restriction digested dystrophin and ANO5 expression constructs. C1-RD lane shows restriction digest product of C1 construct, insert present at ~4.5 kb. GFP-RD lane shows restriction digest product of GFP construct, insert present at ~0.8 kb. GFP lane shows undigested GFP construct. 2c1-RD lane shows restriction digest product of GFP-ANO5 construct, insert present at ~2.8 kb. 2c1 lane shows undigested GFP-Myc construct. 3d1-RD lane shows restriction digest product of ANO5-Myc construct, insert present at ~3 kb. 3d1 lane shows undigested ANO5-Myc construct. 1kbp ladder used with 3000 and 1000bp markers indicated. Biological N = 7. Technical N = 1.

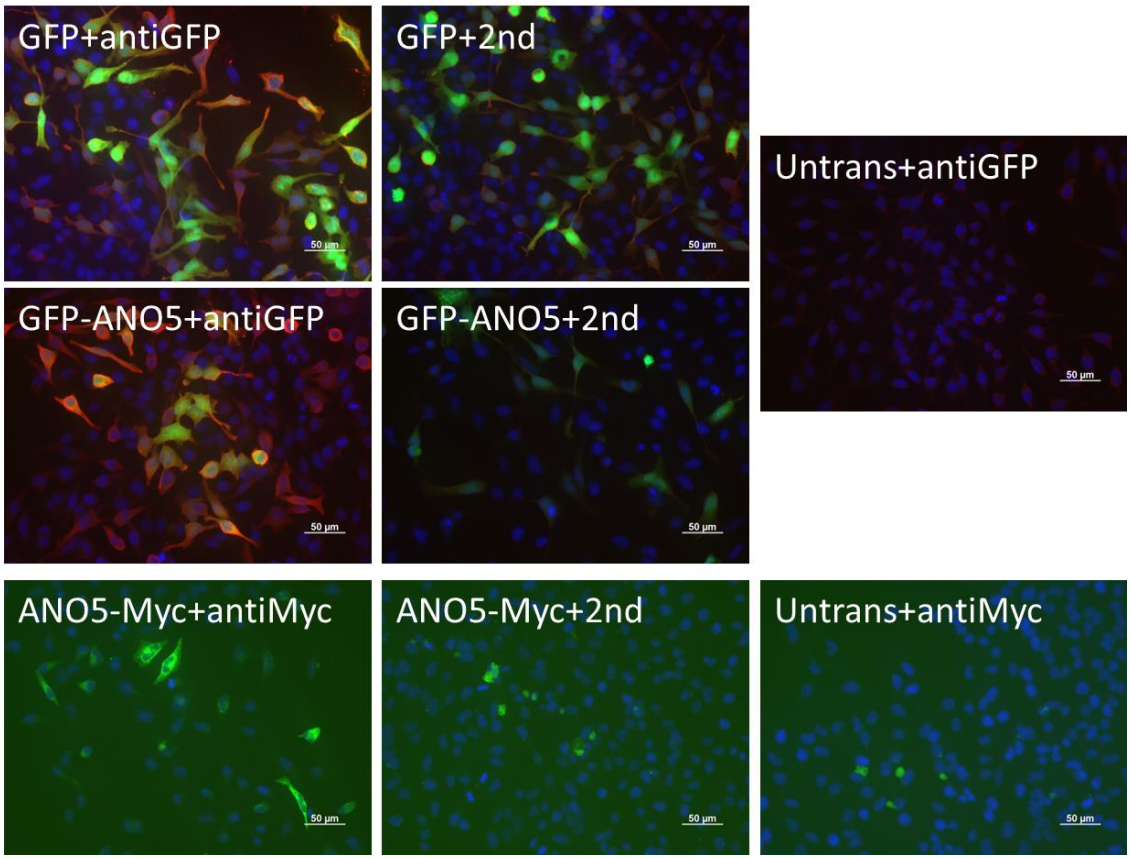

Figure 3.13 GFP and ANO5-tagged construct functionality examination by immunofluorescent staining of transfected HeLa cells. Left hand images are micrographs of transfected constructs + indicated primary and secondary antibodies. Middle images are micrographs of transfected constructs + secondary antibody only. Alexa fluor 594 secondary antibody was used for anti-GFP and secondary antibody only conditions. Alexa fluor 488 secondary antibody was used for anti-Myc (9E10) and secondary antibody only conditions. Right hand images are micrographs of Untransfected + primary and secondary antibodies conditions. All images are taken at x20 magnification (scale bars = 50µm). Biological N = 4. Technical N = 1.

3.7.2 Electroporation of mdx and C57BL/10 mice

Following validation, constructs were used in electroporation experiments utilising both C57BL/10ScSn-Dmd^{mdx} (*mdx*, a mouse model of Duchene muscular dystrophy), and C57BL/10 control mice (BL10). The *mdx* mouse model has weaker plasma membranes (Straub *et al.*, 1997) and it was hoped this would improve uptake of constructs into the muscle tissue following electroporation and improve localisation detection since GFP was not visualised in the initial electroporation attempts in BL10.

Three initial attempts of electroporation experimentation used only GFP and GFP-ANO5, as it was hoped the GFP marker would be sufficient to detect successfully electroporated fibres. However successfully electroporated fibres could not be distinguished from normal fibres as the level and non-specific pattern of fluorescence was unchanged across the muscle sections. Additionally, the same non-specific pattern was observed in non-electroporated control muscle. Immunofluorescent staining for the GFP marker using an anti-GFP antibody was attempted, to improve detection of GFP-positive fibres but this yielded the same non-specific patterns of fluorescence as previous attempts. Additional controls were therefore included in the fourth round of electroporation.

ANO5-MycHis was included in an attempt to use the Myc tag as a second method of identifying ANO5 localisation. Additionally, GFP and ANO5-tagged constructs were co-electroporated with mini-dystrophin constructs (Meng *et al.*, 2016; Reza *et al.*, 2016), which had been detectable following immunofluorescent staining in previous electroporation experiments (Mojgan Reza, unpublished data). Dystrophin is absent from the cytoskeleton of muscle fibres of *mdx* mice (Hoffman *et al.*, 1987). Successfully electroporated mini-dystrophin constructs restore dystrophin to muscle fibres and were therefore used in these experiments as an indicator of successfully electroporated muscle fibres. Comparison of serially sectioned haematoxylin and eosin stained electroporated *mdx* muscle were used to identify the injection site in each condition (Figure 3.14). The site of injection was approximated by identifying signs of muscle repair from morphological features.

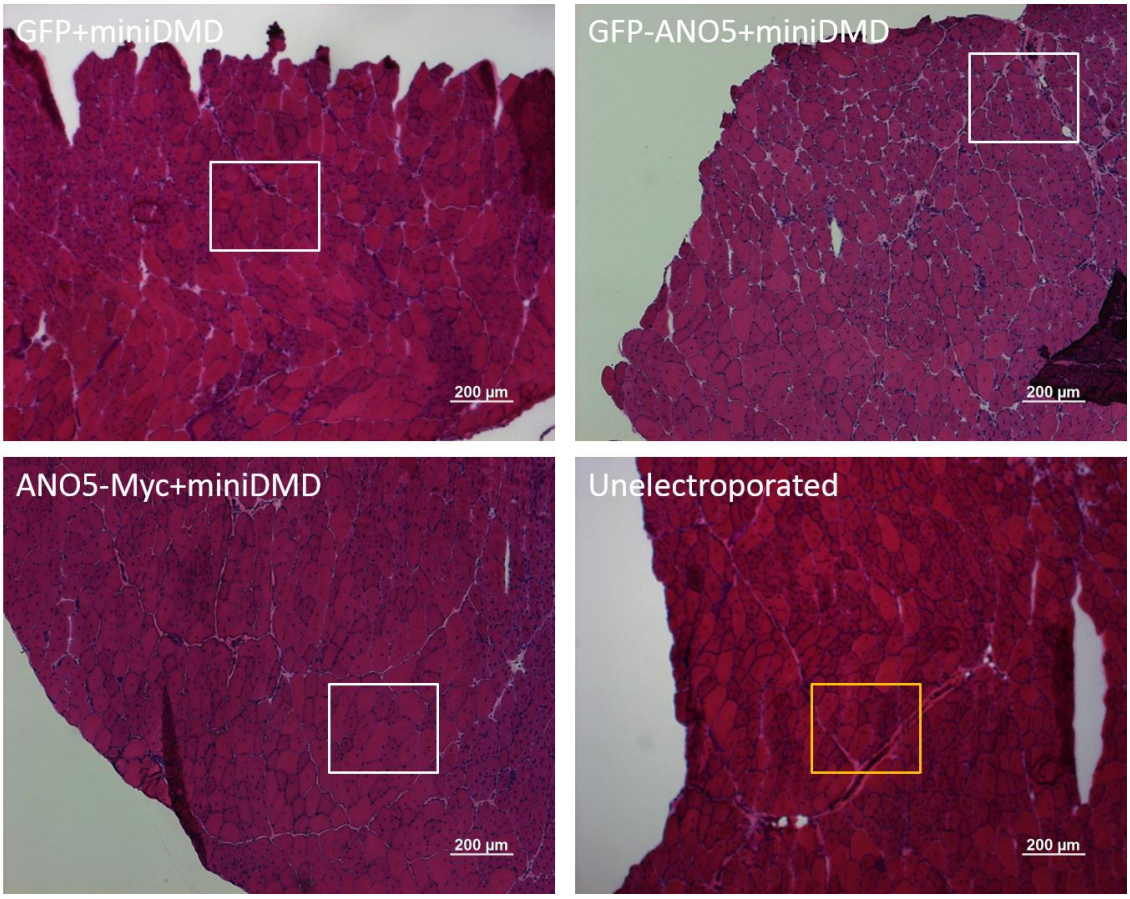

Figure 3.14 Haematoxylin and eosin staining of electroporated mdx mouse muscle sections. Electroporated constructs and unelectroporated control are indicated. miniDMD indicates mini-dystrophin electroporated tissue. Squares indicate the areas of further investigation displayed in Figure 3.15 and Figure 3.16 (White = identified injection site in electroporated muscle; Orange = chosen area of comparison in unelectroporated control). All images taken at x5 magnification (scale bar = 200µm). Biological N = 4. Technical N = 1.

3.7.3 IHC Staining of electroporated mouse muscle

Fluorescent Immunohistochemistry (IHC) staining was used to identify clusters of dystrophin-positive fibres near these sites of injection. The corresponding locations in the serial sections immediately following positively identified sections were then investigated for GFP or Myc fluorescence using additional IHC staining. Unelectroporated controls were also investigated in this way, using dystrophin-positive revertant fibres as controls to compare GFP and Myc tag detection against. Revertant fibres are fibres in which the loss of dystrophin has been naturally overcome and dystrophin is therefore visible following staining (Hoffman *et al.*, 1990).

At x20 magnification there was no detectable difference in the green fluorescence between dystrophin-positive and dystrophin-negative fibres in either GFP-ANO5 or GFP-electroporated muscle (Figure 3.15). However, there appeared to be co-localisation of GFP and anti-GFP stain fluorescence in GFP electroporated muscle when viewed at x63 magnification. In GFP-ANO5 muscle a very faint fluorescence was observable but was not different to that seen in the surrounding dystrophin negative fibres. Furthermore this same fluorescence was also present in unelectroporated *mdx* muscle in fibres identified as dystrophin-positive (Figure 3.15).

Similarly, at x20 magnification in ANO5-MycHis electroporated muscle no obvious fluorescence was observed in dystrophin-positive fibres above that of surrounding dystrophin negative fibres. But at x63 magnification, a fluorescence pattern of internal localisation was observed, which is consistent with that expected from endoplasmic reticulum localisation. In secondary only controls this patterning is not seen (Figure 3.16). However the same pattern of fluorescence is also seen in dystrophin-positive fibres of unelectroporated muscle stained for the Myc tag. This pattern of fluorescence is not seen in dystrophin negative fibres or in secondary antibody only stained sections of unelectroporated muscle (Figure 3.16).

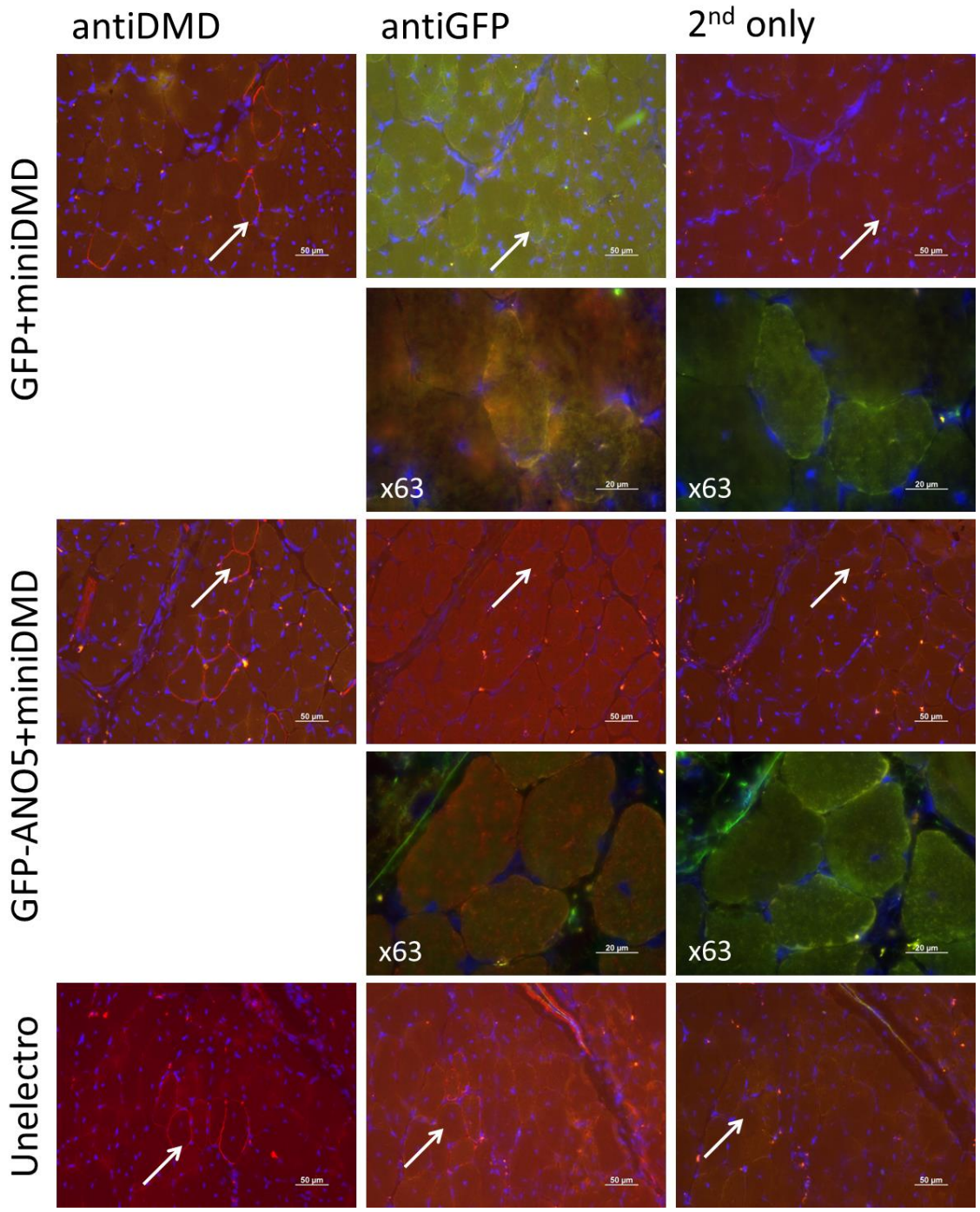

Figure 3.15 Immunofluorescent images of mdx mouse TA muscle electroporated with GFP and GFP-ANO5. Row headings indicate electroporated constructs and unelectroporated controls, column heading indicate primary antibodies and secondary only conditions. miniDMD indicates mini-dystrophin electroporated tissue. Alexa fluor 594 secondary antibody was used for both anti-GFP and anti-DMD primary antibodies. Arrows indicate the dystrophin-positive fibres of interest in each condition. All images are taken at x20 magnification, (scale bars = 50µm) except where indicated as taken at x63 magnification (scale bars = 20µm). Biological N = 3. Technical N = 1.

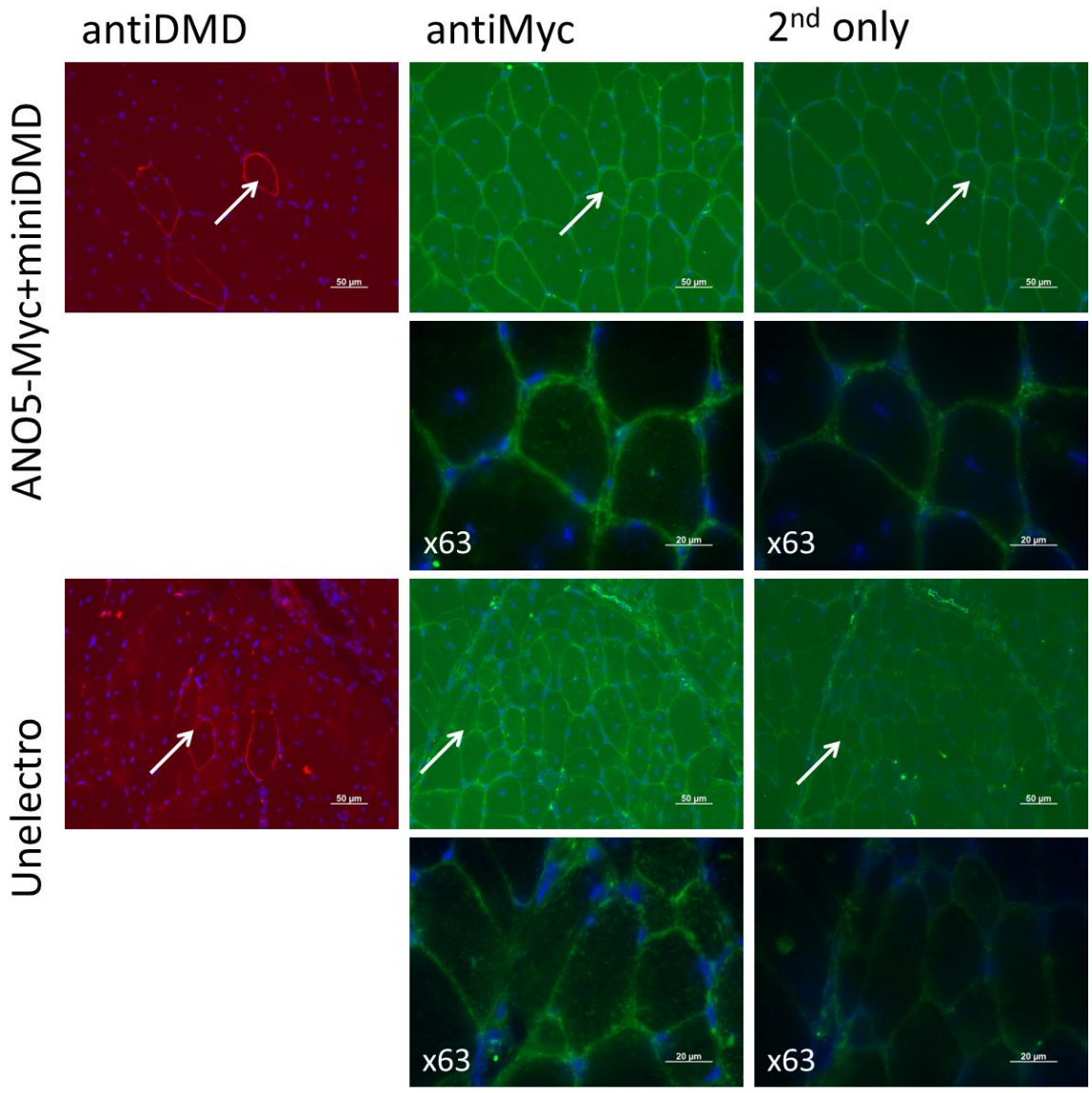

Figure 3.16 Immunofluorescent images of mdx mouse TA muscle electroporated with ANO5-MycHis. Row headings indicate electroporated constructs and unelectroporated controls, column heading indicate primary antibodies and secondary antibody only conditions. miniDMD indicates mini-dystrophin electroporated tissue. Alexa fluor 594 secondary was used for anti-DMD primary antibody, while alexa fluor 488 secondary antibody was used for anti-Myc primary antibody. Arrows indicate the dystrophin-positive fibres of interest in each condition. All images are taken at x20 magnification, (scale bars = 50µm) except where indicated as taken at x63 magnification (scale bars = 20µm). Biological N = 2. Technical N = 1.

3.8 Discussion

None of the Abmart ANO5 antibodies detected overexpressed anoctamin 5 in either Western Blot or IF experiments and as such were deemed sub-optimal for further experimentation. High background produced by Western Blotting of the first batch of antibodies, even highly diluted, was most likely due to the method of production and insufficient filtering and clean-up of the antibodies. Additional cleaning and filtering of the antibodies was not attempted as the high viscosity of this batch of antibodies made them very difficult to work with and it was hoped a second batch of antibodies would be more reliable.

The second batch of antibodies was easier to work with and had reduced background allowing for detection of the same multiple bands by several of the antibodies. However all of these bands were smaller than the predicted molecular weight of ANO5 (~107kDa), suggesting that these antibodies could be unspecifically binding, especially the small ~62kDa band detected in both HeLa and HEK lysates. However, as the two bands at ~40 and 37kDa were only detected in transfected HeLa cell lysates, an alternative explanation for these bands may be that they are remnants of overexpressed ANO5 constructs being broken down and removed from the cell. Failure to detect overexpressed ANO5 by IF is likely due to the antibodies failing to detect the correct epitope tag, as the fluorescence of positively transfected cells, indicated by GFP and Myc fluorescence, was no higher than that of the surrounding untransfected cells.

The failure to identify a workable ANO5 antibody is not unexpected as the identification of a suitable anoctamin 5 antibody has eluded the research and clinical fields for several years. An explanation for this may be that while anoctamin 5 is the most highly expressed anoctamin in skeletal muscle its expression at the cellular level may be highly dependent on specific stimuli acting on the cell, for example induction of scramblase activity (Suzuki *et al.*, 2013). Alternatively, it may be that identification of a suitable specific epitope for anoctamin 5 is hindered due to cross reactivity with the closely related anoctamin 6 also present in the same tissues.

In vitro results using Myc-tagged ANO5 suggest that anoctamin 5 localises to the endoplasmic reticulum in MIN6 cells and the endosomes in NIH 3T3 cells, indicated by positive BIN-1 staining. These findings are consistent with reports of ANO5 localisation in the literature (Tsutsumi et al., 2004; Mizuta et al., 2007). Anoctamin 5

also partially localises to the t-tubules in both undifferentiated and differentiated myoblasts, a finding not previously described.

This finding is of interest given that the related anoctamins ANO1 and 2, have been described as calcium activated chloride channels and that proper action potential generation in the t-tubules are vital for correct muscle contraction. However anoctamin 5 has not yet been found to produce an action potential in the presence of calcium, even when modified to include the current forming loop present in ANO1 (Duran *et al.*, 2012). Similarly, robust chloride conductance has not been recorded in the other anoctamin family members other than ANO1 and 2, though some have been found to function as other ion transporters (Schreiber *et al.*, 2010; Yang *et al.*, 2012; Kunzelmann *et al.*, 2014). Therefore anoctamin 5 may be functioning as a channel for another ion in the t-tubules.

Finally, it was hoped that *in vivo* investigation of electroporated *mdx* muscle would characterise anoctamin 5 localisation in whole tissue, complementing the previous *in vitro* localisation results. From this work, further routes of investigation of the function of anoctamin 5 could be conducted. Unfortunately due to the poor signal to noise ratio of the stained muscle sections, it was not possible to accurately distinguish true signal of tagged ANO5 constructs from background and thereby definitively determine ANO5 localisation.

While electroporation experimentation has worked well for other members of this research team before, in this instance it was unsuccessful. Due to these previous successes, it is therefore unlikely to have been the technique which was at fault. A possible explanation is that while the tagged constructs work well *in vitro*, it may be that *in vivo* these constructs are rapidly broken down and their signal lost amongst the autofluorescence of the muscle. While there is no direct evidence in the literature to support this exact notion, electroporation success and construct retention time within mouse muscle have been found to be affected by factors such as the size of the construct, the co-injection of chemicals to increase membrane permeability (such as hyaluronidase) and even the strain of the mouse (Molnar *et al.*, 2004).

Furthermore, Scudieri *et al.* (2015) suggest that adding tags to constructs can alter their localisation. In their paper investigating ANO6 function, the authors suggest this is as an explanation for the conflicting reports of ANO6 localisation. It is therefore possible that the Myc tag has affected ANO5 expression, changing its localisation in culture,

altering its electroporation efficiency and potentially reducing the retention of the constructs within mouse muscle. Further optimisation of this experimentation may yet yield positive identification of anoctamin 5 localisation. As localisation was only one facet of this project, other routes of investigation were instead followed.

Chapter 4 Investigation of proteins affected by the knockdown of ANO5 in C2C12 cells using 2-Dimensional gel electrophoresis

4.1 Introduction

Identifying that anoctamin 5 localises to the endoplasmic reticulum, and possibly to the t-tubules, in the previous chapter suggests that anoctamin 5 may be involved with calcium homeostasis (Doutheil *et al.*, 2000) and proper protein folding (Hebert and Molinari, 2007). However, precise identification of the function of ANO5 at either the cellular or biochemical level is limited by the lack of an antibody and an ANO5 deficient model system. Despite concerted efforts, the former deficiency has not been remedied.

Lacking access to an animal model of anoctaminopathy, an anoctamin 5 deficient cellular model is required. Knockdown of anoctamin 5 was achieved in C2C12 cells (mouse myoblasts) using a pool of short hairpin RNAs (shRNAs) and validated by reverse transcription PCR (rtPCR). A Control knockdown line was generated in tandem using scrambled shRNAs to confer the same antibiotic resistances and experimental pressures but without affecting gene expression. The anoctamin 5 model was then characterised using 2D gel electrophoresis to better understand what effect, if any, removing anoctamin 5 has on other proteins.

In this chapter the results of the stable knockdown C2C12 generation are presented. The differences in protein expression between the generated clones were subsequently explored using 2D gel electrophoresis, the identified proteins confirmed by Matrix Assisted Laser Desorption/Ionisation tandem Mass Spectrometry (MALDI MS/MS) and western blotting and then investigation of the identified proteins carried out with reference to what their change implies about anoctamin 5 function.

4.1.1 MALDI-MS/MS analysis and identification of proteins

Mass spectrometry (MS) has long been a robust method of identifying and quantifying the isotopic signature, mass and molecular structure of a sample by analysing the mass-to-charge ratio of ions excited from that sample (Wolff and Stephens, 1953). Matrix assisted laser desorption/ionisation (MALDI) mass spectrometry is one variety of mass spectrometry commonly used to identify biomolecules such as proteins (Karas *et al.*, 1987).

In MALDI MS, the "matrix" is typically a crystallised acid which is mixed with the sample and solubilised in water and an organic solvent (to solubilise the hydrophobic elements of the sample). This solution is then applied to a metal plate where the water and organic solvent are evaporated to leave a thin, optically homogenous, crystallised layer containing both the matrix and the sample to be analysed (Karas *et al.*, 1987). This thin layer of the matrix/sample is then irradiated with a pulsed laser causing ablation of the matrix from the plate and formation of a gas in which the sample molecules are ionised (Karas *et al.*, 1987). The ionised molecules can then be accelerated and analysed using the chosen method of MS.

Typically, MALDI MS measures the time of flight (TOF) of excited ions in an electric field of known strength over a given distance (e.g. from the point of excitation to the detector) (Figure 4.1). These measurements are used to calculate the ion's mass-to-charge ratio (Wolff and Stephens, 1953). The accuracy of MS analysis to identify any particular protein from a complex mixture can be increased, whilst also retaining the same level of sensitivity and speed, by using MS machines in series. This process is known as tandem mass spectrometry (MS/MS) and involves using a second round of MS to generate a subpopulation of ions from each of the initial ions excited from the sample (McLafferty and Bockhoff, 1978; McLafferty, 1981).

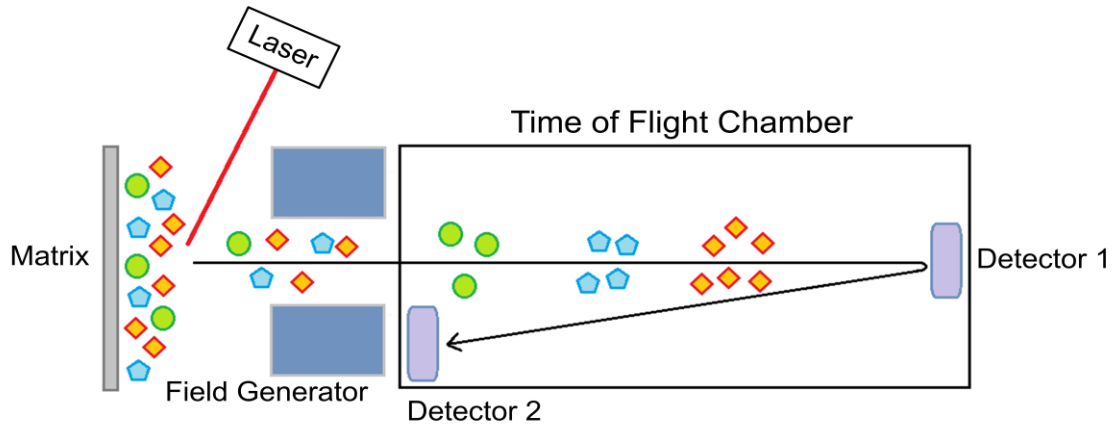

Figure 4.1 Simplified diagram of MALDI MS/MS process. Representations of different molecules contained within the matrix are shown as variously coloured shapes. Following excitation by laser pulses and acceleration from the field generators, the molecules move at different speeds towards the first and second detectors, which then indicates their relative mass to charge ratios.

Samples prepared as part of this project, as well as the internal controls serotransferrin and bovine serum albumin, were analysed by MALDI-MS/MS by the contract research organisation Alphalyse in Denmark. Alphalyse reduced the provided 2D gel electrophoresis spots into individual peptide sequences, concentrated them on a ZipTip micropurification column and deposited onto an anchorship target for analysis using a Bruker Autoflex Speed MALDI TOF/TOF instrument. Partial sequencing was carried out using 15 peptides obtained from the initial reduction of the provided protein material. The mass spectrometry analysis software, Mascot, was then used to compare the resulting data against in house Alphalyse databases compiled from UniProt and NCBI sources. A probability scoring algorithm was then used to identify the most significant non-homologous corresponding protein. The results reported and discussed in this chapter are from their analysis using this process.

4.2 ANO5 knockdown C2C12 generation

In this chapter, a stable ANO5 knockdown C2C12 line was established using ANO5 targeting shRNAs and the effects of ANO5 deficiency at the cellular level characterised using 2D electrophoresis, MALDI MS/MS and western blotting. In the following chapter, results from investigation of ANO5 function as a phospholipid scramblase will be reported using the same generated ANO5 knockdown C2C12 clones.

4.2.1 Cell culture, shRNA transfection and selection

ANO5 specific short hairpin RNAs (shRNA) consisting of a pool of three plasmids, each with different complementary sense and antisense sequences (Table 4.1), were transfected into C2C12 cells to generate an ANO5 knockdown line. Two other separate cultures of C2C12 cells were also transfected with Control shRNA, containing a scrambled sequence, or the GFP construct described in the previous chapter. C2C12 cells were seeded into twelve 100mm tissue culture dishes (5 plates treated with ANO5 shRNA, 5 plates with Control shRNA, 2 plates with GFP) and transfected with shRNA Plasmid Transfection Reagent (sc-108061).

All shRNA plasmids contained puromycin resistance, allowing for selection of transfected clones after 10-12 days treatment with selection media. Selection media was replaced daily and tissue culture dishes were checked for clone formation. GFP cells lacked puromycin resistance and so were used as a selection control. All GFP cells were dead within approximately 3 days post transfection.

Cloning cylinders and trypsin cell dissociation media were used to pick stable clones and transfer them to individual wells of a 24 well plate. A total of 49 clones were picked from dishes (23 clones from ANO5 plates, 26 clones from Control plates). Cells continued to be cultured in selection media, using PBS washes, trypsin dissociation, centrifugation and reseeding cycles to transfer cells to larger tissue culture plates, until cells occupied all wells of 6 well plates. Twenty four clones survived to this stage (14 ANO5 clones, 10 Control clones). Half of the cells of each clone were then resuspended in Cell Recovery Freezing Medium and stored at -80°C, while the other half were seeded into a new 6 well plate for differentiation and RNA extraction. All 24 clones survived selection to the differentiation and RNA extraction phase.

shRNA Name	Hairpin	Sense	Antisense
sc-154403-SHA	GATCCCTGATATGCCA GTTAGTAATTCAAGAG ATTACTAACTGGCATA TCAGTTTTT	CUGAUAUGCCAG UUAGUAAtt	UUACUAACUGGC AUAUCAGtt
sc-154403-SHB	GATCCGAACTATCGTG TTACTGTTTTCAAGAG AAACAGTAACACGATA GTTCTTTTT	GAACUAUCGUGU UACUGUUtt	AACAGUAACACG AUAGUUCtt
sc-154403-SHC	GATCCCATCTGGAGTA GACATATATTCAAGAG ATATATGTCTACTCCA GATGTTTTT	CAUCUGGAGUAG ACAUAUAtt	UAUAUGUCUACU CCAGAUGtt

Table 4.1 Sequences of pooled shRNA used to knockdown ANO5 in C2C12. The "Hairpin" column indicates the sequences of each of the three shRNA's used to knockdown ANO5. The "Sense" and "Antisense" columns indicate the specific sequences used to form the hairpin.

4.2.2 Knockdown validation using differentiation and rt-PCR of selected C2C12 clones

ANO5 expression is upregulated in C2C12 following myogenic differentiation into myotubes but is lowly expressed in undifferentiated C2C12 (Tsutsumi *et al.*, 2005). Therefore to validate the knockdown of the C2C12 cells, RNA was extracted from both Day 0 myoblasts and Day 7 differentiated myotubes for each clone. Upon reaching ~70-80% confluency in each well of a 6 well plate, clones were imaged and half the cells trypsinised, pelleted and stored at -80°C for later Day 0 (D0) time point RNA extraction. The remaining cells were differentiated and imaged at D3, D5 and D7 time points to track differentiation progression. These results show that a total of eight clones from both the ANO5 and Control knockdown C2C12 (four clones in each shRNA condition) form myotubes following 7 days of differentiation (Figure 4.2).

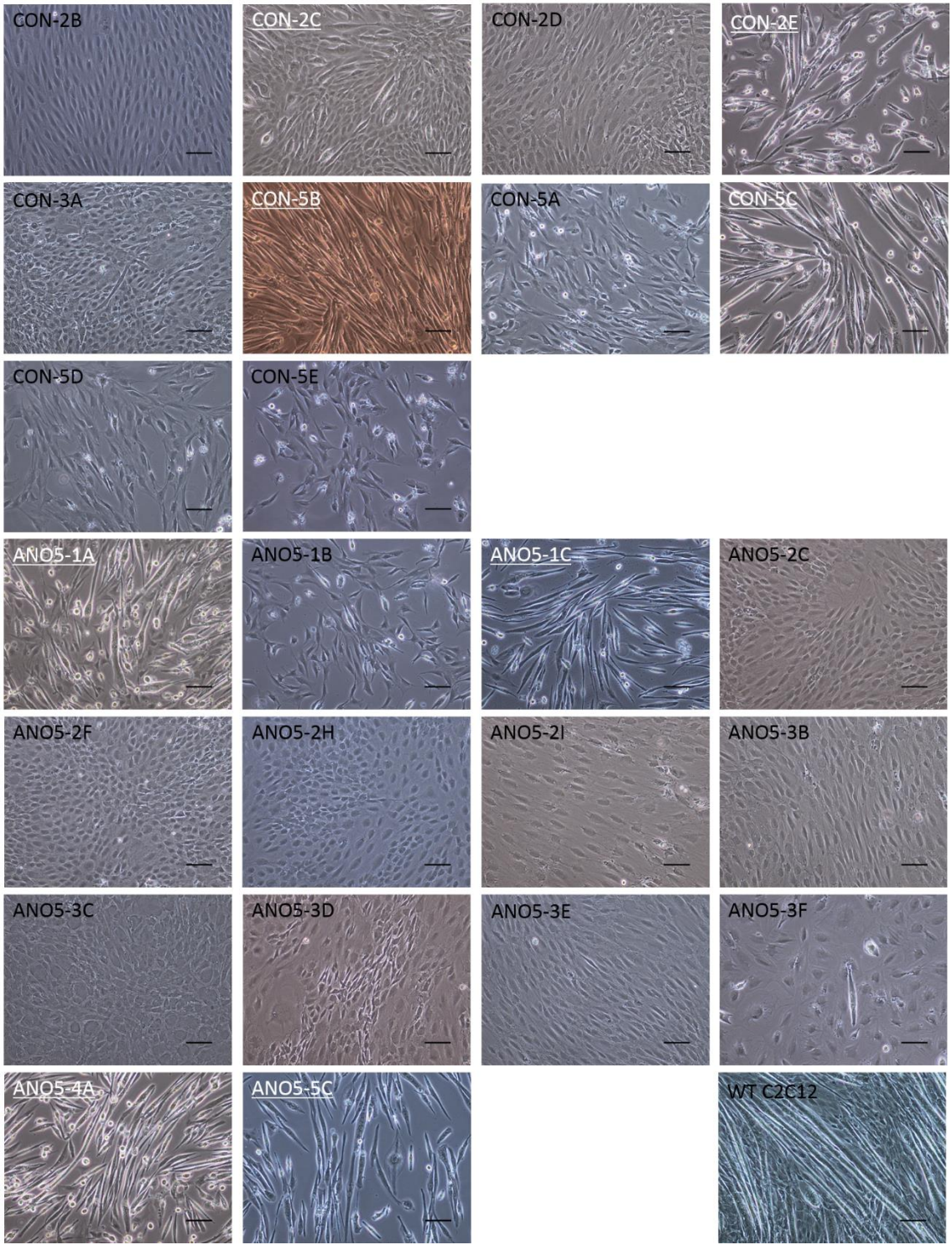

Figure 4.2 D7 time point differentiation of all ANO5 knockdown, Control knockdown and wildtype C2C12 clones. Four clones from each knockdown condition successfully produce myotubes following differentiation, indicated by white underlined labels; Control knockdown clones CON-2C, CON-2E, CON-5B and CON-5C; ANO5 knockdown clones ANO5-1A, ANO5-1C, ANO5-4A and ANO5-5C. All images are taken at x10 magnification (scale bars = 100 um). Biological N = 25. Technical N = 1.

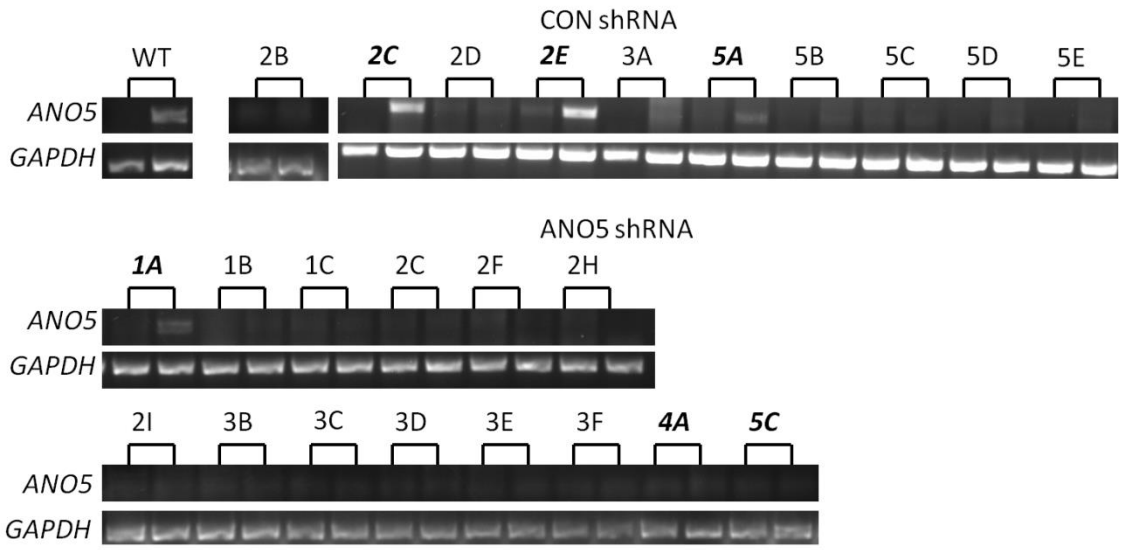

Figure 4.3 Electrophoresis gels of PCR products from undifferentiated and differentiated ANO5 and Control knockdown C2C12 clones. Clone IDs are indicated above each pair of PCR product; D0 samples in the first lane of each pair and D7 samples in the second lane. Bold and italicised clone IDs indicate ANO5 and Control knockdown clones chosen for future experimentation. Due to primer design, all bands are ~500bp in size. Biological N = 25. Technical N = 1.

At the D7 time point, cells were trypsinised, pelleted and stored at -80°C for RNA extraction using Trizol. Paint Pellet was used to assist in recovery of the RNA pellet during isopropanol precipitation. The RNA pellet was resuspended in 30 µl nuclease free water before quantification using a Nanodrop and cDNA synthesis in a LabCycler PCR machine. Generated cDNA was then amplified using ANO5 and GAPDH primers in a standard PCR reaction and visualised on 1% agarose gel under a BioSpectrum Gel Doc-It (Figure 4.3).

GAPDH controls run for each cDNA produced bands of the expected size (~500bp) in each clone and at each time point (Figure 4.3). This confirms that the cDNA for each time point sample had not been degraded and that the reverse transcription reaction was successful. PCR of the cDNA generated from the RNA of the D0 time point showed that, as expected, no bands appeared at this time point in any clone for either ANO5 or Control shRNA treatment. The D7 time point of three Control clones produced bands of the expected size (~500bp) suggesting that these were stable clones with no knockdown (Figure 4.3). These clones have therefore been selected as controls for future experimentation. Apart from a single clone (designated ANO5-1A), no bands were visible for the D7 time points for the ANO5 knockdown clones. This suggests that these

clones were successful stable ANO5 knockdown clones. The very faint band at the D7 time point for ANO5-1A suggests that it is a potential partial knockdown clone (Figure 4.3).

However, during differentiation series both ANO5 and Control myoblasts differentiated poorly, forming very few myotubes or none at all (Figure 4.4). This is either due to the effects of prolonged selection pressure on the myoblasts or due to a loss of differentiation ability in the initial stock of C2C12 myoblasts before the knockdown process began. In either case, the three ANO5 knockdown C2C12 clones which showed the best differentiation were chosen for further functional experimentation (Figure 4.4). As a result ANO5-1A was also included in later experimentation.

The aim of this process was to generate a cellular knockdown model which closely replicated anoctaminopathy patient myoblasts as much as possible. However, the inconsistencies in differentiation ability of the generated myoblasts meant that further organelle fractionation, proteomics and functional experimentation would be carried out on undifferentiated myoblasts rather than myotubes. By doing so though, inherent differences seen between differentiating, proliferating and repair committed muscle cell populations can be avoided (Meola *et al.*, 1991; Gross and Rotwein, 2013). For example, it has been shown that the terminal function of satellite cells (Mauro, 1961), muscle specific stem cells which assist in repairing damaged tissue (Partridge *et al.*, 1978), are strongly influenced by factors influencing the parent population (Gross and Rotwein, 2013). While the clones generated as part of this project will not exactly replicate patient systems, the shared linage and consistent treatment of the clones should increase the validity of observed results.

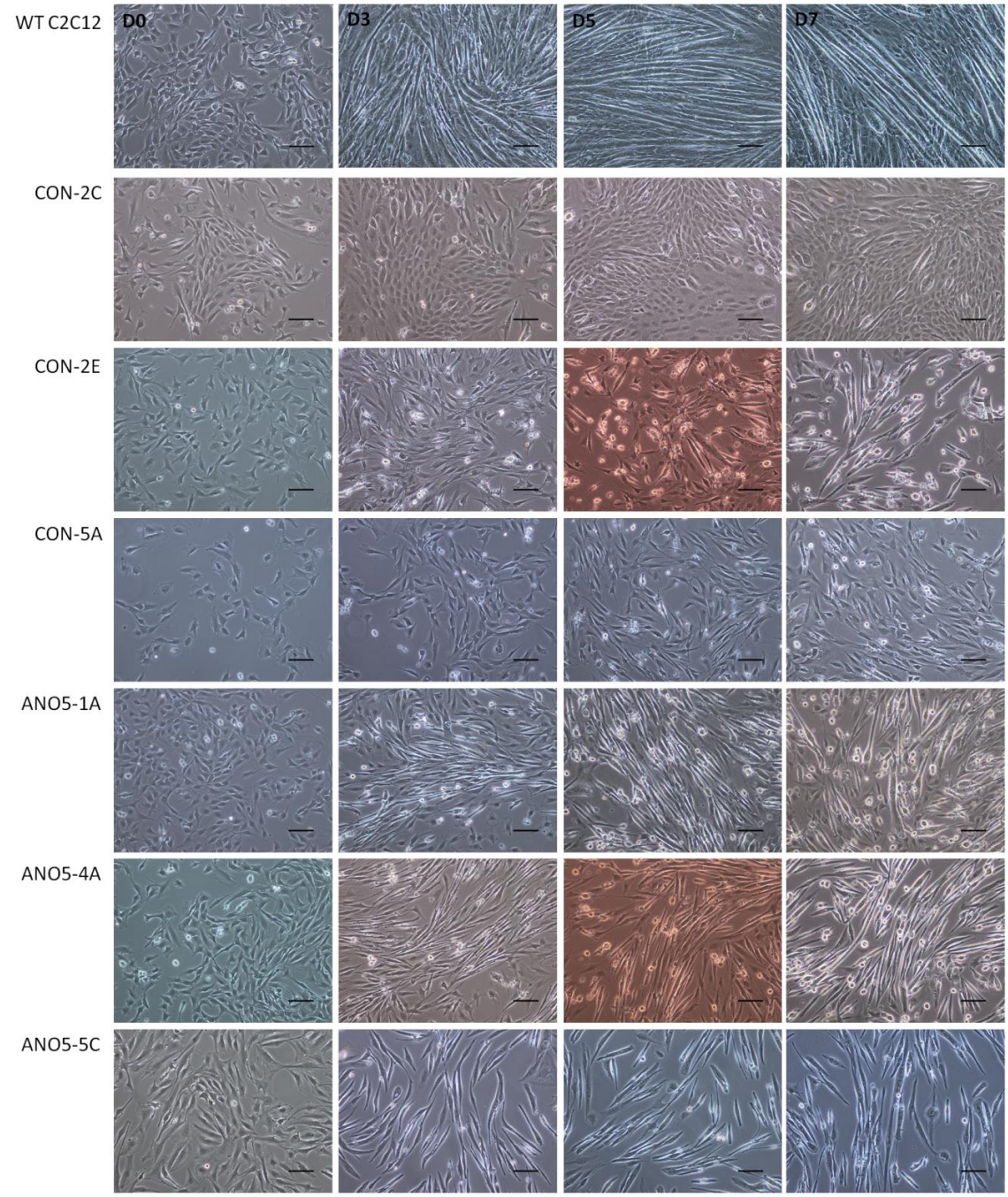

Figure 4.4 Differentiation series of selected ANO5 knockdown, Control knockdown and wild type C2C12. Columns from left to right show representative micrographs of C2C12 differentiation progression (undifferentiated, D3, D5 and D7 time points). All images are taken at x10 magnification (scale bars = 100 um). Biological N = 7. Technical N = 1.

4.3 Subcellular fractionation by differential centrifugation of ANO5 and Control knockdown C2C12

To reduce the complexity of the protein extracts when comparing spots between gels, crude subcellular fractionation was first applied to C2C12 lysates to separate the cellular components into nuclear, mitochondrial and cytoplasmic fractions. The subcellular fractionation protocol developed by Dimauro *et al.* (2012) (Section 2.7.2, Figure 2.2) was used for these experiments. This protocol relies on the differential sedimentation times of the various compartments during ultra-centrifugation in density media to separate proteins into nuclear, mitochondrial and cytoplasmic subcellular fractions. STM buffer was used throughout the protocol rather than detergent based lysis buffers, to reduce degradation to the proteins. For simplicity, ANO5-4A and CON-2C knockdown clones were chosen for 2D gel analysis comparison as these clones grew well in culture, differentiated well and were confirmed to be ANO5 negative and positive by rt-PCR respectively.

4.3.1 2D gel electrophoresis

The three fractionated lysates made using this crude subcellular fractionation (mitochondrial, nuclear and cytoplasmic) were run out using 2 dimensional (2D) electrophoresis using the ZOOM runner IPG system. To minimise experimental variability, each first dimension IPG strip was run at the same time, while second dimension ZOOM gels were prepared and run in pairs of one knockdown and one control sample before subsequent Coomassie staining and visualisation.

4.3.2 Visualisation of protein spots

Coomassie stained 2D gels were imaged using an Odyssey CLx. Test images were taken to ensure the gels were fully within the scanning area of the Odyssey before scanning in the 700 nm spectrum. This spectrum was used at it would accurately detect the blue dye of the Coomassie staining.

The results of these gels show that the subcellular fractionation protocol does reduce the complexity of the proteins present in each lysate (Figure 4.5). The mitochondrial fraction shows the fewest protein spots, with just over ten spots visible on the scanned image of the gel. The majority of these spots are between 36.5 and 97.4 kDa in weight but are spread across the pH gradient of the IPG strip. Both the nuclear and the cytocolic fractions show more protein spots, across a much wider range of molecular weights. Interestingly though, in the nuclear fraction, a clear stopping point for the proteins appears just over halfway across the IPG strip, visible as protein spots all congregating at roughly the same place vertically in the gel at all molecular weights. While the precise pH of the strip at this point is not known, as each IPG strip was always orientated in the same direction in the ZOOM gel, this is the end that moved towards the cathode and is therefore the more acidic end of the IPG strip (pH 8-10). No protein spots are found past this line suggesting that either no proteins in this fraction are found at high pH or that more likely, that none are able to pass the proteins that have migrated to this point. It is possible a barrier of, for example, DNA or polysaccharides has formed at this particular pH. Both can clog the gel pores and effect the overall success of IEF at the acidic end of the gel (Berkelman, 2008).

Of the three lysates the cytoplasmic fraction retains the majority of protein spots. These spots are clearly distinguishable from one another though there are a range of intensities among the spots indicating that some proteins differ in their expression levels within the

cytoplasmic fraction of wild type C2C12. Furthermore there are several examples of bright spots located very close to one another along a horizontal axis, appearing almost like a string. These spots all have very similar molecular weights but have different isoelectric points. These spots are likely phosphorylated forms of the same protein or isoforms of the same protein. The molecular differences between phosphorylated proteins mean that on a 2D gel they might appear with the same molecular weight but different isoelectric points, such as those seen in these gels.

As anoctamin 5 has been suggested to localise to the ER in the literature (Tsutsumi *et al.*, 2004; Mizuta *et al.*, 2007) as well as ER and t-tubules in earlier localisation experiments, only the cytosolic fraction was used to investigate spot differences between ANO5 knockdown and Control knockdown C2C12 lysates.

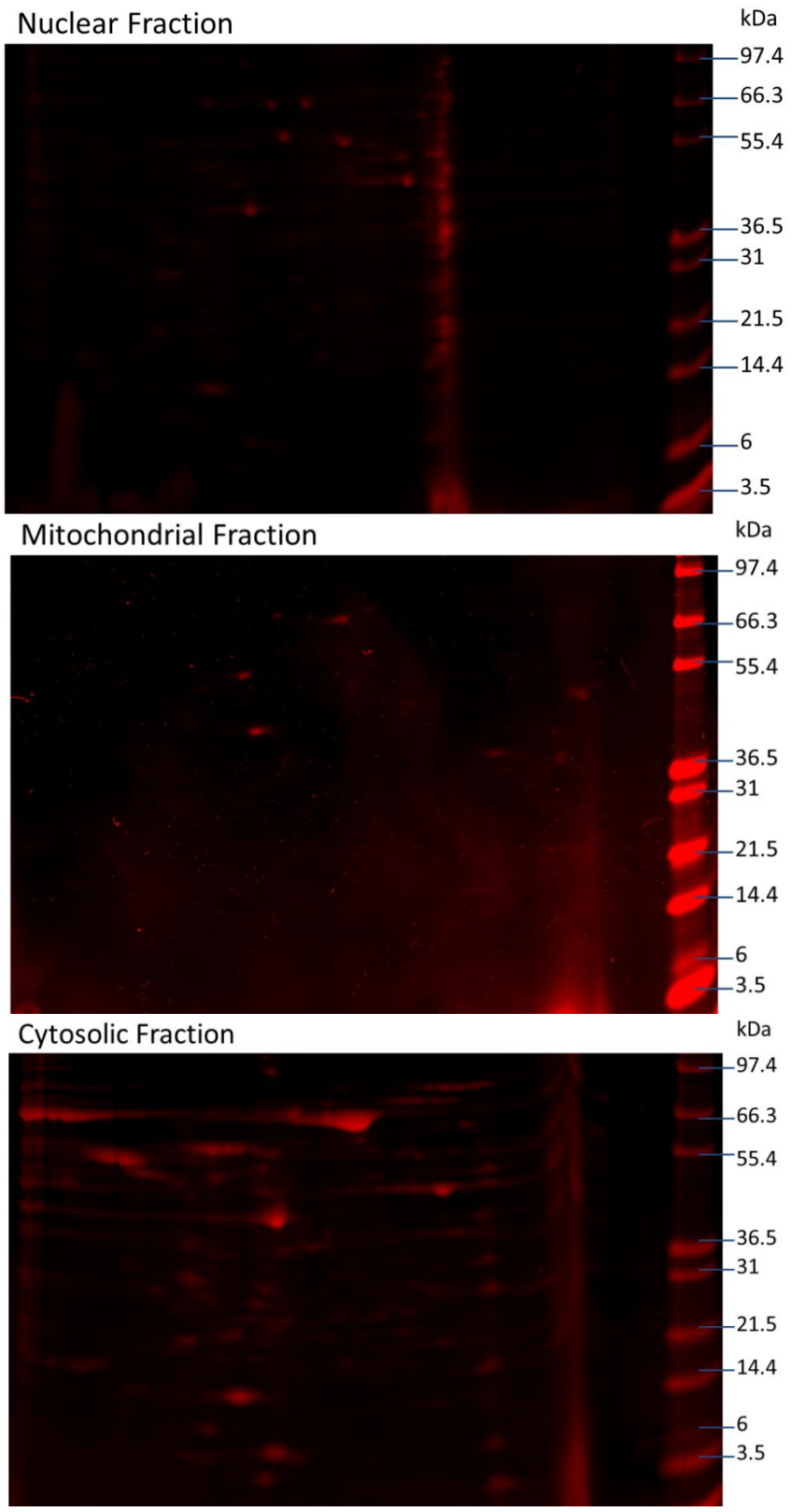

Figure 4.5 Coomassie stained 2D gels of nuclear, mitochondrial and cytosolic subcellular fractions of wild type C2C12. The streaking of spots seen on the right hand side of the cytosolic fraction were caused by an air bubble between the IPG strip and the gel and are not replicated on subsequent gels run with the same lysate fraction. Gels were Coomassie stained and then imaged in the 700nm fluorescence range on a Li-Cor Odyssey CLx infrared imaging system. Biological N = 3. Technical N = 1.

4.4 2D gel electrophoresis of ANO5 knockdown, Control knockdown and wild type C2C12 cytosolic fractions

Triplicate 2DE gels of ANO5-4A and CON-2C lysates were run to accurately confirm differences in the spot populations of gels. Biological, experimental and analytical variability inherently exist within 2DE experimentation and several steps were taken to limit the effect of this variability in these experiments (Choe and Lee, 2003; Zhan and Desiderio, 2003; Bland *et al.*, 2006; Bland *et al.*, 2010). For example, to reduce biological variability enough lysate was fractionated and prepared at the same time to run multiple gels from each lysate. To reduce experimental variability, IEF of IPG strips, SDS PAGE runs of the second dimension and staining steps were run concurrently on samples.

No spot identification software was used to identify spot differences; instead gels were compared side by side and differences in the gels noticed by eye. Comparison by eye was achieved by comparing "constellations" of spots for similarities in patterns. For this, spots with consistent locations across all the replicate gels were used as points from which to check the other spot locations in each gel.

Four spot differences were consistently identified in all three gel replicates (Figure 4.6). Spots labelled as A, B and C, were identified as having increased intensity on the ANO5 knockdown C2C12 lysate while spot D was absent from the ANO5 knockdown gel. These spot differences were found at different molecular weights and pH ranges, though three of them (indicated by arrows A, B and D) were located on the side of the gel nearest the ladder, indicating that they were within the more acidic pH range of the IPG strip. Spot A is ~37 kDa, spot B is 2~3 kDa, spot C is ~56 kDa and spot D is ~7kDa. Spot C is present as several spots along the horizontal axis suggesting that this protein may be phosphorylated or post-translationally modified in some way. It is the only identified spot to show this patterning.

A fourth gel was then run for each cell line for excision of the corresponding spots for MALDI MS/MS. The three spots consistently identified as present or absent on the ANO5 knockdown C2C12 gels (spots A, B and D), along with an additional control spot consistently present on both gels (spot E), were excised from 2-D gels and sent to Alphalyse in Denmark for MALDI MS/MS analysis.

However the fourth spot identified in the triplicate gels (spot C) was not present on the fourth ANO5 knockdown lysate gel and so could not be sent for mass spectrometry analysis and identification. An error in experimental reproducibility may be an explanation for the disappearance of this spot. While the first triplicate gels were all prepared at the same time (i.e. the IPG strips all run through IEF first dimension at the same time) the fourth set of gels were prepared separately. It is unlikely to be an error in biological reproducibility as for each cell line, the fourth gel was from the same biological replicate as the third gel.

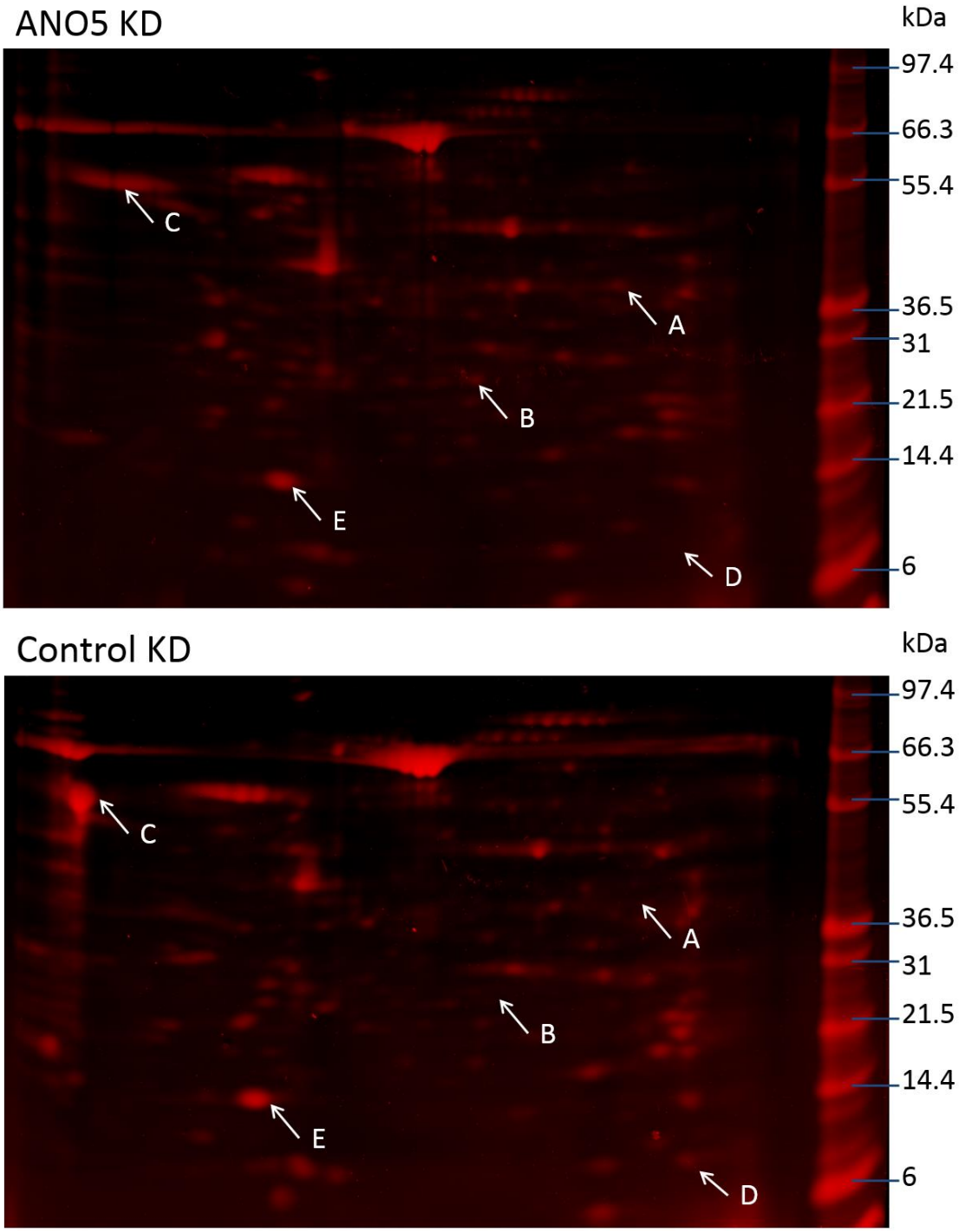

Figure 4.6 Coomassie stained 2D gels of cytosolic fractions of ANO5 and Control knockdown C2C12. Lettered arrows indicate protein spots consistently identified as differentially expressed between replicate gels, except for E which is a control spot which was consistently unchanged across replicates. Both gels shown are the third replicates of triplicate gels run for each knockdown C2C12 line. Gels were Coomassie stained and then imaged in the 700nm fluorescence range on a Li-Cor Odyssey CLx infrared imaging system. Biological N = 2. Technical N = 4.

4.5 MALDI-MS/MS identification and western blot validation of protein spot differences

4.5.1 Alphalyse MALDI MS/MS analysis

Spots identified with consistent differences in intensity between Control and ANO5 knockdown gels were excised from Coomassie stained 2DE gels run using the method described in Section 2.9, only with the addition of being carried out in a Safelab Systems class 1 fume hood, to reduce the collection of contaminants on the gel. Spots excised from these gels were collected into separate Eppendorf tubes and treated with 500µl of distilled deionised water to keep the samples hydrated during shipping. Samples were then sent to the contract research organisation Alphalyse in Denmark for MALDI MS/MS analysis.

Alphalyse identified the spots as Annexin A2 (ANXA2, spot A), Heat shock protein beta 1 (Hsp27 spot B) and S100-A4 protein (S100-A4, spot D) (Table 4.2). The control spot from both gels also sent for analysis was identified as Galectin-1 in both cases (spot E). The majority of the molecular weights of these identified proteins are consistent with the sizes of the spots from the gels (ANXA2 = 38 kDa, Hsp27 = 23 kDa, S100-A4 = 7 kDa), though Galectin-1 has a larger predicted molecular weight than that observed on the gel (predicted molecular weight = 15 kDa, observed molecular weight ~14 kDa).

Additionally, there is a range in the sequence coverage ("Seq.cov") and "Scores" values between each of the identified proteins. The "Seq.cov" values are the percentage of coverage achieved by the sample sequence when compared against the identified protein in the databases. These values are not used to confirm protein identity but rather are used as internal controls. The "Scores" value, or Mascot Score, for a protein is the logarithmic, statistically significant score for how well the peptides identified in the supplied protein spot match with the peptides in the comparison database. A mascot score of more than 90 indicates that, when compared to the nrbd protein database from NCBI, the confidence that the protein has been positively identified is above 95% significance and so can be positively identified as that protein.

The protein with the lowest significance score is S100-A4 (Score = 188). However as the percentage sequence coverage (Seq. cov. = 25%) is greater than the sequence coverage of BSA (Seq. cov. = 24%), one of the internal control samples, and as the

significance score is still well above the level of significance allowed by Alphalyse, it can still be assumed that S100-A4 is the most likely protein identity for spot 3.

The protein with highest significance score and the highest sequence coverage is ANXA2 (Score = 570, Seq. cov = 57%) and so this spot is assumed to be the identified protein.

Hsp27 has a fairly high percentage sequence coverage (Seq. cov. = 53%) but has the second lowest significance score of all the identified proteins (Score = 252). Again though, this is well above the significance scores allowed by Alphalyse and so is the most likely protein identifiable using this identification method.

Sample Name	**Protein found in Database**	**Gene Name**	**Calculated MW**	**Score**	**Seq. cov.**
AB2-A	Annexin A2	Anxa2	38937	570	57%
AB2-B	Heat shock protein beta-1	Hspb1	23057	252	53%
AB2-E	Galectin-1	Lgals1	15198	473	55%
CB2-D	Protein S100-A4	S100a4	11942	188	25%
CB2-E	Galectin-1	Lgals1	15198	327	55%
1pmol transferrin	Serotransferrin	TF	79294	929	51%
62 fmol BSA	Serum albumin	ALB	71244	479	24%

Table 4.2 Proteins identified by MALDI MS/MS analysis by Alphalyse. "Sample name" refers to the name of sample provided to Alphalyse; AB2 or CB2 refers to the gel while the final letter indicates the specific excised spot. "Protein found in database" refers to the details of protein in SwissProt database identified by MALDI MS/MS. "Gene Name" refers to the name of the gene for the protein as found entered on the SwissProt database. "Calculated MW" refers to the molecular weight. "Score" refers to the Mascot Score, the logarithmic, statistically significant score for how well the peptides identified in the supplied protein spot match with the peptides in the comparison database. A mascot score of more than 90 indicates that, when compared to the nrbd protein database from NCBI, the confidence that the protein has been positively identified is above 95% significance. "Seq. cov." refers to the percentage of peptide sequence which matches to sequence found in SwissProt database.

4.5.2 2D gel western blot confirmation of MS/MS identified proteins

To confirm that spots A, B and D were the proteins identified by MALDI MS/MS, triplicate 2D western blots were carried out using the standard 2D Gel Electrophoresis protocol described in Section 2.9 with the addition of protein transfer and immunoblotting (Sections 2.10.3 and 2.10.4) following SDS PAGE. Antibodies specific for ANXA2 (ab41803), Hsp27 (ab2790) and S100-A4 (ab93283) were used to probe western blots of 2D gels run with the same ANO5 knockdown and Control knockdown cytosolic fraction lysates (Figure 4.7, Figure 4.8 and Figure 4.9). Anti-GAPDH antibodies (D16H11 and ab8245) were used as positive loading controls in these experiments.

ANO5 knockdown and Control knockdown blots probed with Hsp27 and S100-A4 are negative for both proteins (Figure 4.7 and Figure 4.8 respectively). Initially this was thought to be because of a low abundance of the proteins on the gel and so the images were overexposed in an attempt to visualise any lowly expressed spots. However, no other spots could be visualised on these blots in this fluorescence channel. Positive detection of GAPDH on Hsp27 and S100-A4 blots confirmed that it was the Hsp27 and S100-A4 antibodies that were failing to detect the specific proteins rather than degradation of the lysates or failure of the transfer during the blotting procedure.

Western blotting using the ANXA2 antibody was successful as several spots are visualised with this antibody (Figure 4.9). Furthermore there is a difference in the spot patterns between the blots for the ANO5 knockdown and Control knockdown lysates. In both knockdown and Control blots there is a spot with a molecular weight of approximately 38 kDa (arrow 1), consistent with the molecular weight of ANXA2 and the position of the spot sent to Alphalyse for identification. In the ANO5 knockdown lysate blot this spot has an increased intensity compared to the corresponding spot in the Control knockdown blot (Figure 4.9).

Probing both knockdown and Control blots with the ANXA2 antibody revealed two additional spots; one at approximately 50kDa (arrow 2) and the other at approximately 16 kDa (arrow 3). However both of these spots have a much smaller expression in the ANO5 knockdown blots than the corresponding spots in the control knockdown blot. In the case of the heavier spot (arrow 2) on the ANO5 knockdown blot, it is very faint (and on one of the triplicate blots, it was completely absent). The lighter spot (arrow 3) on

the Control knockdown covers a wide pH range while it occupies a restricted range on the ANO5 knockdown blot.

These differences in spot intensities were consistently observed across triplicate blots. The precise identities of these additional spots are not known, but given that they are detected by the ANXA2 antibody, they may potentially be modified versions of ANXA2. These results ultimately suggest though that the knockdown of anoctamin 5 in C2C12 affects the expression of annexin A2.

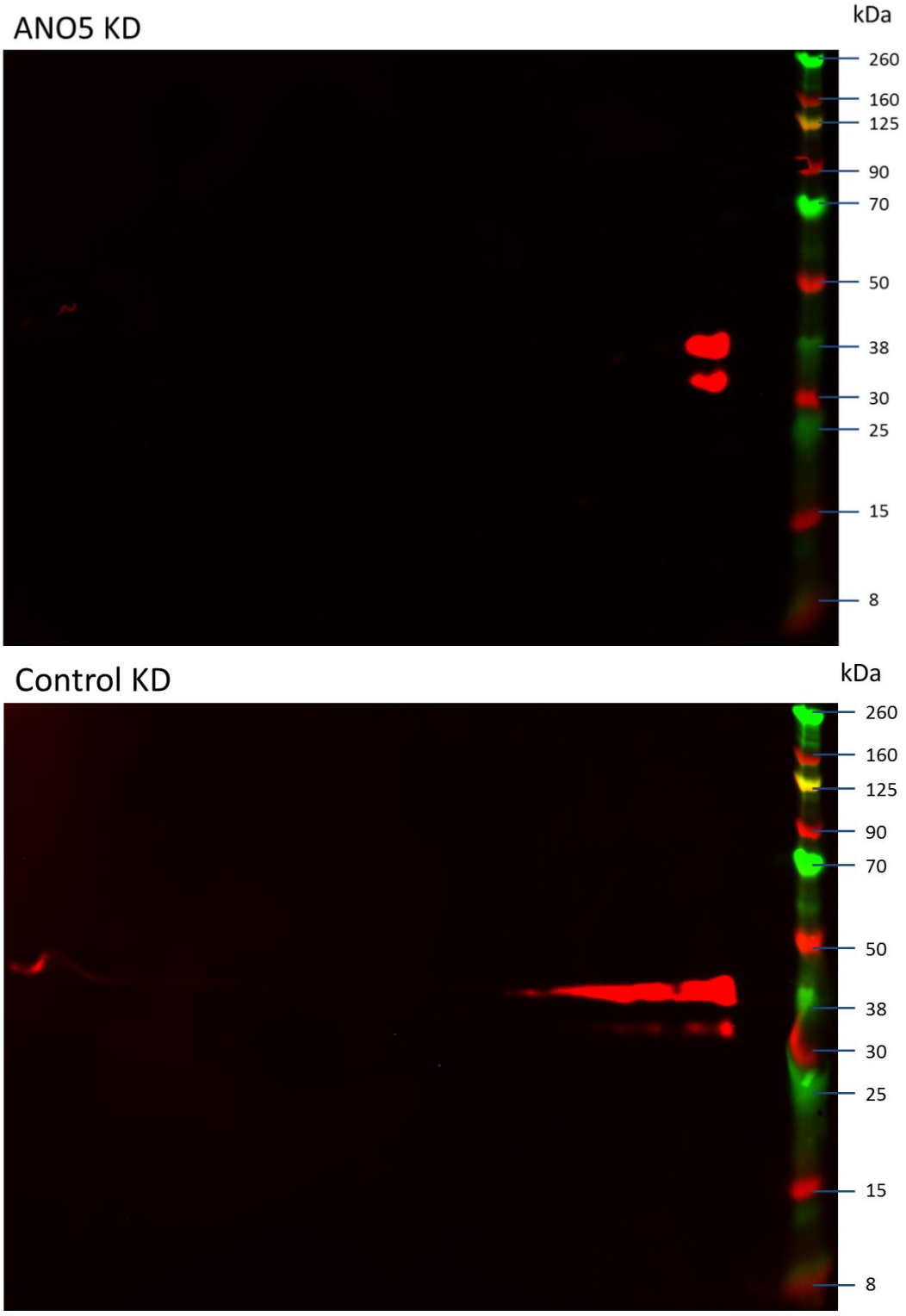

Figure 4.7 2D gel western blots of ANO5 and Control knockdown C2C12 probed with Hsp27 and GAPDH antibodies. No green fluorescence is observed in either blot suggesting that the Hsp27 antibody is unable to detect the protein in these blots. Red fluorescence across the gel between 30-38 kDa indicates positive GAPDH staining. Blots were imaged in both the 700nm and 800nm fluorescence range on a Li-Cor Odyssey CLx infrared imaging system. Biological N = 2. Technical N = 1.

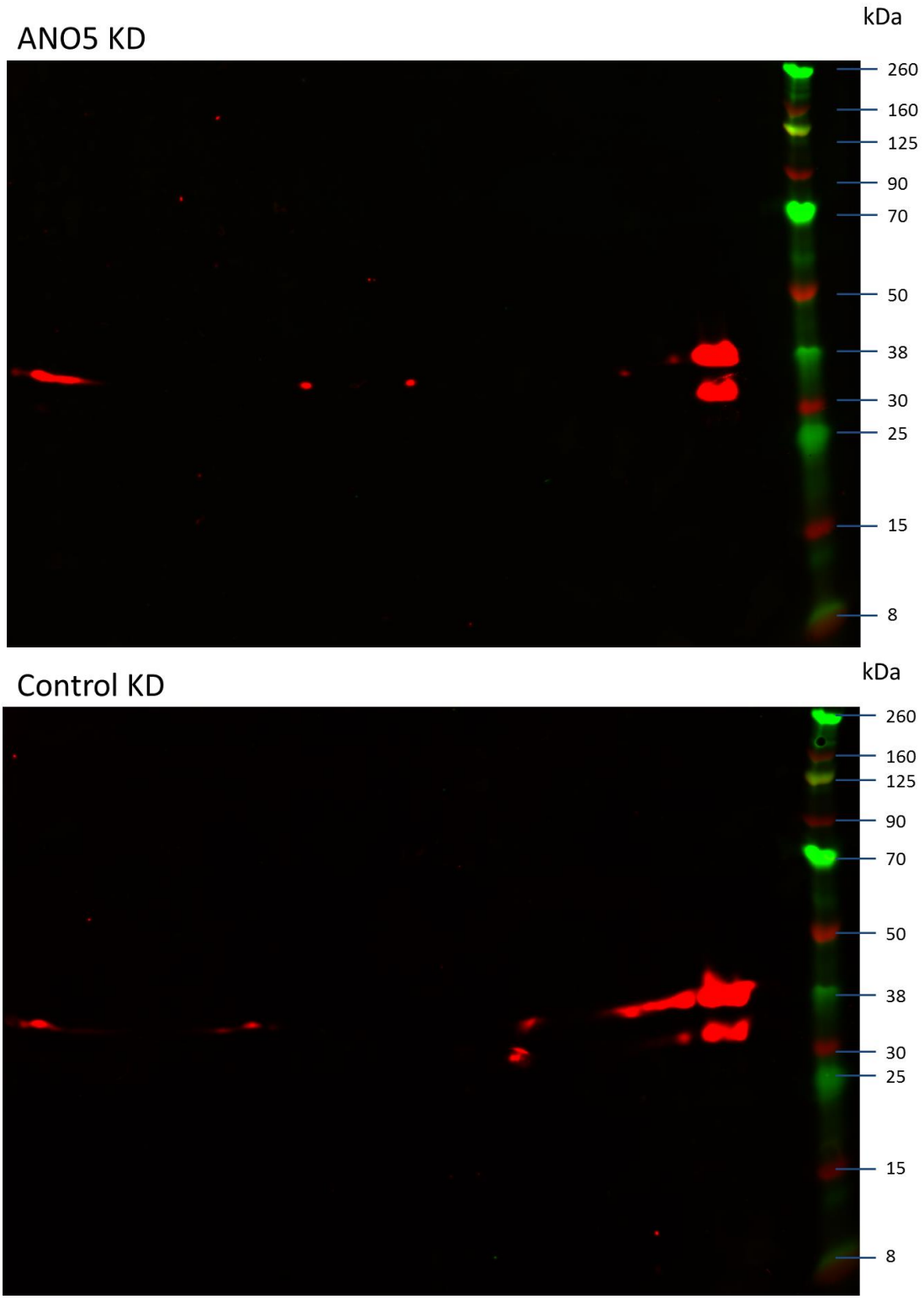

Figure 4.8 2D gel western blots of ANO5 and Control knockdown C2C12 probed with S100-A4 and GAPDH antibodies. No green fluorescence is observed in either blot suggesting that the S100-A4 antibody is unable to detect the protein in these blots. Red fluorescence across the gel between 30-38 kDa indicates positive GAPDH staining. Blots were imaged in both the 700nm and 800nm fluorescence range on a Li-Cor Odyssey CLx infrared imaging system. Biological N = 2. Technical N = 1.

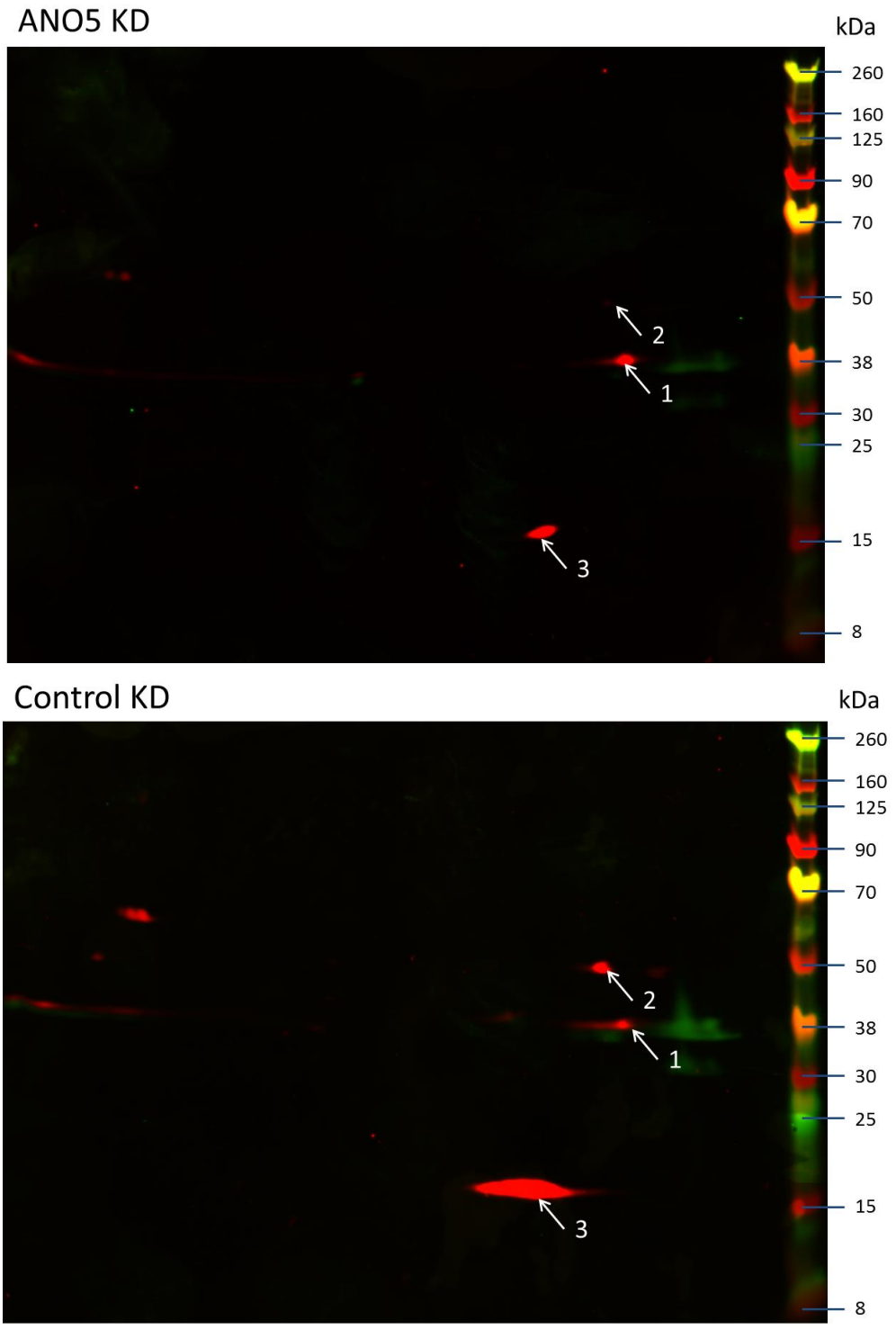

Figure 4.9 2D gel western blots of ANO5 and Control knockdown C2C12 probed with ANXA2 and GAPDH antibodies. Arrow 1 indicates the ANXA2 spot previously identified by MALDI MS/MS. Arrows 2&3 are unidentified spots consistently stained by the ANXA2 antibody across triplicate 2D gel western blots. Both spots are either diminished in intensity or entirely absent from ANO5 blots compared to the Controls. Green fluorescence across the gel between 30-38 kDa indicates positive GAPDH staining. Blots were imaged in both the 700nm and 800nm fluorescence range on a Li-Cor Odyssey CLx infrared imaging system. Biological N = 2. Technical N = 3.

4.6 Western Blot investigation of identified spot proteins

To further investigate the absence of Hsp27 and S100-A4 spots from the 2D gel western blots, SDS-PAGE western blotting was performed using lysates prepared in different buffers. The mini Bradford assay was used to first quantify protein concentration of lysates used for western blots. This protein quantification method was chosen to account for the high concentrations of urea in the solubilisation solution used to prepare the lysates for 2D electrophoresis.

4.6.1 SDS-PAGE

Hand poured, 15% gels (Section 2.10.1) were used to detect S100-A4 as the low molecular weight of the protein makes detection difficult on standard Bis-Tris gels. Hsp27 and Anti-GAPDH, again used as a positive loading control, were run on precast 4-12% Bis-Tris gels. These western blots show that the antibodies do detect bands but that these bands are either the wrong molecular weight (Hsp27) or are only detected in specific lysis buffers (S100-A4) (Figure 4.10).

The Hsp27 antibody detects a single band in all lysates of approximately 62 kDa, though the predicted size of Hsp27 is 23 kDa. The S100-A4 antibody detects bands of the correct size (12 kDa) but only in cytosolic fraction lysates suspended in STM buffer. Lysates prepared in Buffer A, an essential requirement for successful IEF in 2D gels, do not show bands. This suggests that the failure to detect spots using the S100-A4 antibody may be due to the protein being altered by Buffer A during lysis in such a way as to make it undetectable.

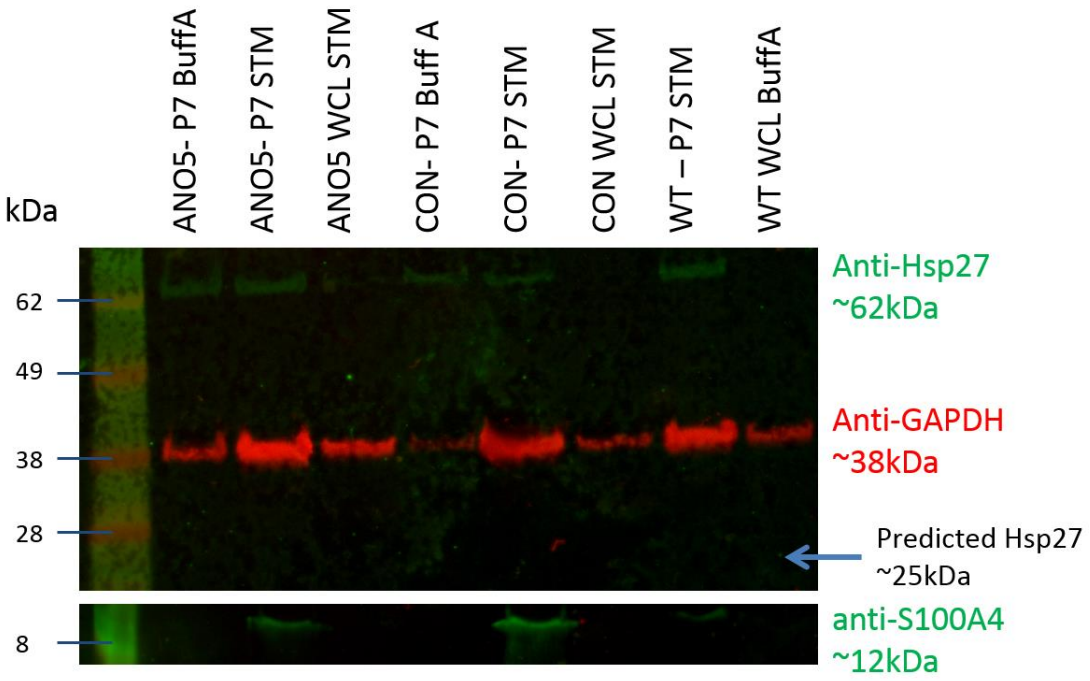

Figure 4.10 Western blot of cytosolic and whole cell knockdown and wild type C2C12 lysates probed with Hsp27, S100-A4 and GAPDH antibodies. The arrow indicates approximately 25 kDa, the predicted size of Hsp27 and where bands were expected to be detected. To resolve the smaller S100-A4 protein the lower image displaying the S100-A4 bands are from a 15% gel. Blots were imaged in both the 700nm (red) and 800nm (green) fluorescence range on a Li-Cor Odyssey CLx infrared imaging system. Biological N = 8. Technical N = 1.

Conversely, SDS-PAGE investigation of ANXA2 showed that differences in lysate preparation did not hinder this antibodies ability to detect the expected 38 kDa band in any lysate sample (Figure 4.11). Rather, the antibody detected multiple bands in all lysate preparations. The majority of these bands are not found on the 2D gels suggesting that these forms of ANXA2 do not migrate on the IPG during IEF. The spots that are present on the 2D gels are found in the bands of this western blot, though the intensities of the bands do not replicate the differences of the spot intensities seen in the 2D gels.

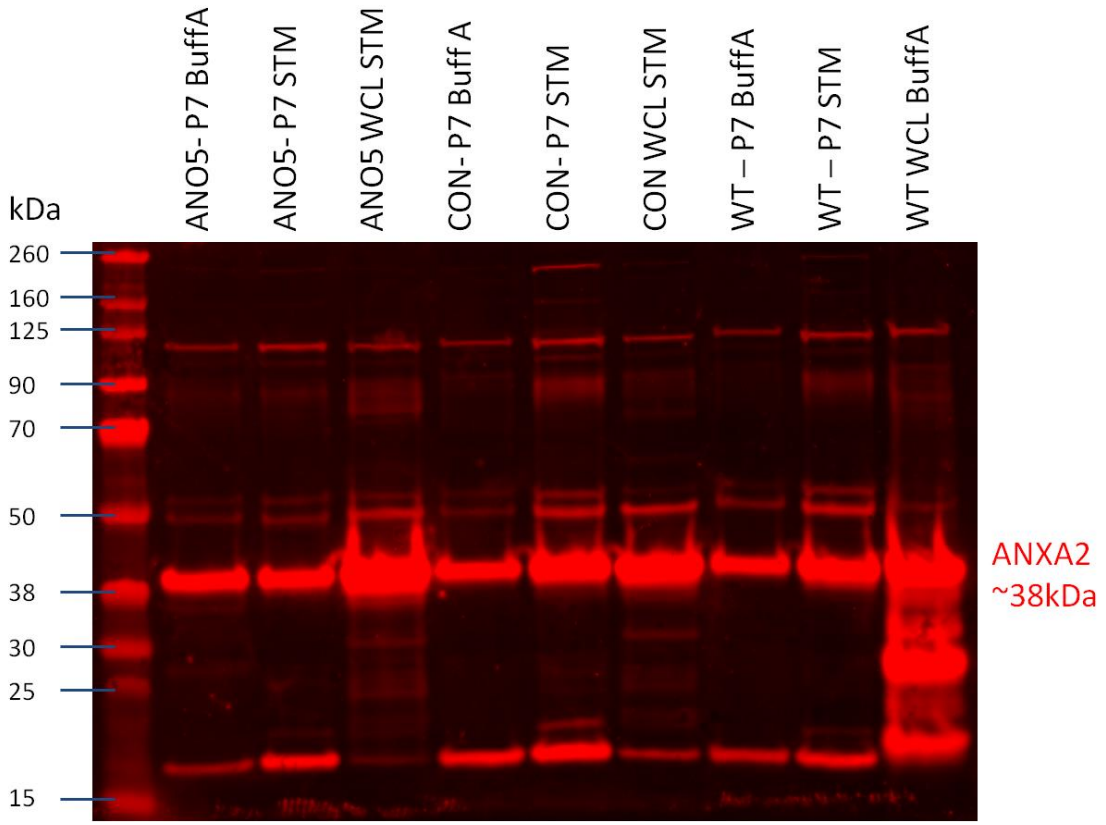

Figure 4.11 Western Blot of cytosolic and whole cell knockdown and wild type C2C12 lysates probed with ANXA2 antibody. A band at ~38 kDa, the expected molecular weight of ANXA2, is observed in all samples. Multiple other bands are also detected by the antibody though these are consistent between samples. Blot imaged in the 700nm (red) fluorescence range on a Li-Cor Odyssey CLx infrared imaging system. Biological N = 9. Technical N = 1.

4.7 Further investigation of identified proteins affected by ANO5 knockdown

ANXA2 is expressed in several tissues and is known to form a heterotetrameric structure with S100-A10 (Bharadwaj *et al.*, 2013). In this structure, two ANXA2 proteins link to opposite sides of two S100-A10 proteins bound around a calcium molecule (Lewit-Bentley *et al.*, 2000). One of the proposed functions of this heterotetramer is membrane fusion. It has been suggested that monomeric ANXA2 proteins which are located within plasma membranes of opposing cellular vesicles or organelles are brought together via two S100-A10 proteins as a central anchor point (Rety *et al.*, 1999). An additional feature of the resulting heterotetrameric structure is that it also increases the stability of S100-A10, preventing it from being disposed of via ubiquitin-mediated degradation (He *et al.*, 2008).

Several other annexins are also closely linked to other S100 proteins, for example ANXA1 and S100-A11 (Rety *et al.*, 2000). Given the apparent relationship between annexins and S100 proteins, it is intriguing that two of these proteins are potentially altered in the cytosol of C2C12 cells when ANO5 is knocked down.

4.7.1 Investigation of ANXA2 and S100-A4 colocalisation in wild type C2C12

Colocalisation of ANXA2 and S100-A4 was investigated in wild type C2C12 using immunofluorescence staining to identify any potential link between the two proteins (Figure 4.12).

These staining data show that the antibody directed against ANXA2 detects filamentous like structures running through the centre of C2C12 cells, including running through the nucleus of the cell (Figure 4.12 A., B. and E.). Other C2C12 which don't show these filamentous structures do still show some potential ANXA2 positivity in their nucleus, observed as purple signal in merged images of red (ANXA2) and blue (DAPI) fluorescence channels. This signal is however much fainter and may potentially be background produced by unspecific binding of the antibody.

Very few C2C12 cells appear to be S100-A4-positive and only because “positive” cells had a marginally brighter green fluorescence than surrounding C2C12 (Figure 4.12). The pattern of staining is diffuse throughout the entire cytoplasm of the cell, with no clearly identifiable structures or organelle populations. From this pattern of staining it was concluded that this was background staining due to unspecific binding and that this

antibody could not sufficiently detect S100-A4 in immunofluorescence experiments. Furthermore, due to this insufficient detection, accurate co-localisation with ANXA2 was not possible.

The possibility of additional background due to co-staining with both antibodies was ruled out by running conditions which used both secondary antibodies but only one of the primary antibodies.

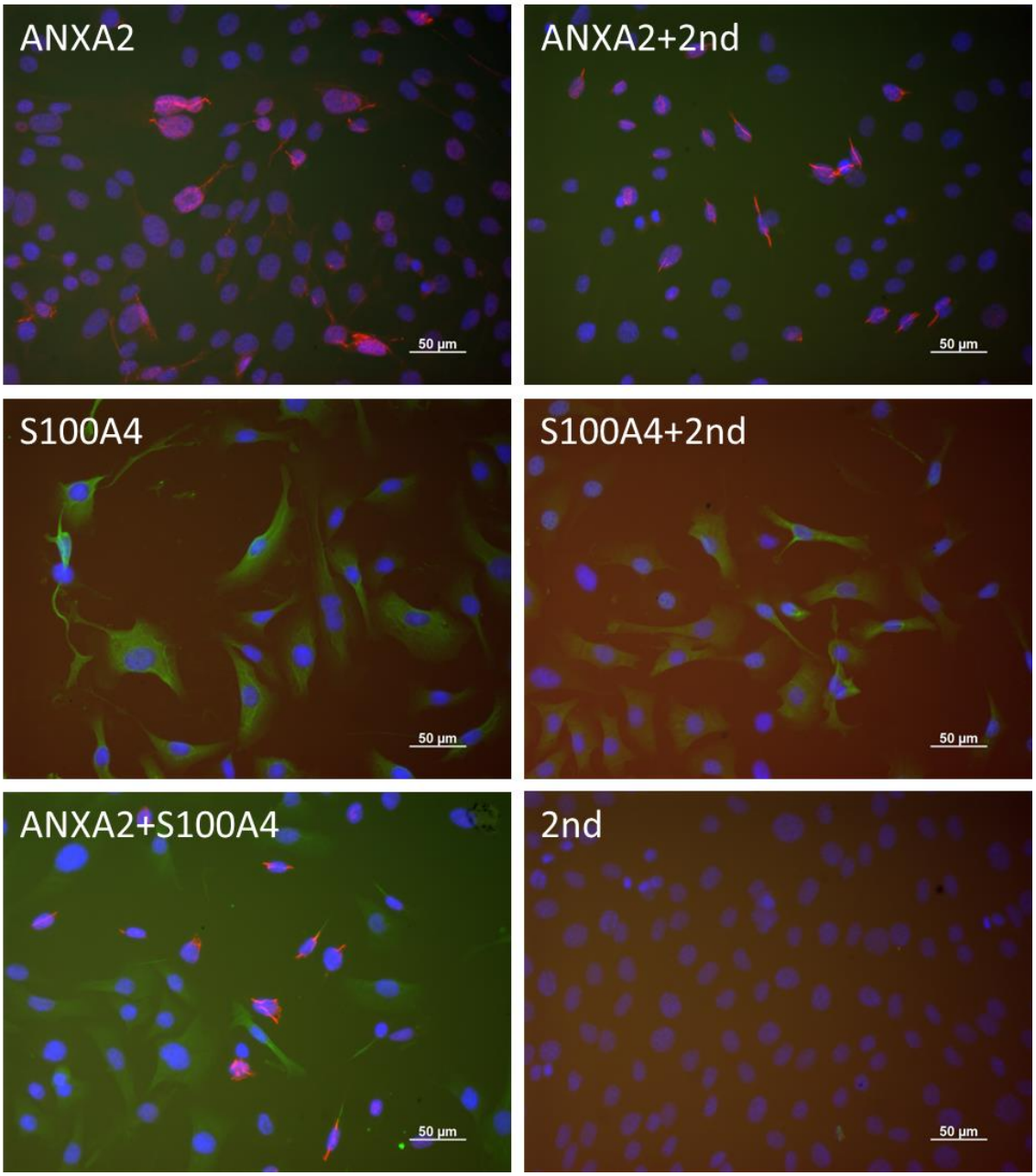

Figure 4.12 Co-localisation of S100-A4 and ANXA2 in wild type C2C12. "ANXA2" stained with anti-ANXA2 + alexa fluor 594 secondary antibody. "S100A4" stained with anti-S100A4 primary antibody + alexa fluor 488 secondary antibody. "ANXA2+S100A4" co-stained with anti-S100A4 and anti-ANXA2 + alexa fluor 488 and 594 secondary antibody. "ANXA2+2nd" and "S100A4+2nd" stained with indicated primary antibody and both 594 and 488 secondary antibodies. "2nd" stained with both 594 and 488 secondary antibodies only. All images are taken at x20 magnification (scale bars = 50µm). Biological N = 4. Technical N = 1.

4.7.2 Investigation of ANXA2 localisation in undifferentiated and differentiated wild type, Control knockdown and ANO5 knockdown C2C12

The previous immunofluorescence and subcellular fractionation experimentation confirm reports from the literature that while ANXA2 is found throughout the cell, as well as secreted into the extracellular space, it is predominantly located in the cytoskeleton and organelles associated with the plasma membrane, the early endosomes for example (Gerke and Moss, 1997). To better understand the role of ANXA2 in C2C12 and what its interaction with ANO5 might be, the localisation of ANXA2 during C2C12 differentiation was investigated. To this end immunofluorescence staining of differentiated C2C12 was carried out to identify ANXA2 localisation during differentiation and to identify any changes to this localisation when ANO5 is knocked down.

Initial investigation of differentiating wild type C2C12 was made using immunofluorescent staining of D1, D3 and D5 time points to track ANXA2 localisation (Figure 4.13). These data show that throughout differentiation from myoblasts to myotubes, the same filamentous structures stained by the ANXA2 antibody as seen in previous experiments (Figure 4.12) are retained throughout the 5 day time series, appearing in approximately 10% of cells.

Specifically, in D1 cells positive for ANXA2, single long spindle like structures are found running the length of the cell. Within each cell, all of these structures run in the same direction, but the direction varies between cells. While this staining pattern was at first thought to just be background, the persistence of this staining pattern in the D3 and D5 time point images suggests that this is a genuine structure within the cells, though similar structures have not been reported in the literature. At the D3 time point these spindle structure become more defined. As with the D1 time point, in the majority of the cells the spindles appears to cross over the nucleus and extend to cover the length of the cell. Finally at D5 a single spindle structure runs the length of formed myotube, again appearing to cross over the multiple nuclei of the myotube.

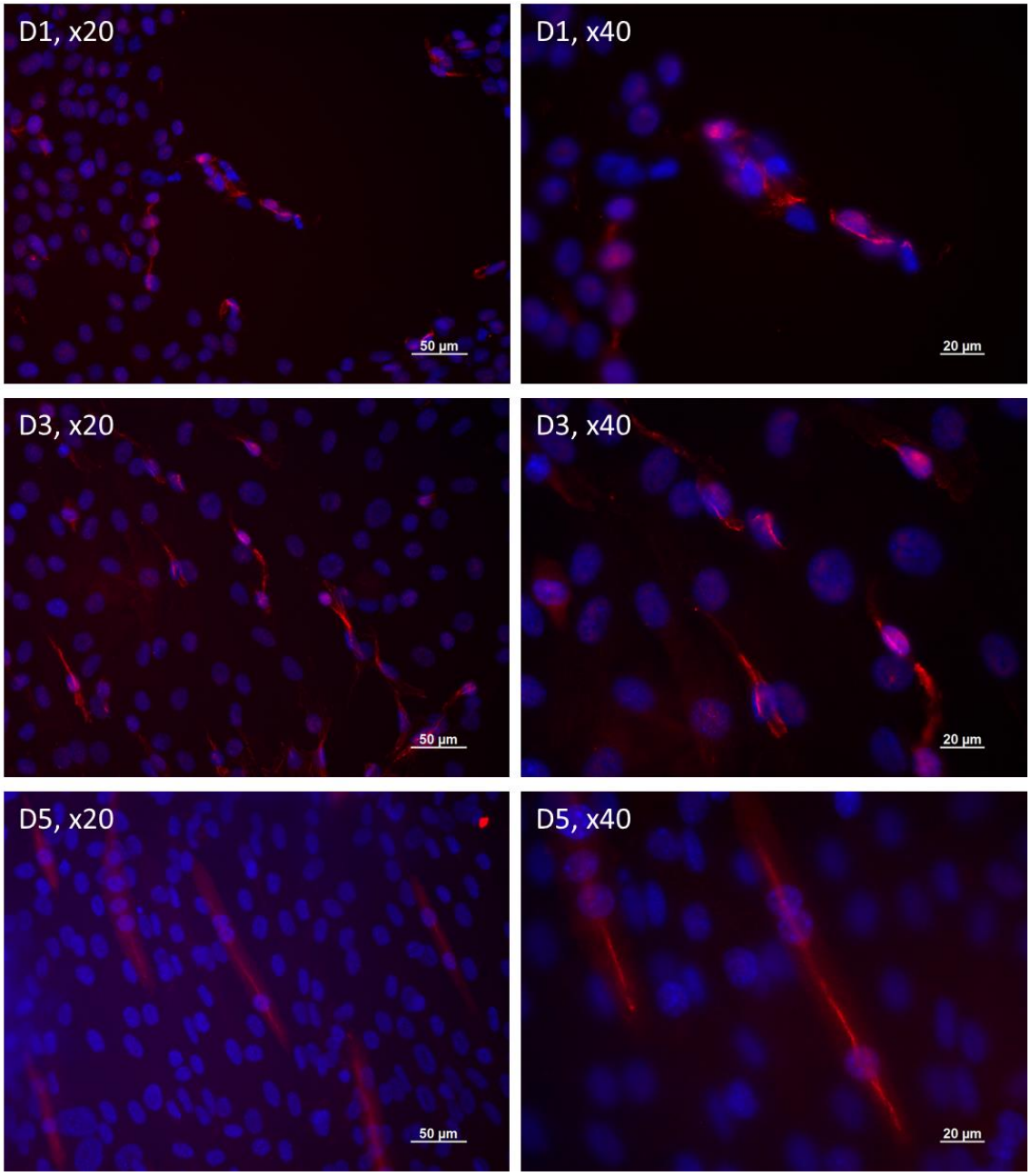

Figure 4.13 ANXA2 localisation in differentiating wild type C2C12. All micrographs show anti-ANXA2 + alexa fluor 594 secondary antibody. Images in the left column are taken at x20 magnification (scale bars = 50µm), the right column of images are taken at x40 magnification (scale bars = 20µm). Biological N = 1. Technical N = 1.

This experimental set up and immunofluorescence staining was repeated on the ANO5-4A and CON-2C knockdown C2C12 clones (Figure 4.14). These data are less informative than the wildtype C2C12 data as these C2C12 do not differentiate as well as the wild type C2C12. They fail to produce multinucleated myotubes even by the D5 time point. They do however line up and elongate, attempting to fuse to form myotubes.

These data show that the spindle like structures are not seen in either cell line. Instead, the pattern of staining seen in these cell lines localises more to the nucleus, evidenced by the purple signal from the overlapping red (ANXA2) and blue (DAPI) staining. There is evidence of cytoplasmic staining in some cells both ANO5 knockdowns and controls, though this is a very diffuse pattern and may just be concentrations of antibody rather than true signal. Considered with the fact that these C2C12 do not differentiate well, ultimately it is not possible to accurately identify ANXA2 localisation in either of these knockdown C2C12 clones and understand how this localisation changes with the knockdown of ANO5.

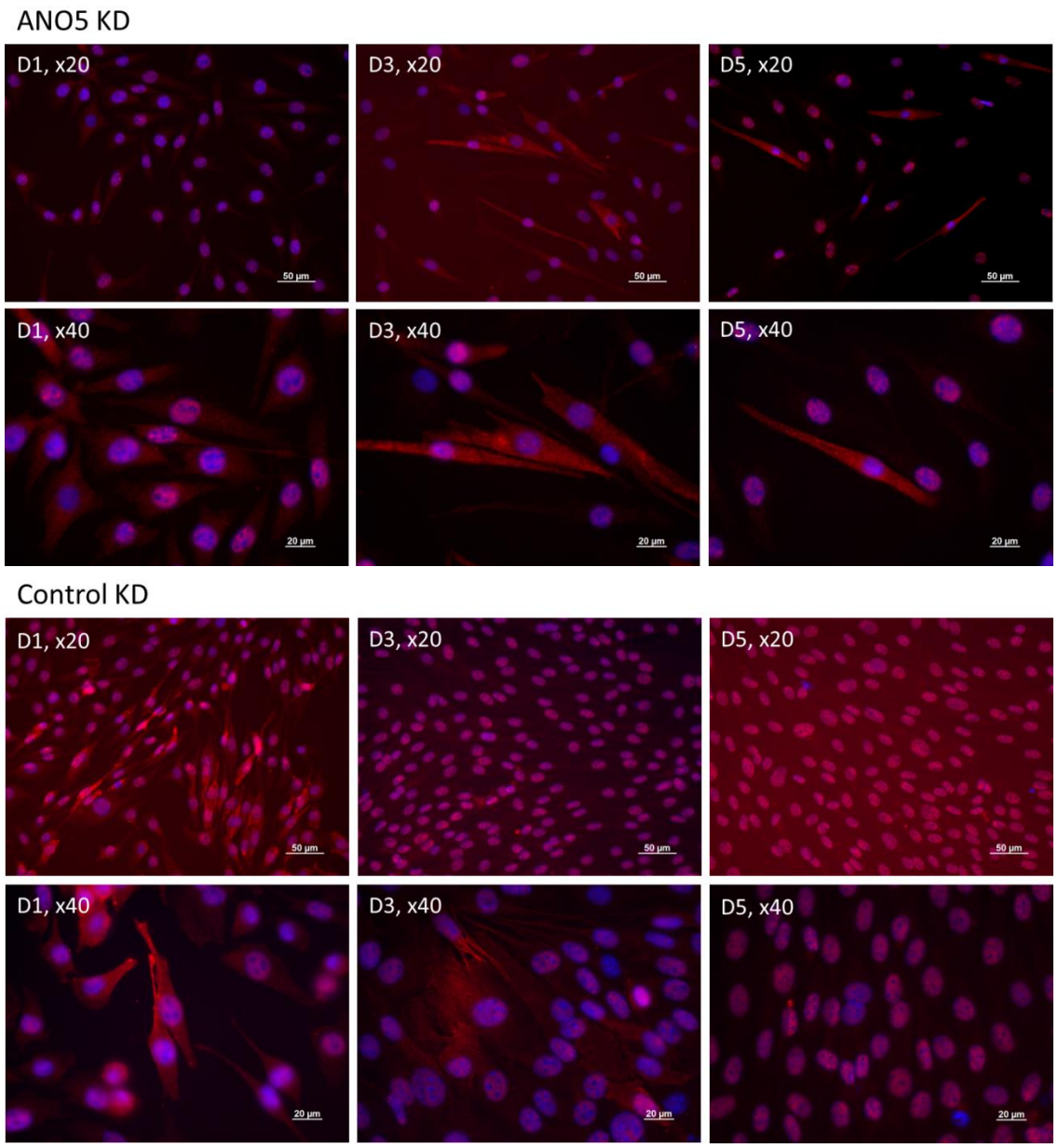

Figure 4.14 Comparison of ANXA2 expression in differentiating ANO5 knockdown and Control knockdown C2C12. All micrographs show anti-ANXA2 and alexa fluor 594 secondary antibody. In both "ANO5 KD" and "Control KD" the top row of images are taken at x20 magnification (scale bars = 50µm), bottom row of images are taken at x40 magnification (scale bars = 20µm). Biological N = 2. Technical N = 1.

4.8 Discussion

Crude subcellular fractionation by differential centrifugation was used to separate C2C12 lysates into nuclear, mitochondrial and cytosolic fractions, reducing the number of protein spots to compare between each gel. Differential centrifugation was used to fractionate lysates as it was the simplest method available to achieve the desired results. More sophisticated methods of subcellular fractionation such as density gradient centrifugation would produce purer fractions for further experimentation (Anderson, 1955). However, as the aim of the fractionation was to reduce the number of spots for subsequent analysis, this method of fractionation was adequate. Additionally this fractionation method was specifically tailored for use with C2C12 cells to maximise the yield and purity of the fractions, using the simplest method possible (Dimauro *et al.*, 2012).

To streamline 2D gel experimentation, but to cover as wide a pH range as possible, only IPG strips with a pH gradient of 3-10 were tested. This means that potentially altered proteins remained undetected because their isoelectric points fall outside of the pH range of the IPG strips used. This is unlikely however as most proteins have isoelectric points within the pH range tested (Schwartz *et al.*, 2001; Weiller *et al.*, 2004). A more likely scenario is that proteins distorted by the lysis and solubilisation process do not enter the gel at all during IEF. For example lipids can bind to proteins and alter their isoelectric point and solubility (Rabilloud, 1999). There are protocols which can be included during lysis to reduce such interference and produce cleaner lysates, but it has been suggested that reducing the handling of protein lysates produces a more informative gel, especially in the first instance (Berkelman, 2008).

Furthermore, a number of proteins may be hidden in lipid rafts. Lipid rafts are found in both external and internal plasma membranes such as the Golgi apparatus and lysosomes, where they are thought to function as organising centres for other proteins involved in cell signalling (Pike, 2003). They are insoluble in non-ionic detergents compared to other parts of the membrane due to the presence of cholesterol, sphingolipids (Moldovan *et al.*, 1995; Brown and London, 1997; Galbiati *et al.*, 2001) and proteins such as caveolin (Perez-Verdaguer *et al.*, 2016). It is likely that other proteins may be undetected because they are contained within these free floating, highly ordered and relatively insoluble regions of the plasma membrane

Conversely, investigating narrower pH ranges would in effect “zoom in” on a portion of the IPG strips already tested and allow for resolution of spots that are very close together and elucidate further potential differences between the knockdown clones. This would be particularly helpful if investigating strings of phosphorylated or post translationally modified proteins.

Only one cell line from each shRNA knockdown condition was used. ANO5-4A and CON-2C gels were run in triplicate for both the initial Coomassie stained gels and the ANXA2 2D western blot investigation with consistent results obtained each time. Therefore the observed differences are likely to be correct for these clones. But to confirm that the observed differences in ANXA2, S100-A4 and Hspb27 are true in all ANO5 deficient C2C12, comparison of other ANO5 deficient cell lines should be investigated.

Spot patterns on triplicate 2D gel western blots of ANXA2 suggest that knocking down ANO5 in C2C12 alters the intensity of the detectable ANXA2. Two other spots, one heavier (spot 2) and one lighter (spot 3), are also present on CON-2C blots which have a reduced expression level on ANO5-4A blots. The identities of these additional spots are not known, but suggestions about its identity can be made using the difference in molecular weights between the ANXA2 spot and spot 2. ANXA2 is subject to several post translational modifications including polyubiquitination (Lauvrak *et al.*, 2005; Bharadwaj *et al.*, 2013), acetylation, glutathionylation and serine and tyrosine phosphorylation (Bharadwaj *et al.*, 2013). Glutathionylation and polyubiquitination are unlikely modifications as the addition of either glutathione (25 kDa) or polyubiquitin (minimum of 17 kDa) would make any potentially modified ANXA2 much larger than the identified spot. Monoubiquitination is a more likely modification as ubiquitin is only 8.5 kDa.

However, there is little direct evidence in the literature to suggest that ANXA2 is monoubiquitinated. Lauvrak *et al.* (2005) have noted however that ANXA2 is involved in endocytosis (Gerke and Moss, 2002) while monoubiquitination is implicated in tagging proteins for the endosomal pathway (Schnell and Hicke, 2003), therefore suggesting that monoubiquitination of ANXA2 is a possibility. If ANXA2 is monoubiquitinated then the absence of spot 2 from the ANO5-4A blots could suggest that the knockdown of ANO5 inhibits the monoubiquitination of ANXA2, potentially removing it from the endosomal pathway.

Finally ANXA2 localisation results show positive staining for filamentous structures within wild type C2C12. This structure persists throughout C2C12 differentiation. The same structure is seen in both ANO5-4A and CON-2C C2C12 myoblasts. However, as both knockdown C2C12 clones differentiate very poorly it is not possible to identify the same structure in differentiated knockdown C2C12. The identity of this structure is not known though this pattern of ANXA2 staining is atypical. The literature reports that ANXA2 can have a diffuse cytosolic localisation (Scharf *et al.*, 2012; Dziduszko and Ozbun, 2013) suggesting either that ANXA2 localises only to this structure in C2C12 cells or that these structures are artefacts.

Chapter 5 Investigation of ANO5 function as a phospholipid scramblase

5.1 Introduction

Anoctamins 1 and 2 have been well established as calcium activated chloride channels (CaCCs) (Caputo *et al.*, 2008; Schroeder *et al.*, 2008; Yang *et al.*, 2008; Stohr *et al.*, 2009). Due to the close sequence homology between anoctamin family members, it was assumed that all anoctamins were CaCCs (Hartzell *et al.*, 2009; Schreiber *et al.*, 2010). However, extensive investigation of the other anoctamins has shown that while anoctamins 6, 7 and 10 produce currents when overexpressed in fisher rat thyroid cells, the current is less than 10% of that produced by anoctamins 1 and 2 in the same cell lines (Schreiber *et al.*, 2010; Duran and Hartzell, 2011). Along with anoctamin 5, several other anoctamins have also been implicated in disease. Mutations in anoctamin 10 have been implicated in brain angiogenesis (Vermeer *et al.*, 2010) and mutations in anoctamin 6 are causative in Scott syndrome (Suzuki *et al.*, 2010; Castoldi *et al.*, 2011), a rare bleeding disorder (Rosing *et al.*, 1985).

The erythrocytes of patients with Scott syndrome fail to undergo coagulation during bleeding because they do not expose phosphatidylserine (PS) at the plasma membrane (Rosing *et al.*, 1985). PS is a key component of the blood coagulation cascade (Spronk *et al.*, 2014) where it is translocated from the inner to the outer leaflet of the plasma membrane by phospholipid scramblases in a calcium dependent manner (Bevers *et al.*, 1982; Bevers *et al.*, 1983). Investigation of ANO6 has confirmed that it is involved in phospholipid scrambling (Suzuki *et al.*, 2010; Scudieri *et al.*, 2015). Furthermore, research suggests that the other non-CaCC anoctamins may also function as phospholipid scramblases (Suzuki *et al.*, 2013).

As well as signalling blood coagulation, PS exposure is also essential for apoptosis (Fadok *et al.*, 1992; Schlegel and Williamson, 2001) and other cellular processes, such as differentiation (Sessions and Horwitz, 1983; Schlegel and Williamson, 2001; van den Eijnde *et al.*, 2001) and wound healing (Middel *et al.*, 2016). In both cases, PS exposure marks the cell as ready for the next step within the relative pathway; fusion with other differentiating cells (Jeong and Conboy, 2011) or accumulation of (Middel *et al.*, 2016) and destruction by phagocytes (Fadok *et al.*, 1992). As ANO6 and ANO5 are the most closely related anoctamins within the family (Duran and Hartzell, 2011) and as differentiation and apoptosis are of high biological importance for correct muscle

maintenance and repair (Hawke and Garry, 2001; Adhihetty and Hood, 2003), one hypothesis is that ANO5 functions as a phospholipid scramblase in the apoptosis of muscle tissue. This chapter reports on the investigation of the phospholipid scramblase ability of ANO5 knockdown C2C12 and patient myoblasts.

5.1.1 Flow cytometry analysis of knockdown C2C12 and patient myoblasts

Flow cytometry is a powerful analysis method capable of recording multiple parameters simultaneously from cell populations (Hulett *et al.*, 1969; Hulett *et al.*, 1973). The technology first appeared in 1965 as a cell sorter, able to discriminate cells on differences in their volume when passed through an electronic field (Fulwyler, 1965). This was then taken a step further in 1969 with the introduction of fluorescence assisted cell sorting (FACS). Here, sub-populations are identified by staining heterogeneous samples with fluorescent markers specific for proteins unique to the desired sub-populations prior to sorting (Hulett *et al.*, 1969). This early technology could only detect one or two colours from stained cells, but current generation cytometers are able to detect more than 20 different colours simultaneously (Bendall *et al.*, 2012). Flow cytometry analysis is now so well established that it is routinely used for a range of diagnostic needs, from vaccine development and transplantation (Lanier, 2014) to screening various patient fluid samples for infection (Bignardi, 2015) and phenotyping blood samples (Maecker, 2009; Hensley-McBain *et al.*, 2014).

Typical fluorescent flow cytometry involves stained cell suspensions being passed through the path of a laser as a single stream. Light emitted from the cells is then picked up by a series of detectors (Figure 5.1 A.). Additional lasers and detectors aligned along the path of flow record multiple fluorescent parameters from each cell. As each cell is recorded as a single event and multiple fluorescent parameters can be gathered from each event, this technology allows for the generation of thousands of data points per cell population. Flow cytometry data must therefore be filtered following acquisition, to identify the populations of interest and discard uninformative data. This can be achieved using appropriate analysis software to select specific population sub-sets, termed “gates” (Figure 5.1 B.). By choosing gates from across several fluorescence channels it is possible to focus on specific cellular sub-populations of interest (Verschoor *et al.*, 2015). For example, while the setup of flow cytometer technology should mean that each event is the analysis of a single cell, it is possible for cells to adhere to one another and for two cells to be analysed as a single event. By plotting the Forward Scatter Height (FSC-

H) and Forward Scatter Area (FSC-A) data on the same graph, these doublets can be identified as events which are "taller" than they are wide and ignored (Figure 5.1 C.).

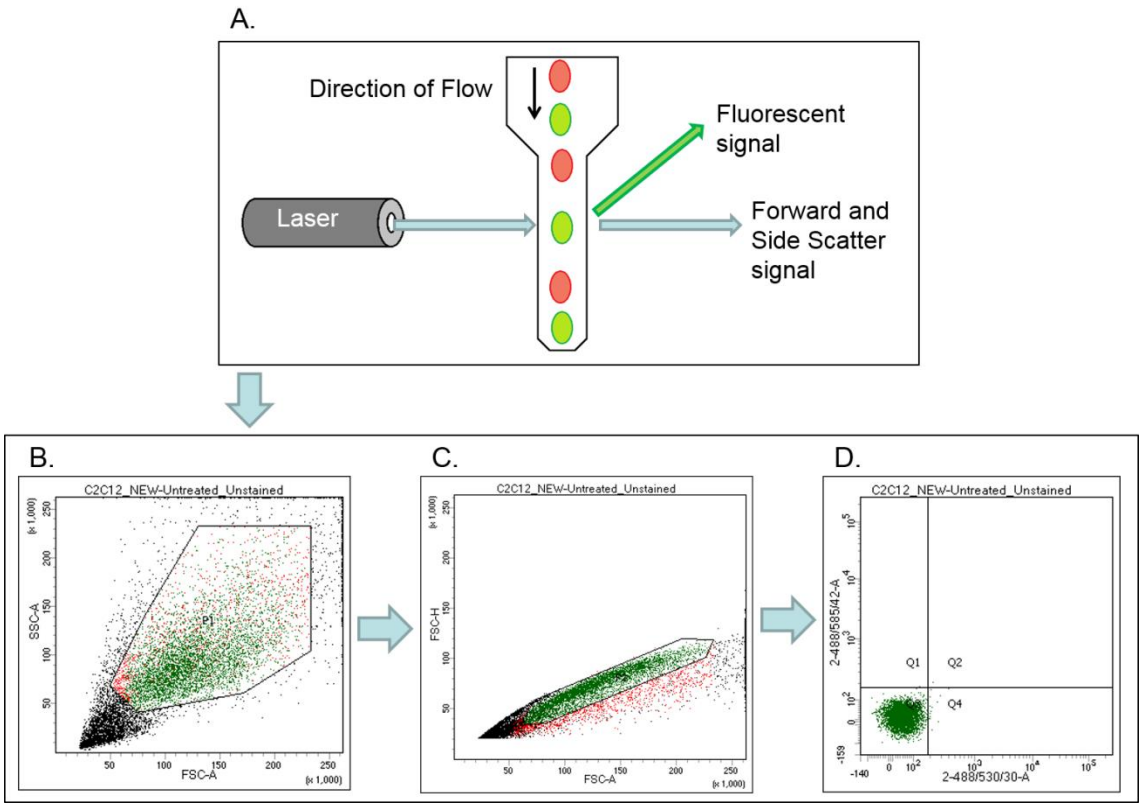

Figure 5.1 Representation of flow cytometry workflow. A. is a simplified diagram of the process occurring within flow cytometry technology. Coloured circles indicate stained cells moving as a single stream in the direction of flow. Only one laser is shown though additional lasers with different emission spectra can then be positioned in the path of the cells for collection of more dye colours. The lower box shows the graphical output of data on FACSDiva software and the order of gating used in these experiments. B. is used to exclude debris (Forward Scatter Area [FSC-A] against Side Scatter Area [SSC-A]); C. is used to exclude doublet cells (FSA against Forward Scatter Height [FSC-H]); D. is the final gated population data collected from each sample, displayed as scatter plot of FITC-AV fluorescence (Axis labelled 2-488/530/30-A) against PI (Axis labelled 2-488/585/42-A). This final plot allows for visualisation of the movement of cell populations following apoptosis treatment.

5.2 Phosphatidylserine exposure during C2C12 differentiation

The exposure of PS on wild type C2C12 during differentiation was investigated by staining cells with FITC conjugated Annexin V (FITC-AV). AV binds to exposed PS in a calcium dependant reaction (Tait and Gibson, 1992; Meers and Mealy, 1993), while differentiation progression was tracked using Alexa Fluor 594 phalloidin which stains the actin filaments, a marker of differentiation (Faulstich *et al.*, 1988; Huang *et al.*, 1992). The aim of this investigation was to confirm that this assay would accurately identify PS exposure in differentiating C2C12. The assay would then be used to characterise differences in PS exposure between ANO5 and Control knockdown C2C12.

Results show that at D1 only one or two C2C12 cells show any FITC-AV positivity and no phalloidin positivity can be observed (Figure 5.2). In the few FITC-AV-positive cells, x63 magnification reveals that FITC-AV appears to have a punctate pattern of staining within the cytoplasm of the cells.

By D3, both FITC-AV and phalloidin positivity are observable, indicating differentiation of myoblasts into myotubes. Detectable FITC-AV fluorescence is seen external to the plasma membrane of cells in clusters of variable size; described as an aggregate staining pattern. External aggregation of FITC-AV is as expected (Jeong and Conboy, 2011), but the location of the FITC-AV staining pattern is not what is expected from the literature (van den Eijnde et al., 2001; Jeong and Conboy, 2011). Rather than aggregating around the cell-cell contact areas, such as the leading ends of the forming myotubes, the aggregation appears to be mostly along the longitudinal plane of the cell. The majority of C2C12 show positive staining with phalloidin, identifiable by the striated pattern of fluorescence along the length of the elongated myoblasts. A few multinucleated myotubes are formed by this time point but are small and not as numerous as the elongated pre-fusion myoblasts.

These staining patterns are also observed in D5 C2C12 though with differences in the levels of fluorescence. Phalloidin staining is now consistent across all myotubes. The level of FITC-AV staining however is reduced and only appears next to a few formed myotubes. Additionally the aggregate staining pattern of FITC-AV remains localised next to the cells but again not in the locations associated with myoblast fusion.

From these data it appears that FITC-AV aggregates on the longitudinal axis of myotubes, an area not expected to show PS exposure. While it is possible that these

findings represent previously unreported localisation for PS, it may also be background or expression of PS not related to differentiation; likely as the localisation detected are not areas associated with myoblast fusion. As such, this assay was determined to be suboptimal for further experimentation and potential differences between ANO5 and Control knockdown C2C12 were not investigated.

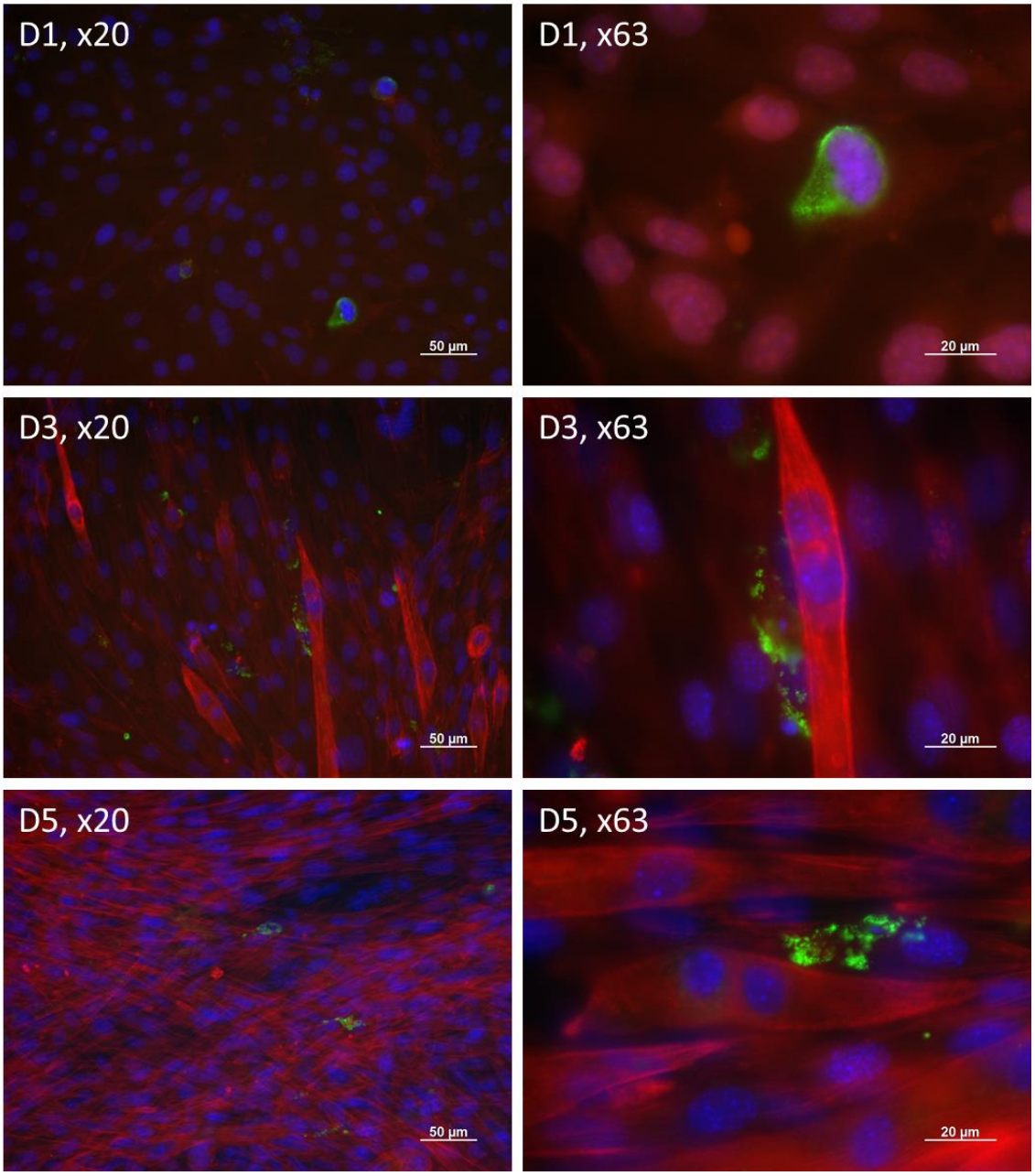

Figure 5.2 FITC-AV and phalloidin staining of differentiating wild type C2C12. Red fluorescence indicates alexa fluor 594 phalloidin staining. Green fluorescence indicates FITC-AV staining. The left column of images are taken at x20 magnification (scale bars = 50µm), right column of images are taken x63 magnification (scale bars = 20µm). Biological N = 1. Technical N = 3.

5.3 Phosphatidylserine exposure during apoptosis in ANO5 knockdown C2C12

PS exposure during apoptosis was investigated using the three selected clones of ANO5 and Control knockdown C2C12 cells generated using ANO5 targeting shRNAs (described in Section 2.2).

The FITC-AV assay, used in the differentiation experimentation in the previous section, was used to detect resulting PS exposure (Figure 5.3). Five random images of each well were collected, the images blinded and the number of FITC-AV-positive cells counted to determine the proportion of FITC-AV-positive cells for each shRNA treatment. FITC-AV-positive cells were identified as any cells showing bright green fluorescence at the plasma membrane. No distinction was made between cells with fluorescence around the full circumference or around just a portion of the cell, all were counted as positive.

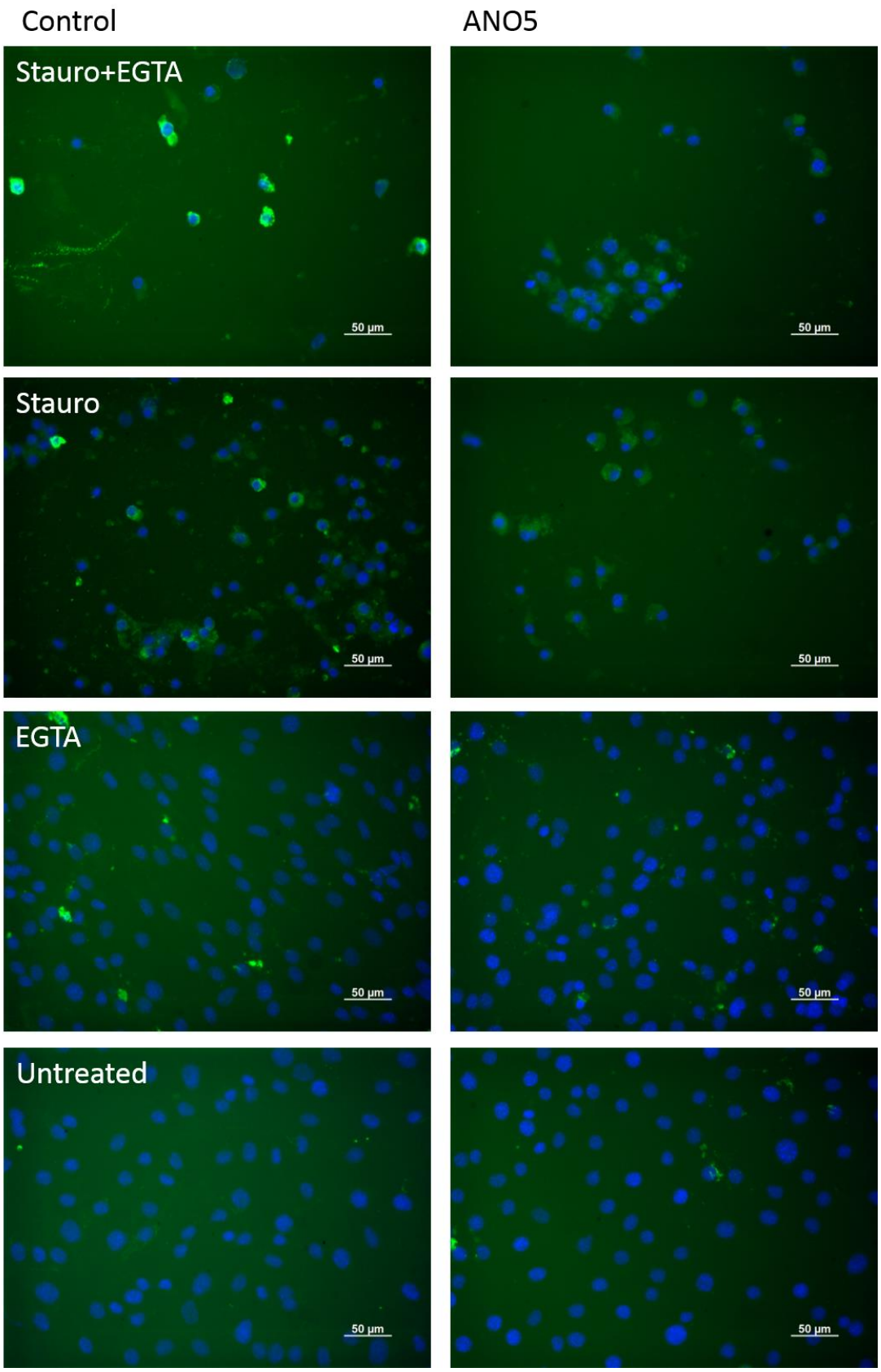

Figure 5.3 Example images of FITC-AV stained Control and ANO5 knockdown C2C12. Labels on right hand column images also apply to left hand column. Images are taken at x20 magnification (scale bars indicate 50µm). Biological N = 4. Technical N = 3.

Chi^2 was used to statistically analyse the difference in the number of positive cells between the ANO5 and Control knockdown C2C12 in each treatment condition (Section 2.14). The combined total of FITC-AV-positive C2C12 from all knockdown clones show that there was a significant difference between the number of FITC-AV-positive cells in both staurosporine+EGTA and staurosporine only treated ANO5 knockdown clones compared to Control knockdown clones (Figure 5.4). There was no significant difference between ANO5 and Control knockdown C2C12 in EGTA and Untreated conditions. This is unsurprising as the level of apoptosis, and consequently FITC-AV positivity, was expected to be very low in the EGTA and Untreated conditions.

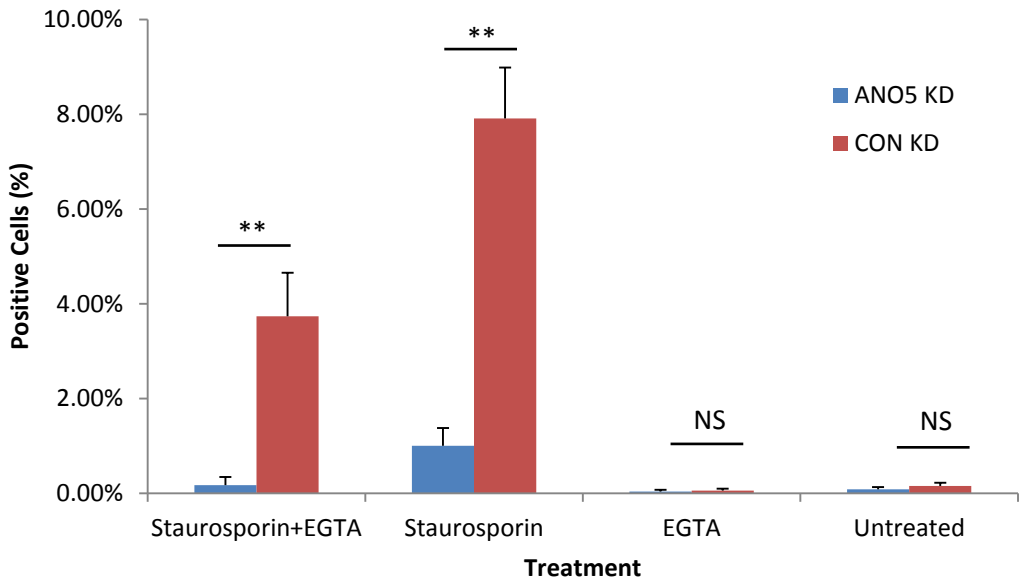

*Figure 5.4 Bar graph of preliminary positive FITC-AV count data for each treatment condition. Blue bars represent combined ANO5 knockdown data for that condition. Red bars represent combined Control knockdown data for that condition. Significant differences calculated using Chi^2 Statistic. ** = $p < 0.001$ at 1 degrees of freedom. NS indicates no significant difference between data. Lines indicate calculated standard error. Biological N = 4. Technical N = 2.*

5.4 Phosphatidylserine exposure potential of knockdown C2C12 investigated using FITC-AV staining and anti-activated caspase 3 staining

To validate the significant difference in PS exposure between ANO5 knockdown and Control knockdown C2C12, the experiment was modified and repeated to include a second immunofluorescent stain for active Caspase 3 (aC3). Activated by binding of the FasL receptors, aC3 is a key part of the apoptotic pathway (Porter and Janicke, 1999), activating other proteins which lead to membrane blebbing (Coleman *et al.*, 2001), DNA fragmentation (Janicke *et al.*, 1998) and chromatin condensation (Sahara *et al.*, 1999). This experiment aimed to test whether the levels of aC3 remained consistent between ANO5 and Control knockdown clones. This would then confirm that ANO5 knockdown has a specific effect on the exposure of PS and was not altering apoptosis pathways in general.

FITC-AV-positive cells were identified by bright green staining of the plasma membrane (Figure 5.5). This staining appears to localise around the nucleus, though this is due to the cell shrinkage during apoptosis (Maeno *et al.*, 2000). FITC-AV-positive cells were classified as any cell that showed green fluorescence around a portion of the cell membrane. Cells that had a bright green staining pattern around the full circumference of the cell were termed “halo” cells and counted as a subset of FITC-AV-positive cells. aC3-positive cells were identified by red fluorescence within the cytoplasm and the nucleus.

Chi^2 analysis of the count data (Table 5.1) show that there is a significant difference between the number of FITC-AV-positive and halo-positive cells between the ANO5 and Control knockdown C2C12 in staurosporine and staurosporine+EGTA treated conditions (in both cases $p < 0.001$, Figure 5.6 A. and B.) confirming the findings of previous experimentation. There is also a statistically significant difference in the number of FITC-AV-positive cells between clones in EGTA and untreated conditions (EGTA $p < 0.03$, Untreated $p < 0.001$), though there is no significant difference in the number of halo-positive cells in these conditions (EGTA $p < 0.15$, Untreated $p < 0.8$).

Statistical analysis of the aC3 data shows that there is no significant difference in the number of aC3-positive cells between the ANO5 and Control knockdown clones in the staurosporine only condition ($p < 0.99$), though there is a statistically significant difference in each other treatment condition (staurosporine+EGTA $p < 0.01$, EGTA $p < 0.001$, Untreated $p < 0.001$, Figure 5.6 C.). Additionally the number of FITC-AV and

aC3-positive cells in the EGTA and Untreated conditions, is marginally higher in ANO5 clones than Control (Figure 5.6 A. B. and C.). This is also the case for the number of aC3-positive cells in the staurosporine condition.

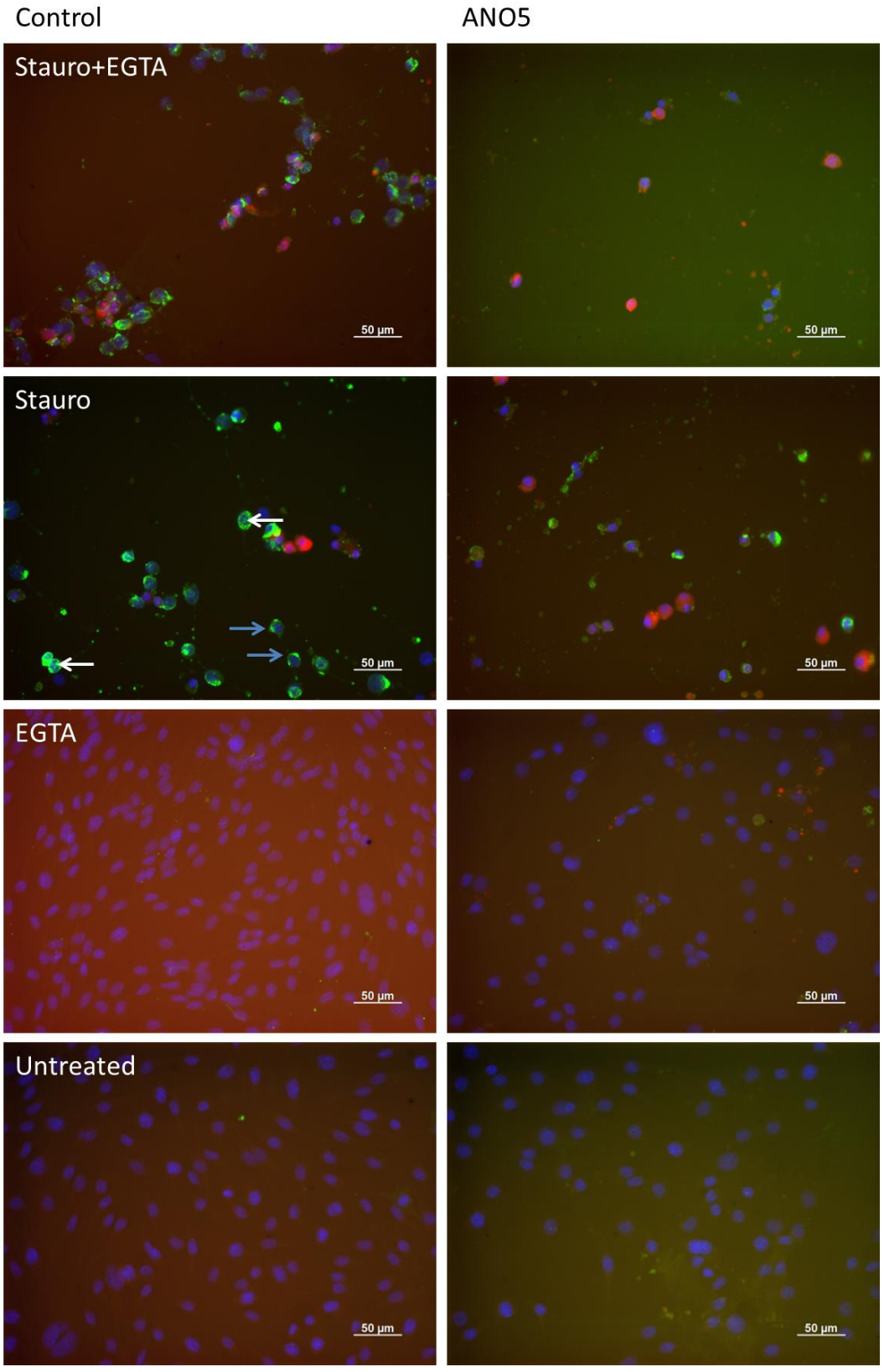

Figure 5.5 Example images of FITC-AV+aC3 stained Control and ANO5 knockdown C2C12. Labels on right hand column images also apply to left hand column. In each image white arrows indicate examples of cells counted as "halo" cells, Blue arrows indicate examples of cells counted as FITC-AV-positive cells. Images are taken at x20 magnification (scale bars indicate 50µm). Biological N = 6. Technical N = 2.

Clone	Treatment	Total Cells	AV cells	Halo Cells	aC3 Cells
ANO5	Stspn+EGTA+AV+anti-C3	250	9	1	99
	Stspn+EGTA+anti-C3	294	1	0	139
	Stspn+AV+anti-C3	677	85	19	198
	Stspn+anti-C3	652	0	0	242
	EGTA+AV+anti-C3	992	10	3	38
	EGTA+anti-C3	1090	0	0	74
	Untreated+AV+anti-C3	1274	15	2	17
	Untreated+anti-C3	1235	0	0	26
CON	Stspn+EGTA+AV+anti-C3	449	124	44	136
	Stspn+EGTA+anti-C3	416	0	0	154
	Stspn+AV+anti-C3	512	132	41	150
	Stspn+anti-C3	1349	0	0	408
	EGTA+AV+anti-C3	1582	8	2	7
	EGTA+anti-C3	1501	0	0	15
	Untreated+AV+anti-C3	1575	6	2	9
	Untreated+anti-C3	1452	0	0	8

Table 5.1 Count data of total number of cells per clone per treatment condition. "AV Cells" indicate the number of cells showing any green fluorescence. "Halo Cells" indicate the number of cells with green fluorescence around their entire circumference. "aC3 Cells" indicate the number of cells showing any red fluorescence. Staurosporine is abbreviated as "Stspn"

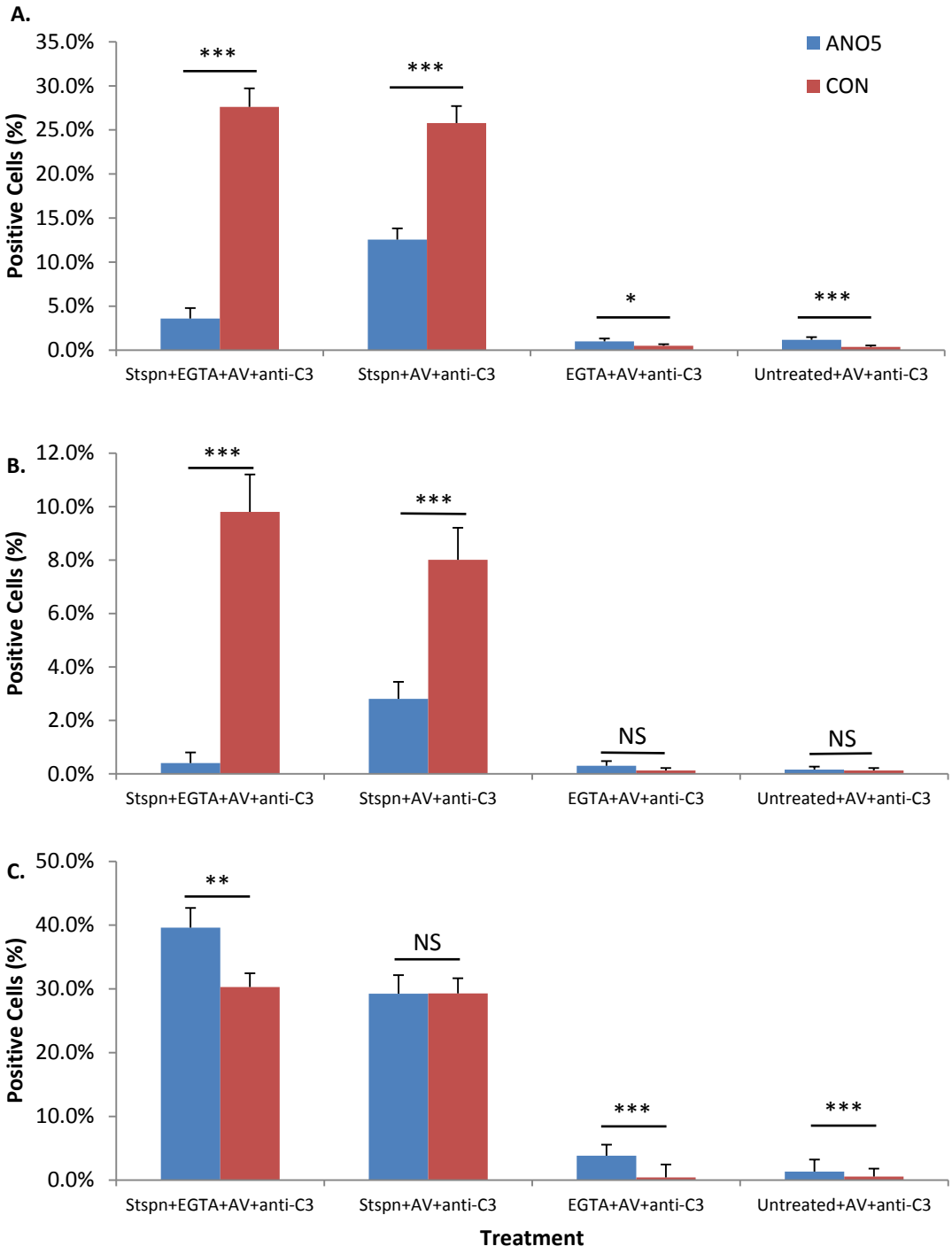

*Figure 5.6 Bar graphs of the percentage of FITC-AV, halo and aC3-positive cells for each treatment condition. Blue bars represent ANO5 knockdown data. Red bars represent Control C2C12 data. A. Percentage of AnnexinV-positive cells. B. Percentage of "Halo"-positive cells C. Percentage of aC3-positive cells. Staurosporine is abbreviated as "Stspn". Significant differences calculated using Chi^2 Statistic. *** indicates significance with $p < 0.001$, ** indicates significance with $p < 0.01$, * indicates significance with $p < 0.03$, all at 1 degree of freedom. NS indicates no significant difference between data. Lines indicate calculated standard error. Biological N = 6. Technical N = 1.*

5.5 Phosphatidylserine exposure potential of patient myoblasts investigated using FITC-AV staining

To investigate the impairment of PS exposure in a more biologically relevant model, the FITC-AV assay was repeated using patient myoblasts. Four myoblast lines were obtained from the Newcastle Biobank; one from a healthy patient control and one each from patients with confirmed genetic diagnoses of LGMD2L (ANO5), LGD2B (DYSF) and LGMD2A (Calpain 3, CAPN3).

Identifying FITC-AV-positive cells was less straight forward for these cell lines than for knockdown C2C12 clones. The cells were more prone to aggregate following apoptosis treatment, leading to a higher level of background associated with the images (Figure 5.7). Despite the differences in cellular response, patient images were still blinded and counted for FITC-AV positivity as per knockdown C2C12 protocols.

Count data from these myoblasts show that across all cell lines the highest percentage of FITC-AV-positive cells remains in staurosporine+EGTA and staurosporine treated conditions. Little or no FITC-AV positivity is detected in EGTA and untreated conditions (Figure 5.8). However, the percentage of FITC-AV-positive cells were highest in DYSF patient myoblasts while the lowest were in the control patient myoblasts. Additionally the percentage of FITC-AV-positive cells in ANO5 patient myoblasts were low in the staurosporine+EGTA treatment condition but very similar to DYSF levels in the staurosporine only condition. The disparity in the number of FITC-AV-positive cells between ANO5, DYSF and CAPN3 patient and control patient lines may be due to experimenter error during cell counting caused by high background from cells aggregating following apoptosis. As such an alternative assay was sought to asses PS exposure ability in patient myoblasts.

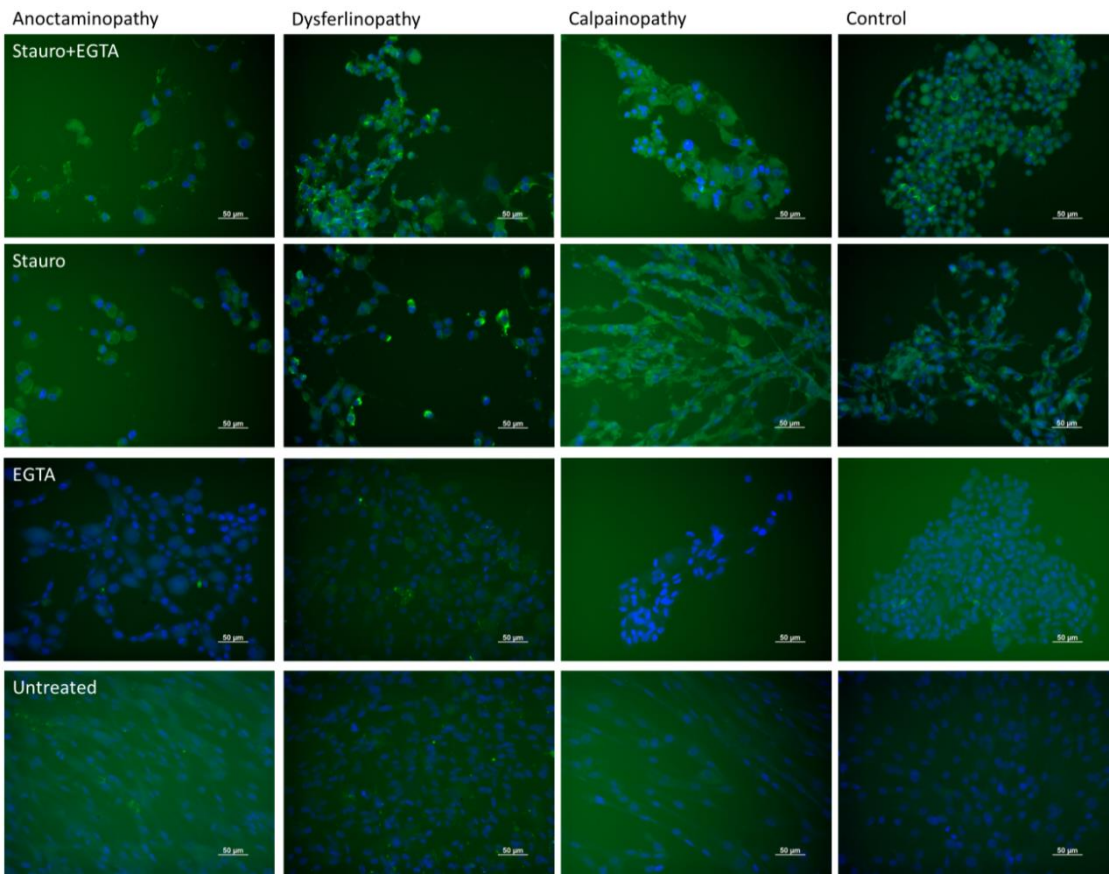

Figure 5.7 Example images of FITC-AV staining for each patient myoblast line. Labels on right hand column images apply across the row. Images are taken at x20 magnification (scale bars indicate 50µm). Biological N = 4. Technical N = 1.

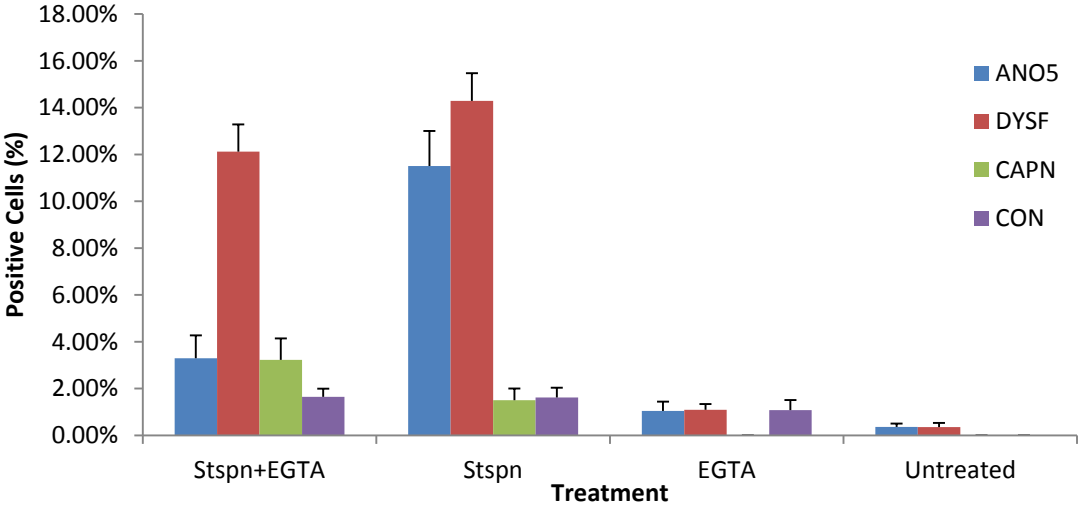

Figure 5.8 Bar graph of the percentage of patient myoblast cells counted as FITC-AV-positive. Blue bars represent ANO5 patient myoblast data. Red bars represent DYSF patient myoblast data. Green bars represent CAPN3 patient myoblast data. Purple bars represent control myoblast data. Staurosporine is abbreviated as "Stspn". Lines indicate calculated standard error. Biological N = 4. Technical N = 1.

5.6 Flow cytometry analysis of phosphatidylserine exposure of knockdown C2C12 and patient myoblasts

To overcome the issue of inconsistent staining of patient myoblasts using the established *in situ* assay, flow cytometry analysis was used to investigate the exposure of PS in patient cells.

Consistency between samples was maintained by first creating a template programme which was used to collect all subsequent data sets. The template included compensation vales for the two lasers used to account for spectral overlap between the FITC-AV and Propidium Iodide (PI) fluorochrome dyes. The compensation values were set by altering the voltage of the detector so that the mean fluorescence of the corresponding dye was within the expected portion of the final P2 scatter plot. For example, when the FITC-AV only sample (Solution 2) was analysed the gates were set so that fluorescence was detected only in the Q3 and Q4 portions of the graph.

5.6.1 Optimisation of apoptosis induction in patient myoblasts

To optimise the protocol, wild type C2C12 and control patient myoblasts were treated with 1µM of staurosporine at 1 hour intervals for 4 hours (Figure 5.9). The percentage of FITC-AV-positive cells were identified as the proportion of events recorded in the Q4 portion of the FITC-AV against PI scatter graph. These data show that the percentage of FITC-AV wild type C2C12 peaks after 1 hour of treatment. Beyond this time point, more and more cells become late apoptotic indicated by increased PI positivity and movement out of the Q4 portion of the scatter plot into the Q2 portion (Figure 5.9 A.).

Under the same treatment conditions however, the percentage of FITC-AV-positive control patient myoblasts remains unchanged. Staurosporine concentration was therefore increased to 50µM and the same time series repeated. These data show that four hours of incubation are required before the percentage of FITC-AV-positive myoblasts begins to increase (Figure 5.9 B.). Due to time restrictions on the project, longer time points were not investigated. Four hour treatment with 50µM staurosporine was used for all subsequent investigation of patient myoblasts responses to apoptotic stimuli.

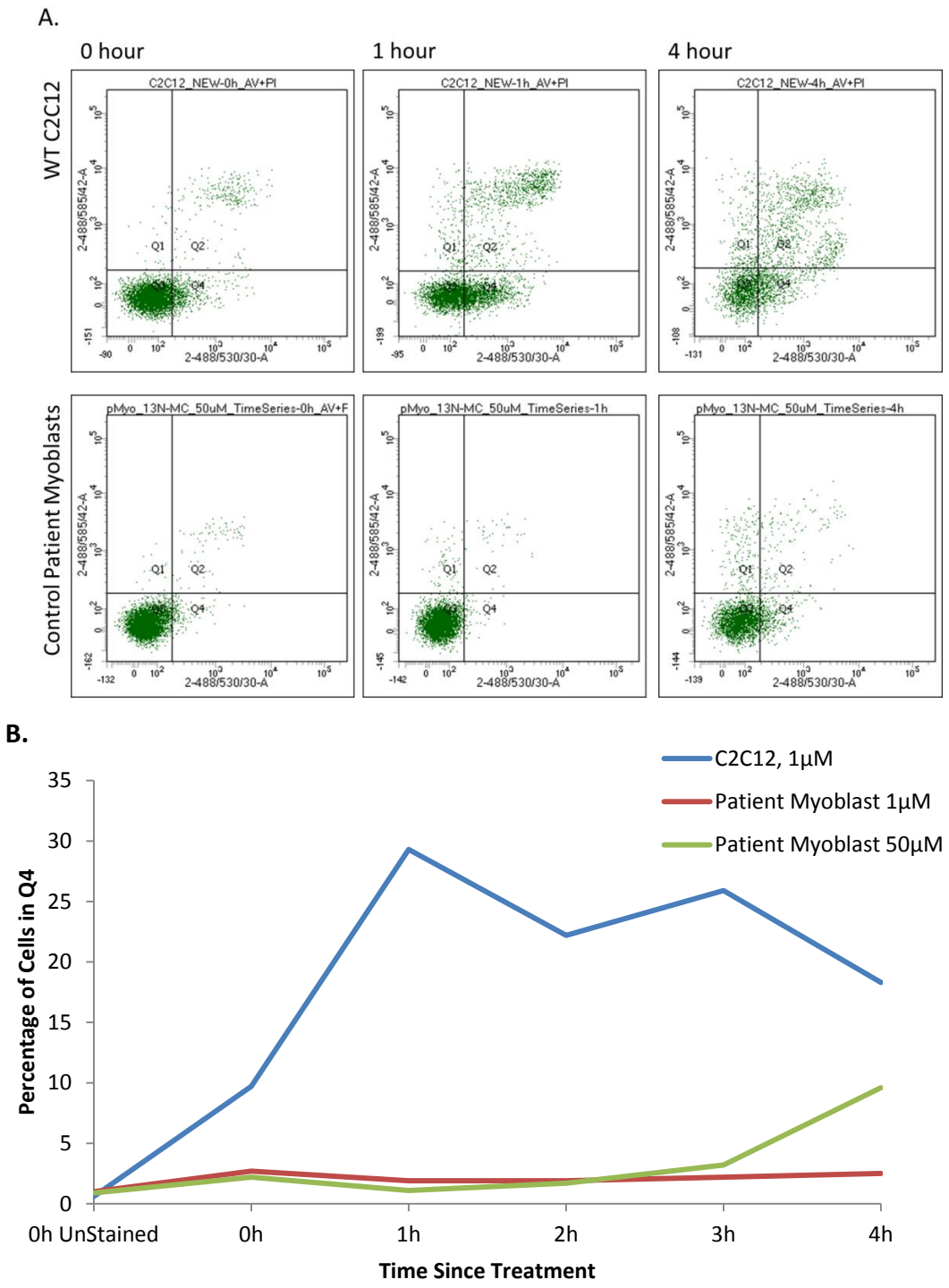

Figure 5.9 Differences in the increase of FITC-AV cells over time between wild type C2C12 and control patient myoblasts. A. Scatter graphs of wild type C2C12 and control patient myoblasts at 0 hour, 1 hour and 4 hour time points. Wild Type C2C12 data shows a more pronounced increase in FITC-AV and PI over the time course than control patient myoblasts. B. Line graph of the proportion of cells within Q4 during a time course of staurosporine treatment. Blue line represents WT C2C12 treated with 1µM staurosporine. Red line represents control patient myoblasts treated with 1µM staurosporine. Green line represents patient myoblasts treated with 50µM staurosporine. Lines indicate calculated standard error. Biological N = 3. Technical N = 1.

5.6.2 Flow cytometry investigation of FITC-AV stained patient myoblasts

The optimised flow cytometry apoptosis protocol was used on six patient myoblast lines, three ANO5 and three DYSF all as age and gender matched as possible, kindly provided by the Muscle Tissue Culture Collection team in Munich, headed by Dr Sabine Krause (Table 5.2). Three new healthy patient controls were also obtained from the Newcastle Biobank.

Each myoblast line was subjectively gated to remove debris and doublet events from the data and select the target cell population of interest. Two scatter plots were used to gate these data. Each point, or "event", on these graphs indicated the data recorded for an individual cell (Figure 5.10 A. and B.). The first graph plotted Forward Scatter Area (FSC-A) against Side Scatter Area (SSC-A), providing a representation of the morphology of the events in the prepared sample. The P1 populations were selected from these data, identified as the group of events clustering in the lower left corner of the graph (around ~50-100 units on both FSC-A and SSC-A axis).

The P1 data was plotted on the second scatter graph to further interrogate the morphology of the cell population and to exclude doublet events. This graph plotted FSC-A against Forward Scatter Height (FSC-H) allowing for exclusion of events which were "taller" than they were "wide", for example two cells which were stuck together in the flow path of the laser and read as one event. This sub-selected population was the P2 population which was used to create the experimental scatter graphs which plotted FITC-AV against PI.

All cell lines were prepared under five different conditions; Untreated/Unstained, Untreated/PI, Untreated/FITC-AV, Untreated/FITC-AV+PI and Staurosporine/FITC-AV+PI. The Untreated/Unstained and Untreated/FITC-AV+PI conditions respectively controlled for the background autofluorescence and apoptosis levels in the cell lines (Figure 5.10 C. and D.). The single dye treatment conditions were used to confirm that the set compensation values of the selected lasers were accurate and were specifically detecting the respective positively stained cells (Figure 5.10 E. and F.).

Cell Line ID	Age at Biopsy	Gender	Mutations
C052-11N-MC000000	31	Male	Healthy Control
C093-13N-MC000000	39	Male	Healthy Control
C128-13N-MC000000	40	Male	Healthy Control
2 DYSF 1015	32	Male	Homozygote frameshift mutation, Exon 26: 3152delG
3 DYSF 1015	58	Female	Exon 6: 610C>T (Arg204X) Exon 12: 1120G>C (Val374Leu)
7 DYSF 1015	39	Female	Exon 27: c.2875C>T = p.Arg959Trp, heterozygote Exon 28: c.2932G>T = p.Glu978Stop, heterozygote
1 ANO5 1015	42	Male	Exon5: c.191dupA bzw. p.Asn64LysfsX15, Exon 6: c.295-1 G>A heterozygote
2 ANO5 1015	44	Male	Exon 7 c.368C>T = p.Ser123Leu, Exon 11: c.1063C>T = p.Leu355Phe, heterozygote
3 ANO5 1015	36	Male	Exon 5: c.191dupA (p.Asn64LysfsX15); Exon 4: c.172 C>T (p.Arg58Trp) heterozygote

Table 5.2 Details of primary patient myoblasts used in this project. DYSF and ANO5 patient myoblasts and mutation data were kindly provided by Dr Sabine Krause's team in Munich from their patient cohort. Control patient myoblasts were kindly provided by the Newcastle Biobank at the John Walton Muscular Dystrophy Research Centre.

To maintain consistency between samples and between cell lines, the same template programme that was created using the data from the wild type C2C12 was used for all patient samples. The validity of the template was confirmed by running the control patient myoblasts first and visually confirming that the template was correctly compensated.

Data from P1 and P2 scatter plots show that following staurosporine treatment the morphology of all the myoblast lines becomes less defined (Figure 5.11). While a clear

population is still definable in the P1 scatter plot across all cell lines, allowing for selection of a P1 population, the distribution of events are spread across the graph.

The change in myoblast morphology is confirmed in the P2 selection scatter graphs (Figure 5.11 B.). Here the pattern of recorded events on the scatter plot suggests that following staurosporine treatment, there is an increase in the number of cells with a height-to-area disparity. Though there is a clearly identified population of cells which conform to the expected width and height, allowing for selection of the P2 population.

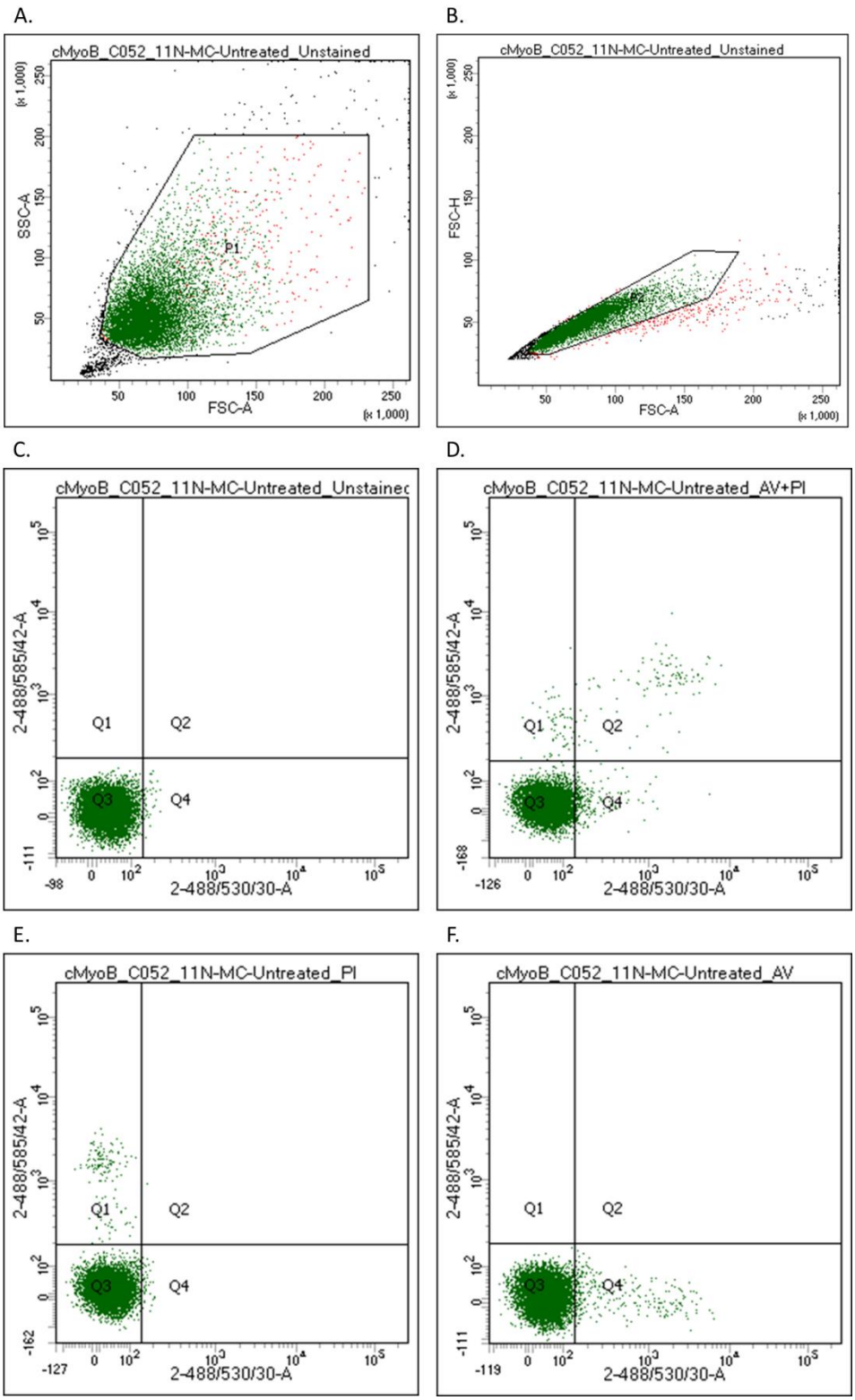

Figure 5.10 Examples of flow cytometry gating work flow. A. Scatter graph of P1 gating, FSC-A against SSC-A. B. Scatter graph of P2 gating, FCS-A against FSC-H. C.-F. Final population scatter graphs, C. Untreated/Unstained control; D. Untreated/FITC-AV+PI background control; E. Untreated/PI only background control; F. Untreated/FITC-AV only background control. Axis labelled 2-488/530/30-A displays FITC-AV fluorescence intensity. Axis labelled 2-488/585/42-A displays PI fluorescence intensity. All axis' are on a logarithmic scale.

A.

Untreated

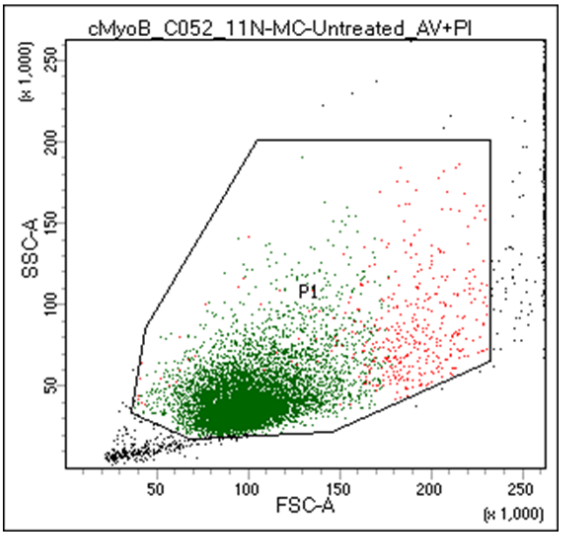

Staurosporine

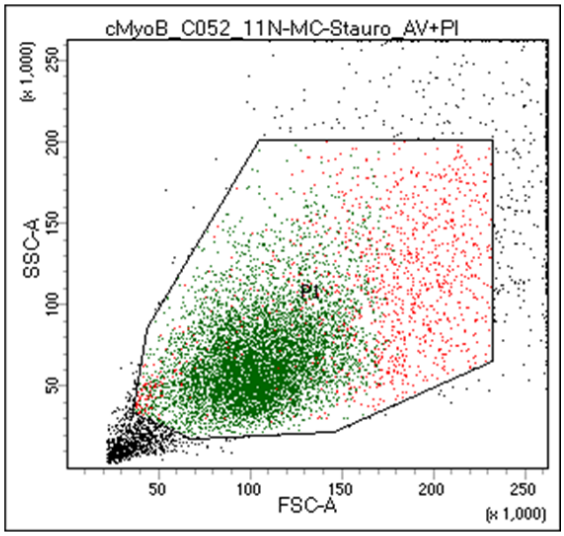

B.

Untreated

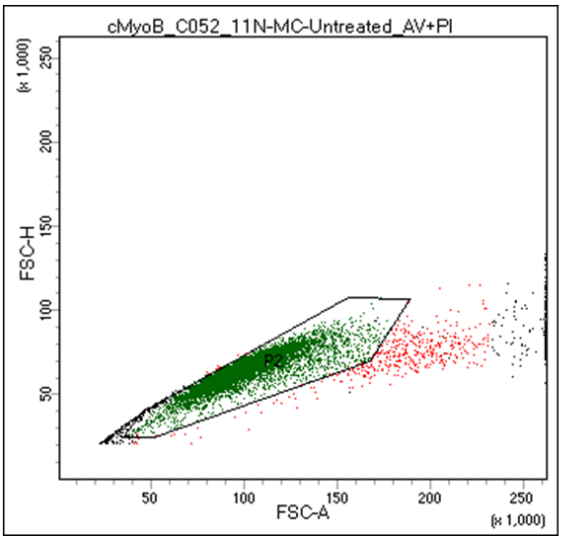

Staurosporine

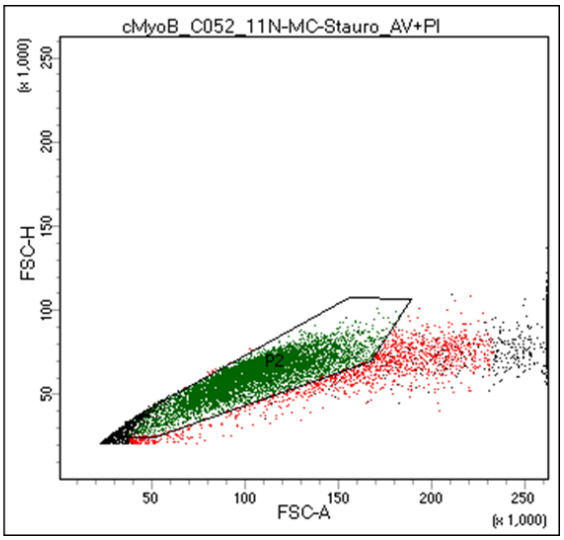

Figure 5.11 Example of the change in control myoblast morphology following 4 hour staurosporine treatment. A. Example P1 gated scatter graphs (FSC-A against SSC-A) of both untreated and staurosporine treated conditions. B. Example P2 gated scatter graphs (FSC-A against FSC-H) of both untreated and staurosporine treated conditions. Red dots indicate P1 gated population. Green dots indicate P2 gated population. All graph axis' are all on a logarithmic scale.

The data from the PI only (Figure 5.12) and FITC-AV only stained control scatter graphs (Figure 5.13) show that the majority of events remain in Q3. This indicates that the majority of cells show little AV or PI positivity and suggests that they are still viable, i.e. non-apoptotic, which has been observed before in earlier time series experiments. The PI only data for the control patient lines show that the majority of other events fall within Q1, the portion of the graph expected for that dye. There are however a number of events in the DYSF and ANO5 lines which are also detected in the Q4 and Q2 portions of the graph. This is not the case for the FITC-AV only condition, where all cell lines showed events only within the Q3 and Q4 portions of the graph. This indicates that there is some background in the FITC-AV laser detection, most likely generated by events included in the P1 and P2 populations which were undergoing early apoptosis. However, as these events were not distributed across the length of the FITC axis and instead restricted to just outside the designated Q1 and Q3 sections of the graph, the compensations applied to the laser detectors were not altered. This ensured more accurate reproducibility between cell lines.

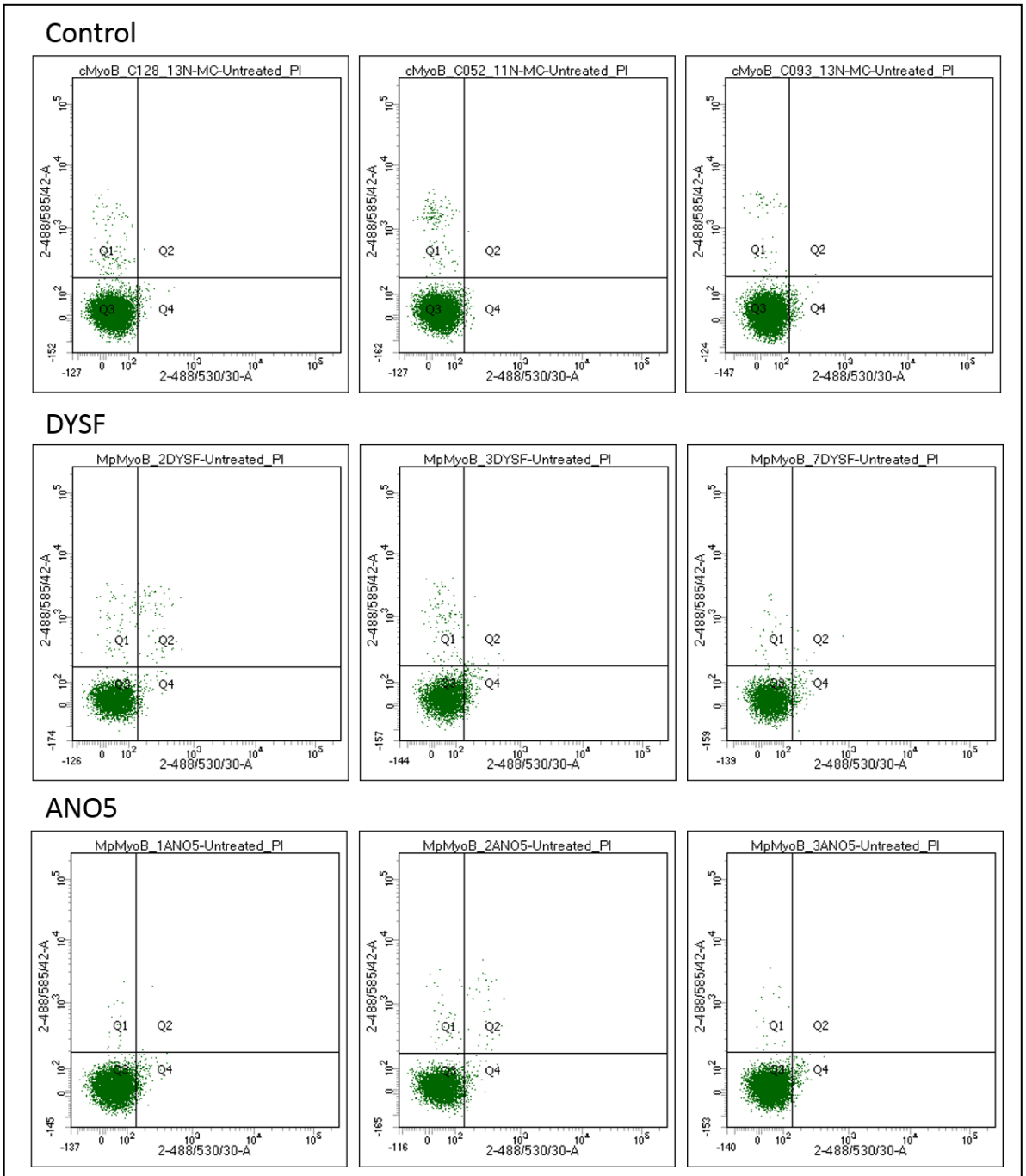

Figure 5.12 Scatter graphs of PI stained untreated control, DYSF and ANO5 patient myoblasts. Axis labels indicate the laser/detector parameters used. Axis labelled 2-488/530/30-A displays FITC-AV fluorescence intensity. Axis labelled 2-488/585/42-A displays PI fluorescence intensity. All axis' are on a logarithmic scale. Biological N = 9. Technical N = 1.

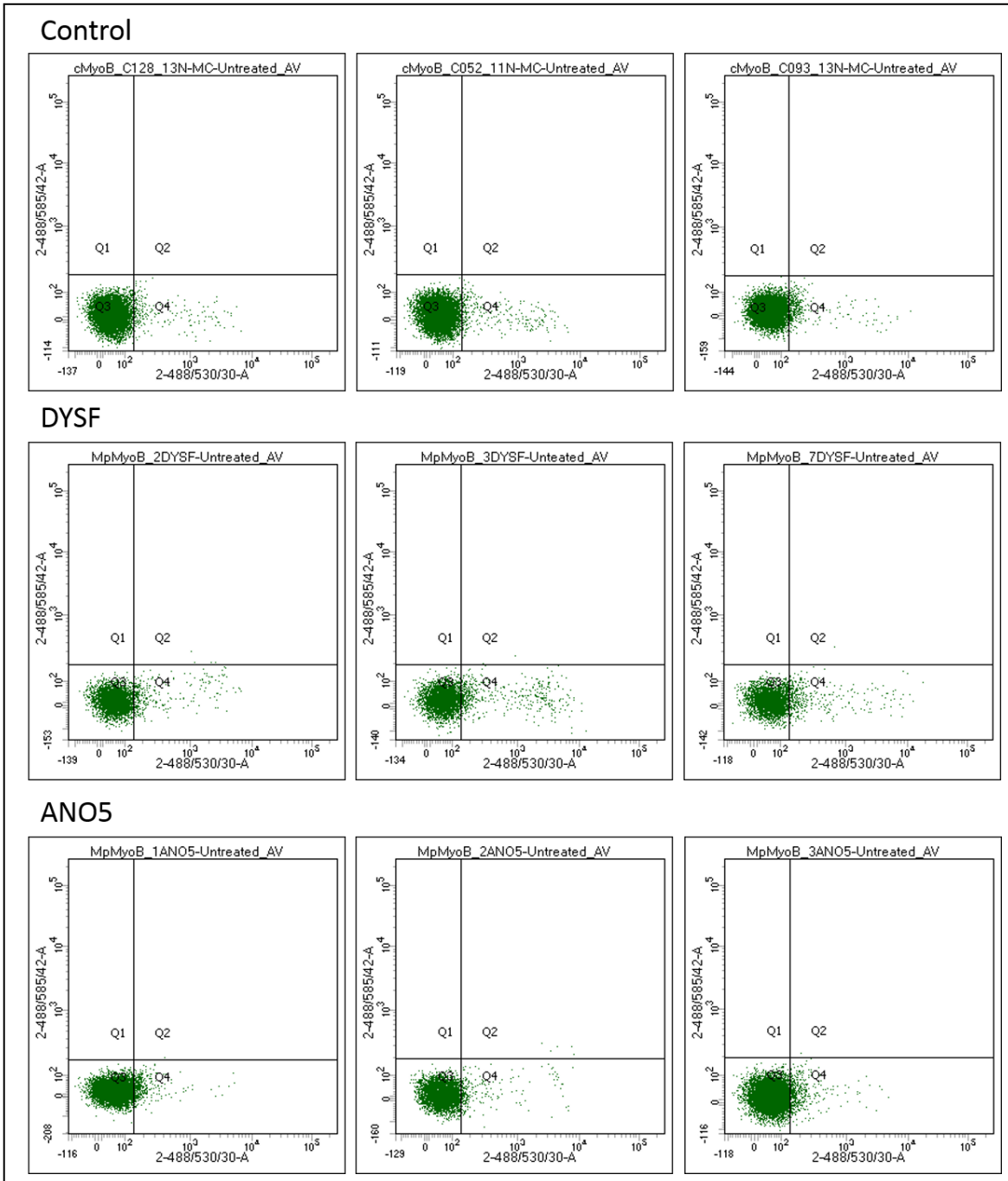

Figure 5.13 Scatter graphs of FITC-AV stained untreated control, DYSF and ANO5 patient myoblasts. Axis labels indicate the laser/detector parameters used. Axis labelled 2-488/530/30-A displays FITC-AV fluorescence intensity. Axis labelled 2-488/585/42-A displays PI fluorescence intensity. All axis' are on a logarithmic scale. Biological N = 9. Technical N = 1.

The data from the experimental scatter graphs for the Staurosporine/FITC-AV+PI condition again consistently show that the majority of events are recorded within the Q3 portion of the graph (Figure 5.14), indicating the majority of cells show little AV or PI positivity. There are however a number of events recorded within the other portions of the graphs indicating the apoptotic events positively stained by FITC-AV and PI.

In control myoblasts, while a portion of events are recorded in the Q4 portion of the graph, a clear population of cells are located in the Q1 and Q2 portions of the graph forming a pattern resembling an upside down “L”. This suggests that control myoblasts, or more likely a subset of them, are becoming PI-positive before they become FITC-AV-positive.

There is a less consistent pattern of distribution between the DYSF and ANO5 myoblast lines. The 3DYSF line shows a clear population of cells which have moved through Q4 and are transitioning up to Q2. In 2DYSF and 7DYSF lines however, while there could be a similar movement of cells as in 3DYSF, the majority of events outside of the Q3 portion of the graph appear roughly equally across Q1, 2 and 4.

This roughly equal distribution of events is also seen in the ANO5 lines, with no clear pattern of cellular movement. However, there appears to be a reduced number of cells in portions Q1, 2, and 4 of the graphs compared to the DYSF lines.

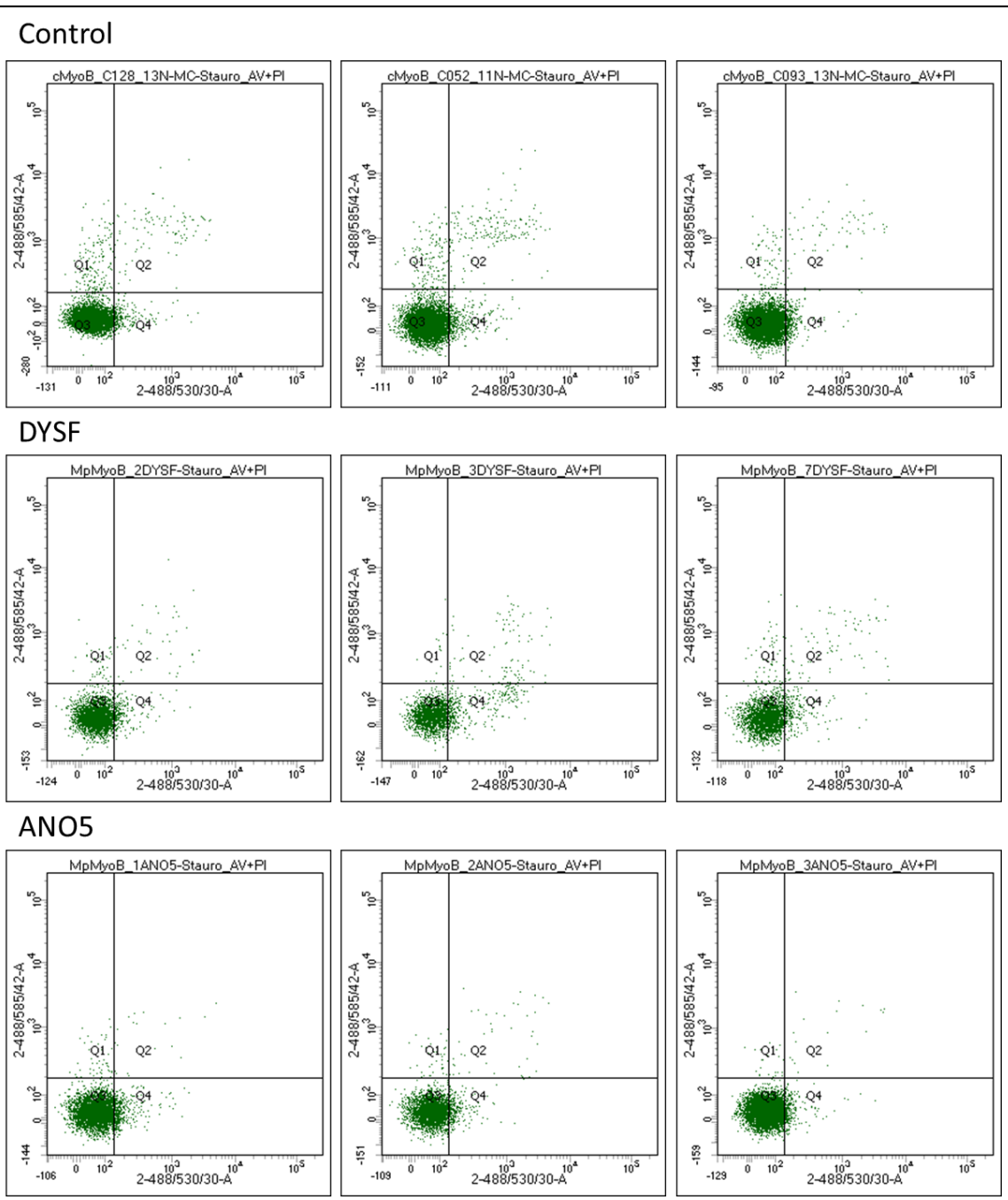

Figure 5.14 Scatter graphs of PI ad FITC-AV stained staurosporine treated control, DYSF and ANO5 patient myoblasts. Gated population data of the staurosporine treated samples. Axis labels indicate the laser/detector parameters used. Axis labelled 2-488/530/30-A displays FITC-AV fluorescence intensity. Axis labelled 2-488/585/42-A displays PI fluorescence intensity. All axis' are on a logarithmic scale. Biological N = 9. Technical N = 1.

5.6.3 Statistical analysis of flow cytometry analysis data

The same Chi^2 statistic used in sections 2.6.2 and 5.4 was again used to statistically analyse the gathered flow cytometry data (Table 5.3). The focus of these experiments were to investigate the difference in FITC-AV binding between patient lines and control myoblasts. To estimate the number of FITC-AV-positive cells the proportion of cells in the Q4 portion of the scatter graph was used. However to more fully understand the data and the differences between the Control and patient cell lines, Chi^2 values were calculated between ANO5 and Control and DYSF and Control patient lines for each quadrant, for each of the five treatment conditions. The hypothesis tested was therefore modified to "There is a difference in the proportion of events present in a given scatter graph quadrant between patient and healthy control myoblasts", with the main hypothesis to be tested being "There is a difference in the proportion of events present in Q4 between patient and healthy control myoblasts".

These data confirm that there are highly significant differences in the proportion of events in the relative quadrant of the scatter graph between patient and control myoblasts in the majority of treatment conditions (Figure 5.15). The exceptions are the DYSF myoblasts in Q1 in the Untreated/PI+FITC-AV condition ($p < 0.15$, Figure 5.15 C.) and both patient myoblast lines in the Q1 and Q2 portions of the Untreated/FITC-AV condition (Figure 5.15 B.). This is the case for the latter quadrants as there are no control myoblast events in these quadrants of the scatter plot under these treatment conditions, meaning that calculation of an expected value, and therefore a Chi^2 statistic, is not possible.

Data from the two control conditions (PI and FITC-AV only) show the baseline distribution of myoblasts across all lines. In the Untreated/FITC-AV condition all myoblasts outside of Q3 appear in Q4, indicating the single staining of FITC-AV (Figure 5.15 B.). Higher percentages of FITC-AV-positive cells in Q4 than in the Untreated/FITC-AV+PI condition can be explained by the absence of a PI stain. Cells that may potentially be PI-positive as well are unable to be detected, meaning they are located in Q4 rather than in Q2. Data for the Untreated/PI condition confirm previous observations that while there are a percentage of cells (<3%) in the Q1 portion of the graph as expected, there are also cells present in both Q2 and Q4 portions of the scatter graph (Figure 5.15 A.). These data indicate background fluorescence detected by the FITC-AV detector. The reason for such a low percentage of PI-positive cells is due to

PI expression in late apoptotic cells. As apoptosis was not induced in these cells, PI expression is expected to be low.

The Untreated/FITC-AV+PI data indicate the base level of apoptosis in the myoblasts. In all cell lines, while there are elevated percentages of cells in Q1 and Q2, the largest percentage is found in Q4 (Figure 5.15 C.). Intriguingly, DYSF myoblasts consistently show the highest percentage positivity compared to ANO5 and control lines. The lowest percentage positivity are found in the control patient myoblasts. ANO5 patient myoblast percentage are shown to be statistically significantly different than control patient myoblasts, but do not have percentages as high as the DYSF lines.

This finding is repeated in the Stauro/FITC-AV+PI condition, though there is an increase in the percentage positivity across cell lines and quadrants, indicating the effect of staurosporine treatment (Figure 5.15 D.). The observation made of control myoblasts having a different pattern of movement through Q1 and Q2 is also seen in these alternative displays of the data. The percentage of control myoblast cells is generally higher in Q1 than compared to the ANO5 and DYSF patient myoblasts. Though small this is a statistically significant difference, supporting the observation that when treated with staurosporine a subset of the control patient myoblasts moves into Q1. However the highest percentage of these cells is still within Q4 also suggesting that another population of cells is reacting to the staurosporine in the same way as the patient myoblasts.

Additionally, these data support previous *in situ* microscopy data showing that control patient myoblasts have the lowest percentage of FITC-AV positivity across cell lines. This suggests that there is an underlying difference in the response of control myoblasts and patient myoblasts to staurosporine treatment. Consequently it is not possible to say if loss of ANO5 affects PS exposure in patient myoblasts.

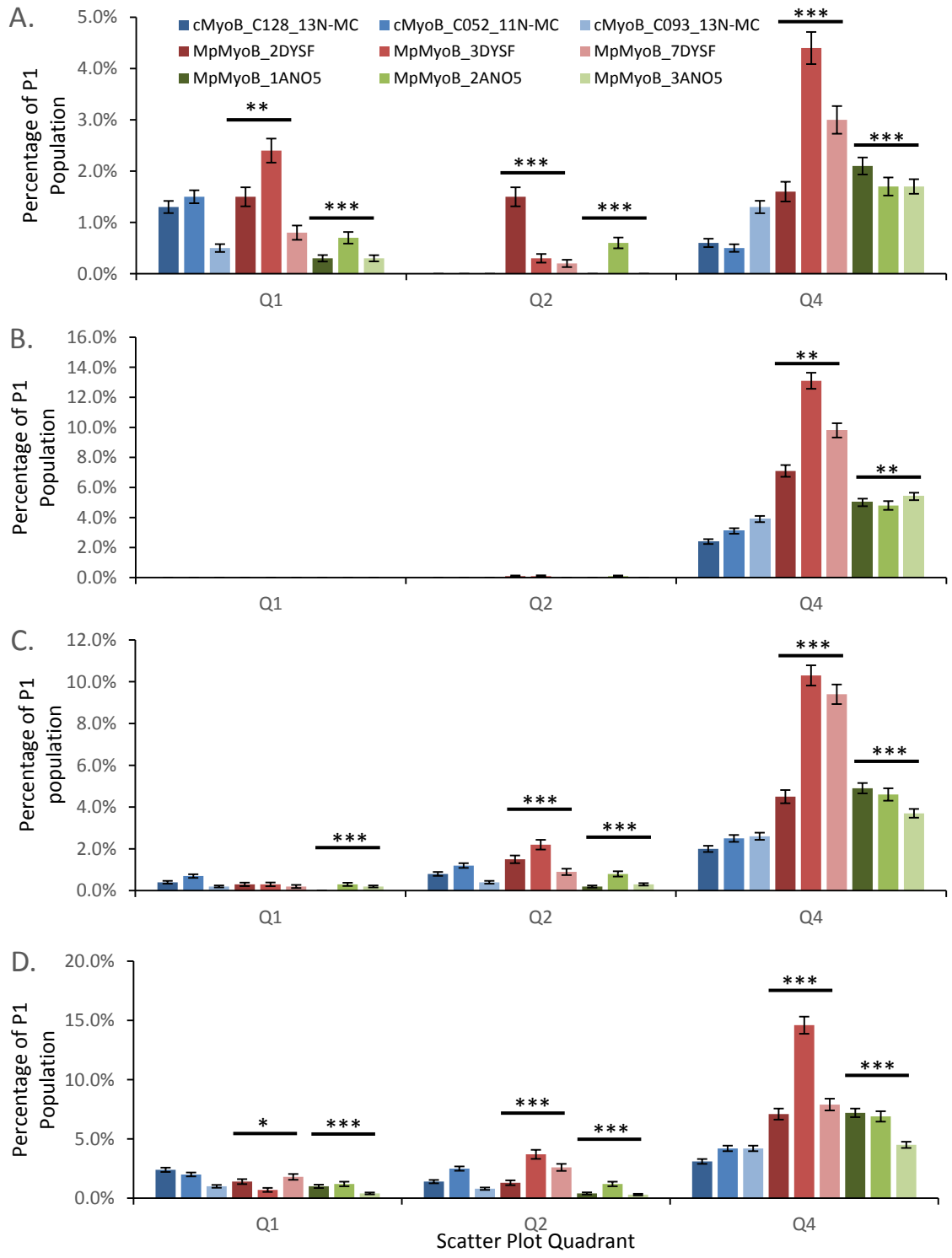

*Figure 5.15 Percentages of cells present in different portions of scatter graphs for each treatment condition. Percentages are calculated from the P2 population of cells. A. Untreated/PI; B. Untreated/FITC-AV; C. Untreated/FITC-AV+PI; D. Stauro/FITC-AV+PI. Blue bars represent control patient myoblasts. Red bars represent DYSF patient myoblasts. Green bars represent ANO5 patient myoblasts. Specific cell line ID codes are given in the legend in A. *** indicates significance with $p < 0.001$, ** indicates significance with $p < 0.01$, * indicates significance with $p < 0.09$, all at 2 degrees of freedom. Lines indicate calculated standard error. Biological N = 9. Technical N = 1.*

A. Untreated_Unstained

Cell Line	Population					
	P1	P2	Q1	Q2	Q3	Q4
cMyoB_C128_13N-MC	9350	9127	0	0	9059	68
cMyoB_C052_11N-MC	9302	9022	0	0	8978	44
cMyoB_C093_13N-MC	9097	8778	0	0	8674	104
MpMyoB_2DYSF	5260	4206	0	8	4033	165
MpMyoB_3DYSF	4986	3995	0	7	3818	170
MpMyoB_7DYSF	5042	4193	0	3	4094	96
MpMyoB_1ANO5	8174	7458	1	1	7346	110
MpMyoB_2ANO5	6523	5541	0	5	5431	105
MpMyoB_3ANO5	8477	8188	0	1	8061	126

B. UnT_PI

Cell Line	Population					
	P1	P2	Q1	Q2	Q3	Q4
cMyoB_C128_13N-MC	9333	9039	113	1	8867	58
cMyoB_C052_11N-MC	9493	9154	137	1	8971	45
cMyoB_C093_13N-MC	9197	8810	47	1	8646	116
MpMyoB_2DYSF	5322	4287	64	64	4091	68
MpMyoB_3DYSF	5299	4279	102	13	3974	190
MpMyoB_7DYSF	4870	4007	32	8	3846	121
MpMyoB_1ANO5	8268	7568	20	2	7386	160
MpMyoB_2ANO5	6447	5429	39	31	5267	92
MpMyoB_3ANO5	8528	8268	22	0	8108	138

C. UnT_AV

Cell Line	Population					
	P1	P2	Q1	Q2	Q3	Q4
cMyoB_C128_13N-MC	9311	8940	0	0	8725	215
cMyoB_C052_11N-MC	9452	8923	0	0	8646	277
cMyoB_C093_13N-MC	9080	8644	0	0	8306	338
MpMyoB_2DYSF	5288	4291	0	4	3981	306
MpMyoB_3DYSF	5059	3999	0	2	3475	522
MpMyoB_7DYSF	4797	3902	0	1	3518	383
MpMyoB_1ANO5	8197	7515	0	1	7137	377
MpMyoB_2ANO5	6316	5309	0	6	5046	257
MpMyoB_3ANO5	8586	8336	0	1	7889	446

D. UnT_AV+PI

	Population					
Cell Line	P1	P2	Q1	Q2	Q3	Q4
cMyoB_C128_13N-MC	9179	8744	38	74	8453	179
cMyoB_C052_11N-MC	9458	9020	61	104	8628	227
cMyoB_C093_13N-MC	9126	8637	19	34	8356	228
MpMyoB_2DYSF	5373	4324	13	64	4051	196
MpMyoB_3DYSF	4985	3904	10	86	3407	401
MpMyoB_7DYSF	4706	3895	9	37	3482	367
MpMyoB_1ANO5	8186	7505	3	14	7120	368
MpMyoB_2ANO5	6020	4979	13	39	4697	230
MpMyoB_3ANO5	8518	8250	18	21	7907	304

E. Stauro_AV+PI

	Population					
Cell Line	P1	P2	Q1	Q2	Q3	Q4
cMyoB_C128_13N-MC	7953	7034	168	96	6554	216
cMyoB_C052_11N-MC	8366	7083	143	176	6467	297
cMyoB_C093_13N-MC	8064	7420	75	61	6976	308
MpMyoB_2DYSF	3896	3064	42	39	2765	218
MpMyoB_3DYSF	3481	2388	17	88	1935	348
MpMyoB_7DYSF	3839	2960	54	78	2595	233
MpMyoB_1ANO5	6449	4954	51	18	4530	355
MpMyoB_2ANO5	4333	3321	41	39	3012	229
MpMyoB_3ANO5	7138	6191	25	17	5873	276

Table 5.3 Raw flow cytometry counts for each gated population of each patient cell line under each treatment condition.

5.7 Investigation of ANO5 translocation during apoptosis

As ANO5 is an intracellularly expressed protein, how the knockdown of ANO5 affects PS exposure at the plasma membrane is unclear (Duran *et al.*, 2012). One hypothesis is that ANO5 is located to specific vesicle populations which move to the sarcolemma when the cell is stimulated by apoptotic signals. To test this hypothesis, the localisation of ANO5 to specific vesicle compartments and the subsequent movement of these organelle populations to the plasma membrane following apoptotic stimulation was investigated using transient transfection of Myc-tagged ANO5 in tandem with dyes which label the cell lysosomes.

5.7.1 Lysotracker staining optimisation

LysoTracker Red DND99 is a red dye which localises to the lysosomes of cells (Diwu *et al.*, 1994). Optimisation of staining was carried out on wild type C2C12. These data show that staining was successful at all concentrations (70, 60 and 50nM) though with different signal to background ratios, depending on concentration and length of staining (Figure 5.16). The pattern of staining follows a punctate pattern within the cytoplasm of the cells. Rapid signal loss was an issue when imaging however, especially at higher magnifications so more detailed investigation could not be made. From these data, staining with 70nM of lysotracker for 1 hour was chosen as optimal conditions. These conditions gave the brightest signal-to-noise staining of lysosomes and so, it was hoped, the longest retention of signal when combined with immunofluorescence staining.

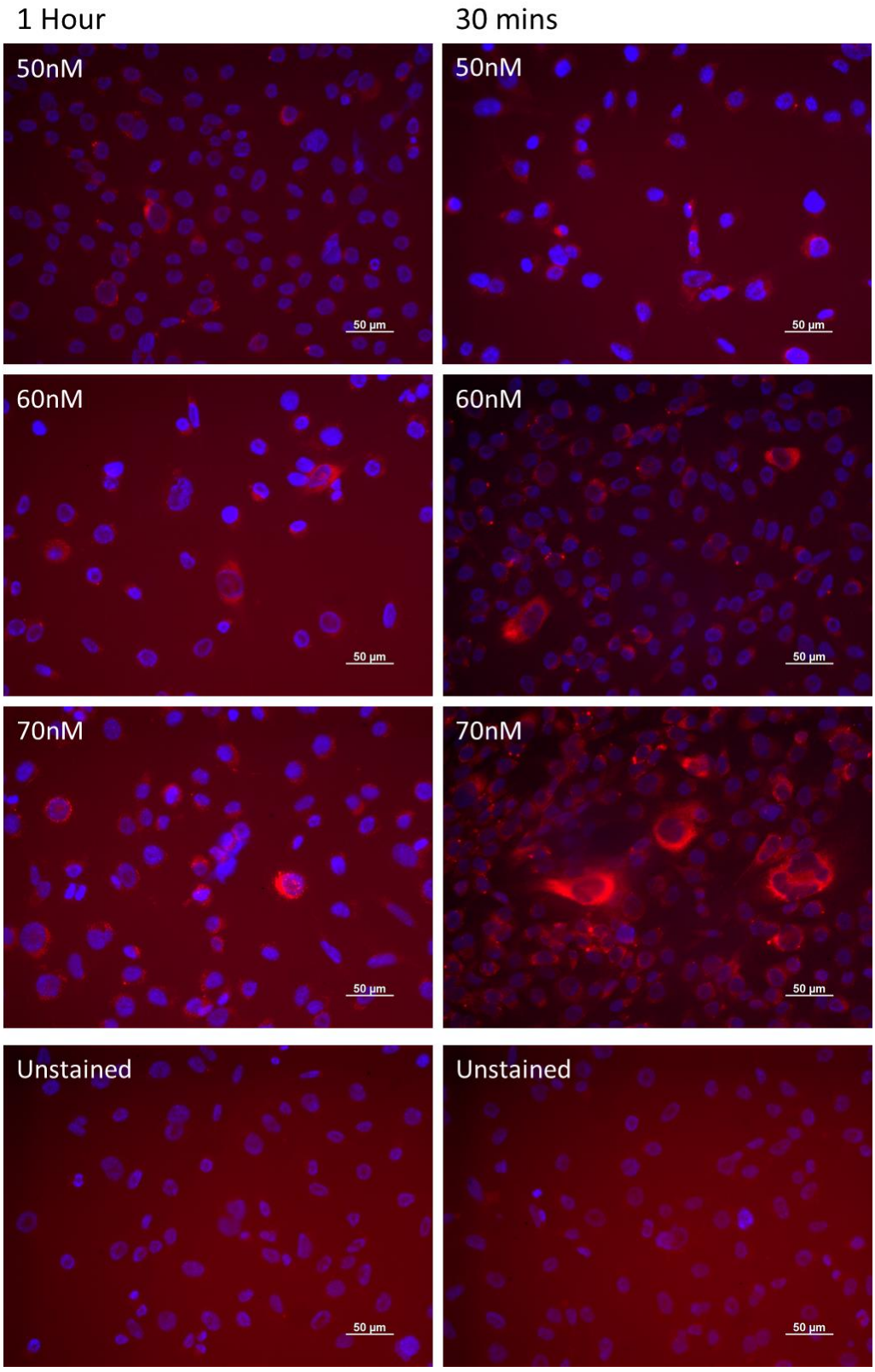

Figure 5.16 Optimisation of LysoTracker concentrations and treatment time. Left hand column indicates 1 hour of LysoTracker treatment. Right hand column indicates 30 minutes of LysoTracker treatment All images are taken at x20 magnification (scale bars = 50µm). Biological N = 4. Technical N = 2.

5.7.2 Tandem ANO5-Myc immunofluorescence and Lysotracker staining

Localisation of anoctamin 5 in relation to lysosomes was investigated using tandem LysoTracker and standard IF staining of ANO5 and GFP constructs transiently transfected into wild type C2C12.

Micrographs of C2C12 stained with both Lysotracker and 9E10 primary antibody show that transfection of and staining for the ANO5-Myc construct was successful (Figure 5.17). The pattern of Myc staining is the same as has been observed previously; a punctate pattern throughout the cytoplasm but with concentrations of staining close to the nucleus. This staining pattern is not present in untransfected and only with secondary antibody-stained conditions suggesting that this is true signal. There appears to be some LysoTracker positivity in the co-stained condition, but only a few fluorescent spots are observable and are present in only in Myc-negative cells.

However, untransfected cells stained with LysoTracker show the same staining pattern as untransfected and unstained cells. This suggests that the staining seen in the LysoTracker only stained cells are background, most likely caused by rapid bleaching of the LysoTracker signal. It is therefore likely that all the Lysotracker staining is background. These data suggest that while transfection and staining of the ANO5-Myc construct was successful, accurate detection of the lyosomes using the selected LysoTracker staining parameters failed.

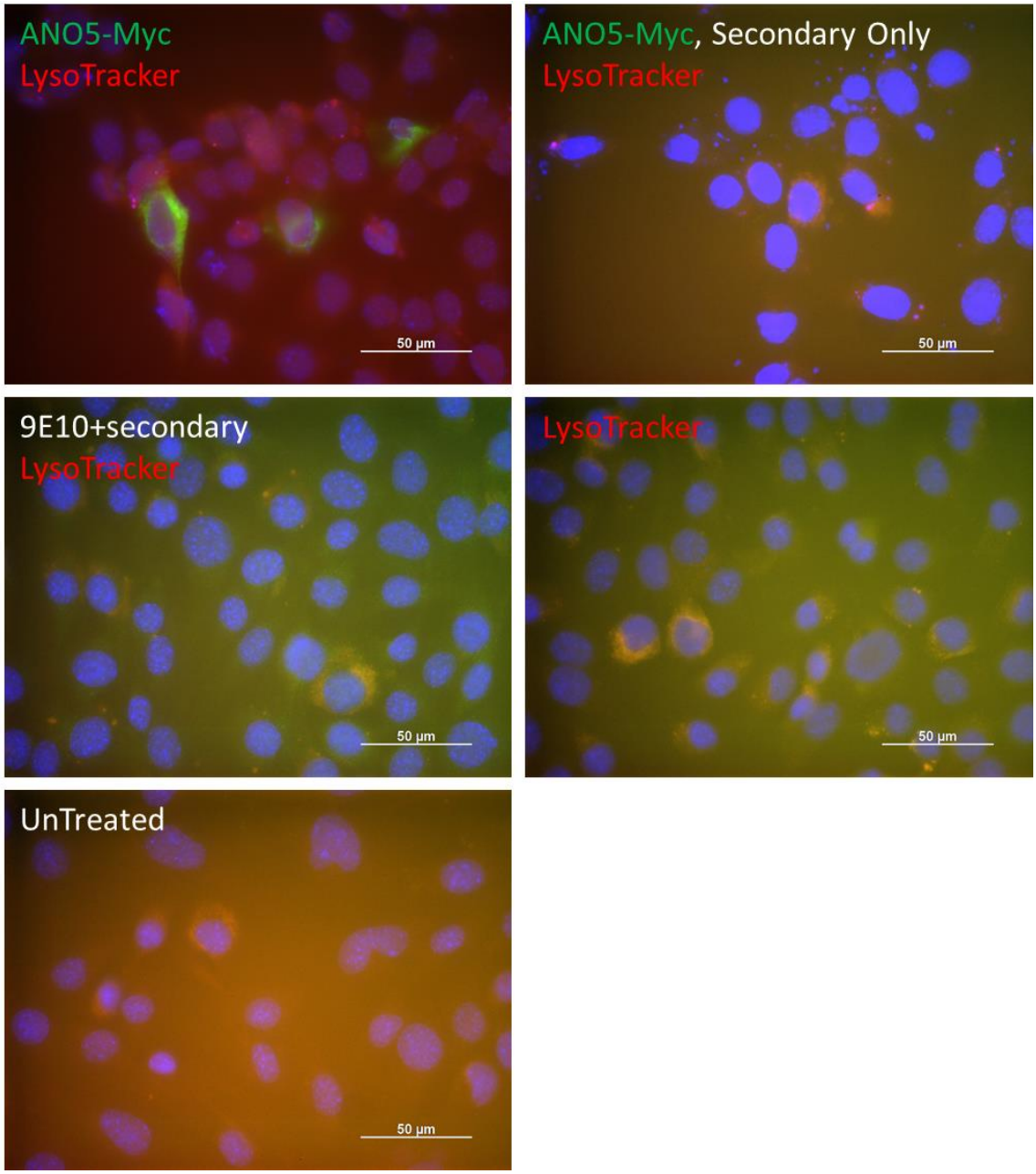

Figure 5.17 LysoTracker colocalisation with ANO5-Myc. Red fluorescence indicates LysoTracker stain. Green fluorescence indicates 9E10 (anti-Myc) antibody + alexa fluor 488 secondary antibody. All images are taken at x40 magnification (scale bars = 50µm). Biological N = 3. Technical N = 1.

5.7.3 ANO5-Myc and GFP co-expression during apoptosis

Movement of ANO5 during apoptosis was still investigated by observing expression of Myc tagged ANO5 before and after induction of apoptosis. This was achieved by sequentially combining the transfection, apoptosis induction and immunofluorescent staining protocols of previous experimentation. ANO5-Myc constructs were transiently transfected into wild type C2C12 and then either fixed and imaged or treated with staurosporine and EGTA combinations to induce apoptosis. Slides were incubated for 4 hours under normal tissue culture conditions before standard fixation and IF staining. GFP constructs were also transfected into C2C12 as transfection controls and as a control for construct retention following apoptosis induction. The GFP construct was used for this purpose as it has a higher transfection efficiency (~50%) compared to tagged ANO5 constructs (~7-10%). It was hoped that the higher transfection efficiency would mean that a proportion of GFP-positive cells would be retained even following apoptosis induction.

Results show that transfected ANO5-Myc and GFP constructs remain detectable following apoptotic treatments (Figure 5.18). The number of detectable transfectants appears to be related to the initial transfection efficiency as while a number of GFP-positive cells were detectable post-treatment, only one or two ANO5-Myc-positive cells remained post-treatment.

From the transfectants remaining in each apoptosis treatment condition, it is clear that transfected cells undergo the same processes post-treatment such as shrinking of the cytoplasm. However Myc-positive staining appears to remain throughout the cytoplasm, with no observable concentrations of expression near the plasma membrane. GFP transfected into C2C12 also show no change in expression pattern post-treatment. Expression of these GFP constructs remains within the cytoplasm of the cells with only the additional Myc tag staining being detected on the membrane.

These results therefore suggest that while it is still possible to detect transfected ANO5-Myc and GFP constructs post-apoptosis treatment, there appears to be no difference in the localisation of ANO5 between apoptotic and non-apoptotic C2C12.

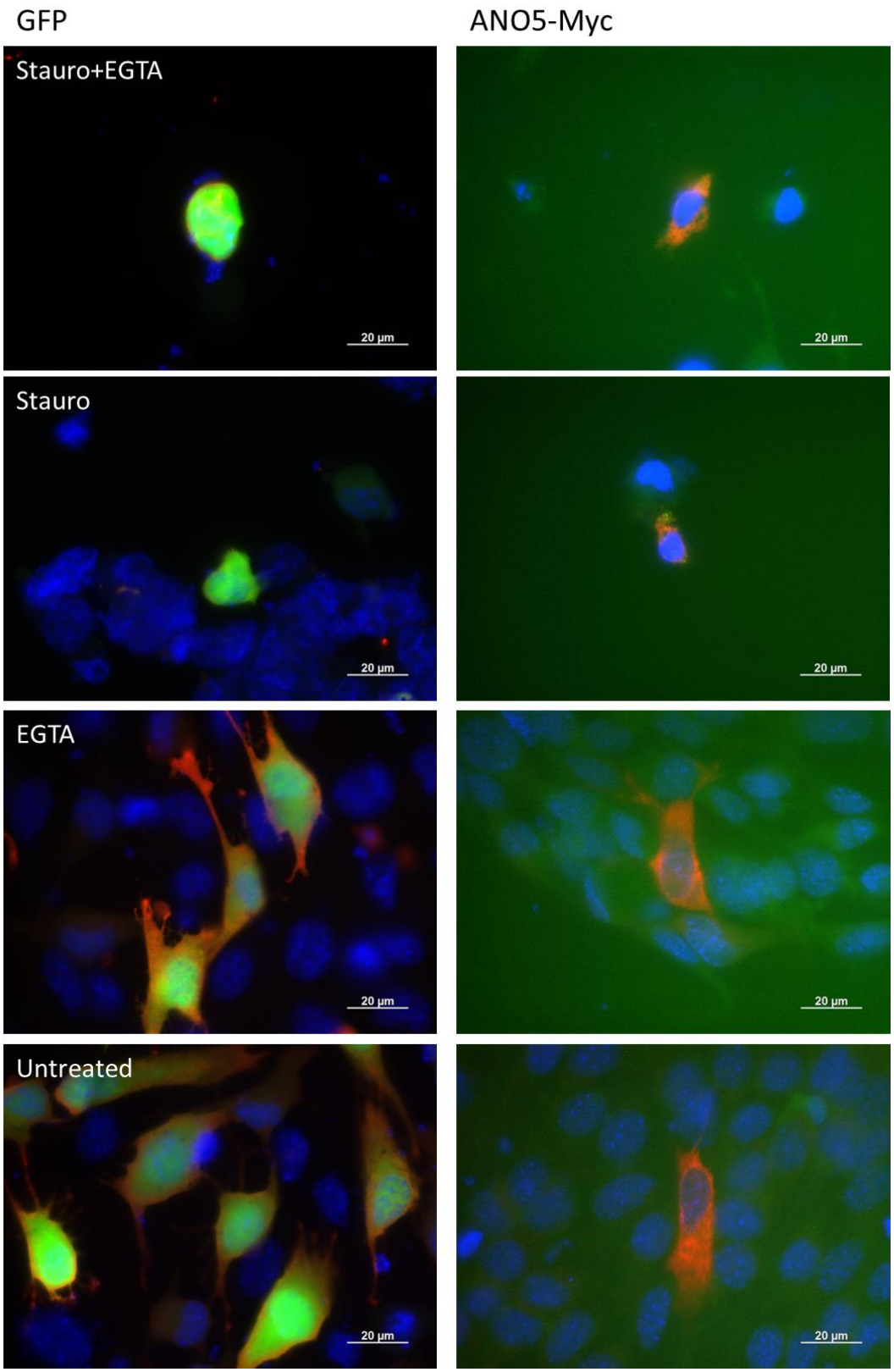

Figure 5.18 Translocation of overexpressed ANO5-Myc during apoptosis. Red fluorescence is of 9E10 (anti-Myc) antibody + alexa fluor 594 secondary antibody. Green fluorescence is of GFP fluorescence and is only present in GFP transfected cells. Staurosporine and EGTA combinations used to induce apoptosis are indicated. All images are taken at x63 magnification (scale bars = 20µm). Biological N = 2. Technical N = 1.

5.8 Discussion

The low FITC-AV and phalloidin positivity detected in D1 C2C12 is not surprising as relatively little expression of these proteins is expected at this time point (van der Ven *et al.*, 1992). Phalloidin is well established as a marker of F-actin (Faulstich *et al.*, 1988; Huang *et al.*, 1992) and the expression pattern in these data are consistent with reports from the literature (van der Ven *et al.*, 1992; Engler *et al.*, 2004). However the detected expression of FITC-AV is different from that reported in the literature. While expected to form aggregates on the external leaflet of the plasma membrane (Jeong and Conboy, 2011), the localisation of these aggregates is not at cell-cell contact points, where fusion would be expected to occur (van den Eijnde *et al.*, 2001).

An explanation for the localisation of FITC-AV aggregates to the longitudinal portion of forming myotubes may be that these are actually collections of excess FITC-AV and that these aggregates are not binding to PS. Increased levels of FITC-AV fluorescence from these aggregates may also mean that true fluorescence signal of PS bound FITC-AV remains undetected or overlooked. To account for this, sites of expected fusion were specifically investigated for low levels of FITC-AV but found no detectable FITC-AV staining. This ultimately suggests that this particular assay was not suitable to detect PS exposure during myoblast differentiation. An alternative, more sensitive assay may be more effective and identify sites of PS exposure during differentiation.

The FITC-AV assay was successfully utilised in apoptosis experiments with knockdown C2C12. The statistically significant difference in the number of FITC-AV-positive cells between ANO5 and control knockdown C2C12 suggests that knockdown of ANO5 is reducing the ability of C2C12 to expose PS at the plasma membrane. Additionally, the non-significant difference in the number of aC3-positive cells in the experimental, staurosporine only condition also suggests that the knockdown specifically affects PS exposure. However, the statistically significant differences in aC3 positivity in staurosporine+EGTA, EGTA only and untreated conditions opposes this conclusion and instead suggests that knocking down ANO5 may be having a general effect on the apoptotic pathway of the cells.

One explanation for the significant difference in the number of aC3-positive cells in these conditions may lie in the observation that the number of FITC-AV-positive cells is higher in ANO5 knockdown C2C12 in the EGTA only and untreated conditions. This may suggest that the ANO5 knockdown C2C12 have an increased rate of apoptosis over

the control knockdowns leading to increased aC3 activation and a significant difference in the aC3 values for the same experimental conditions.

The statistically significant aC3 values could also be explained by the relatively restricted number of knockdown clones compared. Increasing the number of knockdown clones compared would increase the accuracy of the Chi^2 statistic, for both aC3 and FITC-AV positivity. This would ultimately increase the validity of the finding that knocking down ANO5 specifically impacts PS exposure in C2C12. Additionally, a second marker of apoptosis could be run to confirm these data. Poly(ADP-Ribose) Polymerase-1 (PARP-1) would be a good choice as it is activates a caspase-independent apoptotic pathway(Yu *et al.*, 2002). This would be a useful additional confirmation step as other studies investigating the utility of various apoptotic markers have found variability in the correlation between the expression of markers and visible apoptotic morphology in the same cells (Holubec *et al.*, 2005).

The microscopy protocol for this assay was insufficient for detecting differences between patient myoblast lines. It was hoped that flow cytometry analysis in tandem with a larger number of patient myoblast lines would allow for successful investigation of PS exposure in these cells. However as the majority of myoblasts remain in Q3 across all cell lines, indicating that these cells remain viable, these data ultimately show that a better method of apoptosis induction, such as by the Fas/Fas-L pathway (Waring and Mullbacher, 1999), should be applied in future work. Investigation of alternative apoptosis induction methods would also be useful in understanding whether loss of ANO5 and DYSF makes myoblasts more susceptible to staurosporine than control lines, explaining the larger percentage population values for patient myoblasts.

The protocol could be further optimised by using time series data rather than single time point data. To maintain consistency with *in situ* data these experiments only sought to collect single time point data. But time series data would more accurately show the response of the cells from the moment of treatment through to a desired end point, potentially right up to death of the entire population.

Possible explanations for the differences seen between patient lines, such as an apparent sub-population of cells moving through Q1 to Q2 in control patient myoblast lines but not in ANO5 and DYSF patient lines, include differences in the constituent sub populations of cells between control and patient lines. This leads to an altered overall population in the control patient myoblasts which becomes PI-positive quicker than

AV-positive. To combat this issue preliminary cell sorting before running the assay would increase the purity of the primary myoblast population. Using a series of cytometry suitable dyes targeted against cell specific antigens, it would be possible to pre-screen the total cell population specifically for myoblasts. Flow cytometry is an exceptionally powerful tool, with the ability to record data from several colours simultaneously. Using only two colour channels in these experiments, while appropriate for the assay used, did not utilise the full power of this technology. Other assays have used multiple dyes to select for populations of a single cell type, for example for phenotype experiments involving t-cell populations (Chattopadhyay and Roederer, 2012). In tandem with an optimal method of inducing apoptosis, selecting stains for specific cell populations would allow for a greater understanding of the cellular dynamics at play during apoptosis between these patient lines.

Ultimately, flow cytometry is still a very powerful tool for investigating apoptosis and with a more rigorously optimised protocol this technology has the potential to be very informative and provide a very good follow up to this study. Indeed, flow cytometry has been used by other researchers to investigate ANO6 and its role in phospholipid scrambling in blood cells (Fujii *et al.*, 2015).

The question of how the intracellular protein ANO5 is affecting the arrangement of phospholipids in the plasma membrane remains unanswered as ANO5-Myc does not relocate following staurosporine treatment. Despite this, one possible explanation for the change in PS exposure between ANO5 and Control knockdown C2C12 cell clones might be that ANO5 regulates the phospholipid scrambling pathway rather than acting as a phospholipid scramblase its self. Conflicting research on ANO6 function has shown it both exhibiting and lacking scramblase function in different cell lines (Suzuki *et al.*, 2010; Segawa *et al.*, 2011; Yang *et al.*, 2012). This has led to the suggestion that it is not a scramblase but rather a regulator of other scramblase proteins (Yang *et al.*, 2012). It is therefore possible that the role of ANO5 is also as a regulator of scramblases.

To answer this important question, a potential improvement to the protocol would be to include a positive control more suitable for vesicle translocation. The GFP construct used in this experimentation is a very good control for transfection efficiency but does not control for altered localisation during apoptosis. Using targeted antibody staining to identify vesicle compartments rather than using fluorescently tagged markers such as LysoTracker might improve the stability of signal and allow for increased examination

of the trafficking of internal compartments.

Chapter 6 Discussion

6.1 Localisation of anoctamin 5

6.1.1 Attempted identification of an ANO5 specific antibody

The first aim of this research project was to identify the specific intracellular localisation of anoctamin 5. Without a confirmed antibody against anoctamin 5, the first step of this research was to characterise nine commercially sourced antibodies and identify the most suitable for detecting anoctamin 5. As none of these antibodies proved to be useful in immunofluorescence or western blot investigation, tagged anoctamin 5 constructs were instead utilised.

The identification of a suitable anoctamin 5 antibody has eluded the research field for several years. While several papers claim to have used or developed ANO5 antibodies (Mizuta *et al.*, 2007; Gyobu *et al.*, 2015; Tian *et al.*, 2015; Griffin *et al.*, 2016), no consensus had been reached on a reliable antibody prior to the start of this project. This appears to stem from the historic use of antibodies in diagnosing patients and the initial failures of developed ANO5 antibodies to do so (Bolduc *et al.*, 2010; Milone *et al.*, 2012).

However some antibodies now appear to show consensus in western blotting experiments of myoblasts and muscle extracts. Both Mizuta *et al.* (2007) and Gyobu *et al.* (2015) consistently detect ANO5 at approximately 100kDa in myoblasts, while Gyobu *et al.* (2015) and Griffin *et al.* (2016) detect broad bands around 400-500kDa in BN PAGE and western blot of muscle tissue respectively. Griffin *et al.* (2016) in particular detect a very broad smear in muscle tissue which they suggest is due to post translational modifications such as glycosylation and ubiquitination. Similar consistency between histological examinations using ANO5 antibodies is less clear. Recent papers have reported the use of ANO5 antibodies for immunofluorescent localisation but such work is currently limited (Tian *et al.*, 2015). To our knowledge, no review of currently available ANO5 antibodies has been conducted, though would perhaps identify a consensus antibody at least suitable for research purposes.

6.1.2 Localisation investigation using fluorescently tagged anoctamin 5

Fluorescently tagged anoctamin 5 constructs were successfully localised to the endoplasmic reticulum, in line with predicted localisation (Tsutsumi *et al.*, 2004), and partially localised to the t-tubules in cell culture models. However, electroporation

experiments, which other members of the John Walton Muscular Dystrophy Research Centre had used to successfully express mini-dystrophin constructs in mouse tissue, were unsuccessful. Scudieri *et al.* (2015) suggest that adding tags to constructs can alter their localisation. In their paper investigating ANO6 function, the authors suggest this is as an explanation for the conflicting reports of ANO6 localisation. Additionally, disagreement in the localisation of DYSF following membrane wounding between Bansal *et al.* (2003) and Klinge *et al.* (2007) has been suggested to be due to the epitope tagging of DYSF in the latter study (Cooper and McNeil, 2015). It is therefore possible that in the current project, the Myc tag has affected ANO5 protein expression, reducing the retention of the constructs within mouse muscle.

6.2 Function of anoctamin 5

6.2.1 Knock down of anoctamin 5 affects the abundance of annexin A2 in C2C12 cells

The data from the current study suggest that the knock down of ANO5 alters the abundance of annexin A2 in C2C12, to our knowledge the first instance of a relationship between these two proteins. Annexin A2 often appears in the literature involved with LGMDs and sarcolemmal repair (Draeger *et al.*, 2010; Roostalu and Strahle, 2012; Demonbreun *et al.*, 2015). Along with annexin A1, it has been identified as a binding partner of dysferlin suggesting an involvement in LGMD2B pathology (Lennon *et al.*, 2003; Cagliani *et al.*, 2005). Wound repair and ANXA2 distribution in the sarcolemma are both significantly disrupted in dysferlin deficient mice (Bansal *et al.*, 2003; Lennon *et al.*, 2003; Han and Campbell, 2007). Very recent research has further expanded on the role of ANXA2 in myofibril repair and regeneration. Defour *et al.* (2017) have identified ANXA2 as responsible for myofibril repair and the pro-inflammatory response. ANXA2-deficient mice showed reduced body and muscle mass, decreased grip and forelimb strengths increasing muscle weakness which with age relative to wild type counterparts. Defour *et al.* (2017) also compared the ANXA2-deficient mice to DYSF-deficient mice and found reduced histopathology, fewer regenerating fibres and differences in inflammatory gene expression. Defour *et al.* (2017) suggest that the lack of myofibril repair and inflammatory response in ANXA2-deficient mice is due to the pro-inflammatory role of ANXA2 in myofiber repair when expressed extracellularly.

Understanding of the role of annexins in plasma membrane processes is increasing and the data from this study further strengthens the argument of a relationship between ANXA2 and the limb girdle muscular dystrophies. These data also support the suggestions of similar functions or a close association between anoctamin 5 and dysferlin as both these intracellular proteins have now been suggested as interacting with annexin A2 in pathways resulting in changes at the plasma membrane (Roostalu and Strahle, 2012). However protein interaction screening or improved co-localisation experiments would help clarify the particular roles each of these causative genes plays in LGMD pathology and especially address the question of whether a direct protein-protein interaction exists between these proteins.

The possible effect on annexin A2 abundance is also of interest as the monomere has been found to be involved with chloride channel regulation (Kubista *et al.*, 1999) while

the ANXA2/S00A10 heterotetramere has been suggested to be responsible for ion channel trafficking from intracellular sites to the plasma membrane and speculated to be required to tether ion channel to cytoskeleton of the plasma membrane (Gerke *et al.*, 2005). Annexin A2 has been localised to lipid rafts within the plasma membrane (Oliferenko *et al.*, 1999). Lipid rafts are small, highly dynamic and transient regions of the membrane (Pierini and Maxfield, 2001) suggested as being involved in recruiting signalling cascade proteins (Cherukuri *et al.*, 2001).

Finally, annexin A2 has also been suggested as necessary for osteoblastic mineralization. Gillette and Nielsen-Preiss (2004) identified that overexpression of ANXA2 resulted in increased alkaline phosphatase activity and mineralisation of osteoblasts. Given that dominant mutations in ANO5 lead to the bone disease Gnathodiaphyseal dysplasia (GDD), investigation of the relationship between anoctamin 5 and annexin A2 in osteoblasts should be undertaken.

6.2.2 Knocking down anoctamin 5 reduces the phospholipid scramblase ability of C2C12

Following establishment of a knock down C2C12 line, specific investigation of anoctamin 5 function as a phospholipid scramblase was pursued. This investigation was undertaken due to the close homology between ANO5 and ANO6 and the established phospholipid scramblase function of ANO6. The working hypothesis was that impaired scramblase function during apoptosis led to impaired immune response, increased inflammation processes and dystrophic pathology. These data confirm that ANO5 knock down affects PS exposure which could lead to an impaired apoptotic response or inflammatory response during myofiber regeneration seen in some LGMD2L patients (Hicks *et al.*, 2011).

6.1.1 A hypothetical vesicle population containing anoctamin 5 and annexin A2

The initial hypothesis of anoctamin 5 functioning as a phospholipid scramblase, can now be expanded to include the altered annexin A2 abundance in ANO5 knock down C2C12. Annexin A2 aggregate vesicles and lipid rafts to the cytosolic side of the plasma membrane in a calcium dependent manner (Babiychuk and Draeger, 2000) and have been suggested as intracellular calcium sensors (Monastyrskaya *et al.*, 2007). Furthermore, annexin A2 has been found to be required for binding and aggregation of vesicles containing PS (Blackwood and Ernst, 1990; Menke *et al.*, 2005). Annexin A2

may hypothetically act as a calcium sensor in vesicles containing anoctamin 5 and PS. Upon increase in internal calcium concentration annexin A2 traffics the vesicle to the plasma membrane and facilitates fusion of the vesicle with the plasma membrane. Anoctamin 5 and PS are then inserted into the plasma membrane where anoctamin 5 scrambles the membrane, exposing the excess PS. ANXA2 expression disruption by the loss of ANO5 would then impair beneficial accumulation of vesicles, which has been observed by electron microscopy investigation of muscle biopsies of two Finnish LGMD2L patients (Mahjneh *et al.*, 2010). A similar model for PS trafficking to the membrane during apoptosis has been suggested by Mirnikjoo *et al.* (2009b). The authors suggest that a pseudo-membrane repair response occurs following increases in intracellular calcium which involves the fusion of PS rich lysosomes to the plasma membrane.

However, this hypothesis conflicts with the data that overexpressed ANO5-Myc is intracellularly located and does not traffic to the plasma membrane during apoptosis. While the addition of the Myc tag may be affecting the true intracellular localisation of ANO5, an alternative hypothesis may be that anoctamin 5 is not trafficked to the plasma membrane but rather fulfils an intracellular scramblase function which has a downstream impact on PS exposure at the plasma membrane. While investigation of internal PS exposure, and by extension intracellular scramblase activity, is very difficult because of the inherent changes to lipid structure caused by transfecting probes and other molecules directed against PS, evidence suggests that scramblase activity is required for exposing PS to the cytosol following synthesis in the ER (Leventis and Grinstein, 2010). Hypothetically, if anoctamin 5 controlled scramblase activity was impaired in the ER then there may be a reduction in total cellular PS, leading to the observed PS reduction at the plasma membrane.

There are however inconsistencies with this counter theory. For example, while PS is one of the lowest phospholipids in terms of overall abundance (Leventis and Grinstein, 2010), the majority of PS produced is immediately trafficked to the mitochondria where it is degraded by decarboxylation to produce phosphatidylethanolamine (PE) (Tamura *et al.*, 2012; Vance and Tasseva, 2013). So while impaired production of PS may not significantly affect its own directly associated functions, it would have a knock on effect by impairing PE production which has been shown to be embryonic lethal in mice and lead to fragmented mitochondria (Steenbergen *et al.*, 2005). PS has been suggested as

important for other intracellular processes, but these are regulated by ATP dependant flippases and not scramblases (Leventis and Grinstein, 2010).

6.3 A role for anoctamin 5 containing vesicles in plasma membrane repair

Investigation of anoctamin 5 presence in such a vesicle population and its response to plasma membrane wounding has recently been carried out, research which was unknown during the write up of this project. Tian *et al.* (2015) localised endogenous anoctamin5 to an unknown intracellular vesicle population using immunofluorescence techniques as well as commercially purchased antibodies against anoctamin 5. The pattern of localisation reported by Tian *et al.* (2015) is the same as the localisation experiments reported in this project. However the authors found that the pattern of anoctamin 5 localisation was not consistent with the pattern of lysosome localisation (identified by co-staining with the lysosome marker LAMP2), supporting the possibility of a novel vesicle population containing anoctamin 5.

Tian *et al.* (2015) further establish that anoctamin 5 translocates to the plasma membrane following wounding with saponin. They suggest that anoctamin 5 is responding to the increased calcium concentrations following wounding due to its function as a CaCC. However, they also report that anoctamin 5 only translocates to the plasma membrane during wounding events. Increases in intracellular calcium are not enough to move anoctamin 5 to the plasma membrane. Their assumption that anoctamin 5 functions as a CaCC is also odd given the close homology with ANO6 (Hartzell *et al.*, 2009) and the increasing understanding that all anoctamins other than ANO1 and ANO2 are more likely phospholipid scramblases than CaCCs (Whitlock and Hartzell, 2016a).

Additionally, the authors used kidney (HEK293) and lung (CFBE) cells to investigate anoctamin 5 localisation during membrane repair rather than a muscle cell line. They justify this choice by showing exogenous expression of anoctamin 5 in these cells and citing similar previous findings by Tsutsumi *et al.* (2004). This is still an unusual selection however as while Tsutsumi *et al.* (2004) do report expression of anoctamin 5 in these tissues, they also report four to twelve times higher anoctamin 5 expression in skeletal muscle and bone tissues. Tian *et al.* (2015) also acknowledge the known LGMD and MMD dystrophies caused by recessive anoctamin 5 mutations, which further compounds this less than optimal choice of cell lines.

6.3.1 Relation to other membrane repair proteins

The very recent identification of the complex interaction of dysferlin and annexin family members in membrane repair (Roostalu and Strahle, 2012; Demonbreun *et al.*,

2016b), in tandem with these data reported by Tian *et al.* (2015) support the likelihood of anoctamin 5 localisation to an unknown vesicle population. Furthermore they tantalisingly suggest a position for anoctamin 5 within the repair pathway.

Evidence in both mouse (Demonbreun *et al.*, 2016b) and zebrafish (Roostalu and Strahle, 2012) models suggest that following plasma membrane wounding there is ordered, independent, recruitment of dysferlin enriched vesicles followed by accumulation of annexin A6. In mice this is through the formation of a "shoulder" region adjacent to the injury site and a "repair cap" above the injury site (respectively formed by the accumulation of DYSF and ANXA6) while in zebrafish Dysf and Anxa6 (the zebrafish orthologs of their respective human genes) accumulation at the site of damage form a seal. In both species, this then prompts the recruitment of annexin A2 and annexin A1. Indeed zebrafish deficient for either Dysf or Anxa6 fail to recruit Anxa2a or Anxa1a (again, the zebrafish orthologs of their respective human genes) to the wound site (Roostalu and Strahle, 2012).

Hypothetically, it may be that the recruitment of ANXA2 prompts the recruitment of ANO5 contained in the cytoplasmic vesicle population. Under the current hypothesis this occurs simultaneously with PS recruitment but currently all that has been confirmed is that PS enrichment of the injury site is preceded by both DYSF and the annexins (Demonbreun *et al.*, 2016b). Further investigation is required to confirm the presence of PS in the same vesicles as ANO5.

Additionally, while it has been suggested that endosomes and exocytosis of lysosomes are involved in wound repair (Reddy *et al.*, 2001; Idone *et al.*, 2008), the exact identity of this anoctamin 5 containing vesicle population is unclear. In zebrafish, intracellular vesicles detected by marking proteins including Lamp1 and 2, Laptm4a and specific Rab family members (1a, 5a, 6a, 7 and 27a) do not play a role in wound healing (Roostalu and Strahle, 2012) and anoctamin 5 did not co-localise with LAMP2 *in vivo* supporting the suggestion that it is not contained within a lysosome (Tian *et al.*, 2015).

Furthermore, while Demonbreun *et al.* (2016b) suggest that exposure of PS leads to phagocytosis and the inflammatory response, further work should be carried out to understand if this is the precise purpose of PS exposure or if membrane fusion with satellite cells is the specific end point. Perhaps ANO5 scrambling varies depending on the situation of the cell. Finally, how the repair patch is removed currently remains unknown (Cooper and McNeil, 2015).

6.4 Interrogation of developed ANO5 knockout mouse models

Within the last few years, two different groups simultaneously published characterisations of ANO5 knock out mouse lines, the first publications of in depth investigation of such a model (Gyobu *et al.*, 2015; Xu *et al.*, 2015). Xu *et al.* (2015) validated the knock out using rt-PCR of mRNA with four different primer sets, none of which detected ANO5 in knock out samples. Gyobu *et al.* (2015) also used PCR using one forward and two reverse primers (one against the wild type and one against the mutant allele) to identify the ANO5 knock out genotype mice. However both authors also report that their models do not recapitulate the muscular dystrophy phenotypes of patients in either muscle histology or contractile response (Table 6.1), despite Xu *et al.* (2015) investigating older 18 month old mice at rest. Xu *et al.* (2015) also investigated potential protective effects from increased expression in other anoctamins but found no increase over that observed in the wild type mice. Gyobu *et al.* (2015) however reported reduced fertility due to decreased sperm motility in their model. While $ANO5^{-/-}$ sperm morphology was unchanged and the sperm could still move, their velocity was significantly reduced compared to wild type derived sperm. The authors suggest that the decreased motility is due to the effect of ANO5 on spermatogenesis. Although these mouse models obviously do not represent a suitable phenocopy of the human disorder, one might speculate about their suitability in unravelling proteins (beyond the anoctamin family) protecting skeletal muscle from vulnerability. Unbiased protein profiling utilizing different muscle derived from knock-out animals and wildtype-littermates would represent a promising step towards this goal.

The lack of an overt phenotype is unsurprising as other mouse models for more severe muscular dystrophies have only a mild phenotype when compared to patients. For example the *mdx* mouse, the standard model of Duchenne, lacks the replacement of muscle by fatty infiltrate seen in patients, as well as showing improved muscle regeneration (Coulton *et al.*, 1988). Proposed explanations for a comparatively reduced phenotype in the *mdx* mouse include other proteins, such as utrophin and sarcoglycan, compensating for the loss of dystrophin in mice (Grady *et al.*, 1997; Li *et al.*, 2009) and a species specific protective/compensatory mechanism in the mouse muscle (McGreevy *et al.*, 2015). Both authors acknowledge that anoctamin 5 may not fulfil the same function in mice as it does in humans due to the general differences in human and murine physiology. Xu *et al.* (2015) suggest that genetic, environmental, metabolic and

immunological differences between mice and humans may contribute to the differences in phenotype.

Recently, Griffin *et al.* (2016) also developed an ANO5 knock out mouse model, though histological and clinical examination revealed that their model exhibited several phenotypes consistent with the LGMD2L presentation in patients (Table 6.1). As with the other models, ANO5 knock out was confirmed via RT-PCR, here with primers spanning exons 10-14 and 17-20 (>99% reduction in ANO5). Mice were found to have high CK levels (~2 fold higher than wild types), variable muscle force contraction (~15% reduced diaphragm muscle contraction, but unaffected in extensor disitorum longus (EDL) and tibialis anterior (TA) muscle), reduced muscle fibre diameter in gastrocnemius (GAS) and TA muscle and reduced exercise tolerance. Furthermore Griffin *et al.* (2016) also report impaired myoblast fusion as well as muscle regeneration following cardiotoxin injection, subsequently rescued by AAV delivery of human ANO5-FLAG. The development of all three of these models are steps forward but the most recent model will be of greatest benefit in the study of ANO5 function.

Table 6.1 Comparison of the different ANO5 knockout mouse models developed since the beginning of this project. Authors and models are presented in order of online publication date; Gyobu et al. (2015) 14th December, Xu et al. (2015) 21st December and Griffin et al. (2016) 11th March.

	Gyobu *et al.* (2015)	**Xu *et al.* (2015)**	**Griffin *et al.* (2016)**
Reported Age of Mice (assay dependant)	6-7 months (histological examination) 7-10 months (CK extractions) 2-6 months (sperm examination) 3 months (fertility assessment, 5 months post breeding);	7, 14, and 21 day time points 4, 8 and 18 month time points	1, 3, 7, 14, 30 and 90 day time points 7.5, 10 month time points
Details of Knockout	ANO5 Exon 2 replaced with neo-loxP cassette; C57BL6/J ES cells positive for the vector were injected into BALB/c mice blastocysts, $ANO5^{+/NeoFRT}$ mice crossed with CAG-CRE mice to obtain $ANO5^{+/-}$ mouse which was then backcrossed to obtain target	Exon 1 and 1.6kb upstream of ANO5 replaced with neomycin selection casstte, C57BL6/J mouse background backcrossed for 6 generations to generate homozygotes	Null ANO5 transcript created by splicing to lacZ trapping element after exon 8, C57BL6 mouse background backcrossed for 4 generations to the wild type to generate homozygotes
Muscle Examined	Only tibialis anterior muscle mentioned though testis also investigated	Gastrocnemius and quadriceps muscle (molecular and histopathological examination) Gastrocnemius and tibialis anterior (Muscle mass) Extensor Digitorum Longus (contractile measurements) cardic muscle also investigated	Tibialis anterior muscle (electron microscopy, morphometrics) Gastrocnemius muscle (morphometrics) Quadriceps Muscle (SDH staining) FDB muscle (membrane repair) Extensor Digitorum Longus (force generation)
Phenotype	No dystrophy phenotype observed Defect in sperm motility suggested to be due to faulty spermatogenesis,. $ANO5^{+/+}$ females bred with $ANO5^{-/-}$ males produced approximately half as many pups compared with $ANO5^{+/+}$ and $ANO^{-/-}$ females bred with $ANO5^{+/+}$ males	No dystrophy phenotype observed: muscle mass, musculature unaffected, nonstatisitcally significant central nucleation of quadriceps, DYSF and DGC unaffected, cellular repair unaffected, cardiac abilities unaffected	Dystrophy phenotype observed: Mild histopathology, variable muscle weakness, exercise intolerance, impaired regeneration and elevated CK levels

A possible reason for the different observed pathologies in the three models may be the genetic background of the mice. While all three had a C57NL6 background, both the Xu *et al.* (2015) and Gyobu *et al.* (2015) models were on the C57NL6/J substrain. Detailed investigation has been conducted on the effect of the genetic background of a mouse on its phenotype. Coley *et al.* (2016) compared the functional, histological, biochemical and molecular phenotypes of *mdx* mice against D2-mdx mice, *mdx* mice bred on a DBA/2J background rather than a C57BL/10 background. The authors found that functionally *mdx* mice displayed a hypertrophic phenotype while D2-mdx mice showed an atrophic phenotype. Furthermore Demonbreun *et al.* (2016a) identified different membrane repair abilities between 129T2/SvEmsJ and C57BL/6J mouse strains both bred to be dysferlin-deficient. Macrophage infiltration and movement of ANXA6 to the site of injury were both increased in the C57BL/6J mouse, suggesting that this background intensifies the dysferlin pathology.

Unlike other C57NL6 substrains, the C57NL6/J substrain has been found to have a functional deletion in the nicotinamide nucleotide transhydrogenase (Nnt) gene (Toye *et al.*, 2005; Freeman *et al.*, 2006b). The Nnt gene is responsible for insulin secretion and detoxification of reactive oxygen species (Freeman *et al.*, 2006a; Freeman *et al.*, 2006b), making the C57NL6/J substrain physiologically different to the other models. Furthermore, several single nucleotide polymorphisms (SNPs) have been found to be different between several C57NL/6 subtypes, highlighting the need to carefully consider the genetic heritage of a mouse before its implementation in developing a new model (Mekada *et al.*, 2009).

A more likely explanation though is Griffin *et al.* (2016) own suggestion that their model accurately replicates the LGMD2L phenotype because of the location of the disruption. Xu *et al.* (2015) and Gyobu *et al.* (2015) inserted disruptions in exons 1 and 2 respectively, while Griffin *et al.* (2016) targeted exons 8 and 9 and admit that they therefore cannot exclude the possibility of partial transcription of ANO5 preceding these exons. As the common causative c.191dupA mutation for LGMD2L is located on exon 5 they continue by suggesting that this partial transcript may result in pathology. No further investigation of this theory or the stability of the transcript is mentioned by Griffin *et al.* (2016) and so a vital route of further investigation would be following up on this possibility.

Given the stronger pathological implications of the location of the mutation, this is the more likely reason for the differences in the models. However the differences in the genetic backgrounds of the mice should still be kept in mind when using these mice in future research, especially if studies compare between them.

6.4.1 Implications of new ANO5 models to this project

During their investigation, Xu *et al.* (2015) also used microarray analysis to identify 81 upregulated genes and 893 downregulated genes in their knock out model. From these genes the authors identify several which are involved with lipid metabolism and suggest that anoctamin 5 might play a role in metabolic homeostasis and the complement pathway. In the context of the current study, while S100A4 and Hspb27 were not among the lists of up or down regulated genes, ANXA2 is identified as down regulated by just over 4-fold. While this finding further supports a link between ANO5 and ANXA2 abundance, the reduced transcription of ANXA2 found by Xu *et al.* (2015) would appear to conflict with the observed increase in spot intensity seen in the 2D gels of the current study. However transcription and translation of a protein are not necessarily correlated. Disparity in the correlation between protein and transcript abundances have reported, suggested to be due to post-translational modification or degradation of the proteins (de Sousa Abreu *et al.*, 2009). Given the increased understanding of the role of annexins in membrane fusion and membrane repair, the downregulation of ANXA2 recorded in the Xu *et al.* (2015) model requires further investigation and a clearer understanding of its relationship to the overall expression of annexin A2. Simultaneous investigation of both ANXA2 transcript and protein abundances the Xu *et al.* (2015) model may reveal that an increased abundance of protein occurs from reduced transcript.

Griffin *et al.* (2016) and Gyobu *et al.* (2015) report conflicting localisation for FLAG-tagged ANO5 in their investigations. Griffin *et al.* (2016) observed sarcolemmal localisation following AAV delivery to rescue membrane repair while Gyobu *et al.* (2015) identified ER localisation in C2C12 and mouse skeletal muscle. Gyobu *et al.* (2015) suggest that this is the natural localisation of ANO5 and support this finding with an ANO1/ANO5 chimera, created by altering the SCRD region of ANO5 with the corresponding region in ANO1, localising to the plasma membrane which is the recorded localisation of ANO1. However, Gyobu *et al.* (2015) also report that the chimera shows strong scramblase function, conflicting with the established function of

ANO1 but supporting the established functions of the other anoctamin family members (Whitlock and Hartzell, 2016a) and the membrane repair defects reported by Griffin *et al.* (2016). Given that the sarcolemmal localisation of FLAG-ANO5 reported by Griffin *et al.* (2016) was during investigation of the ability of transfected ANO5 to rescue membrane repair, these findings suggest that the localisation of ANO5 may be dependent on the situation of and pressures on the tissue at that time, supporting the possibility of ANO5 existing in a transient vesicle population. Moreover, membrane proteins are produced in the ER and it is thus not a surprise that plasma membrane resident proteins can also be detected in the ER/Golgi system; especially not under circumstances like forced over-expresssion via transient transfection.

6.5 Identification of anoctamin5 function through investigation of GDD

GDD, the rare bone disease characterised by sclerosis of tubular bones, cemento-osseous lesions in the jaw bone and skeletal fragility (Akasaka *et al.*, 1969; Riminucci *et al.*, 2001) caused by autosomal dominant mutations in ANO5 (Akasaka *et al.*, 1969), is a relatively unexplored research avenue in terms of identifying anoctamin 5 functionality. But, if the ultimate aim is to understand functionality in general, then investigation of anoctamin 5 in the context of GDD does allow for a second or parallel route for understanding anoctamin 5 if not the LGMD2L phenotype specifically. While phenotypically very different, differences in expression and protein-protein interactions between ANO5 and GDD patients could be illuminating.

Intriguingly anoctamin 6 has been shown to be important for mineralisation of osteoblasts in mice (Ehlen *et al.*, 2013). Two lines of ANO6 null mice were found to have delayed bone formation both pre and post-natally as well as deformities of the long bones, ribs and skull. Furthermore, PS exposure was found to also be impaired in the osteoblasts of ANO6 null mice. Ehlen *et al.* (2013) explain that osteoblast mineralisation is thought to be promoted by the formation of matrix vesicles (Gillette and Nielsen-Preiss, 2004; Genge *et al.*, 2008) and that in hypertrophic chondrocytes scrambling of the plasma membrane is responsible for the release of these matrix vesicles (Damek-Poprawa *et al.*, 2006). They note that Scott Syndrome patients have a bleeding disorder rather than bone deformity and suggest that the differences in phenotype between ANO6 null mice and these patients may be due to differences in anoctamin 6 function between mice and humans. They explain that while they did not investigate a bleeding phenotype in these mice, they did not observe any obvious instances of increased bleeding, for example in females following birth.

Given this function of anoctamin 6 in osteoclasts, similar investigation of the phospholipid scrambling ability of ANO5 null osteoclasts is imperative. While the three different ANO5 null mouse models could be utilised and compared to track their bone formation, ideally an additional ANO5 mouse model with dominant mutations, and therefore more accurately replicating human GDD mutations, would be of use. Confirmation of the similarity of these mice to the GDD phenotype as well as investigation of scramblase activity in primary osteoclasts would confirm that anoctamin 5 is involved with redistribution of the plasma membrane and that it is the specific tissue in which it is expressed which determines its final function.

6.6 Investigation of asymptomatic anoctamin 5 patients to identify potential compensatory/protective pathways

The goal of any translational research is to improve the diagnosis, treatment, or quality of life for patients. This has become especially important for anoctamin 5 as the frequency of ANO5 mutations within patient populations are now understood to be higher than previously thought (Hicks *et al.*, 2011). This has led to the suggestion that genetic screening for ANO5 should be a priority for patients presenting with even a suspected LGMD2L pathology, namely late age onset of asymmetrical limb-girdle weakness and significantly elevated creatine kinase (CK) levels (Sarkozy *et al.*, 2013; van der Kooi *et al.*, 2013).

Significantly elevated CK levels have also often been noted in asymptomatic individuals positive for ANO5 mutations (Sarkozy *et al.*, 2013). These individuals were often screened due to their relatedness to LGMD2L patients, who were in turn identified due to re-interrogation of patient data with new screening techniques for ANO5 mutations (van der Kooi *et al.*, 2013). Investigating anoctamin 5 function in these asymptomatic individuals may help to explain why they remain asymptomatic, despite having ANO5 mutations and CK levels equivalent to LGMD2L patients.

Also of interest to the progression of ANO5 is the relationship between exercise and the onset of LGMD2L. Cases have been reported of either high exercise ability of patients (Mahjneh *et al.*, 2010) or exercise intolerance before the onset of LGMD2L pathology (Milone *et al.*, 2012). Given the increasing evidence of the role of ANO5 at the sarcolemma, the link between exercise ability preceding onset is worth investigation especially with the availability of a reliable mouse model. A particularly intriguing case was recently reported by Blackburn *et al.* (2016) where they describe a 22 year old female athlete with progressive muscle weakness and back pain during exercise. Subsequent genetic analysis revealed two previously reported frameshift mutations in ANO5. Blackburn *et al.* (2016) note this is an intriguing case given the comparatively early age of onset and severity of pathology. The case is also of interest as the patient is female who are not often affected by LGMD pathology, but also as these are previously reported mutations, highlighting the lack of a genotype phenotype correlation.

While there has as yet been no clear genotype/phenotype correlation in anoctaminopathy patients, investigation of the other anoctamins suggests that genotype changes may alter their function. Scudieri *et al.* (2015) have identified differences in

expression and phospholipid scramblase and ion channel function between three different variants of ANO6. Alternative splice variants of ANO1 and 2 have also been shown to have reduced CaCC functionality (Ferrera *et al.*, 2009; Ponissery Saidu *et al.*, 2013). Variation in anoctamin sequences may therefore lead to variability of function. Deeper investigation of the correlation and differences between mutations of anoctaminopathy patients and their phenotypes may reveal further routes of investigation.

6.7 Future Work

Several routes of follow up should be pursued to fully understand the scramblase function of anoctamin 5 and how this fits with the other anoctamin family members. First, *in silico* modelling of the structure of anoctamin 5 can be carried out to confirm its structural similarity to other anoctamins with investigated structures such as anoctamin 6 and the TMEM16 homologue from *Nectaria haematococca* (nhTMEM16) (Brunner *et al.*, 2014). Secondly, LGMD2L patient derived cells, and potentially the knock down cells developed in this project, could be further characterised using electrophysiology investigation for their response to changes in calcium. Identification of a high affinity anoctamin 5 antibody would also be of great benefit to both academic research and the simplicity and speed of patient diagnosis. Alternatively, methods of protein localisation that do not require an antibody, such as LOPIT, could be utilised to answer outstanding questions about anoctamin 5 localisation. Finally, investigation of the specificity of ANO5 as a phospholipid scramblase should be investigated, given the increasing evidence for a relationship between ANO5, phospholipid scrambling, DYSF, annexins, membrane fusion and repair. This is of particular interest now that several ANO5 mouse models are available to examine this function.

6.7.1 Structural investigation of anoctamin 5 through in silico modelling

In silico modelling of anoctamin 5 structure would allow for direct comparisons with the structures of other anoctamins which have already been investigated. Brunner *et al.* (2014) used x-ray crystallography to characterise the structure of nhTMEM16, a homologue of the anoctamins in the fungus *Nectria haematococca*, and identify conserved regions found throughout the family. Yu *et al.* (2015) also recently identified the sequence within anoctamin 6 which they suggest is responsible for phospholipid scramblase activity. Through a series of electrophysiology studies, they confirmed that the amino acid sequence between amino acids 525 -559 in anoctamin 6 was able to confer anoctamin 1 with robust phospholipid scramblase activity in the presence of excess calcium. Anoctamin 1 is normally negative for scramblase activity. Furthermore, within this region, which they term the scrambling domain (SCRD), nine amino acids are essential for the phospholipid scrambling activity in anoctamin 6. They also suggest that the weak non-selective ion channel activity observed for anoctamin 6 by previous studies is a by-product of the scramblase activity and is not the function of anoctamin 6.

Bethel and Grabe (2016) have recently built on the understanding of this domain by identifying two regions in the SCRD of nhTMEM, termed the S_C and S_E sites, which are facilitate movement of lipids from one leaflet to the other. The sites are each located at either end of the scrambling pore but within the sequence of the SCRD domain; the S_C at the cytoplasmic leaflet and the S_E at the extracellular leaflet. Both sites are conserved in all mammalian anoctamins, though the key basic and acidic residues of the S_E site have flipped positions compared to the model nhTMEM. Bethel and Grabe (2016) argue that it is the opposite charges of the residues which is important rather than the order of the charge. The S_C site meanwhile, is only present in mammalian anoctamins with scramblase function, therefore excluding ANO1 and 2. This suggests that there are additional structural factors required for the correct function of ANOs.

While in depth structural modelling would take time, the clear importance of this region to the specific function of anoctamins means that immediate work could and should be undertaken into the homology of this region between anoctamin 5 and anoctamin 6.

6.7.2 Electrophysiology studies to investigate intracellular calcium handling of anoctamin 5

Through electrophysiological experimentation of anoctamin 6, ion channel activity thought to be associated with robust phospholipid scramblase activity has been found to be a by-product rather than a direct function. Additionally simultaneous imaging of cells during patch clamp experiments has clarified the relationship between calcium increase and activation of phospholipid scrambling (Yu *et al.*, 2015). It would therefore be pertinent to use electrophysiological experiments to further understanding of the anoctamin 5 reaction to increases of intracellular calcium in over expressing and knock down cells. Patient derived cells, or the ANO5 knock down C2C12 lines developed as part of this project, could be investigated using such techniques, yielding results relatively quickly.

While anoctamin 5 has not shown any channel forming ability thus far (Tran *et al.*, 2014), anoctamin 6 channel activity was only observed after delayed activation and under much higher concentrations of calcium than required for anoctamin 1 and anoctamin 2 activation. Investigation of this function in anoctamin 5 would also have to allow for a considerable difference from those observed for anoctamin 1 and anoctamin 2. Furthermore, Brunner *et al.* (2014) suggest that while calcium binding is most likely

common across the anoctamin family there may be additional modes of regulation for the specific family members. As anoctamin 5 is the only anoctamin to be strongly expressed in musculoskeletal tissue, it may have a more specific method of activation than the other anoctamins.

Ultimately, identifying the relationship between increases in internal calcium concentration, scramblase activity and any potential channel formation in ANO5 deficient cells would resolve questions around anoctamin 5 such as its intracellular localisation despite its scramblase function. This would then increase the understanding in relation to the other anoctamins, such as anoctamin 6 which it is closely related to and anoctamin 7 which is also intracellularly localised (Duran and Hartzell, 2011).

6.7.3 Utility and characterisation of potential anoctamin 5 antibody

While work is ongoing to develop an anoctamin 5 antibody, none are currently commercially available. Western blotting results appear to be consistent between a few developed antibodies (Mizuta *et al.*, 2007; Gyobu *et al.*, 2015; Griffin *et al.*, 2016), but a review of the histological suitability of all currently available antibodies would be of great benefit. From a research perspective, consensus on a reliable ANO5 antibody would lead to resolution of several questions about this protein for example subcellular localisation and differential expression during processes such as apoptosis and differentiation. To our knowledge, no such review of currently published ANO5 antibodies has been conducted but would perhaps be a useful step in understanding the remaining issues surrounding a suitable anoctamin 5 antibody. Additionally a reliable antibody would impact on patient diagnosis as diagnosis could be achieved by western blot or immunohistochemistry. As such it would be of considerable value to diagnostic labs who would be able to finally incorporate antibody tests for anoctamin 5 into routine screens. Of course, precise data concerning the subcellular localisation of ANO5 would be beneficial in terms of a reliable evaluation of developed antibodies.

6.7.4 Localisation of ANO5 using LOPIT, an isotope tagging method

Given the difficulty in identifying a suitable anoctamin 5 antibody and the potential interference to protein-to-protein interactions caused by tagging ANO5, an alternative method for investigating anoctamin 5 localisation should be used. While fractionation methods are an alternative possibility, they have an inherent “blind spot” when investigating proteins in the endomembrane system, such as membrane proteins. For

example organelles would be either so similar in size or are in such a constant state of flux, moving from the ER to the membrane (Wu *et al.*, 2004; Sadowski *et al.*, 2006), that distinguishing between "resident" or "transient" proteins in a pure fraction would be very difficult. However, LOPIT (localisation of organelle proteins by isotope tagging), developed by Sadowski *et al.* (2006), combines amine-specific stable isotope tagging, 2D liquid chromatography and MS/MS to localise proteins to a particular subcellular compartment and as such offers high specificity with no need for an antibody. LOPIT works by comparing the MS/MS data from the target protein against the MS/MS data of known subcellular organelle markers distributed along a gradient. A protein is considered to localise to a specific subcellular compartment when the MS/MS profiles of the two proteins matches. While accurately localising transient proteins (for example, proteins that traffic between the ER and Golgi) is still tricky with this procedure, LOPIT is still of considerably use given the current situation of anoctamin 5 antibody research. Additional studies focussing on (new) protein-binding partners of ANO5 would also strengthen the understanding of its subcellular localisation and thus be helpful for the interpretation of the LOPIT data addressing the endogenous ANO5 protein.

6.7.5 Further investigation of the ANO5 knock out mouse and specificity of ANO5 as a phospholipid scramblase

The development of three ANO5 knock out mouse is also very encouraging for future studies. While the models developed by Xu *et al.* (2015) and Gyobu *et al.* (2015) do not have dystrophic phenotypes they can still be used as a basis for further investigation, and are arguably of more interest than the Griffin *et al.* (2016) model in terms of identifying compensatory mechanisms and developing therapies for LGMD2L patients. Xu *et al.* (2015) and Gyobu *et al.* (2015) show that they have successfully knocked out ANO5 in their models perhaps suggesting that the lack of a dystrophy in their models may be due to a compensatory or protective mechanism. Broad examination of the relative expression of other proteins in these models may identify other proteins which take over the functions of ANO5 and prevent the dystrophic phenotype. Further comparison with the Griffin *et al.* (2016) model and patient derived cells would then reveal more about the interplay between ANO5 and related proteins.

Additionally, further characterisation of all three mouse models in regard to their phospholipid scrambling ability and membrane repair ability is essential. Investigation

of scramblase ability was limited across these animal models, while developing evidence suggests that it should be routine. Xu *et al.* (2015) did not investigate scramblase function at all and while Gyobu *et al.* (2015) did, only the ability of various anoctamins and their chimeras expressed in Ba/F3 cells (murine pro-B cells) are reported. Despite the lack of an overt dystrophic phenotype in the Xu *et al.* (2015) and Gyobu *et al.* (2015) mice, investigation for impaired phospholipid scrambling would still be informative. Based on the results of the current study and those of Griffin *et al.* (2016) whose model displayed impaired muscle repair processes and myoblast fusion, further investigation of all these models from the specific perspective of phospholipid scrambling is essential. Specific questions in the research field that currently remain but which could be investigated using these models include the specificity of the anoctamins and the lipids that they transport and if calcium is the only essential requirement for anoctamin mediated phospholipid scrambling (Whitlock and Hartzell, 2016a).

Finally, all of these models also provide a source of primary material for research, as has been achieved with other anoctamin mouse models (Yu *et al.*, 2015). While not eliminating the need for patient samples, a more readily available source of primary material for study would be invaluable for the longitudinal studies required to fully investigate anoctaminopathy phenotypes.

6.7.6 Investigation of ANO5 function in plasma membrane repair

Within the last couple of years, multiple labs have identified new links between anoctamin 5, PS, annexin and dysferlin, namely the formation of repair patches and increased exposure of PS following wounding (Roostalu and Strahle, 2012; Tian *et al.*, 2015; Demonbreun *et al.*, 2016b). Further investigation into the role of anoctamin 5 in plasma membrane resealing should therefore be carried out. Specific identification of anoctamin 5 localisation in relation to dysferlin, PS and annexins A1, A2 and A6 before, during and following wounding would be illuminating and potentially validate the proposed hypothetical vesicle population.

Given the observation of the highly ordered accumulation of proteins to the site of repair, it may be that ANXA2 is the sensor for the recruitment of the vesicle population to the site of injury, detecting the accumulation of ANXA6. Comparison of recruitment of membrane repair proteins in DYSF, ANXA6 and ANO5-null mice following

wounding would be of benefit as well as the localisation of these proteins in each of these mice.

6.8 Conclusions

Based on these data presented in the current project, anoctamin 5 is an internally expressed protein, which is involved in phospholipid scrambling of PS due to apoptotic stimuli. Abundance of annexin A2 has been identified as altered by the knock down of ANO5. Because of the association of annexin A2 with vesicle population aggregation and membrane fusion and repair, this may suggest that anoctamin 5 is trafficked to the plasma membrane when required. Knock down of ANO5 alters the composition of the internal vesicles in which it is held, affecting the function or binding of annexin A2. This research provides first steps towards understanding anoctamin 5 function and suggests an involvement in phospholipid scrambling.

Since the end of the experimental phase of this project several papers have been published which shed light on questions surrounding anoctamin 5, namely the phospholipid scramblase ability of the other anoctamin family members particularly ANO6 (Scudieri *et al.*, 2015; Yu *et al.*, 2015), what role phospholipid scramblases play in muscle (Demonbreun *et al.*, 2015) and the relationship between ANO5, DYSF, ANXA2 and muscle regeneration (Griffin *et al.*, 2016). The data presented in this thesis compliment these discoveries and provide the first step in confirming and understanding ANO5 as a phospholipid scramblase.

If carried out again with the information now available, this project would most likely have focussed less on the involvement of ANO5 as a phospholipid scramblase in apoptosis and rather on further investigating its role in membrane repair or membrane fusion. Prior to the start of this project however, investigation of apoptosis was the simplest route of investigation to identify ANO5 function as a scramblase. Future work should use the information gleaned here (knock down of ANO5 in C2C12 effects ANXA2 abundance as well as a loss of scramblase function) as well as, if possible, the developed ANO5 deficient mouse model (Griffin *et al.*, 2016) to more fully investigate and understand phospholipid scramblase ability of ANO5 in relation to apoptosis, membrane repair and membrane fusion pathways.

References

Achanzar, W.E. and Ward, S. (1997) 'A nematode gene required for sperm vesicle fusion', *J Cell Sci*, 110 (Pt 9), pp. 1073-81.

Adhihetty, P.J. and Hood, D.A. (2003) 'Mechanisms of apoptosis in skeletal muscle', *BAM-PADOVA-*, 13(4), pp. 171-180.

Ahluwalia, J., Ly, J.Q., Norman, E., Costello, R.F., Jr. and Beall, D.P. (2007) 'Gnathodiaphyseal dysplasia', *Clin Imaging*, 31(1), pp. 67-9.

Akasaka, Y., Nakajima, T., Koyama, K., Furuya, K. and Mitsuka, Y. (1969) '[Familial cases of a new systemic bone disease, hereditary gnatho-diaphyseal sclerosis]', *Nihon Seikeigeka Gakkai Zasshi*, 43(5), pp. 381-94.

Andersen, J.P., Vestergaard, A.L., Mikkelsen, S.A., Mogensen, L.S., Chalat, M. and Molday, R.S. (2016) 'P4-ATPases as Phospholipid Flippases-Structure, Function, and Enigmas', *Front Physiol*, 7, p. 275.

Anderson, N.G. (1955) 'Studies on isolated cell components. VIII. High resolution gradient differential centrifugation', *Exp Cell Res*, 9(3), pp. 446-59.

Avila-Sakar, A.J., Kretsinger, R.H. and Creutz, C.E. (2000) 'Membrane-bound 3D structures reveal the intrinsic flexibility of annexin VI', *J Struct Biol*, 130(1), pp. 54-62.

Babiychuk, E.B. and Draeger, A. (2000) 'Annexins in cell membrane dynamics. Ca(2+)-regulated association of lipid microdomains', *J Cell Biol*, 150(5), pp. 1113-24.

Bach, J.R. and Martinez, D. (2011) 'Duchenne muscular dystrophy: continuous noninvasive ventilatory support prolongs survival', *Respir Care*, 56(6), pp. 744-50.

Bansal, D., Miyake, K., Vogel, S.S., Groh, S., Chen, C.C., Williamson, R., McNeil, P.L. and Campbell, K.P. (2003) 'Defective membrane repair in dysferlin-deficient muscular dystrophy', *Nature*, 423(6936), pp. 168-72.

Bashir, R., Britton, S., Strachan, T., Keers, S., Vafiadaki, E., Lako, M., Richard, I., Marchand, S., Bourg, N., Argov, Z., Sadeh, M., Mahjneh, I., Marconi, G., Passos-Bueno, M.R., Moreira Ede, S., Zatz, M., Beckmann, J.S. and Bushby, K. (1998) 'A gene related to Caenorhabditis elegans spermatogenesis factor fer-1 is mutated in limb-girdle muscular dystrophy type 2B', *Nat Genet*, 20(1), pp. 37-42.

Bastian, A., Mageriu, V., Micu, G. and Manole, E. (2015) 'The Growing Family of Limb-Girdle Muscular Dystrophies: Old and Newly Identified Members', *Rom J Intern Med*, 53(1), pp. 13-24.

Bastian, J. and Nakajima, S. (1974) 'Action potential in the transverse tubules and its role in the activation of skeletal muscle', *J Gen Physiol*, 63(2), pp. 257-78.

Behin, A., Laforêt, P., Cossée, M., Deburgrave, N., Orhant, L., Kaplan, J.C., Stojkovic, T., Leturcq, F. and Eymard, B. (2011) 'P2.49 Myopathies with mutations in anoctamin

5: Phenotype and gene mutations in a French cohort', *Neuromuscular Disorders*, 21(9–10), p. 675.

Bendall, S.C., Nolan, G.P., Roederer, M. and Chattopadhyay, P.K. (2012) 'A deep profiler's guide to cytometry', *Trends Immunol*, 33(7), pp. 323-32.

Berkelman, T. (2008) 'Removal of interfering substances in samples prepared for two-dimensional (2-D) electrophoresis', *Methods Mol Biol*, 424, pp. 51-62.

Bethel, N.P. and Grabe, M. (2016) 'Atomistic insight into lipid translocation by a TMEM16 scramblase', *Proc Natl Acad Sci U S A*, 113(49), pp. 14049-14054.

Betz, R.C., Schoser, B.G., Kasper, D., Ricker, K., Ramirez, A., Stein, V., Torbergsen, T., Lee, Y.A., Nothen, M.M., Wienker, T.F., Malin, J.P., Propping, P., Reis, A., Mortier, W., Jentsch, T.J., Vorgerd, M. and Kubisch, C. (2001) 'Mutations in CAV3 cause mechanical hyperirritability of skeletal muscle in rippling muscle disease', *Nat Genet*, 28(3), pp. 218-9.

Bevers, E.M., Comfurius, P., van Rijn, J.L., Hemker, H.C. and Zwaal, R.F. (1982) 'Generation of prothrombin-converting activity and the exposure of phosphatidylserine at the outer surface of platelets', *Eur J Biochem*, 122(2), pp. 429-36.

Bevers, E.M., Comfurius, P. and Zwaal, R.F. (1983) 'Changes in membrane phospholipid distribution during platelet activation', *Biochim Biophys Acta*, 736(1), pp. 57-66.

Bharadwaj, A., Bydoun, M., Holloway, R. and Waisman, D. (2013) 'Annexin A2 heterotetramer: structure and function', *Int J Mol Sci*, 14(3), pp. 6259-305.

Bignardi, G.E. (2015) 'Flow cytometry for the microscopy of body fluids in patients with suspected infection', *J Clin Pathol*, 68(11), pp. 870-8.

Bisceglia, L., Zoccolella, S., Torraco, A., Piemontese, M.R., Dell'Aglio, R., Amati, A., De Bonis, P., Artuso, L., Copetti, M., Santorelli, F.M., Serlenga, L., Zelante, L., Bertini, E. and Petruzzella, V. (2010) 'A new locus on 3p23-p25 for an autosomal-dominant limb-girdle muscular dystrophy, LGMD1H', *Eur J Hum Genet*, 18(6), pp. 636-41.

Bitbol, M., Fellmann, P., Zachowski, A. and Devaux, P.F. (1987) 'Ion regulation of phosphatidylserine and phosphatidylethanolamine outside-inside translocation in human erythrocytes', *Biochim Biophys Acta*, 904(2), pp. 268-82.

Bitto, E. and Cho, W. (1998) 'Roles of individual domains of annexin I in its vesicle binding and vesicle aggregation: a comprehensive mutagenesis study', *Biochemistry*, 37(28), pp. 10231-7.

Blackburn, P.R., Selcen, D., Jackson, J.L., Guthrie, K.J., Cousin, M.A., Boczek, N.J., Clift, K.E., Klee, E.W., Dimberg, E.L. and Atwal, P.S. (2016) 'Early-onset limb-girdle muscular dystrophy-2L in a female athlete', *Muscle Nerve*.

Blackwood, R.A. and Ernst, J.D. (1990) 'Characterization of Ca2(+)-dependent phospholipid binding, vesicle aggregation and membrane fusion by annexins', *Biochem J*, 266(1), pp. 195-200.

Bland, A.M., D'Eugenio, L.R., Dugan, M.A., Janech, M.G., Almeida, J.S., Zile, M.R. and Arthur, J.M. (2006) 'Comparison of variability associated with sample preparation in two-dimensional gel electrophoresis of cardiac tissue', *J Biomol Tech*, 17(3), pp. 195-9.

Bland, A.M., Janech, M.G., Almeida, J.S. and Arthur, J.M. (2010) 'Sources of variability among replicate samples separated by two-dimensional gel electrophoresis', *J Biomol Tech*, 21(1), pp. 3-8.

Bolduc, V., Marlow, G., Boycott, K.M., Saleki, K., Inoue, H., Kroon, J., Itakura, M., Robitaille, Y., Parent, L., Baas, F., Mizuta, K., Kamata, N., Richard, I., Linssen, W.H., Mahjneh, I., de Visser, M., Bashir, R. and Brais, B. (2010) 'Recessive mutations in the putative calcium-activated chloride channel Anoctamin 5 cause proximal LGMD2L and distal MMD3 muscular dystrophies', *Am J Hum Genet*, 86(2), pp. 213-21.

Bonnemann, C.G., Modi, R., Noguchi, S., Mizuno, Y., Yoshida, M., Gussoni, E., McNally, E.M., Duggan, D.J., Angelini, C. and Hoffman, E.P. (1995) 'Beta-sarcoglycan (A3b) mutations cause autosomal recessive muscular dystrophy with loss of the sarcoglycan complex', *Nat Genet*, 11(3), pp. 266-73.

Bonnemann, C.G., Wang, C.H., Quijano-Roy, S., Deconinck, N., Bertini, E., Ferreiro, A., Muntoni, F., Sewry, C., Beroud, C., Mathews, K.D., Moore, S.A., Bellini, J., Rutkowski, A. and North, K.N. (2014) 'Diagnostic approach to the congenital muscular dystrophies', *Neuromuscul Disord*, 24(4), pp. 289-311.

Borst, P., Zelcer, N. and van Helvoort, A. (2000) 'ABC transporters in lipid transport', *Biochim Biophys Acta*, 1486(1), pp. 128-44.

Boye, T.L. and Nylandsted, J. (2016) 'Annexins in plasma membrane repair', *Biol Chem*, 397(10), pp. 961-9.

Brockington, M., Blake, D.J., Prandini, P., Brown, S.C., Torelli, S., Benson, M.A., Ponting, C.P., Estournet, B., Romero, N.B., Mercuri, E., Voit, T., Sewry, C.A., Guicheney, P. and Muntoni, F. (2001a) 'Mutations in the fukutin-related protein gene (FKRP) cause a form of congenital muscular dystrophy with secondary laminin alpha2 deficiency and abnormal glycosylation of alpha-dystroglycan', *Am J Hum Genet*, 69(6), pp. 1198-209.

Brockington, M., Yuva, Y., Prandini, P., Brown, S.C., Torelli, S., Benson, M.A., Herrmann, R., Anderson, L.V., Bashir, R., Burgunder, J.M., Fallet, S., Romero, N., Fardeau, M., Straub, V., Storey, G., Pollitt, C., Richard, I., Sewry, C.A., Bushby, K., Voit, T., Blake, D.J. and Muntoni, F. (2001b) 'Mutations in the fukutin-related protein gene (FKRP) identify limb girdle muscular dystrophy 2I as a milder allelic variant of congenital muscular dystrophy MDC1C', *Hum Mol Genet*, 10(25), pp. 2851-9.

Brown, D.A. and London, E. (1997) 'Structure of detergent-resistant membrane domains: does phase separation occur in biological membranes?', *Biochem Biophys Res Commun*, 240(1), pp. 1-7.

Brunner, J.D., Lim, N.K., Schenck, S., Duerst, A. and Dutzler, R. (2014) 'X-ray structure of a calcium-activated TMEM16 lipid scramblase', *Nature*, 516(7530), pp. 207-12.

Bushby, K. (2009) 'Diagnosis and management of the limb girdle muscular dystrophies', *Pract Neurol*, 9(6), pp. 314-23.

Bushby, K., Finkel, R., Birnkrant, D.J., Case, L.E., Clemens, P.R., Cripe, L., Kaul, A., Kinnett, K., McDonald, C., Pandya, S., Poysky, J., Shapiro, F., Tomezsko, J. and Constantin, C. (2010) 'Diagnosis and management of Duchenne muscular dystrophy, part 1: diagnosis, and pharmacological and psychosocial management', *Lancet Neurol*, 9(1), pp. 77-93.

Bushby, K.M. (1995) 'Diagnostic criteria for the limb-girdle muscular dystrophies: report of the ENMC Consortium on Limb-Girdle Dystrophies', *Neuromuscul Disord*, 5(1), pp. 71-4.

Bushby, K.M. (1999) 'Making sense of the limb-girdle muscular dystrophies', *Brain*, 122 (Pt 8), pp. 1403-20.

Cagliani, R., Magri, F., Toscano, A., Merlini, L., Fortunato, F., Lamperti, C., Rodolico, C., Prelle, A., Sironi, M., Aguennouz, M., Ciscato, P., Uncini, A., Moggio, M., Bresolin, N. and Comi, G.P. (2005) 'Mutation finding in patients with dysferlin deficiency and role of the dysferlin interacting proteins annexin A1 and A2 in muscular dystrophies', *Hum Mutat*, 26(3), p. 283.

Campbell, G.R., Chamley-Campbell, J., Groschel-Stewart, U., Small, J.V. and Anderson, P. (1979) 'Antibody staining of 10-nm (100-A) filaments in cultured smooth, cardiac and skeletal muscle cells', *J Cell Sci*, 37, pp. 303-22.

Caputo, A., Caci, E., Ferrera, L., Pedemonte, N., Barsanti, C., Sondo, E., Pfeffer, U., Ravazzolo, R., Zegarra-Moran, O. and Galietta, L.J. (2008) 'TMEM16A, a membrane protein associated with calcium-dependent chloride channel activity', *Science*, 322(5901), pp. 590-4.

Carbone, I., Bruno, C., Sotgia, F., Bado, M., Broda, P., Masetti, E., Panella, A., Zara, F., Bricarelli, F.D., Cordone, G., Lisanti, M.P. and Minetti, C. (2000) 'Mutation in the CAV3 gene causes partial caveolin-3 deficiency and hyperCKemia', *Neurology*, 54(6), pp. 1373-6.

Carles, A., Millon, R., Cromer, A., Ganguli, G., Lemaire, F., Young, J., Wasylyk, C., Muller, D., Schultz, I., Rabouel, Y., Dembele, D., Zhao, C., Marchal, P., Ducray, C., Bracco, L., Abecassis, J., Poch, O. and Wasylyk, B. (2006) 'Head and neck squamous cell carcinoma transcriptome analysis by comprehensive validated differential display', *Oncogene*, 25(12), pp. 1821-31.

Castoldi, E., Collins, P.W., Williamson, P.L. and Bevers, E.M. (2011) 'Compound heterozygosity for 2 novel TMEM16F mutations in a patient with Scott syndrome', *Blood*, 117(16), pp. 4399-400.

Chalfie, M., Tu, Y., Euskirchen, G., Ward, W.W. and Prasher, D.C. (1994) 'Green fluorescent protein as a marker for gene expression', *Science*, 263(5148), pp. 802-5.

Chattopadhyay, P.K. and Roederer, M. (2012) 'Cytometry: today's technology and tomorrow's horizons', *Methods*, 57(3), pp. 251-8.

Cheng, E.H., Kirsch, D.G., Clem, R.J., Ravi, R., Kastan, M.B., Bedi, A., Ueno, K. and Hardwick, J.M. (1997) 'Conversion of Bcl-2 to a Bax-like death effector by caspases', *Science*, 278(5345), pp. 1966-8.

Cherkashin, A.P., Kolesnikova, A.S., Tarasov, M.V., Romanov, R.A., Rogachevskaja, O.A., Bystrova, M.F. and Kolesnikov, S.S. (2015) 'Expression of calcium-activated chloride channels Ano1 and Ano2 in mouse taste cells', *Pflugers Arch*.

Cherukuri, A., Dykstra, M. and Pierce, S.K. (2001) 'Floating the raft hypothesis: lipid rafts play a role in immune cell activation', *Immunity*, 14(6), pp. 657-60.

Choe, L.H. and Lee, K.H. (2003) 'Quantitative and qualitative measure of intralaboratory two-dimensional protein gel reproducibility and the effects of sample preparation, sample load, and image analysis', *Electrophoresis*, 24(19-20), pp. 3500-7.

Cohn, R.D. and Campbell, K.P. (2000) 'Molecular basis of muscular dystrophies', *Muscle Nerve*, 23(10), pp. 1456-71.

Coleman, M.L., Sahai, E.A., Yeo, M., Bosch, M., Dewar, A. and Olson, M.F. (2001) 'Membrane blebbing during apoptosis results from caspase-mediated activation of ROCK I', *Nat Cell Biol*, 3(4), pp. 339-45.

Coley, W.D., Bogdanik, L., Vila, M.C., Yu, Q., Van Der Meulen, J.H., Rayavarapu, S., Novak, J.S., Nearing, M., Quinn, J.L., Saunders, A., Dolan, C., Andrews, W., Lammert, C., Austin, A., Partridge, T.A., Cox, G.A., Lutz, C. and Nagaraju, K. (2016) 'Effect of genetic background on the dystrophic phenotype in mdx mice', *Hum Mol Genet*, 25(1), pp. 130-45.

Cooper, S.T. and McNeil, P.L. (2015) 'Membrane Repair: Mechanisms and Pathophysiology', *Physiol Rev*, 95(4), pp. 1205-40.

Cotta, A., Carvalho, E., da-Cunha-Junior, A.L., Paim, J.F., Navarro, M.M., Valicek, J., Menezes, M.M., Nunes, S.V., Xavier Neto, R., Takata, R.I. and Vargas, A.P. (2014) 'Common recessive limb girdle muscular dystrophies differential diagnosis: why and how?', *Arq Neuropsiquiatr*, 72(9), pp. 721-34.

Coulton, G.R., Morgan, J.E., Partridge, T.A. and Sloper, J.C. (1988) 'The mdx mouse skeletal muscle myopathy: I. A histological, morphometric and biochemical investigation', *Neuropathol Appl Neurobiol*, 14(1), pp. 53-70.

Courjaret, R., Hodeify, R., Hubrack, S., Ibrahim, A., Dib, M., Daas, S. and Machaca, K. (2016) 'The Ca2+-activated Cl- channel Ano1 controls microvilli length and membrane surface area in the oocyte', *J Cell Sci*, 129(13), pp. 2548-58.

Creutz, C.E. and Snyder, S.L. (2005) 'Interactions of annexins with the mu subunits of the clathrin assembly proteins', *Biochemistry*, 44(42), pp. 13795-806.

Crutzen, R., Virreira, M., Markadieu, N., Shlyonsky, V., Sener, A., Malaisse, W.J., Beauwens, R., Boom, A. and Golstein, P.E. (2015) 'Anoctamin 1 (Ano1) is required for glucose-induced membrane potential oscillations and insulin secretion by murine beta-cells', *Pflugers Arch*.

Daftary, A.S., Crisanti, M., Kalra, M., Wong, B. and Amin, R. (2007) 'Effect of long-term steroids on cough efficiency and respiratory muscle strength in patients with Duchenne muscular dystrophy', *Pediatrics*, 119(2), pp. e320-4.

Daleke, D.L. (2003) 'Regulation of transbilayer plasma membrane phospholipid asymmetry', *J Lipid Res*, 44(2), pp. 233-42.

Daleke, D.L. (2007) 'Phospholipid flippases', *J Biol Chem*, 282(2), pp. 821-5.

Daleke, D.L. and Lyles, J.V. (2000) 'Identification and purification of aminophospholipid flippases', *Biochim Biophys Acta*, 1486(1), pp. 108-27.

Damek-Poprawa, M., Golub, E., Otis, L., Harrison, G., Phillips, C. and Boesze-Battaglia, K. (2006) 'Chondrocytes utilize a cholesterol-dependent lipid translocator to externalize phosphatidylserine', *Biochemistry*, 45(10), pp. 3325-36.

Dauner, K., Lissmann, J., Jeridi, S., Frings, S. and Mohrlen, F. (2012) 'Expression patterns of anoctamin 1 and anoctamin 2 chloride channels in the mammalian nose', *Cell Tissue Res*, 347(2), pp. 327-41.

Dauner, K., Mobus, C., Frings, S. and Mohrlen, F. (2013) 'Targeted expression of anoctamin calcium-activated chloride channels in rod photoreceptor terminals of the rodent retina', *Invest Ophthalmol Vis Sci*, 54(5), pp. 3126-36.

de Sousa Abreu, R., Penalva, L.O., Marcotte, E.M. and Vogel, C. (2009) 'Global signatures of protein and mRNA expression levels', *Mol Biosyst*, 5(12), pp. 1512-26.

Defour, A., Medikayala, S., Van der Meulen, J.H., Hogarth, M.W., Holdreith, N., Malatras, A., Duddy, W., Boehler, J., Nagaraju, K. and Jaiswal, J.K. (2017) 'Annexin A2 links poor myofiber repair with inflammation and adipogenic replacement of the injured muscle', *Hum Mol Genet*.

Demonbreun, A.R., Allen, M.V., Warner, J.L., Barefield, D.Y., Krishnan, S., Swanson, K.E., Earley, J.U. and McNally, E.M. (2016a) 'Enhanced Muscular Dystrophy from Loss of Dysferlin Is Accompanied by Impaired Annexin A6 Translocation after Sarcolemmal Disruption', *Am J Pathol*, 186(6), pp. 1610-22.

Demonbreun, A.R., Biersmith, B.H. and McNally, E.M. (2015) 'Membrane fusion in muscle development and repair', *Semin Cell Dev Biol*.

Demonbreun, A.R., Quattrocelli, M., Barefield, D.Y., Allen, M.V., Swanson, K.E. and McNally, E.M. (2016b) 'An actin-dependent annexin complex mediates plasma membrane repair in muscle', *J Cell Biol*, 213(6), pp. 705-18.

Demonbreun, A.R., Rossi, A.E., Alvarez, M.G., Swanson, K.E., Deveaux, H.K., Earley, J.U., Hadhazy, M., Vohra, R., Walter, G.A., Pytel, P. and McNally, E.M. (2014) 'Dysferlin and myoferlin regulate transverse tubule formation and glycerol sensitivity', *Am J Pathol*, 184(1), pp. 248-59.

Dimauro, I., Pearson, T., Caporossi, D. and Jackson, M.J. (2012) 'A simple protocol for the subcellular fractionation of skeletal muscle cells and tissue', *BMC Res Notes*, 5, p. 513.

Dinant, C., van Royen, M.E., Vermeulen, W. and Houtsmuller, A.B. (2008) 'Fluorescence resonance energy transfer of GFP and YFP by spectral imaging and quantitative acceptor photobleaching', *J Microsc*, 231(Pt 1), pp. 97-104.

Dini, L., Ruzittu, M.T. and Falasca, L. (1996) 'Recognition and phagocytosis of apoptotic cells', *Scanning Microsc*, 10(1), pp. 239-51; discussion 251-2.

Diwu, Z., Zhang, Y. and Haugland, R.P. (1994) 'Novel site-selective fluorescent probes for lysosome and acidic organelle staining and long-term tracking', *Cytometry*, 18(77).

Doutheil, J., Althausen, S., Treiman, M. and Paschen, W. (2000) 'Effect of nitric oxide on endoplasmic reticulum calcium homeostasis, protein synthesis and energy metabolism', *Cell Calcium*, 27(2), pp. 107-15.

Doyle, D.A., Morais Cabral, J., Pfuetzner, R.A., Kuo, A., Gulbis, J.M., Cohen, S.L., Chait, B.T. and MacKinnon, R. (1998) 'The structure of the potassium channel: molecular basis of K+ conduction and selectivity', *Science*, 280(5360), pp. 69-77.

Draeger, A., Sanchez-Freire, V., Monastyrskaya, K., Hoppeler, H., Mueller, M., Breil, F., Mohaupt, M.G. and Babiychuk, E.B. (2010) 'Statin therapy and the expression of genes that regulate calcium homeostasis and membrane repair in skeletal muscle', *Am J Pathol*, 177(1), pp. 291-9.

Duran, C. and Hartzell, H.C. (2011) 'Physiological roles and diseases of Tmem16/Anoctamin proteins: are they all chloride channels?', *Acta Pharmacol Sin*, 32(6), pp. 685-92.

Duran, C., Qu, Z., Osunkoya, A.O., Cui, Y. and Hartzell, H.C. (2012) 'ANOs 3-7 in the anoctamin/Tmem16 Cl- channel family are intracellular proteins', *Am J Physiol Cell Physiol*, 302(3), pp. C482-93.

Durbeej, M. and Campbell, K.P. (2002) 'Muscular dystrophies involving the dystrophin-glycoprotein complex: an overview of current mouse models', *Curr Opin Genet Dev*, 12(3), pp. 349-61.

Dziduszko, A. and Ozbun, M.A. (2013) 'Annexin A2 and S100A10 regulate human papillomavirus type 16 entry and intracellular trafficking in human keratinocytes', *J Virol*, 87(13), pp. 7502-15.

Eagle, M., Baudouin, S.V., Chandler, C., Giddings, D.R., Bullock, R. and Bushby, K. (2002) 'Survival in Duchenne muscular dystrophy: improvements in life expectancy since 1967 and the impact of home nocturnal ventilation', *Neuromuscul Disord*, 12(10), pp. 926-9.

Ehlen, H.W., Chinenkova, M., Moser, M., Munter, H.M., Krause, Y., Gross, S., Brachvogel, B., Wuelling, M., Kornak, U. and Vortkamp, A. (2013) 'Inactivation of anoctamin-6/Tmem16f, a regulator of phosphatidylserine scrambling in osteoblasts, leads to decreased mineral deposition in skeletal tissues', *J Bone Miner Res*, 28(2), pp. 246-59.

Emery, A.E. (2002) 'The muscular dystrophies', *Lancet*, 359(9307), pp. 687-95.

Emery, A.E. and Emery, M.L. (1993) 'Edward Meryon (1809-1880) and muscular dystrophy', *J Med Genet*, 30(6), pp. 506-11.

Enari, M., Sakahira, H., Yokoyama, H., Okawa, K., Iwamatsu, A. and Nagata, S. (1998) 'A caspase-activated DNase that degrades DNA during apoptosis, and its inhibitor ICAD', *Nature*, 391(6662), pp. 43-50.

Engler, A.J., Griffin, M.A., Sen, S., Bonnemann, C.G., Sweeney, H.L. and Discher, D.E. (2004) 'Myotubes differentiate optimally on substrates with tissue-like stiffness: pathological implications for soft or stiff microenvironments', *J Cell Biol*, 166(6), pp. 877-87.

Ervasti, J.M. and Campbell, K.P. (1993) 'A role for the dystrophin-glycoprotein complex as a transmembrane linker between laminin and actin', *J Cell Biol*, 122(4), pp. 809-23.

Fadok, V.A., de Cathelineau, A., Daleke, D.L., Henson, P.M. and Bratton, D.L. (2001) 'Loss of phospholipid asymmetry and surface exposure of phosphatidylserine is required for phagocytosis of apoptotic cells by macrophages and fibroblasts', *J Biol Chem*, 276(2), pp. 1071-7.

Fadok, V.A., Voelker, D.R., Campbell, P.A., Cohen, J.J., Bratton, D.L. and Henson, P.M. (1992) 'Exposure of phosphatidylserine on the surface of apoptotic lymphocytes triggers specific recognition and removal by macrophages', *J Immunol*, 148(7), pp. 2207-16.

Fanin, M., Nascimbeni, A.C., Fulizio, L. and Angelini, C. (2005) 'The frequency of limb girdle muscular dystrophy 2A in northeastern Italy', *Neuromuscul Disord*, 15(3), pp. 218-24.

Faulstich, H., Zobeley, S., Rinnerthaler, G. and Small, J.V. (1988) 'Fluorescent phallotoxins as probes for filamentous actin', *J Muscle Res Cell Motil*, 9(5), pp. 370-83.

Ferrera, L., Caputo, A., Ubby, I., Bussani, E., Zegarra-Moran, O., Ravazzolo, R., Pagani, F. and Galietta, L.J. (2009) 'Regulation of TMEM16A chloride channel properties by alternative splicing', *J Biol Chem*, 284(48), pp. 33360-8.

Fliegel, L., Burns, K., MacLennan, D.H., Reithmeier, R.A. and Michalak, M. (1989) 'Molecular cloning of the high affinity calcium-binding protein (calreticulin) of skeletal muscle sarcoplasmic reticulum', *J Biol Chem*, 264(36), pp. 21522-8.

Freeman, H., Shimomura, K., Cox, R.D. and Ashcroft, F.M. (2006a) 'Nicotinamide nucleotide transhydrogenase: a link between insulin secretion, glucose metabolism and oxidative stress', *Biochem Soc Trans*, 34(Pt 5), pp. 806-10.

Freeman, H.C., Hugill, A., Dear, N.T., Ashcroft, F.M. and Cox, R.D. (2006b) 'Deletion of nicotinamide nucleotide transhydrogenase: a new quantitive trait locus accounting for glucose intolerance in C57BL/6J mice', *Diabetes*, 55(7), pp. 2153-6.

Frosk, P., Greenberg, C.R., Tennese, A.A., Lamont, R., Nylen, E., Hirst, C., Frappier, D., Roslin, N.M., Zaik, M., Bushby, K., Straub, V., Zatz, M., de Paula, F., Morgan, K., Fujiwara, T.M. and Wrogemann, K. (2005) 'The most common mutation in FKRP

causing limb girdle muscular dystrophy type 2I (LGMD2I) may have occurred only once and is present in Hutterites and other populations', *Hum Mutat*, 25(1), pp. 38-44.

Frosk, P., Weiler, T., Nylen, E., Sudha, T., Greenberg, C.R., Morgan, K., Fujiwara, T.M. and Wrogemann, K. (2002) 'Limb-girdle muscular dystrophy type 2H associated with mutation in TRIM32, a putative E3-ubiquitin-ligase gene', *Am J Hum Genet*, 70(3), pp. 663-72.

Fujii, T., Sakata, A., Nishimura, S., Eto, K. and Nagata, S. (2015) 'TMEM16F is required for phosphatidylserine exposure and microparticle release in activated mouse platelets', *Proc Natl Acad Sci U S A*, 112(41), pp. 12800-5.

Fulwyler, M.J. (1965) 'Electronic separation of biological cells by volume', *Science*, 150(3698), pp. 910-1.

Galbiati, F., Razani, B. and Lisanti, M.P. (2001) 'Emerging themes in lipid rafts and caveolae', *Cell*, 106(4), pp. 403-11.

Gamez, J., Navarro, C., Andreu, A.L., Fernandez, J.M., Palenzuela, L., Tejeira, S., Fernandez-Hojas, R., Schwartz, S., Karadimas, C., DiMauro, S., Hirano, M. and Cervera, C. (2001) 'Autosomal dominant limb-girdle muscular dystrophy: a large kindred with evidence for anticipation', *Neurology*, 56(4), pp. 450-4.

Gazzerro, E., Sotgia, F., Bruno, C., Lisanti, M.P. and Minetti, C. (2010) 'Caveolinopathies: from the biology of caveolin-3 to human diseases', *Eur J Hum Genet*, 18(2), pp. 137-45.

Geisow, M.J., Fritsche, U., Hexham, J.M., Dash, B. and Johnson, T. (1986) 'A consensus amino-acid sequence repeat in Torpedo and mammalian Ca2+-dependent membrane-binding proteins', *Nature*, 320(6063), pp. 636-8.

Genge, B.R., Wu, L.N. and Wuthier, R.E. (2008) 'Mineralization of annexin-5-containing lipid-calcium-phosphate complexes: modulation by varying lipid composition and incubation with cartilage collagens', *J Biol Chem*, 283(15), pp. 9737-48.

Gerke, V., Creutz, C.E. and Moss, S.E. (2005) 'Annexins: linking Ca2+ signalling to membrane dynamics', *Nat Rev Mol Cell Biol*, 6(6), pp. 449-61.

Gerke, V. and Moss, S.E. (1997) 'Annexins and membrane dynamics', *Biochim Biophys Acta*, 1357(2), pp. 129-54.

Gerke, V. and Moss, S.E. (2002) 'Annexins: from structure to function', *Physiol Rev*, 82(2), pp. 331-71.

Ghaoui, R., Benavides, T., Lek, M., Waddell, L.B., Kaur, S., North, K.N., MacArthur, D.G., Clarke, N.F. and Cooper, S.T. (2016) 'TOR1AIP1 as a cause of cardiac failure and recessive limb-girdle muscular dystrophy', *Neuromuscul Disord*, 26(8), pp. 500-3.

Ghaoui, R., Cooper, S.T., Lek, M., Jones, K., Corbett, A., Reddel, S.W., Needham, M., Liang, C., Waddell, L.B., Nicholson, G., O'Grady, G., Kaur, S., Ong, R., Davis, M., Sue, C.M., Laing, N.G., North, K.N., MacArthur, D.G. and Clarke, N.F. (2015) 'Use of

Whole-Exome Sequencing for Diagnosis of Limb-Girdle Muscular Dystrophy: Outcomes and Lessons Learned', *JAMA Neurol*, 72(12), pp. 1424-32.

Gilchrist, J.M., Pericak-Vance, M., Silverman, L. and Roses, A.D. (1988) 'Clinical and genetic investigation in autosomal dominant limb-girdle muscular dystrophy', *Neurology*, 38(1), pp. 5-9.

Gillette, J.M. and Nielsen-Preiss, S.M. (2004) 'The role of annexin 2 in osteoblastic mineralization', *J Cell Sci*, 117(Pt 3), pp. 441-9.

Gonzalez-Perez, P., Gallano, P., Gonzalez-Quereda, L., Rivas-Infante, E., Teijeira, S., Navarro, C. and Bautista-Lorite, J. (2009) 'Phenotypic variability in a Spanish family with a Caveolin-3 mutation', *J Neurol Sci*, 276(1-2), pp. 95-8.

Grady, R.M., Teng, H., Nichol, M.C., Cunningham, J.C., Wilkinson, R.S. and Sanes, J.R. (1997) 'Skeletal and cardiac myopathies in mice lacking utrophin and dystrophin: a model for Duchenne muscular dystrophy', *Cell*, 90(4), pp. 729-38.

Griffin, D.A., Johnson, R.W., Whitlock, J.M., Pozsgai, E.R., Heller, K.N., Grose, W.E., Arnold, W.D., Sahenk, Z., Hartzell, H.C. and Rodino-Klapac, L.R. (2016) 'Defective membrane fusion and repair in Anoctamin5-deficient muscular dystrophy', *Hum Mol Genet*, 25(10), pp. 1900-1911.

Grimm, T. (1984) 'Genetic counseling in Becker type X-linked muscular dystrophy. II: Practical considerations', *Am J Med Genet*, 18(4), pp. 719-23.

Gross, S.M. and Rotwein, P. (2013) 'Live cell imaging reveals marked variability in myoblast proliferation and fate', *Skelet Muscle*, 3(1), p. 10.

Guan, L., Song, Y., Gao, J., Gao, J. and Wang, K. (2016) 'Inhibition of calcium-activated chloride channel ANO1 suppresses proliferation and induces apoptosis of epithelium originated cancer cells', *Oncotarget*, 7(48), pp. 78619-78630.

Guha, U., Gomes, W.A., Kobayashi, T., Pestell, R.G. and Kessler, J.A. (2002) 'In vivo evidence that BMP signaling is necessary for apoptosis in the mouse limb', *Dev Biol*, 249(1), pp. 108-20.

Gumerson, J.D. and Michele, D.E. (2011) 'The dystrophin-glycoprotein complex in the prevention of muscle damage', *J Biomed Biotechnol*, 2011, p. 210797.

Gyobu, S., Miyata, H., Ikawa, M., Yamazaki, D., Takeshima, H., Suzuki, J. and Nagata, S. (2015) 'A Role of TMEM16E Carrying a Scrambling Domain in Sperm Motility', *Mol Cell Biol*, 36(4), pp. 645-59.

Hampton, M.B., Vanags, D.M., Porn-Ares, M.I. and Orrenius, S. (1996) 'Involvement of extracellular calcium in phosphatidylserine exposure during apoptosis', *FEBS Lett*, 399(3), pp. 277-82.

Han, R. and Campbell, K.P. (2007) 'Dysferlin and muscle membrane repair', *Curr Opin Cell Biol*, 19(4), pp. 409-16.

Hartzell, H.C., Yu, K., Xiao, Q., Chien, L.T. and Qu, Z. (2009) 'Anoctamin/TMEM16 family members are Ca2+-activated Cl- channels', *J Physiol*, 587(Pt 10), pp. 2127-39.

Hauser, M.A., Conde, C.B., Kowaljow, V., Zeppa, G., Taratuto, A.L., Torian, U.M., Vance, J., Pericak-Vance, M.A., Speer, M.C. and Rosa, A.L. (2002) 'myotilin Mutation found in second pedigree with LGMD1A', *Am J Hum Genet*, 71(6), pp. 1428-32.

Hauser, M.A., Horrigan, S.K., Salmikangas, P., Torian, U.M., Viles, K.D., Dancel, R., Tim, R.W., Taivainen, A., Bartoloni, L., Gilchrist, J.M., Stajich, J.M., Gaskell, P.C., Gilbert, J.R., Vance, J.M., Pericak-Vance, M.A., Carpen, O., Westbrook, C.A. and Speer, M.C. (2000) 'Myotilin is mutated in limb girdle muscular dystrophy 1A', *Hum Mol Genet*, 9(14), pp. 2141-7.

Hawke, T.J. and Garry, D.J. (2001) 'Myogenic satellite cells: physiology to molecular biology', *J Appl Physiol (1985)*, 91(2), pp. 534-51.

He, K.L., Deora, A.B., Xiong, H., Ling, Q., Weksler, B.B., Niesvizky, R. and Hajjar, K.A. (2008) 'Endothelial cell annexin A2 regulates polyubiquitination and degradation of its binding partner S100A10/p11', *J Biol Chem*, 283(28), pp. 19192-200.

Hebert, D.N. and Molinari, M. (2007) 'In and out of the ER: protein folding, quality control, degradation, and related human diseases', *Physiol Rev*, 87(4), pp. 1377-408.

Hensley-McBain, T., Heit, A., De Rosa, S.C., McElrath, M.J. and Andersen-Nissen, E. (2014) 'Optimization of a whole blood phenotyping assay for enumeration of peripheral blood leukocyte populations in multicenter clinical trials', *J Immunol Methods*, 411, pp. 23-36.

Hicks, D., Sarkozy, A., Muelas, N., Koehler, K., Huebner, A., Hudson, G., Chinnery, P.F., Barresi, R., Eagle, M., Polvikoski, T., Bailey, G., Miller, J., Radunovic, A., Hughes, P.J., Roberts, R., Krause, S., Walter, M.C., Laval, S.H., Straub, V., Lochmuller, H. and Bushby, K. (2011) 'A founder mutation in Anoctamin 5 is a major cause of limb-girdle muscular dystrophy', *Brain*, 134, pp. 171-182.

Hochreiter-Hufford, A. and Ravichandran, K.S. (2013) 'Clearing the dead: apoptotic cell sensing, recognition, engulfment, and digestion', *Cold Spring Harb Perspect Biol*, 5(1), p. a008748.

Hoffman, E.P., Brown, R.H., Jr. and Kunkel, L.M. (1987) 'Dystrophin: the protein product of the Duchenne muscular dystrophy locus', *Cell*, 51(6), pp. 919-28.

Hoffman, E.P., Morgan, J.E., Watkins, S.C. and Partridge, T.A. (1990) 'Somatic reversion/suppression of the mouse mdx phenotype in vivo', *J Neurol Sci*, 99(1), pp. 9-25.

Holubec, H., Payne, C.M., Bernstein, H., Dvorakova, K., Bernstein, C., Waltmire, C.N., Warneke, J.A. and Garewal, H. (2005) 'Assessment of apoptosis by immunohistochemical markers compared to cellular morphology in ex vivo-stressed colonic mucosa', *J Histochem Cytochem*, 53(2), pp. 229-35.

Huang, F., Zhang, H., Wu, M., Yang, H., Kudo, M., Peters, C.J., Woodruff, P.G., Solberg, O.D., Donne, M.L., Huang, X., Sheppard, D., Fahy, J.V., Wolters, P.J., Hogan,

B.L., Finkbeiner, W.E., Li, M., Jan, Y.N., Jan, L.Y. and Rock, J.R. (2012) 'Calcium-activated chloride channel TMEM16A modulates mucin secretion and airway smooth muscle contraction', *Proc Natl Acad Sci U S A*, 109(40), pp. 16354-9.

Huang, Z.J., Haugland, R.P., You, W.M. and Haugland, R.P. (1992) 'Phallotoxin and actin binding assay by fluorescence enhancement', *Anal Biochem*, 200(1), pp. 199-204.

Huber, R., Romisch, J. and Paques, E.P. (1990) 'The crystal and molecular structure of human annexin V, an anticoagulant protein that binds to calcium and membranes', *Embo j*, 9(12), pp. 3867-74.

Hulett, H.R., Bonner, W.A., Barrett, J. and Herzenberg, L.A. (1969) 'Cell sorting: automated separation of mammalian cells as a function of intracellular fluorescence', *Science*, 166(3906), pp. 747-9.

Hulett, H.R., Bonner, W.A., Sweet, R.G. and Herzenberg, L.A. (1973) 'Development and application of a rapid cell sorter', *Clin Chem*, 19(8), pp. 813-6.

Huxley, A.F. and Taylor, R.E. (1958) 'Local activation of striated muscle fibres', *J Physiol*, 144(3), pp. 426-41.

Idone, V., Tam, C., Goss, J.W., Toomre, D., Pypaert, M. and Andrews, N.W. (2008) 'Repair of injured plasma membrane by rapid Ca2+-dependent endocytosis', *J Cell Biol*, 180(5), pp. 905-14.

Inouye, S. and Tsuji, F.I. (1994) 'Aequorea green fluorescent protein. Expression of the gene and fluorescence characteristics of the recombinant protein', *FEBS Lett*, 341(2-3), pp. 277-80.

Jaiswal, J.K., Marlow, G., Summerill, G., Mahjneh, I., Mueller, S., Hill, M., Miyake, K., Haase, H., Anderson, L.V., Richard, I., Kiuru-Enari, S., McNeil, P.L., Simon, S.M. and Bashir, R. (2007) 'Patients with a non-dysferlin Miyoshi myopathy have a novel membrane repair defect', *Traffic*, 8(1), pp. 77-88.

Janicke, R.U., Sprengart, M.L., Wati, M.R. and Porter, A.G. (1998) 'Caspase-3 is required for DNA fragmentation and morphological changes associated with apoptosis', *J Biol Chem*, 273(16), pp. 9357-60.

Jarry, J., Rioux, M.F., Bolduc, V., Robitaille, Y., Khoury, V., Thiffault, I., Tetreault, M., Loisel, L., Bouchard, J.P. and Brais, B. (2007) 'A novel autosomal recessive limb-girdle muscular dystrophy with quadriceps atrophy maps to 11p13-p12', *Brain*, 130(Pt 2), pp. 368-80.

Jeong, J. and Conboy, I.M. (2011) 'Phosphatidylserine directly and positively regulates fusion of myoblasts into myotubes', *Biochem Biophys Res Commun*, 414(1), pp. 9-13.

Johnson, F.H., Gershman, L.C., Waters, J.R., Reynolds, G.T., Saiga, Y. and Shimomura, O. (1962) 'QUANTUM EFFICIENCY OF CYPRIDINA LUMINESCENCE, WITH A NOTE ON THAT OF AEQUOREA', *Journal of Cellular and Comparative Physiology*, 60(1), pp. 85-&.

Karas, M., Bachmann, D., Bahr, U. and Hillenkamp, F. (1987) 'Matrix-Assisted Ultraviolet Laser Desorption of Non-Volatile Compounds', *International Journal of Mass Spectrometry and Ion Processes*, 78, pp. 53-68.

Katoh, M. (2004) 'GDD1 is identical to TMEM16E, a member of the TMEM16 family', *Am J Hum Genet*, 75(5), pp. 927-8; author reply 928-9.

Katoh, M. and Katoh, M. (2004) 'Identification and characterization of TMEM16E and TMEM16F genes in silico', *Int J Oncol*, 24(5), pp. 1345-9.

Kerr, J.F., Wyllie, A.H. and Currie, A.R. (1972) 'Apoptosis: a basic biological phenomenon with wide-ranging implications in tissue kinetics', *Br J Cancer*, 26(4), pp. 239-57.

Kinali, M., Arechavala-Gomeza, V., Cirak, S., Glover, A., Guglieri, M., Feng, L., Hollingsworth, K.G., Hunt, D., Jungbluth, H., Roper, H.P., Quinlivan, R.M., Gosalakkal, J.A., Jayawant, S., Nadeau, A., Hughes-Carre, L., Manzur, A.Y., Mercuri, E., Morgan, J.E., Straub, V., Bushby, K., Sewry, C., Rutherford, M. and Muntoni, F. (2011) 'Muscle histology vs MRI in Duchenne muscular dystrophy', *Neurology*, 76(4), pp. 346-53.

Klinge, L., Laval, S., Keers, S., Haldane, F., Straub, V., Barresi, R. and Bushby, K. (2007) 'From T-tubule to sarcolemma: damage-induced dysferlin translocation in early myogenesis', *Faseb j*, 21(8), pp. 1768-76.

Kubista, H., Hawkins, T.E., Patel, D.R., Haigler, H.T. and Moss, S.E. (1999) 'Annexin 5 mediates a peroxide-induced Ca(2+) influx in B cells', *Curr Biol*, 9(23), pp. 1403-6.

Kuhn, M., Glaser, D., Joshi, P.R., Zierz, S., Wenninger, S., Schoser, B. and Deschauer, M. (2016) 'Utility of a next-generation sequencing-based gene panel investigation in German patients with genetically unclassified limb-girdle muscular dystrophy', *J Neurol*, 263(4), pp. 743-50.

Kunzelmann, K., Kongsuphol, P., Aldehni, F., Tian, Y., Ousingsawat, J., Warth, R. and Schreiber, R. (2009) 'Bestrophin and TMEM16-Ca(2+) activated Cl(-) channels with different functions', *Cell Calcium*, 46(4), pp. 233-41.

Kunzelmann, K., Nilius, B., Owsianik, G., Schreiber, R., Ousingsawat, J., Sirianant, L., Wanitchakool, P., Bevers, E.M. and Heemskerk, J.W. (2014) 'Molecular functions of anoctamin 6 (TMEM16F): a chloride channel, cation channel, or phospholipid scramblase?', *Pflugers Arch*, 466(3), pp. 407-14.

Kurosaka, K., Takahashi, M., Watanabe, N. and Kobayashi, Y. (2003) 'Silent cleanup of very early apoptotic cells by macrophages', *J Immunol*, 171(9), pp. 4672-9.

Kurosaka, K., Watanabe, N. and Kobayashi, Y. (2002) 'Potentiation by human serum of anti-inflammatory cytokine production by human macrophages in response to apoptotic cells', *J Leukoc Biol*, 71(6), pp. 950-6.

Laing, N.G., Davis, M.R., Bayley, K., Fletcher, S. and Wilton, S.D. (2011) 'Molecular diagnosis of duchenne muscular dystrophy: past, present and future in relation to implementing therapies', *Clin Biochem Rev*, 32(3), pp. 129-34.

Lalonde, M.R., Kelly, M.E. and Barnes, S. (2008) 'Calcium-activated chloride channels in the retina', *Channels (Austin)*, 2(4), pp. 252-60.

Lanier, L.L. (2014) 'Just the FACS', *J Immunol*, 193(5), pp. 2043-4.

Lauvrak, S.U., Hollas, H., Doskeland, A.P., Aukrust, I., Flatmark, T. and Vedeler, A. (2005) 'Ubiquitinated annexin A2 is enriched in the cytoskeleton fraction', *FEBS Lett*, 579(1), pp. 203-6.

Lee, E., Marcucci, M., Daniell, L., Pypaert, M., Weisz, O.A., Ochoa, G.C., Farsad, K., Wenk, M.R. and De Camilli, P. (2002) 'Amphiphysin 2 (Bin1) and T-tubule biogenesis in muscle', *Science*, 297(5584), pp. 1193-6.

Lee, Y.H., Tan, H.T. and Chung, M.C. (2010) 'Subcellular fractionation methods and strategies for proteomics', *Proteomics*, 10(22), pp. 3935-56.

Lennon, N.J., Kho, A., Bacskai, B.J., Perlmutter, S.L., Hyman, B.T. and Brown, R.H., Jr. (2003) 'Dysferlin interacts with annexins A1 and A2 and mediates sarcolemmal wound-healing', *J Biol Chem*, 278(50), pp. 50466-73.

Leventis, P.A. and Grinstein, S. (2010) 'The distribution and function of phosphatidylserine in cellular membranes', *Annu Rev Biophys*, 39, pp. 407-27.

Lewit-Bentley, A., Rety, S., Sopkova-de Oliveira Santos, J. and Gerke, V. (2000) 'S100-annexin complexes: some insights from structural studies', *Cell Biol Int*, 24(11), pp. 799-802.

Lhermusier, T., Chap, H. and Payrastre, B. (2011) 'Platelet membrane phospholipid asymmetry: from the characterization of a scramblase activity to the identification of an essential protein mutated in Scott syndrome', *J Thromb Haemost*, 9(10), pp. 1883-91.

Li, D., Long, C., Yue, Y. and Duan, D. (2009) 'Sub-physiological sarcoglycan expression contributes to compensatory muscle protection in mdx mice', *Hum Mol Genet*, 18(7), pp. 1209-20.

Li, M.O., Sarkisian, M.R., Mehal, W.Z., Rakic, P. and Flavell, R.A. (2003) 'Phosphatidylserine receptor is required for clearance of apoptotic cells', *Science*, 302(5650), pp. 1560-3.

Li, S., Kimura, E., Ng, R., Fall, B.M., Meuse, L., Reyes, M., Faulkner, J.A. and Chamberlain, J.S. (2006) 'A highly functional mini-dystrophin/GFP fusion gene for cell and gene therapy studies of Duchenne muscular dystrophy', *Hum Mol Genet*, 15(10), pp. 1610-22.

Liewluck, T., Winder, T.L., Dimberg, E.L., Crum, B.A., Heppelmann, C.J., Wang, Y., Bergen, H.R., 3rd and Milone, M. (2013) 'ANO5-muscular dystrophy: clinical, pathological and molecular findings', *Eur J Neurol*, 20(10), pp. 1383-9.

Linssen, W.H., de Visser, M., Notermans, N.C., Vreyling, J.P., Van Doorn, P.A., Wokke, J.H., Baas, F. and Bolhuis, P.A. (1998) 'Genetic heterogeneity in Miyoshi-type distal muscular dystrophy', *Neuromuscul Disord*, 8(5), pp. 317-20.

Linssen, W.H., Notermans, N.C., Van der Graaf, Y., Wokke, J.H., Van Doorn, P.A., Howeler, C.J., Busch, H.F., De Jager, A.E. and De Visser, M. (1997) 'Miyoshi-type distal muscular dystrophy. Clinical spectrum in 24 Dutch patients', *Brain*, 120 (Pt 11), pp. 1989-96.

Little, A.A., McKeever, P.E. and Gruis, K.L. (2013) 'Novel mutations in the Anoctamin 5 gene (ANO5) associated with limb-girdle muscular dystrophy 2L', *Muscle Nerve*, 47(2), pp. 287-91.

Liu, J., Aoki, M., Illa, I., Wu, C., Fardeau, M., Angelini, C., Serrano, C., Urtizberea, J.A., Hentati, F., Hamida, M.B., Bohlega, S., Culper, E.J., Amato, A.A., Bossie, K., Oeltjen, J., Bejaoui, K., McKenna-Yasek, D., Hosler, B.A., Schurr, E., Arahata, K., de Jong, P.J. and Brown, R.H., Jr. (1998) 'Dysferlin, a novel skeletal muscle gene, is mutated in Miyoshi myopathy and limb girdle muscular dystrophy', *Nat Genet*, 20(1), pp. 31-6.

Lopez-Marques, R.L., Theorin, L., Palmgren, M.G. and Pomorski, T.G. (2014) 'P4-ATPases: lipid flippases in cell membranes', *Pflugers Arch*, 466(7), pp. 1227-40.

MacKinnon, R. (2004) 'Nobel Lecture. Potassium channels and the atomic basis of selective ion conduction', *Biosci Rep*, 24(2), pp. 75-100.

Maecker, H.T. (2009) 'Multiparameter flow cytometry monitoring of T cell responses', *Methods Mol Biol*, 485, pp. 375-91.

Maeno, E., Ishizaki, Y., Kanaseki, T., Hazama, A. and Okada, Y. (2000) 'Normotonic cell shrinkage because of disordered volume regulation is an early prerequisite to apoptosis', *Proc Natl Acad Sci U S A*, 97(17), pp. 9487-92.

Magri, F., Del Bo, R., D'Angelo, M.G., Gandossini, S., Corti, S., Lucchini, V., Napoli, L., Moggio, M. and Comi, G.P. (2011) 'P2.50 LGMD2L in Italian population: New mutations and clinical and morphological aspects', *Neuromuscular Disorders*, 21(9–10), p. 675.

Mahjneh, I., Jaiswal, J., Lamminen, A., Somer, M., Marlow, G., Kiuru-Enari, S. and Bashir, R. (2010) 'A new distal myopathy with mutation in anoctamin 5', *Neuromuscul Disord*, 20(12), pp. 791-5.

Mandinova, A., Atar, D., Schafer, B.W., Spiess, M., Aebi, U. and Heizmann, C.W. (1998) 'Distinct subcellular localization of calcium binding S100 proteins in human smooth muscle cells and their relocation in response to rises in intracellular calcium', *J Cell Sci*, 111 (Pt 14), pp. 2043-54.

Marconi, C., Brunamonti Binello, P., Badiali, G., Caci, E., Cusano, R., Garibaldi, J., Pippucci, T., Merlini, A., Marchetti, C., Rhoden, K.J., Galietta, L.J., Lalatta, F., Balbi, P. and Seri, M. (2013) 'A novel missense mutation in ANO5/TMEM16E is causative for gnathodiaphyseal dyplasia in a large Italian pedigree', *Eur J Hum Genet*, 21(6), pp. 613-9.

Markham, L.W., Kinnett, K., Wong, B.L., Woodrow Benson, D. and Cripe, L.H. (2008) 'Corticosteroid treatment retards development of ventricular dysfunction in Duchenne muscular dystrophy', *Neuromuscul Disord*, 18(5), pp. 365-70.

Marlow, G., Bolduc, V., Boycott, K.M., Saleki, K., Inoue, H., Kroon, J., Itakura, M., Robitaille, Y., Parent, L., Baas, F., Mizuta, K., Kamata, N., Richard, I., Linssen, W., Mahjneh, I., de Visser, M., Brais, B. and Bashir, R. 'P13 Identification of a novel group of muscular dystrophies, the Anoctaminopathies, caused by recessive mutations in the putative calcium activated chloride channel, ANO5', *Neuromuscular Disorders*, 20, p. S8.

Matos, L.L., Trufelli, D.C., de Matos, M.G. and da Silva Pinhal, M.A. (2010) 'Immunohistochemistry as an important tool in biomarkers detection and clinical practice', *Biomark Insights*, 5, pp. 9-20.

Matsuda, C., Hayashi, Y.K., Ogawa, M., Aoki, M., Murayama, K., Nishino, I., Nonaka, I., Arahata, K. and Brown, R.H., Jr. (2001) 'The sarcolemmal proteins dysferlin and caveolin-3 interact in skeletal muscle', *Hum Mol Genet*, 10(17), pp. 1761-6.

Mattheij, N.J., Braun, A., van Kruchten, R., Castoldi, E., Pircher, J., Baaten, C.C., Wulling, M., Kuijpers, M.J., Kohler, R., Poole, A.W., Schreiber, R., Vortkamp, A., Collins, P.W., Nieswandt, B., Kunzelmann, K., Cosemans, J.M. and Heemskerk, J.W. (2015) 'Survival protein anoctamin-6 controls multiple platelet responses including phospholipid scrambling, swelling, and protein cleavage', *Faseb j*.

Matthews, H.R. and Reisert, J. (2003) 'Calcium, the two-faced messenger of olfactory transduction and adaptation', *Curr Opin Neurobiol*, 13(4), pp. 469-75.

Mauro, A. (1961) 'Satellite cell of skeletal muscle fibers', *J Biophys Biochem Cytol*, 9, pp. 493-5.

McGreevy, J.W., Hakim, C.H., McIntosh, M.A. and Duan, D. (2015) 'Animal models of Duchenne muscular dystrophy: from basic mechanisms to gene therapy', *Dis Model Mech*, 8(3), pp. 195-213.

McLafferty, F.W. (1981) 'Tandem mass spectrometry', *Science*, 214(4518), pp. 280-287.

McLafferty, F.W. and Bockhoff, F.M. (1978) 'Separation/Identification System for Complex Mixtures Using Mass Separation and Mass Spectral Characterization', *Analytical Chemistry*, 50(1), pp. 69-76.

McNeil, P.L. and Khakee, R. (1992) 'Disruptions of muscle fiber plasma membranes. Role in exercise-induced damage', *Am J Pathol*, 140(5), pp. 1097-109.

Meers, P. and Mealy, T. (1993) 'Calcium-dependent annexin V binding to phospholipids: stoichiometry, specificity, and the role of negative charge', *Biochemistry*, 32(43), pp. 11711-21.

Mekada, K., Abe, K., Murakami, A., Nakamura, S., Nakata, H., Moriwaki, K., Obata, Y. and Yoshiki, A. (2009) 'Genetic differences among C57BL/6 substrains', *Exp Anim*, 58(2), pp. 141-9.

Meng, J., Counsell, J.R., Reza, M., Laval, S.H., Danos, O., Thrasher, A., Lochmuller, H., Muntoni, F. and Morgan, J.E. (2016) 'Autologous skeletal muscle derived cells

expressing a novel functional dystrophin provide a potential therapy for Duchenne Muscular Dystrophy', *Sci Rep*, 6, p. 19750.

Menke, M., Gerke, V. and Steinem, C. (2005) 'Phosphatidylserine membrane domain clustering induced by annexin A2/S100A10 heterotetramer', *Biochemistry*, 44(46), pp. 15296-303.

Meola, G., Velicogna, M., Brigato, C., Pizzul, S., Rotondo, G. and Scarlato, G. (1991) 'Growth and differentiation of myogenic clones from adult human muscle cell cultures', *Eur J Basic Appl Histochem*, 35(3), pp. 219-31.

Mercuri, E. and Muntoni, F. (2013) 'Muscular dystrophies', *Lancet*, 381(9869), pp. 845-60.

Meryon, E. (1852) 'On Granular and Fatty Degeneration of the Voluntary Muscles', *Med Chir Trans*, 35, pp. 73-84.1.

Middel, V., Zhou, L., Takamiya, M., Beil, T., Shahid, M., Roostalu, U., Grabher, C., Rastegar, S., Reischl, M., Nienhaus, G.U. and Strahle, U. (2016) 'Dysferlin-mediated phosphatidylserine sorting engages macrophages in sarcolemma repair', *Nat Commun*, 7, p. 12875.

Milone, M., Liewluck, T., Winder, T.L. and Pianosi, P.T. (2012) 'Amyloidosis and exercise intolerance in ANO5 muscular dystrophy', *Neuromuscul Disord*, 22(1), pp. 13-5.

Minetti, C., Sotgia, F., Bruno, C., Scartezzini, P., Broda, P., Bado, M., Masetti, E., Mazzocco, M., Egeo, A., Donati, M.A., Volonte, D., Galbiati, F., Cordone, G., Bricarelli, F.D., Lisanti, M.P. and Zara, F. (1998) 'Mutations in the caveolin-3 gene cause autosomal dominant limb-girdle muscular dystrophy', *Nat Genet*, 18(4), pp. 365-8.

Mirnikjoo, B., Balasubramanian, K. and Schroit, A.J. (2009a) 'Mobilization of lysosomal calcium regulates the externalization of phosphatidylserine during apoptosis', *J Biol Chem*, 284(11), pp. 6918-23.

Mirnikjoo, B., Balasubramanian, K. and Schroit, A.J. (2009b) 'Suicidal membrane repair regulates phosphatidylserine externalization during apoptosis', *J Biol Chem*, 284(34), pp. 22512-6.

Mirsaeidi, M., Gidfar, S., Vu, A. and Schraufnagel, D. (2016) 'Annexins family: insights into their functions and potential role in pathogenesis of sarcoidosis', *J Transl Med*, 14, p. 89.

Mizuta, K., Tsutsumi, S., Inoue, H., Sakamoto, Y., Miyatake, K., Miyawaki, K., Noji, S., Kamata, N. and Itakura, M. (2007) 'Molecular characterization of GDD1/TMEM16E, the gene product responsible for autosomal dominant gnathodiaphyseal dysplasia', *Biochem Biophys Res Commun*, 357(1), pp. 126-32.

Moldovan, N.I., Heltianu, C., Simionescu, N. and Simionescu, M. (1995) 'Ultrastructural evidence of differential solubility in Triton X-100 of endothelial vesicles and plasma membrane', *Exp Cell Res*, 219(1), pp. 309-13.

Molnar, M.J., Gilbert, R., Lu, Y., Liu, A.B., Guo, A., Larochelle, N., Orlopp, K., Lochmuller, H., Petrof, B.J., Nalbantoglu, J. and Karpati, G. (2004) 'Factors influencing the efficacy, longevity, and safety of electroporation-assisted plasmid-based gene transfer into mouse muscles', *Mol Ther*, 10(3), pp. 447-55.

Monastyrskaya, K., Babiychuk, E.B. and Draeger, A. (2009) 'The annexins: spatial and temporal coordination of signaling events during cellular stress', *Cell Mol Life Sci*, 66(16), pp. 2623-42.

Monastyrskaya, K., Babiychuk, E.B., Hostettler, A., Rescher, U. and Draeger, A. (2007) 'Annexins as intracellular calcium sensors', *Cell Calcium*, 41(3), pp. 207-19.

Moore, S.A., Shilling, C.J., Westra, S., Wall, C., Wicklund, M.P., Stolle, C., Brown, C.A., Michele, D.E., Piccolo, F., Winder, T.L., Stence, A., Barresi, R., King, N., King, W., Florence, J., Campbell, K.P., Fenichel, G.M., Stedman, H.H., Kissel, J.T., Griggs, R.C., Pandya, S., Mathews, K.D., Pestronk, A., Serrano, C., Darvish, D. and Mendell, J.R. (2006) 'Limb-girdle muscular dystrophy in the United States', *J Neuropathol Exp Neurol*, 65(10), pp. 995-1003.

Morise, H., Shimomura, O., Johnson, F.H. and Winant, J. (1974) 'Intermolecular energy transfer in the bioluminescent system of Aequorea', *Biochemistry*, 13(12), pp. 2656-62.

Moss, S.E. and Morgan, R.O. (2004) 'The annexins', *Genome Biol*, 5(4), p. 219.

Munnix, I.C., Harmsma, M., Giddings, J.C., Collins, P.W., Feijge, M.A., Comfurius, P., Heemskerk, J.W. and Bevers, E.M. (2003) 'Store-mediated calcium entry in the regulation of phosphatidylserine exposure in blood cells from Scott patients', *Thromb Haemost*, 89(4), pp. 687-95.

Nakano, M., Fukuda, M., Kudo, T., Matsuzaki, N., Azuma, T., Sekine, K., Endo, H. and Handa, T. (2009) 'Flip-flop of phospholipids in vesicles: kinetic analysis with time-resolved small-angle neutron scattering', *J Phys Chem B*, 113(19), pp. 6745-8.

Narayanaswami, P., Weiss, M., Selcen, D., David, W., Raynor, E., Carter, G., Wicklund, M., Barohn, R.J., Ensrud, E., Griggs, R.C., Gronseth, G. and Amato, A.A. (2014) 'Evidence-based guideline summary: diagnosis and treatment of limb-girdle and distal dystrophies: report of the guideline development subcommittee of the American Academy of Neurology and the practice issues review panel of the American Association of Neuromuscular & Electrodiagnostic Medicine', *Neurology*, 83(16), pp. 1453-63.

Nigro, V., de Sa Moreira, E., Piluso, G., Vainzof, M., Belsito, A., Politano, L., Puca, A.A., Passos-Bueno, M.R. and Zatz, M. (1996) 'Autosomal recessive limb-girdle muscular dystrophy, LGMD2F, is caused by a mutation in the delta-sarcoglycan gene', *Nat Genet*, 14(2), pp. 195-8.

Nigro, V. and Savarese, M. (2014) 'Genetic basis of limb-girdle muscular dystrophies: the 2014 update', *Acta Myol*, 33(1), pp. 1-12.

Niks, E.H. and Aartsma-Rus, A. (2017) 'Exon skipping: a first in class strategy for Duchenne muscular dystrophy', *Expert Opin Biol Ther*, 17(2), pp. 225-236.

Noguchi, S., McNally, E.M., Ben Othmane, K., Hagiwara, Y., Mizuno, Y., Yoshida, M., Yamamoto, H., Bonnemann, C.G., Gussoni, E., Denton, P.H., Kyriakides, T., Middleton, L., Hentati, F., Ben Hamida, M., Nonaka, I., Vance, J.M., Kunkel, L.M. and Ozawa, E. (1995) 'Mutations in the dystrophin-associated protein gamma-sarcoglycan in chromosome 13 muscular dystrophy', *Science*, 270(5237), pp. 819-22.

Norwood, F.L., Harling, C., Chinnery, P.F., Eagle, M., Bushby, K. and Straub, V. (2009) 'Prevalence of genetic muscle disease in Northern England: in-depth analysis of a muscle clinic population', *Brain*, 132(Pt 11), pp. 3175-86.

Ohlendieck, K., Ervasti, J.M., Matsumura, K., Kahl, S.D., Leveille, C.J. and Campbell, K.P. (1991) 'Dystrophin-related protein is localized to neuromuscular junctions of adult skeletal muscle', *Neuron*, 7(3), pp. 499-508.

Oliferenko, S., Paiha, K., Harder, T., Gerke, V., Schwarzler, C., Schwarz, H., Beug, H., Gunthert, U. and Huber, L.A. (1999) 'Analysis of CD44-containing lipid rafts: Recruitment of annexin II and stabilization by the actin cytoskeleton', *J Cell Biol*, 146(4), pp. 843-54.

Olive, M., Goldfarb, L.G., Shatunov, A., Fischer, D. and Ferrer, I. (2005) 'Myotilinopathy: refining the clinical and myopathological phenotype', *Brain*, 128(Pt 10), pp. 2315-26.

Parton, R.G. and Simons, K. (2007) 'The multiple faces of caveolae', *Nat Rev Mol Cell Biol*, 8(3), pp. 185-94.

Partridge, T.A., Grounds, M. and Sloper, J.C. (1978) 'Evidence of fusion between host and donor myoblasts in skeletal muscle grafts', *Nature*, 273(5660), pp. 306-8.

Penttila, S., Palmio, J., Suominen, T., Raheem, O., Evila, A., Muelas Gomez, N., Tasca, G., Waddell, L.B., Clarke, N.F., Barboi, A., Hackman, P. and Udd, B. (2012) 'Eight new mutations and the expanding phenotype variability in muscular dystrophy caused by ANO5', *Neurology*, 78(12), pp. 897-903.

Perez-Verdaguer, M., Capera, J., Martinez-Marmol, R., Camps, M., Comes, N., Tamkun, M.M. and Felipe, A. (2016) 'Caveolin interaction governs Kv1.3 lipid raft targeting', *Sci Rep*, 6, p. 22453.

Peterle, E., Fanin, M., Semplicini, C., Padilla, J.J., Nigro, V. and Angelini, C. (2013) 'Clinical phenotype, muscle MRI and muscle pathology of LGMD1F', *J Neurol*, 260(8), pp. 2033-41.

Pierini, L.M. and Maxfield, F.R. (2001) 'Flotillas of lipid rafts fore and aft', *Proc Natl Acad Sci U S A*, 98(17), pp. 9471-3.

Pike, L.J. (2003) 'Lipid rafts: bringing order to chaos', *J Lipid Res*, 44(4), pp. 655-67.

Pomorski, T. and Menon, A.K. (2006) 'Lipid flippases and their biological functions', *Cellular and Molecular Life Sciences CMLS*, 63(24), pp. 2908-2921.

Ponissery Saidu, S., Stephan, A.B., Talaga, A.K., Zhao, H. and Reisert, J. (2013) 'Channel properties of the splicing isoforms of the olfactory calcium-activated chloride channel Anoctamin 2', *J Gen Physiol*, 141(6), pp. 691-703.

Poppe, M., Cree, L., Bourke, J., Eagle, M., Anderson, L.V., Birchall, D., Brockington, M., Buddles, M., Busby, M., Muntoni, F., Wills, A. and Bushby, K. (2003) 'The phenotype of limb-girdle muscular dystrophy type 2I', *Neurology*, 60(8), pp. 1246-51.

Porter, A.G. and Janicke, R.U. (1999) 'Emerging roles of caspase-3 in apoptosis', *Cell Death Differ*, 6(2), pp. 99-104.

Putcha, G.V., Harris, C.A., Moulder, K.L., Easton, R.M., Thompson, C.B. and Johnson, E.M., Jr. (2002) 'Intrinsic and extrinsic pathway signaling during neuronal apoptosis: lessons from the analysis of mutant mice', *J Cell Biol*, 157(3), pp. 441-53.

Rabilloud, T. (1999) 'Solubilization of proteins in 2-D electrophoresis. An outline', *Methods Mol Biol*, 112, pp. 9-19.

Ramos, G.C., Fernandes, D., Charao, C.T., Souza, D.G., Teixeira, M.M. and Assreuy, J. (2007) 'Apoptotic mimicry: phosphatidylserine liposomes reduce inflammation through activation of peroxisome proliferator-activated receptors (PPARs) in vivo', *Br J Pharmacol*, 151(6), pp. 844-50.

Rawat, R., Cohen, T.V., Ampong, B., Francia, D., Henriques-Pons, A., Hoffman, E.P. and Nagaraju, K. (2010) 'Inflammasome up-regulation and activation in dysferlin-deficient skeletal muscle', *Am J Pathol*, 176(6), pp. 2891-900.

Raynal, P. and Pollard, H.B. (1994) 'Annexins: the problem of assessing the biological role for a gene family of multifunctional calcium- and phospholipid-binding proteins', *Biochim Biophys Acta*, 1197(1), pp. 63-93.

Reddy, A., Caler, E.V. and Andrews, N.W. (2001) 'Plasma membrane repair is mediated by Ca(2+)-regulated exocytosis of lysosomes', *Cell*, 106(2), pp. 157-69.

Repetto, S., Bado, M., Broda, P., Lucania, G., Masetti, E., Sotgia, F., Carbone, I., Pavan, A., Bonilla, E., Cordone, G., Lisanti, M.P. and Minetti, C. (1999) 'Increased number of caveolae and caveolin-3 overexpression in Duchenne muscular dystrophy', *Biochem Biophys Res Commun*, 261(3), pp. 547-50.

Rety, S., Osterloh, D., Arie, J.P., Tabaries, S., Seeman, J., Russo-Marie, F., Gerke, V. and Lewit-Bentley, A. (2000) 'Structural basis of the Ca(2+)-dependent association between S100C (S100A11) and its target, the N-terminal part of annexin I', *Structure*, 8(2), pp. 175-84.

Rety, S., Sopkova, J., Renouard, M., Osterloh, D., Gerke, V., Tabaries, S., Russo-Marie, F. and Lewit-Bentley, A. (1999) 'The crystal structure of a complex of p11 with the annexin II N-terminal peptide', *Nat Struct Biol*, 6(1), pp. 89-95.

Reza, M., Laval, S.H., Roos, A., Carr, S. and Lochmuller, H. (2016) 'Optimization of Internally Deleted Dystrophin Constructs', *Hum Gene Ther Methods*, 27(5), pp. 174-186.

Richard, I., Hogrel, J.Y., Stockholm, D., Payan, C.A., Fougerousse, F., Eymard, B., Mignard, C., Lopez de Munain, A., Fardeau, M. and Urtizberea, J.A. (2016) 'Natural history of LGMD2A for delineating outcome measures in clinical trials', *Ann Clin Transl Neurol*, 3(4), pp. 248-65.

Richards, M., Coppee, F., Thomas, N., Belayew, A. and Upadhyaya, M. (2012) 'Facioscapulohumeral muscular dystrophy (FSHD): an enigma unravelled?', *Hum Genet*, 131(3), pp. 325-40.

Riminucci, M., Collins, M.T., Corsi, A., Boyde, A., Murphey, M.D., Wientroub, S., Kuznetsov, S.A., Cherman, N., Robey, P.G. and Bianco, P. (2001) 'Gnathodiaphyseal dysplasia: a syndrome of fibro-osseous lesions of jawbones, bone fragility, and long bone bowing', *J Bone Miner Res*, 16(9), pp. 1710-8.

Roberds, S.L., Leturcq, F., Allamand, V., Piccolo, F., Jeanpierre, M., Anderson, R.D., Lim, L.E., Lee, J.C., Tome, F.M., Romero, N.B. and et al. (1994) 'Missense mutations in the adhalin gene linked to autosomal recessive muscular dystrophy', *Cell*, 78(4), pp. 625-33.

Rock, K.L. and Kono, H. (2008) 'The inflammatory response to cell death', *Annu Rev Pathol*, 3, pp. 99-126.

Roostalu, U. and Strahle, U. (2012) 'In vivo imaging of molecular interactions at damaged sarcolemma', *Dev Cell*, 22(3), pp. 515-29.

Rosing, J., Bevers, E.M., Comfurius, P., Hemker, H.C., van Dieijen, G., Weiss, H.J. and Zwaal, R.F. (1985) 'Impaired factor X and prothrombin activation associated with decreased phospholipid exposure in platelets from a patient with a bleeding disorder', *Blood*, 65(6), pp. 1557-61.

Rybakova, I.N., Patel, J.R. and Ervasti, J.M. (2000) 'The dystrophin complex forms a mechanically strong link between the sarcolemma and costameric actin', *J Cell Biol*, 150(5), pp. 1209-14.

Saccone, V., Palmieri, M., Passamano, L., Piluso, G., Meroni, G., Politano, L. and Nigro, V. (2008) 'Mutations that impair interaction properties of TRIM32 associated with limb-girdle muscular dystrophy 2H', *Hum Mutat*, 29(2), pp. 240-7.

Sadowski, P.G., Dunkley, T.P., Shadforth, I.P., Dupree, P., Bessant, C., Griffin, J.L. and Lilley, K.S. (2006) 'Quantitative proteomic approach to study subcellular localization of membrane proteins', *Nat Protoc*, 1(4), pp. 1778-89.

Sahara, S., Aoto, M., Eguchi, Y., Imamoto, N., Yoneda, Y. and Tsujimoto, Y. (1999) 'Acinus is a caspase-3-activated protein required for apoptotic chromatin condensation', *Nature*, 401(6749), pp. 168-73.

Sarkozy, A., Deschauer, M., Carlier, R.Y., Schrank, B., Seeger, J., Walter, M.C., Schoser, B., Reilich, P., Leturq, F., Radunovic, A., Behin, A., Laforet, P., Eymard, B., Schreiber, H., Hicks, D., Vaidya, S.S., Glaser, D., Carlier, P.G., Bushby, K., Lochmuller, H. and Straub, V. (2012) 'Muscle MRI findings in limb girdle muscular dystrophy type 2L', *Neuromuscul Disord*, 22 Suppl 2, pp. S122-9.

Sarkozy, A., Hicks, D., Hudson, J., Laval, S.H., Barresi, R., Hilton-Jones, D., Deschauer, M., Harris, E., Rufibach, L., Hwang, E., Bashir, R., Walter, M.C., Krause, S., van den Bergh, P., Illa, I., Penisson-Besnier, I., De Waele, L., Turnbull, D., Guglieri, M., Schrank, B., Schoser, B., Seeger, J., Schreiber, H., Glaser, D., Eagle, M., Bailey, G., Walters, R., Longman, C., Norwood, F., Winer, J., Muntoni, F., Hanna, M., Roberts, M., Bindoff, L.A., Brierley, C., Cooper, R.G., Cottrell, D.A., Davies, N.P., Gibson, A., Gorman, G.S., Hammans, S., Jackson, A.P., Khan, A., Lane, R., McConville, J., McEntagart, M., Al-Memar, A., Nixon, J., Panicker, J., Parton, M., Petty, R., Price, C.J., Rakowicz, W., Ray, P., Schapira, A.H., Swingler, R., Turner, C., Wagner, K.R., Maddison, P., Shaw, P.J., Straub, V., Bushby, K. and Lochmuller, H. (2013) 'ANO5 Gene Analysis in a Large Cohort of Patients with Anoctaminopathy: Confirmation of Male Prevalence and High Occurrence of the Common Exon 5 Gene Mutation', *Hum Mutat*.

Savarese, M., Di Fruscio, G., Tasca, G., Ruggiero, L., Janssens, S., De Bleecker, J., Delpech, M., Musumeci, O., Toscano, A., Angelini, C., Sacconi, S., Santoro, L., Ricci, E., Claes, K., Politano, L. and Nigro, V. (2015) 'Next generation sequencing on patients with LGMD and nonspecific myopathies: Findings associated with ANO5 mutations', *Neuromuscul Disord*, 25(7), pp. 533-41.

Scharf, B., Clement, C.C., Wu, X.-X., Morozova, K., Zanolini, D., Follenzi, A., Larocca, J.N., Levon, K., Sutterwala, F.S., Rand, J., Cobelli, N., Purdue, E., Hajjar, K.A. and Santambrogio, L. (2012) 'Annexin A2 binds to endosomes following organelle destabilization by particulate wear debris', *Nat Commun*, 3, p. 755.

Schindler, R.F., Scotton, C., Zhang, J., Passarelli, C., Ortiz-Bonnin, B., Simrick, S., Schwerte, T., Poon, K.L., Fang, M., Rinne, S., Froese, A., Nikolaev, V.O., Grunert, C., Muller, T., Tasca, G., Sarathchandra, P., Drago, F., Dallapiccola, B., Rapezzi, C., Arbustini, E., Di Raimo, F.R., Neri, M., Selvatici, R., Gualandi, F., Fattori, F., Pietrangelo, A., Li, W., Jiang, H., Xu, X., Bertini, E., Decher, N., Wang, J., Brand, T. and Ferlini, A. (2016) 'POPDC1(S201F) causes muscular dystrophy and arrhythmia by affecting protein trafficking', *J Clin Invest*, 126(1), pp. 239-53.

Schlegel, R.A. and Williamson, P. (2001) 'Phosphatidylserine, a death knell', *Cell Death Differ*, 8(6), pp. 551-63.

Schnell, J.D. and Hicke, L. (2003) 'Non-traditional functions of ubiquitin and ubiquitin-binding proteins', *J Biol Chem*, 278(38), pp. 35857-60.

Schreiber, R., Uliyakina, I., Kongsuphol, P., Warth, R., Mirza, M., Martins, J.R. and Kunzelmann, K. (2010) 'Expression and function of epithelial anoctamins', *J Biol Chem*, 285(10), pp. 7838-45.

Schroeder, B.C., Cheng, T., Jan, Y.N. and Jan, L.Y. (2008) 'Expression cloning of TMEM16A as a calcium-activated chloride channel subunit', *Cell*, 134(6), pp. 1019-29.

Schwartz, R., Ting, C.S. and King, J. (2001) 'Whole proteome pI values correlate with subcellular localizations of proteins for organisms within the three domains of life', *Genome Res*, 11(5), pp. 703-9.

Scudieri, P., Caci, E., Venturini, A., Sondo, E., Pianigiani, G., Marchetti, C., Ravazzolo, R., Pagani, F. and Galietta, L.J. (2015) 'Ion channel and lipid scramblase activity

associated with expression of TMEM16F/ANO6 isoforms', *J Physiol*, 593(17), pp. 3829-48.

Segawa, K., Suzuki, J. and Nagata, S. (2011) 'Constitutive exposure of phosphatidylserine on viable cells', *Proc Natl Acad Sci U S A*, 108(48), pp. 19246-51.

Selcen, D. and Engel, A.G. (2004) 'Mutations in myotilin cause myofibrillar myopathy', *Neurology*, 62(8), pp. 1363-71.

Servian-Morilla, E., Takeuchi, H., Lee, T.V., Clarimon, J., Mavillard, F., Area-Gomez, E., Rivas, E., Nieto-Gonzalez, J.L., Rivero, M.C., Cabrera-Serrano, M., Gomez-Sanchez, L., Martinez-Lopez, J.A., Estrada, B., Marquez, C., Morgado, Y., Suarez-Calvet, X., Pita, G., Bigot, A., Gallardo, E., Fernandez-Chacon, R., Hirano, M., Haltiwanger, R.S., Jafar-Nejad, H. and Paradas, C. (2016) 'A POGLUT1 mutation causes a muscular dystrophy with reduced Notch signaling and satellite cell loss', *EMBO Mol Med*, 8(11), pp. 1289-1309.

Sessions, A. and Horwitz, A.F. (1983) 'Differentiation-related differences in the plasma membrane phospholipid asymmetry of myogenic and fibrogenic cells', *Biochim Biophys Acta*, 728(1), pp. 103-11.

Shalaby, S., Mitsuhashi, H., Matsuda, C., Minami, N., Noguchi, S., Nonaka, I., Nishino, I. and Hayashi, Y.K. (2009) 'Defective myotilin homodimerization caused by a novel mutation in MYOT exon 9 in the first Japanese limb girdle muscular dystrophy 1A patient', *J Neuropathol Exp Neurol*, 68(6), pp. 701-7.

Shang, L., Hao, J.J., Zhao, X.K., He, J.Z., Shi, Z.Z., Liu, H.J., Wu, L.F., Jiang, Y.Y., Shi, F., Yang, H., Zhang, Y., Liu, Y.Z., Zhang, T.T., Xu, X., Cai, Y., Jia, X.M., Li, M., Zhan, Q.M., Li, E.M., Wang, L.D., Wei, W.Q. and Wang, M.R. (2016) 'ANO1 protein as a potential biomarker for esophageal cancer prognosis and precancerous lesion development prediction', *Oncotarget*, 7(17), pp. 24374-82.

Shokeir, M.H. and Kobrinsky, N.L. (1976) 'Autosomal recessive muscular dystrophy in Manitoba Hutterites', *Clin Genet*, 9(2), pp. 197-202.

Simionescu, N., Siminoescu, M. and Palade, G.E. (1975) 'Permeability of muscle capillaries to small heme-peptides. Evidence for the existence of patent transendothelial channels', *J Cell Biol*, 64(3), pp. 586-607.

Smolina, N., Kostareva, A., Bruton, J., Karpushev, A., Sjoberg, G. and Sejersen, T. (2015) 'Primary Murine Myotubes as a Model for Investigating Muscular Dystrophy', *Biomed Res Int*, 2015, p. 594751.

Solari, F.A., Mattheij, N.J., Burkhart, J.M., Swieringa, F., Collins, P.W., Cosemans, J.M., Sickmann, A., Heemskerk, J.W. and Zahedi, R.P. (2016) 'Combined Quantification of the Global Proteome, Phosphoproteome, and Proteolytic Cleavage to Characterize Altered Platelet Functions in the Human Scott Syndrome', *Mol Cell Proteomics*, 15(10), pp. 3154-3169.

Song, K.S., Scherer, P.E., Tang, Z., Okamoto, T., Li, S., Chafel, M., Chu, C., Kohtz, D.S. and Lisanti, M.P. (1996) 'Expression of caveolin-3 in skeletal, cardiac, and smooth muscle cells. Caveolin-3 is a component of the sarcolemma and co-fractionates with

dystrophin and dystrophin-associated glycoproteins', *J Biol Chem*, 271(25), pp. 15160-5.

Spenneberg, R., Osterloh, D. and Gerke, V. (1998) 'Phospholipid vesicle binding and aggregation by four novel fish annexins are differently regulated by Ca2+', *Biochim Biophys Acta*, 1448(2), pp. 311-9.

Spronk, H.M., ten Cate, H. and van der Meijden, P.E. (2014) 'Differential roles of tissue factor and phosphatidylserine in activation of coagulation', *Thromb Res*, 133 Suppl 1, pp. S54-6.

Starling, A., Kok, F., Passos-Bueno, M.R., Vainzof, M. and Zatz, M. (2004) 'A new form of autosomal dominant limb-girdle muscular dystrophy (LGMD1G) with progressive fingers and toes flexion limitation maps to chromosome 4p21', *Eur J Hum Genet*, 12(12), pp. 1033-40.

Steenbergen, R., Nanowski, T.S., Beigneux, A., Kulinski, A., Young, S.G. and Vance, J.E. (2005) 'Disruption of the phosphatidylserine decarboxylase gene in mice causes embryonic lethality and mitochondrial defects', *J Biol Chem*, 280(48), pp. 40032-40.

Stehlikova, K., Skalova, D., Zidkova, J., Mrazova, L., Vondracek, P., Mazanec, R., Vohanka, S., Haberlova, J., Hermanova, M., Zamecnik, J., Soucek, O., Oslejskova, H., Dvorackova, N., Solarova, P. and Fajkusova, L. (2014) 'Autosomal recessive limb-girdle muscular dystrophies in the Czech Republic', *BMC Neurol*, 14, p. 154.

Stohr, H., Heisig, J.B., Benz, P.M., Schoberl, S., Milenkovic, V.M., Strauss, O., Aartsen, W.M., Wijnholds, J., Weber, B.H. and Schulz, H.L. (2009) 'TMEM16B, a novel protein with calcium-dependent chloride channel activity, associates with a presynaptic protein complex in photoreceptor terminals', *J Neurosci*, 29(21), pp. 6809-18.

Straub, V., Rafael, J.A., Chamberlain, J.S. and Campbell, K.P. (1997) 'Animal models for muscular dystrophy show different patterns of sarcolemmal disruption', *J Cell Biol*, 139(2), pp. 375-85.

Suzuki, J., Fujii, T., Imao, T., Ishihara, K., Kuba, H. and Nagata, S. (2013) 'Calcium-dependent phospholipid scramblase activity of TMEM16 protein family members', *J Biol Chem*, 288(19), pp. 13305-16.

Suzuki, J., Umeda, M., Sims, P.J. and Nagata, S. (2010) 'Calcium-dependent phospholipid scrambling by TMEM16F', *Nature*, 468(7325), pp. 834-8.

Sveen, M.L., Schwartz, M. and Vissing, J. (2006) 'High prevalence and phenotype-genotype correlations of limb girdle muscular dystrophy type 2I in Denmark', *Ann Neurol*, 59(5), pp. 808-15.

Tait, J.F. and Gibson, D. (1992) 'Phospholipid binding of annexin V: effects of calcium and membrane phosphatidylserine content', *Arch Biochem Biophys*, 298(1), pp. 187-91.

Tamura, Y., Onguka, O., Itoh, K., Endo, T., Iijima, M., Claypool, S.M. and Sesaki, H. (2012) 'Phosphatidylethanolamine biosynthesis in mitochondria: phosphatidylserine

(PS) trafficking is independent of a PS decarboxylase and intermembrane space proteins UPS1P and UPS2P', *J Biol Chem*, 287(52), pp. 43961-71.

Tateyama, M., Aoki, M., Nishino, I., Hayashi, Y.K., Sekiguchi, S., Shiga, Y., Takahashi, T., Onodera, Y., Haginoya, K., Kobayashi, K., Iinuma, K., Nonaka, I., Arahata, K. and Itoyama, Y. (2002) 'Mutation in the caveolin-3 gene causes a peculiar form of distal myopathy', *Neurology*, 58(2), pp. 323-5.

Tawil, R., van der Maarel, S.M. and Tapscott, S.J. (2014) 'Facioscapulohumeral dystrophy: the path to consensus on pathophysiology', *Skelet Muscle*, 4, p. 12.

Taylor, P.R., Carugati, A., Fadok, V.A., Cook, H.T., Andrews, M., Carroll, M.C., Savill, J.S., Henson, P.M., Botto, M. and Walport, M.J. (2000) 'A hierarchical role for classical pathway complement proteins in the clearance of apoptotic cells in vivo', *J Exp Med*, 192(3), pp. 359-66.

Thompson, R. and Straub, V. (2016) 'Limb-girdle muscular dystrophies - international collaborations for translational research', *Nat Rev Neurol*, 12(5), pp. 294-309.

Thornberry, N.A. and Lazebnik, Y. (1998) 'Caspases: enemies within', *Science*, 281(5381), pp. 1312-6.

Tian, Y., Wright, J., Cebotaru, L., Wang, H. and Guggino, W.B. (2015) 'Anoctamin 5 is related to plasma membrane repair', *JSM Regenerative Medicine & Bioengineering*, 3(1).

Tidball, J.G. (2005) 'Inflammatory processes in muscle injury and repair', *Am J Physiol Regul Integr Comp Physiol*, 288(2), pp. R345-53.

Toti, F., Satta, N., Fressinaud, E., Meyer, D. and Freyssinet, J.M. (1996) 'Scott syndrome, characterized by impaired transmembrane migration of procoagulant phosphatidylserine and hemorrhagic complications, is an inherited disorder', *Blood*, 87(4), pp. 1409-15.

Towomey, C. and McCarthy, J.V. (2005) 'Pathways of apoptosis and importance in development', *Journal of Cellular and Molecular Medicine*, 9(2), p. 14.

Toye, A.A., Lippiat, J.D., Proks, P., Shimomura, K., Bentley, L., Hugill, A., Mijat, V., Goldsworthy, M., Moir, L., Haynes, A., Quarterman, J., Freeman, H.C., Ashcroft, F.M. and Cox, R.D. (2005) 'A genetic and physiological study of impaired glucose homeostasis control in C57BL/6J mice', *Diabetologia*, 48(4), pp. 675-86.

Tran, T.T., Tobiume, K., Hirono, C., Fujimoto, S., Mizuta, K., Kubozono, K., Inoue, H., Itakura, M., Sugita, M. and Kamata, N. (2014) 'TMEM16E (GDD1) exhibits protein instability and distinct characteristics in chloride channel/pore forming ability', *J Cell Physiol*, 229(2), pp. 181-90.

Tsutsumi, S., Inoue, H., Sakamoto, Y., Mizuta, K., Kamata, N. and Itakura, M. (2005) 'Molecular cloning and characterization of the murine gnathodiaphyseal dysplasia gene GDD1', *Biochem Biophys Res Commun*, 331(4), pp. 1099-106.

Tsutsumi, S., Kamata, N., Vokes, T.J., Maruoka, Y., Nakakuki, K., Enomoto, S., Omura, K., Amagasa, T., Nagayama, M., Saito-Ohara, F., Inazawa, J., Moritani, M., Yamaoka, T., Inoue, H. and Itakura, M. (2004) 'The novel gene encoding a putative transmembrane protein is mutated in gnathodiaphyseal dysplasia (GDD)', *Am J Hum Genet*, 74(6), pp. 1255-61.

Tyler, F.H. and Stephens, F.E. (1950) 'Studies in disorders of muscle. II Clinical manifestations and inheritance of facioscapulohumeral dystrophy in a large family', *Ann Intern Med*, 32(4), pp. 640-60.

Urtizberea, J.A., Bassez, G., Leturcq, F., Nguyen, K., Krahn, M. and Levy, N. (2008) 'Dysferlinopathies', *Neurol India*, 56(3), pp. 289-97.

van den Eijnde, S.M., van den Hoff, M.J., Reutelingsperger, C.P., van Heerde, W.L., Henfling, M.E., Vermeij-Keers, C., Schutte, B., Borgers, M. and Ramaekers, F.C. (2001) 'Transient expression of phosphatidylserine at cell-cell contact areas is required for myotube formation', *J Cell Sci*, 114(Pt 20), pp. 3631-42.

van der Kooi, A.J., Ledderhof, T.M., de Voogt, W.G., Res, C.J., Bouwsma, G., Troost, D., Busch, H.F., Becker, A.E. and de Visser, M. (1996) 'A newly recognized autosomal dominant limb girdle muscular dystrophy with cardiac involvement', *Ann Neurol*, 39(5), pp. 636-42.

van der Kooi, A.J., Ten Dam, L., Frankhuizen, W.S., Straathof, C.S., van Doorn, P.A., de Visser, M. and Ginjaar, I.B. (2013) 'ANO5 mutations in the Dutch limb girdle muscular dystrophy population', *Neuromuscul Disord*.

van der Ven, P.F., Schaart, G., Jap, P.H., Sengers, R.C., Stadhouders, A.M. and Ramaekers, F.C. (1992) 'Differentiation of human skeletal muscle cells in culture: maturation as indicated by titin and desmin striation', *Cell Tissue Res*, 270(1), pp. 189-98.

van Helvoort, A., Smith, A.J., Sprong, H., Fritzsche, I., Schinkel, A.H., Borst, P. and van Meer, G. (1996) 'MDR1 P-glycoprotein is a lipid translocase of broad specificity, while MDR3 P-glycoprotein specifically translocates phosphatidylcholine', *Cell*, 87(3), pp. 507-17.

van Meer, G., Voelker, D.R. and Feigenson, G.W. (2008) 'Membrane lipids: where they are and how they behave', *Nat Rev Mol Cell Biol*, 9(2), pp. 112-24.

Vance, J.E. and Tasseva, G. (2013) 'Formation and function of phosphatidylserine and phosphatidylethanolamine in mammalian cells', *Biochim Biophys Acta*, 1831(3), pp. 543-54.

Verhoven, B., Schlegel, R.A. and Williamson, P. (1995) 'Mechanisms of phosphatidylserine exposure, a phagocyte recognition signal, on apoptotic T lymphocytes', *J Exp Med*, 182(5), pp. 1597-601.

Vermeer, S., Hoischen, A., Meijer, R.P., Gilissen, C., Neveling, K., Wieskamp, N., de Brouwer, A., Koenig, M., Anheim, M., Assoum, M., Drouot, N., Todorovic, S., Milic-Rasic, V., Lochmuller, H., Stevanin, G., Goizet, C., David, A., Durr, A., Brice, A., Kremer, B., van de Warrenburg, B.P., Schijvenaars, M.M., Heister, A., Kwint, M., Arts,

P., van der Wijst, J., Veltman, J., Kamsteeg, E.J., Scheffer, H. and Knoers, N. (2010) 'Targeted next-generation sequencing of a 12.5 Mb homozygous region reveals ANO10 mutations in patients with autosomal-recessive cerebellar ataxia', *Am J Hum Genet*, 87(6), pp. 813-9.

Verschoor, C.P., Lelic, A., Bramson, J.L. and Bowdish, D.M. (2015) 'An Introduction to Automated Flow Cytometry Gating Tools and Their Implementation', *Front Immunol*, 6, p. 380.

Vieira, N.M., Naslavsky, M.S., Licinio, L., Kok, F., Schlesinger, D., Vainzof, M., Sanchez, N., Kitajima, J.P., Gal, L., Cavacana, N., Serafini, P.R., Chuartzman, S., Vasquez, C., Mimbacas, A., Nigro, V., Pavanello, R.C., Schuldiner, M., Kunkel, L.M. and Zatz, M. (2014) 'A defect in the RNA-processing protein HNRPDL causes limb-girdle muscular dystrophy 1G (LGMD1G)', *Hum Mol Genet*, 23(15), pp. 4103-10.

Vorgerd, M., Ricker, K., Ziemssen, F., Kress, W., Goebel, H.H., Nix, W.A., Kubisch, C., Schoser, B.G. and Mortier, W. (2001) 'A sporadic case of rippling muscle disease caused by a de novo caveolin-3 mutation', *Neurology*, 57(12), pp. 2273-7.

Walter, M.C., Petersen, J.A., Stucka, R., Fischer, D., Schroder, R., Vorgerd, M., Schroers, A., Schreiber, H., Hanemann, C.O., Knirsch, U., Rosenbohm, A., Huebner, A., Barisic, N., Horvath, R., Komoly, S., Reilich, P., Muller-Felber, W., Pongratz, D., Muller, J.S., Auerswald, E.A. and Lochmuller, H. (2004) 'FKRP (826C>A) frequently causes limb-girdle muscular dystrophy in German patients', *J Med Genet*, 41(4), p. e50.

Walton, J.N. and Nattrass, F.J. (1954) 'On the classification, natural history and treatment of the myopathies', *Brain*, 77(2), pp. 169-231.

Waring, P. and Mullbacher, A. (1999) 'Cell death induced by the Fas/Fas ligand pathway and its role in pathology', *Immunol Cell Biol*, 77(4), pp. 312-7.

Watzele, G. and Berger, E.G. (1990) 'Near identity of HeLa cell galactosyltransferase with the human placental enzyme', *Nucleic Acids Res*, 18(23), p. 7174.

Weiler, T., Greenberg, C.R., Zelinski, T., Nylen, E., Coghlan, G., Crumley, M.J., Fujiwara, T.M., Morgan, K. and Wrogemann, K. (1998) 'A gene for autosomal recessive limb-girdle muscular dystrophy in Manitoba Hutterites maps to chromosome region 9q31-q33: evidence for another limb-girdle muscular dystrophy locus', *Am J Hum Genet*, 63(1), pp. 140-7.

Weiller, G.F., Caraux, G. and Sylvester, N. (2004) 'The modal distribution of protein isoelectric points reflects amino acid properties rather than sequence evolution', *Proteomics*, 4(4), pp. 943-9.

Weiss, H.J., Vicic, W.J., Lages, B.A. and Rogers, J. (1979) 'Isolated deficiency of platelet procoagulant activity', *Am J Med*, 67(2), pp. 206-13.

West, R.B., Corless, C.L., Chen, X., Rubin, B.P., Subramanian, S., Montgomery, K., Zhu, S., Ball, C.A., Nielsen, T.O., Patel, R., Goldblum, J.R., Brown, P.O., Heinrich, M.C. and van de Rijn, M. (2004) 'The novel marker, DOG1, is expressed ubiquitously in gastrointestinal stromal tumors irrespective of KIT or PDGFRA mutation status', *Am J Pathol*, 165(1), pp. 107-13.

Whitlock, J.M. and Hartzell, H.C. (2016a) 'Anoctamins/TMEM16 Proteins: Chloride Channels Flirting with Lipids and Extracellular Vesicles', *Annu Rev Physiol*.

Whitlock, J.M. and Hartzell, H.C. (2016b) 'A Pore Idea: the ion conduction pathway of TMEM16/ANO proteins is composed partly of lipid', *Pflugers Arch*, 468(3), pp. 455-73.

Williamson, P., Bevers, E.M., Smeets, E.F., Comfurius, P., Schlegel, R.A. and Zwaal, R.F. (1995) 'Continuous analysis of the mechanism of activated transbilayer lipid movement in platelets', *Biochemistry*, 34(33), pp. 10448-55.

Williamson, P., Christie, A., Kohlin, T., Schlegel, R.A., Comfurius, P., Harmsma, M., Zwaal, R.F. and Bevers, E.M. (2001) 'Phospholipid scramblase activation pathways in lymphocytes', *Biochemistry*, 40(27), pp. 8065-72.

Williamson, P., Kulick, A., Zachowski, A., Schlegel, R.A. and Devaux, P.F. (1992) 'Ca2+ induces transbilayer redistribution of all major phospholipids in human erythrocytes', *Biochemistry*, 31(27), pp. 6355-60.

Wokke, B.H., van den Bergen, J.C., Versluis, M.J., Niks, E.H., Milles, J., Webb, A.G., van Zwet, E.W., Aartsma-Rus, A., Verschuuren, J.J. and Kan, H.E. (2014) 'Quantitative MRI and strength measurements in the assessment of muscle quality in Duchenne muscular dystrophy', *Neuromuscul Disord*, 24(5), pp. 409-16.

Wolff, M.M. and Stephens, W.E. (1953) 'A Pulsed Mass Spectrometer with Time Dispersion', *Review of Scientific Instruments*, 24(616), pp. 6161-617.

Wu, C.C., MacCoss, M.J., Mardones, G., Finnigan, C., Mogelsvang, S., Yates, J.R., 3rd and Howell, K.E. (2004) 'Organellar proteomics reveals Golgi arginine dimethylation', *Mol Biol Cell*, 15(6), pp. 2907-19.

Xu, J., El Refaey, M., Xu, L., Zhao, L., Gao, Y., Floyd, K., Karaze, T., Janssen, P.M. and Han, R. (2015) 'Genetic disruption of Ano5 in mice does not recapitulate human ANO5-deficient muscular dystrophy', *Skelet Muscle*, 5, p. 43.

Yang, H., Kim, A., David, T., Palmer, D., Jin, T., Tien, J., Huang, F., Cheng, T., Coughlin, S.R., Jan, Y.N. and Jan, L.Y. (2012) 'TMEM16F forms a Ca2+-activated cation channel required for lipid scrambling in platelets during blood coagulation', *Cell*, 151(1), pp. 111-22.

Yang, Y.D., Cho, H., Koo, J.Y., Tak, M.H., Cho, Y., Shim, W.S., Park, S.P., Lee, J., Lee, B., Kim, B.M., Raouf, R., Shin, Y.K. and Oh, U. (2008) 'TMEM16A confers receptor-activated calcium-dependent chloride conductance', *Nature*, 455(7217), pp. 1210-5.

Yoshida, M., Suzuki, A., Yamamoto, H., Noguchi, S., Mizuno, Y. and Ozawa, E. (1994) 'Dissociation of the complex of dystrophin and its associated proteins into several unique groups by n-octyl beta-D-glucoside', *Eur J Biochem*, 222(3), pp. 1055-61.

Yu, K., Whitlock, J.M., Lee, K., Ortlund, E.A., Cui, Y.Y. and Hartzell, H.C. (2015) 'Identification of a lipid scrambling domain in ANO6/TMEM16F', *Elife*, 4, p. e06901.

Yu, S.W., Wang, H., Poitras, M.F., Coombs, C., Bowers, W.J., Federoff, H.J., Poirier, G.G., Dawson, T.M. and Dawson, V.L. (2002) 'Mediation of poly(ADP-ribose) polymerase-1-dependent cell death by apoptosis-inducing factor', *Science*, 297(5579), pp. 259-63.

Zachowski, A. (1993) 'Phospholipids in animal eukaryotic membranes: transverse asymmetry and movement', *Biochem J*, 294 (Pt 1), pp. 1-14.

Zatz, M., de Paula, F., Starling, A. and Vainzof, M. (2003) 'The 10 autosomal recessive limb-girdle muscular dystrophies', *Neuromuscul Disord*, 13(7-8), pp. 532-44.

Zhan, X. and Desiderio, D.M. (2003) 'Differences in the spatial and quantitative reproducibility between two second-dimensional gel electrophoresis systems', *Electrophoresis*, 24(11), pp. 1834-46.

Zimmermann, T. (2005) 'Spectral imaging and linear unmixing in light microscopy', *Adv Biochem Eng Biotechnol*, 95, pp. 245-65.

Zwaal, R.F. and Schroit, A.J. (1997) 'Pathophysiologic implications of membrane phospholipid asymmetry in blood cells', *Blood*, 89(4), pp. 1121-32.